PEOPLE'S DEMOCRATIC REPUBLIC OF ALGERIA
MINISTRY OF HIGHER EDUCATION
AND SCIENTIFIC RESEARCH

UNIVERSITY OF JIJEL

Faculty of Sciences and Technology

Department of Automatic Control

This thesis is submitted in fulfillment of the requirement for the degree

DOCTORAT 3^{th} cycle (LMD)

Option: Automatic and systems

Presented by **Ihab Abderraouf BOULHAM**

Theme

$\mathscr{L}_1$ Adaptive Control for Fractional-Order Systems

---

Defended on: 03/07/2024 in front of the Examination Committee:

Mr.	Toufik BOUDEN	Professor	University of Jijel	President
Mr.	Ahsene BOUBAKIR	Professor	University of Jijel	Supervisor
Mr.	Abdesselem BOULKROUNE	Professor	University of Jijel	Examiner
Mr.	Samir LADACI	Professor	ENP, Algiers	Examiner
Mr.	M Salah ABDELOUAHAB	Professor	University Center of Mila	Examiner

Academic Year 2023/2024

Abstract

Fractional-order calculus has attracted the attention of scholars in the areas of control and system analysis. However, despite its notable advantages, $\mathscr{L}_1$ adaptive control technique remains unexplored in this field. This thesis introduces an extension of this technique to fractional-order systems. Firstly, a new fractional-order $\mathscr{L}_1$ adaptive controller is proposed for a class of fractional-order systems with matched uncertainties and external disturbances. Then, the controller is generalized to the case of multiple-input multiple-output incommensurate systems. The extension of the methodology is possible thanks to the use of a fractional-order sliding surface, simplifying the control architecture and facilitating stability analysis. In the pursuit of enhancing the developed controller, neural networks are employed to handle time-varying input gain and unmodeled dynamics. Additionally, fuzzy logic systems are implemented to tackle various sources of uncertainty within the system. These include unknown input nonlinearities, unmodeled system dynamics, and external disturbances. The analysis of the obtained theoretical and simulation results confirms that the developed strategies guarantee closed-loop stability maintaining the key features of the $\mathscr{L}_1$ adaptive controller.

Keywords: $\mathscr{L}_1$ adaptive control, Fractional-order uncertain systems, Fractional-order sliding surface, Neural networks, Fuzzy logic, Model-free control.

Résumé

Le calcul d'ordre fractionnaire a attiré l'attention des chercheurs dans le domaine de l'automatique et de l'analyse des systèmes. Cependant, malgré ses avantages considérables, la technique de la commande $\mathscr{L}_1$ adaptative reste inexplorée dans ce domaine. Cette thèse introduit une extension de cette technique de commande aux systèmes d'ordre fractionnaire. Premièrement, une nouvelle commande $\mathscr{L}_1$ adaptative à ordre fractionnaire est proposée pour une classe de systèmes d'ordre fractionnaire avec des incertitudes et des perturbations externes. Ensuite, la commande est généralisée au cas des systèmes incommensurables à entrées multiples et à sorties multiples. L'extension de la méthodologie est rendue possible grâce à l'utilisation d'une surface de glissement d'ordre fractionnaire, simplifiant l'architecture de contrôle et facilitant l'analyse de la stabilité. Dans le but d'améliorer la commande développée, des réseaux de neurones sont utilisés pour gérer les gains d'entrée variant dans le temps et les dynamiques non modélisées. De plus, des systèmes de logique floue sont mis en œuvre pour aborder diverses sources d'incertitude au sein du système. Celles-ci comprennent des non-linéarités d'entrée inconnues, des dynamiques non modélisées, et des perturbations externes. L'analyse des résultats théoriques et des simulations obtenues confirment que les stratégies développées garantissent la stabilité en boucle fermée tout en préservant les caractéristiques clés de la commande $\mathscr{L}_1$ adaptative.

Mots clés: Commande $\mathscr{L}_1$ adaptative, Systèmes d'ordre fractionnaire, Surface de glissement d'ordre fractionnaire, Réseaux de neurones, Logique floue, Commande sans modèle.

ملخص

الحساب الكسري جذب انتباه الباحثين في مجالات التحكم وتحليل الأنظمة. على الرغم من مزاياها الملحوظة، تظل تقنية التحكم التكيفي $\mathscr{L}_1$ غير مستكشَفة في هذا المجال. تقدم هذه الرسالة تمديدا لهذه التقنية لتشمل الأنظمة ذي الرتبة الكسرية. أولاً، يُقترح تحكم تكيفي $\mathscr{L}_1$ جديد للأنظمة ذات الدرجات الكسرية والخاضعة لمتغيرات غير معروفة واضطرابات الخارجية. ثم، يُعمم التحكم لحالة الأنظمة الكسرية متعددة المتغيرات. إن توسيع مخطط التحكم يكون ممكنًا بفضل استخدام سطح انزلاق ذو درجة كسرية، مما يُبسِّط هندسة التحكم ويُيسِّر تحليل الاستقرار. في سعي لتعزيز التحكم، يتم استخدام الشبكات العصبية للتعامل مع معدل الإدخال المتغير مع الزمن و الديناميات الغير المعروفة. بالإضافة إلى ذلك، يتم تطبيق أنظمة المنطق الضبابي لمواجهة مصادر مختلفة لعدم اليقين داخل النظام. تشمل هذه العناصر عدم الخطية في الإدخال، الديناميات الغير المعروفة، والاضطرابات الخارجية. تحليل النتائج النظرية وعمليات المحاكاة التي تم الحصول عليها يؤكد أن الاستراتيجيات المطورة تضمن استقرار النظام مع الحفاظ على الخصائص الرئيسية للتحكم التكيفي $\mathscr{L}_1$.

الكلمات المفتاحية: تحكم تكيفي $\mathscr{L}_1$، أنظمة ذات درجة كسرية، سطح انزلاق ذو درجة كسرية، الشبكات العصبية، المنطق الغامض، تحكم دون نموذج.

"*One remains a scholar as long as they*
are in pursuit of knowledge.
Once they believe they have attained it,
ignorance begins."

Ibn Qutaybah, 889 AD, Baghdad, Iraq

Acknowledgments

Above all, I extend my deepest gratitude to The Almighty Allah for the wisdom and perseverance bestowed upon me throughout the course of this research work and, indeed, throughout my life. Working on this thesis has been a rewarding journey, and I sincerely hope that readers will find it not only interesting and useful but also comfortable to peruse.

Foremost, my heartfelt appreciation goes to my supervisor, Professor **Ahsene BOUBAKIR**, whose inspiring guidance, encouragement, and unwavering support were instrumental in the completion of this work. His timely assistance and dedicated efforts have played a pivotal role in presenting the findings encapsulated in this thesis, and I consider myself fortunate to have had the privilege of working under his mentorship.

I am equally indebted to Professor **Toufik BOUDEN**, Professor **Abdesselem BOULKROUNE**, Professor **Samir LADACI**, and Professor **Mohammed Salah ABDELOUAHAB** for graciously agreeing to serve on the examination committee for my thesis.

Special thanks are extended to Professor **Salim LABIOD** for his invaluable suggestions, comments, and contributions to this research endeavor. I am evenly grateful to Doctor **Toufik SOUANEF**, lecturer at Cranfield University (United Kingdom), for warmly welcoming me to the Center for Aeronautics and providing valuable advice. Our fruitful scientific discussions have significantly contributed to the enhancement of this work.

My sincere thanks also go to my parents, sisters, brother, and friends whose unwavering support and encouragement have been a constant throughout this journey. Regardless of the difficulties encountered, their steadfast belief in me has been a driving force. I express my utmost admiration to all my family members and relatives for the positive encouragement showered upon me during the entirety of this research work.

Ihab Abderraouf Boulham.

Contents

List of Figures

List of Tables

List of Acronyms

ASMC	Adaptive Sliding Mode Control
BIBO	Bounded-Input Bounded-Output
CFANNC	Command-filtered Adaptive Neural Network Controller
CRONE	Commande Robuste d'Ordre Non Entier
DAC	Direct Adaptive Control
FFOL1AC	Fuzzy Fractional-Order $\mathscr{L}_1$ Adaptive Controller
FLSs	Fuzzy Logic Systems
FOCs	Fractional-Order Controllers
FOCSs	Fractional-Order Chaotic Systems
FODEs	Fractional-Order Differential Equations
FOL1AC	Fractional-Order $\mathscr{L}_1$ Adaptive Controller
FOLSs	Fractional-Order Linear Systems
FOMCON	Fractional-Order Modeling and Control
FONLSs	Fractional-Order Nonlinear Systems
FOPID	Fractional-Order Proportional Integral Derivative
FOSMC	Fractional-Order Sliding Mode Control
FOSs	Fractional-Order Systems
FOTF	Fractional-Order Transfer Functions
IAC	Indirect Adaptive Control
IOCs	Integer-order Controllers
MFOL1AC	Multivariable Fractional-Order $\mathscr{L}_1$ Adaptive
MIMO	Controller Multiple-Input Multiple-Output
MRAC	Model Reference Adaptive Control
NN	Neural Networks
NNFOL1AC	Neural Network Fractional-Order $\mathscr{L}_1$ Adaptive
PID	Controller Proportional Integral Derivative
RBFNN	Radial Basis Function Neural Network
SISO	Single-Input Single-Output

SMADRC	Sliding Mode Active Disturbance Rejection Controller
STD	Standard Deviation

Introduction

Fractional-order calculus is a mathematical field with a rich history spanning 300 years. Its origins can be traced to a question posed by L'Hopital in September 1695, discussing the meaning of a derivative of order 0.5 [1]. This question led to the birth of what we now call fractional-order calculus, opening up new paths for developments and explorations. In essence, fractional-order calculus is an extension of integer-order calculus allowing generalization of derivatives and integrals to encompass non-integer, arbitrary real, and complex orders [2]. Consequently, terms such as "fractional-order", "non-integer order", and "generalized order" are often used interchangeably in academic literature. Among these terms, "fractional-order" is the most commonly used, and adopted in our work.

Although fractional-order calculus emerged during the same historical period as integer-order calculus, it proceeded to experience comparatively slower development trajectory. For a significant portion of its history, the concept remained largely confined to theoretical frameworks without practical applications. The ability to address real-world problems was hindered by the absence of a structured solution [3]. Fractional-order calculus garnered the attention of renowned mathematicians including Euler, Lagrange, Cauchy, and Fourier during the 18^{th} and 19^{th} centuries. They mentioned the concept in their works and contributed to its early development. The first recorded application of a fractional-order operator can be traced back to 1823 when Niels Henrik Abel employed the concept to tackle an integral equation fond in the tautochrone problem [3, 4]. Subsequently, developing fractional operators and investigating their properties to solve Fractional-Order Differential Equations (FODEs) became the focal points of extensive research in the field [1, 3]. Within literature, Numerous definitions of fractional-order derivatives and integration have been suggested and out of the available definitions, three are gained prevalence: Riemann-Liouville's definition [5, 6], Grünwald-Letnikov's definition [7–10], and Caputo's definition [6, 11].

Over the past three decades, various approximation methods came into existence along with the advancement in the technology of high-speed computing. This progress paved the way for the integration of fractional-order calculus into physical problems and engineering applications [12]. These applications cover a wide range of fields, such as robotics [13], signal processing [14], electrical circuits [15], bio-engineering [16], and economic processes

[17], etc. Consequently, fractional-order calculus played a significant role in successfully explaining and solving many important phenomena such as the conservation of mass [18], and groundwater flow [19]. Compared to integer-order, fractional-order calculus has the ability to represent high-order dynamical systems using fewer coefficients, thanks to the arbitrary order that offers more flexibility and degree of freedom to accurately present a specific behavior. Besides, fractional-order derivative is a non-local operator, and proves particularly useful in modeling any physical system with hereditary or memory effects [6]. In some cases, fractional-order models have been considered more accurate descriptions of some system dynamics compared to conventional models based on integer-order calculus [20].

The integration of fractional-order calculus in control systems has garnered significant interest among researchers owing to its inherent advantages. As fractional-order calculus allows for more realistic representations of both linear and nonlinear dynamics, particularly in systems known as Fractional-Order Systems (FOSs). Consequently, the development of control mechanisms for this class of systems is an important task. Podlubny [21,22] proposed various methodologies to solve FODEs and applied these methods in control theory. He also emphasized that Fractional-Order Controllers (FOCs) are the most effective method to achieve optimal performance for a fractional-order system [23]. As expected, FOCs offer greater flexibility in adjusting control gains and provide more degrees of freedom, ultimately enhancing closed-loop performance, control accuracy, and control signal efficiency compared to Integer-order Controllers (IOCs) [24]. The Fractional-Order Proportional Integral Derivative (FOPID) controller, was proposed by Podlubny [23], is a typical example of FOCs. It extends the conventional Proportional Integral Derivative (PID) controller by incorporating fractional-order integral and derivative actions, introducing two additional parameters for tuning. Podlubny's work in [22] presents different methods for tuning and designing the FOPID, proving its superior performance compared to the PID [25]. The applicability of the FOPID has been validated in various engineering problems [26, 27], and many contributions discussed its advantages in different scenarios, including non-minimum phase systems [28], higher-order systems [29], Fractional-Order Nonlinear Systems (FONLSs) [1], and time-delayed systems [30].

The growing interest in FOSs and FOCs motivated researchers to propose different control designs that extend the integer-order control methodologies to fractional-order systems. Examples of such controllers include the Fractional-Order Sliding Mode Control (FOSMC) [31], the fractional-order adaptive control [32], and the fractional-order model predictive control [33]. It also led to the investigation of chaotic behavior of FONLSs. This behavior is rather complex and can observed for some nonlinear systems. Several mathematical definitions exist to characterize such behavior [1]. All of which share the common feature of extreme sensitivity to small variations of initial conditions [1]. The phenomena can be recognized through the application of the Lyapunov exponent criteria, wherein the presence of a positive Lyapunov exponent serves as an indicator of a chaotic

behavior [34]. The concept of Fractional-Order Chaotic Systems (FOCSs) was introduced through the fractional-order Chua's circuit [15], which demonstrated chaotic behavior in systems at orders below three, showing a phenomenon that cannot be observed in integer-order counterparts. The concept sparked further research into FOCSs alongside their synchronization and control schemes. To date, FOCSs extensions from integer-order ones have been widely studied. Notable examples include the fractional-order Arneodo's system [35], the fractional-order Lorenz system [36], and the fractional-order Duffing-Holmes system [37]. Furthermore, other studies have focused on addressing the fractional-order synchronization problem, such as projective synchronization [38], impulsive synchronization [39], and complete synchronization [40], etc.

Adaptive control is an expression that refers to a closed-loop controller that possesses the ability to adjust its parameters automatically to effectively overcome any change in system dynamics, parameters, and perturbations. Research in this field was motivated by the aviation and aerospace industries; a decent controller (autopilot in this case) is required to deal with the dynamic characteristics of an aircraft that differ with the change in speed and altitude. An adaptive control strategy can play a key role in achieving closed-loop stability for nonlinear systems that involve uncertainties and unmodeled dynamics [41,42]. The literature on research and applications of this control strategy is rich in different schemes that fall under its definition, such as self-oscillating adaptive controller and Model Reference Adaptive Control (MRAC) [43]. MRAC is a typical adaptive approach with a theory based on combining a control law and an adaptive law, where the adaptive law is an online estimation for system uncertainties while the control law is a mathematical formula designed from the ideal case of the closed-loop system. The latter can be obtained using the estimated parameters, and the calculated control law is used to achieve and preserve the stability of the closed-loop system.

Adaptive control encompasses two different strategies: Indirect Adaptive Control (IAC) and Direct Adaptive Control (DAC). The concept behind the IAC is to continuously estimate the uncertain quantities in real-time and uses the calculated values to configure the stabilizing control law. In contrast, the DAC focuses on the direct estimation of the appropriate control law gains to achieve stability in a closed-loop system [44]. Control gains are consequently, not constants but also variate dynamically, and the mentioned approaches have demonstrated their capabilities to effectively handle uncertainties, perturbations, and variations by acquiring their proper estimations and ensuring reliable closed-loop performances. Nonetheless, dating back to the early research on adaptive control during the 1950s [45], it was predominantly considered as a tool to control slowly varying uncertain systems. In order to maintain the robustness of the controlled system, designers typically opted for low adaptation gains within adaptive closed-loop schemes [46]. Otherwise, the system may encounter the so-called parameter drifting and bursting in the presence of fast adaptations, these phenomena entail a temporary lack of predictability and repeatability in the system's response. This, in turn, can lead to the occurrence of

high-frequency oscillations and a reduction in transient performance [47]. It was mentioned in [48] that even for a stable closed-loop adaptive system, the latter can show arbitrarily poor transient performances. Transient performance can be described as the performance of the closed-loop system before the convergence of the adaptive parameters, which occurs during the learning or process phase. Many factors can affect the transient performance, including the adaptive gains of the controller, the initial conditions of the system, the desired inputs, and the uncertain parameters. A number of studies have been conducted to investigate the convergence and the robustness of adaptive controllers, with many of them suggesting some modifications to enhance the performance of the strategy. The σ-modification [49] and the e-modification [50] were proposed based on damping the adaptive laws; the idea relies on the limitation of the adaptation loop gain and the elimination of its integral action, which helps in addressing the issue of parameter drifting. The authors in [51] suggested a composite strategy that uses both the tracking and prediction errors in a new adaptive law; as a result, they were able to limit the oscillatory behavior caused by high adaptive gains. A high-gain switching MRAC [52] was proposed to achieve an arbitrarily decent tracking performance compared to the one delivered by the conventional MRAC. Additional modifications to adaptive controllers can be found in [53–55]. However, none of the mentioned efforts addressed certain transient performance aspects as outlined in [44]. These aspects include the insertion of the control signal within the calculated bounds, guaranteeing that any change in the system or the reference input will not cause an oscillatory control signal or unacceptable transient performances, as well as, suggesting improvements to the adaptive controller that are not related to high-gain feedback.

As a recent modification, Cao and Hovakimyan [46,56] essentially introduced $\mathscr{L}_1$ adaptive control to address the problem of MRAC by providing a robust response in the presence of fast adaptations. The key improvement lies in the fact that the $\mathscr{L}_1$ adaptive control scheme guarantees desired transient performances with analytically provable bounds for system input and output signals simultaneously, those high control performances can be achieved for a closed-loop system even when confronted with uncertainties, perturbations, and unmodeled dynamics [57]. In contrast to MRAC, the $\mathscr{L}_1$ adaptive control methodology permits the designer to utilize high adaptation gains without sacrificing robustness. In other words, fast adaptations are beneficial for both robustness and performance, while the coupling between the two is solved by using a low-pass filter in the adaptive control channel [44]. Besides, the mentioned low-pass filter, the architecture of the $\mathscr{L}_1$ adaptive controller includes many components, namely a state predictor, a control law, and adaptive laws [58]. The optimal performance of $\mathscr{L}_1$ adaptive control can be attained by employing an auxiliary ideal closed-loop reference system, which is the result of the elimination of the uncertainties within the controlled system. For that reason, the filtered control signal is sensitized to ensure that the actual system response tracks that of the closed-loop reference system. In this case, the implementation of a low-pass fil-

ter serves the purpose of avoiding high-frequency control signals with the comprehension that any uncertainty in the feedback loop can be only compensated within a specific bandwidth [44]. An $\mathscr{L}_1$ norm condition can be deduced; any design parameter value chosen within the range of this condition will guarantee closed-loop stability, however, a thoughtful selection is required to maximize performance.

Contribution of the Thesis

In the field of fractional-order adaptive controllers, several works have been proposed over the years focusing on one or more classes of FOSs. Up to this date, $\mathscr{L}_1$ adaptive control design for FOSs has not been documented in existing literature. Indeed, the main motivation of this thesis is to extend the application of the $\mathscr{L}_1$ adaptive scheme, which exhibited advantages for both integer linear and nonlinear systems, to different classes of FOSs. Furthermore, the aims and major contributions of this thesis that set it apart from other existing studies are listed as follows:

- Design of a new fractional-order $\mathscr{L}_1$ adaptive controller for a general FOSs with matched uncertainties and bounded time-varying external disturbances. The findings on this scheme are supported by extensive numerical simulations and comparative studies.
- Design of a Multivariable Fractional-Order $\mathscr{L}_1$ Adaptive Controller (MFOL1AC) for a general class of FOSs with model uncertainties, time-varying external disturbances, and unknown constant input gain. The proposed controller is applied to control Multiple-Input Multiple-Output (MIMO) incommensurate FOSs as well as high-dimensional fractional-order hyper-chaotic systems.
- Design of a Neural Network Fractional-Order $\mathscr{L}_1$ Adaptive Controller (NNFOL1AC) for a general class FONLSs that are subject to uncertain dynamics and unknown time-varying input gain. The conducted numerical simulations focus on the cases of unknown constant and time-varying input gains.
- Design a Fuzzy Fractional-Order $\mathscr{L}_1$ Adaptive Controller (FFOL1AC) considering a class of FONLSs that are subject to uncertain dynamics and unknown input nonlinearities (dead-zone and sector nonlinearities). The proposed controller is applied for chaos synchronization problems.

Outline

The remaining sections of the thesis are structured in the form of chapters as follows:

Chapter 1 provides a concise overview of fractional-order calculus, defining fractional-order integrals and derivatives, and discussing their respective Laplace transform properties. It examines the advantages and disadvantages of these concepts and describes fractional-order systems, including their stability conditions. Additionally, this chapter discusses the implementation of fractional-order operators and includes a literature review on fractional-order adaptive controllers.

Chapter 2 offers an overview of the fundamental architecture of model reference and $\mathscr{L}_1$ adaptive controllers, highlighting the key differences and advantages of each method. Through comparative performance analysis, the chapter demonstrates the superior benefits of the $\mathscr{L}_1$ adaptive controller. Additionally, it includes a comprehensive literature review on $\mathscr{L}_1$ adaptive control, providing a thorough background and context for the discussion.

Chapter 3 introduces the idea of the fractional-order $\mathscr{L}_1$ adaptive controller for a class of fractional-order systems subject to matched uncertainties and bounded time-varying external disturbances. Initially, a suitable form of a fractional-order sliding surface is selected to simplify the control design and the stability analysis. Then the control structure is derived based on $\mathscr{L}_1$ adaptive control methodology, which includes a control law, an adaptive mechanism, and a predictor. Finally, a detailed numerical simulation is provided focusing on the cases of constant and time-varying uncertainties and external disturbances.

Chapter 4 extends the idea of previous chapter to encompass multiple-input multiple-output fractional-order systems by designing a multivariable fractional-order $\mathscr{L}_1$ adaptive controller. This chapter introduces a new aspect to the proposed controller, specifically addressing the challenge posed by unknown input gain. Consequently, a distinct control structure is employed to effectively manage this uncertainty, complementing its capability to handle unmodeled dynamics and external disturbances. It also focuses the applicability of the proposed scheme to control incommensurate order and hyper-chaotic systems via numerical simulations.

Chapter 5 addresses the design of a neural network fractional-order $\mathscr{L}_1$ adaptive controller for a class of fractional-order nonlinear systems. Mainly focusing on the incorporation of a neural network as an online estimator in the control structure, and its role to handle uncertain nonlinear dynamics and unknown time-varying input gain inherent to the considered system. Finally, two scenarios are considered to test the efficiency of the controller: chaos suppression of fractional-order systems, and the case of unknown time-varying input gain through the control of fractional-order nonlinear systems.

Chapter 6 deals with the control of fractional-order systems in the case of input

nonlinearity. The suggested controller includes a fuzzy system, which takes the role of an online estimator for system nonlinear uncertain functions which helps in the handling of the input nonlinearities. In this chapter, the focus of the simulations is shifted to synchronization problems, where the controller is used to achieve master-slave synchronizations between two different 2-dimensional and 3-dimensional fractional-order chaotic systems.

List of Publications

This thesis is deeply rooted to the work produced by the author, as encapsulated in the following list of publications:

- Boulham, Ihab Abderraouf, Ahsene Boubakir, and Salim Labiod. "$\mathscr{L}_1$ adaptive controller design for a class of fractional order uncertain systems." *Mathematics and Computers in Simulation* 193 (2022): 232-249.

- Boulham, Ihab Abderraouf, Ahsene Boubakir, and Salim Labiod. "Neural network $\mathscr{L}_1$ adaptive control for a class of uncertain fractional order nonlinear systems." *Integration* 83 (2022): 1-11.

- Boulham, Ihab Abderraouf, Ahsene Boubakir, and Salim Labiod. "Fuzzy $\mathscr{L}_1$ adaptive controller for chaos synchronization of uncertain fractional-order chaotic systems with input nonlinearities." *Transactions of the Institute of Measurement and Control* (2023): 01423312221148241.

Chapter 1

Generalities on Fractional Calculus

1.1 Introduction

Calculus is a branch of mathematics concerned with the study of how functions change. It offers a methodical framework for modeling and comprehending systems that involve varying quantities or dynamic processes. By employing calculus, the behavior of such models can be predicted based on their properties [3]. As calculus developed, its scope expanded to include fractional or non-integer orders, resulting in more generalized versions. Fractional calculus is a branch of mathematics that employs real or complex number powers of integration and differentiation to characterize the dynamic behavior of systems across domains [2]. Within the field of fractional calculus, the literature contains numerous definitions of fractional-order derivatives and integrals. A simple approach to define fractional-order integrals is the generalization of n-fold integrals [20]. The concept described above gave rise to the formulation of the Riemann-Liouville integral, which was the base to introduce certain definitions of the fractional-order derivative [21]. These derivatives are important in describing FODEs [59], and eventually, FOSs.

In control theory, system stability is a critical property, that can be studied both in time and frequency domains. The emergence of FOSs has led to a rising interest in exploring and analyzing their stability within academia [1]. While the field of stability analysis for these particular systems is not extensively explored, many significant findings have been discussed in existing literature [3]. Investigations in this field revealed that the stability behavior of Fractional-Order Linear Systems (FOLSs) is distinct from that of the integer-order ones but also relies upon the roots of the characteristic polynomial equation [60].

Understanding the stability of these systems is important because it directly influences and explains their behavior. Toward this end, this chapter present a brief overview on fractional calculus, focusing on the fractional-order derivatives, FOSs, and their stability analysis. The rest of the chapter is divided into 6 sections and organized as follows. Section 1.2 provides a general introduction into fractional calculus by addressing the formulation of fractional-order integral and derivative operators. Section 1.3 describes different repre-

sentations of linear and nonlinear FOSs. Section 1.4 provides a general understanding on the stability of FOSs. Section 1.5 deals with the problem of implementing fractional-order operators. Section 1.7 concludes the chapter.

1.2 Fractional Calculus

Fractional calculus is a concept that was discovered several centuries ago, and their applications in modeling physical systems and control theory have been vastly studied in recent years. However, this concept remains obscure to a significant portion of the academic community. Therefore, this section will focus on providing a concise introduction.

1.2.1 Fractional-Order Operators

As previously stated, fractional calculus is a mathematical field that tackles the possibility of using real or complex number power of integration and differentiation. The term β is used in this study to indicate the order of the fractional operator. Consequently, the fractional-order integro-differential operator can be represented as ${}_bD_t^\beta$, with t and b being the limits of the operation. The fractional operator can be classified into three forms based on the value of β: derivative for $\mathbb{R}(\beta) > 0$, integration for $\mathbb{R}(\beta) < 0$, and identity for $\mathbb{R}(\beta) = 0$. The overall idea is simply summarized in the subsequent expression

$$ {}_bD_t^\beta = \begin{cases} \frac{d^\beta}{dt^\beta}, & \mathbb{R}(\beta) > 0 \\ 1, & \mathbb{R}(\beta) = 0 \\ \int_b^t (d\tau)^\beta, & \mathbb{R}(\beta) < 0 \end{cases} \tag{1.1} $$

In this study, the order β is assumed to be a real number. However, it is worth noting that it can also be a complex number [24]. In what follows, we will highlight certain fundamental properties of the fractional operator as reported in [6, 20]:

- For $\beta = n$ where n is an integer number, the fractional operator ${}_bD_t^n$ gives the same results as the integer-order operator, that is

$$ {}_bD_t^n g(t) = \frac{d^n g(t)}{dt^n} \tag{1.2} $$

- For $\beta = 0$ the operation ${}_bD_t^\beta$ behaves as the identity operator, that is

$$ {}_bD_t^0 g(t) = g(t) \tag{1.3} $$

- For two scalars a_1 and a_2 and two continuous differentiable functions $g(t)$ and $f(t)$, the fractional-order derivative and integration are linear operations and agree with

the expression that follows

$$ {}_bD_t^{\beta}(a_1 g(t) + a_2 f(t)) = a_1 {}_bD_t^{\beta} g(t) + a_2 {}_bD_t^{\beta} f(t) \tag{1.4} $$

1.2.2 Some Important Functions in Fractional Calculus

After defining the fractional operator, it is important to address some special functions that are often encountered in fractional calculus.

1.2.2.1 Gamma Function

The Gamma function $\Gamma(\beta)$ is a mathematical function that provide an extension for factorial operations to real or complex numbers. Therefore, it is a fundamental element in the majority of fractional-order operator definitions. The definition of the Gamma function is given as follows

Definition 1.1. [5, 6, 61] The Gamma function is defined in the following form

$$ \Gamma(\beta) = \int_0^{\infty} t^{\beta-1} e^{-t} dt, \mathbb{R}(\beta) > 0 \tag{1.5} $$

with β is a complex number. □

The most important property of the Gamma function is derived from the above definition and states that

$$ \Gamma(\beta + 1) = \beta\Gamma(\beta) \tag{1.6} $$

here β is a real number. The previous property further implies that

$$ \begin{aligned} \Gamma(n+1) &= n\Gamma(n) \\ &= n(n-1)! \\ &= n! \end{aligned} \tag{1.7} $$

where $n \in \mathbb{N}$ and $\mathbb{N}$ is a set of positive integers.

1.2.2.2 Mittag-Leffler Function

The Mittag-Leffler function is a generalization of the exponential function which plays a significant role in the solution of FODEs, similar to how the exponential function does in the solution of their integer-order counterparts. Within the four known forms, the most often used are the 1-parameter and 2-parameter representations given in equations (1.8) and (1.9), receptively [5, 6, 61]

$$ E_{\beta}(x) = \sum_{k=0}^{\infty} \frac{x^k}{\Gamma(\beta k + 1)}, \beta > 0 \tag{1.8} $$

$$E_{\beta,\alpha}(x) = \sum_{k=0}^{\infty} \frac{x^k}{\Gamma(\beta k + \alpha)}, \beta > 0, \alpha > 0 \tag{1.9}$$

The relation between the 1-parameter and 2-parameter representations is given in what follows

$$E_{\beta,1}(x) = \sum_{k=0}^{\infty} \frac{x^k}{\Gamma(\beta k + 1)} = E_\beta(x) \tag{1.10}$$

Some of the most essential relations of the Mittag-Leffler function are given as

$$E_{1,1}(x) = E_1(x) = e^x \tag{1.11}$$

and

$$E_{1,2}(x) = \frac{e^x - 1}{x} \tag{1.12}$$

1.2.3 Fractional-Order Integral

In the area of fractional-order calculus, there exist several methods for generalizing the order of integrals to non-integer values [61]. One well-known formulation, proposed by Cauchy, represents an n-fold integral as a convolution integral. This strategy provides a simple access to the idea. The formula is given by the following theorem

Theorem 1.1. [6] The n-fold integral of the function $g(t)$ is the following

$${}_0I_t^n g(t) = \int_0^t \frac{(t-\tau)^{n-1}}{(n-1)!} g(\tau) d\tau, n \in \mathbb{N} \tag{1.13}$$

with $\mathbb{N}$ is a set of positive integers. □

A fractional-order integral generalizes the definition of integer-order integral. Therefore, as stated in (1.7), the factorial operation $(n-1)!$ found in the n-fold integral (1.13) can be replaced with the continuous Gamma function for $n \in \mathbb{R}$. Based on that, the Riemann-Liouville integral can be introduced in the subsequent definition as

Definition 1.2. [20, 21] The Riemann-Liouville integral of the fractional-order $0 < \beta < 1$ is given as follows

$${}_0I_t^\beta g(t) = {}_0D_t^{-\beta} g(t) = \frac{1}{\Gamma(\beta)} \int_0^t \frac{g(\tau)}{(t-\tau)^{1-\beta}} d\tau \tag{1.14}$$

where $g(t)$ represents a casual function of t, i.e., $g(t) = 0$ for all $t < 0$, and $\Gamma(\beta)$ is the Gamma function introduced in Definition 1.1. □

1.2.4 Fractional-Order Derivatives

The definition of fractional-order derivative is more straightforward. It builds upon the understanding of both the fractional-order integral and the conventional integer-order derivative. The literature offers several definitions of fractional-order derivatives and integrals, each with its own suitability, complexity, and accuracy for different scenarios. In this subsection, we will explore two possible ways to define the fractional-order derivative, each of which will result in a different definition.

1.2.4.1 Riemann-Liouville's Definition for Fractional Derivative

The Riemann-Liouville derivative can be obtained by repeatedly performing fractional-order integration (1.14), followed by an appropriate number of integer-order differentiation. The derivative is given by the following definition

Definition 1.3. [5,6] The Riemann-Liouville fractional derivative of order $\beta > 0$ is given as

$$ {}^{RL}_{0}D^{\beta}_{t} g(t) = D^{n} D^{-(n-\beta)} g(t) = \frac{d^{n}}{dt^{n}} \left[\frac{1}{\Gamma(n-\beta)} \int_{0}^{t} \frac{g(\tau)}{(t-\tau)^{1+\beta-n}} d\tau \right] \tag{1.15} $$

with $n-1 < \beta < n$ and $n \in \mathbb{N}$. □

1.2.4.2 Caputo's Definition for Fractional Derivative

The fractional-order derivative given by Caputo [11] employs an alternate methodology. Indeed, it follows an opposing approach compared to the Riemann-Liouville derivative. The Caputo fractional derivative is summarized in the definition that follows

Definition 1.4. [6,11] The Caputo fractional derivative of order $\beta > 0$ is given as

$$ {}^{C}_{0}D^{\beta}_{t} g(t) = D^{-(n-\beta)} D^{n} g(t) = \frac{1}{\Gamma(n-\beta)} \int_{0}^{t} \frac{g^{(n)}(\tau)}{(t-\tau)^{1+\beta-n}} d\tau \tag{1.16} $$

with $n-1 < \beta < n$ and $n \in \mathbb{N}$. □

1.2.5 Properties of Riemann-Liouville and Caputo Derivatives

In this subsection, we focus on certain significant properties of fractional-order derivatives defined in the preceding sections. It is worth noting that due to brevity reasons, we would not delve into the demonstration of these properties. For further details, refer to the works in [2,7–10].

- The Riemann-Liouville and Caputo derivatives of a constant C are given by the equations (1.17) and (1.18), respectively

$$ {}^{RL}_{0}D^{\beta}_{t}C = \frac{Ct^{-\beta}}{\Gamma(1-\beta)} \tag{1.17} $$

$$ {}^{C}_{0}D^{\beta}_{t}C = 0 \tag{1.18} $$

- The relation between the Riemann-Liouville derivative and the Caputo derivative can be summarized by the following equations

$$ {}^{RL}_{0}D^{\beta}_{t}g(t) = {}^{C}_{0}D^{\beta}_{t}g(t) + \sum_{k=0}^{n-1} \frac{t^{k-\beta}}{\Gamma(k-\beta+1)} g^{(k)}(0^{+}) \tag{1.19} $$

$$ {}^{C}_{0}D^{\beta}_{t}g(t) = {}^{RL}_{0}D^{\beta}_{t}\left(g(t) - \sum_{k=0}^{n-1} g^{(k)}(0^{+})\frac{t^{k}}{k!}\right) \tag{1.20} $$

- The relation between the Riemann-Liouville derivative and the Riemann-Liouville integral is given by the equation that follows

$$ {}_{0}I^{\beta}_{t}\,{}^{RL}_{0}D^{\beta}_{t}g(t) = g(t) - \sum_{k=0}^{n-1} \left[{}^{RL}_{0}D^{\beta-k}_{t}g(t)\right]_{t=0} \frac{t^{\beta-k}}{\Gamma(\beta-k+1)} \tag{1.21} $$

- The relation between the Caputo derivative and the Riemann-Liouville integral can be summarized by the following equation

$$ {}_{0}I^{\beta}_{t}\,{}^{C}_{0}D^{\beta}_{t}g(t) = g(t) - \sum_{k=0}^{n-1} g^{(k)}(0)\frac{t^{k}}{k!} \tag{1.22} $$

- For $n = 1$, we have

$$ {}^{C}_{0}D^{\beta}_{t}g(t)\,{}_{0}I^{\beta}_{t}g(t) = {}^{RL}_{0}D^{\beta}_{t}g(t)\,{}_{0}I^{\beta}_{t}g(t) = g(t) \tag{1.23} $$

- For $0 < \beta < 1$, the following inequality holds for all $t \geq 0$

$$ \frac{1}{2}\,{}^{C}_{0}D^{\beta}_{t}(g(t))^{2} \leq g(t)\,{}^{C}_{0}D^{\beta}_{t}g(t) \tag{1.24} $$

- For $0 < \beta < 1$, and for $\bar{g}(t) \in \mathbb{R}^{n}$ a differentiable function vector, the following inequality holds for all $t \geq 0$

$$ \frac{1}{2}\,{}^{C}_{0}D^{\beta}_{t}(\bar{g}^{T}(t)P\bar{g}(t)) \leq \bar{g}^{T}(t)P\,{}^{C}_{0}D^{\beta}_{t}\bar{g}(t) \tag{1.25} $$

with $P \in \mathbb{R}^{n\times n}$ is a positive definite and symmetric constant matrix.

- For $\beta \geq \alpha \geq 0$ the following equality holds for the Caputo derivative

$$ {}_0^C D_t^{\beta} \, {}_0^C D_t^{-\alpha}(g(t)) = {}_0^C D_t^{\beta-\alpha}(g(t)) \tag{1.26} $$

- The Caputo fractional derivative can be found using the following equation

$$ {}_0^C D_t^{\beta} g(t) = {}_0^{RL} D_t^{-([\beta]-\beta)}(g^{[\beta]}(t)) \tag{1.27} $$

  and $[\beta]$ represents the integer part of β.

1.2.6 Laplace Transform of Fractional-Order Operators

The Laplace transform is a widely employed mathematical technique to manage engineering problems. The name "Laplace" was derived after Pierre-Simon Laplace, who developed the transform during his studies on probability theory. In this section, we will provide an overview of the Laplace transform applied to integer-order calculus, followed by an explanation of its use for fractional-orders.

1.2.6.1 Generalities on Laplace Transform

Basically, the Laplace transform is a linear operation that is utilized to transform a function $g(t)$ to a function $G(s)$ through the integral expression that follows [1, 20]

$$ G(s) = L\{g(t); s\} = \int_0^{\infty} g(t) e^{-st} dt \tag{1.28} $$

where t and s are the real and complex arguments, respectively. The function $G(s)$ is referred to as the transform of $g(t)$, whereas $g(t)$ is called the original function. The transform exhibits a highly beneficial property whereby many operations and relationships performed on the original function $g(t)$ can be more easily managed when applied to the transformed function $G(s)$.

It is possible to restore the original function from its transform function using the inverse Laplace transform, which is provided in the following expression [20]

$$ g(t) = L^{-1}\{G(s); t\} = \int_{c-j\infty}^{c+j\infty} G(s) e^{st} ds, c = \mathbb{R}(s) > c_0 \tag{1.29} $$

with c_0 is located in the right half-plane of the absolute convergence of the integral (1.28). The evaluation of the inverse Laplace transform from (1.29) is relatively complicated. However, it has the potential to deliver some valuable insights into the behavior of the unknown function $g(t)$ [1]. The rest of this section is related to the Laplace transform of fractional-order integrals and derivatives, for that reason we consider the lower limit

$b = 0$.

1.2.6.2 Laplace Transform of Fractional-Order Integrals

Theorem 1.2. [1,6] The Laplace transform of Riemann-Liouville integral is given in the subsequent expression [1,6]

$$L\left\{{}_0I_t^{\beta} g(t); s\right\} = s^{-\beta} G(s) \tag{1.30}$$

with $\beta \in \mathbb{R}^+$. □

1.2.6.3 Laplace Transform of Fractional-Order Derivatives

Theorem 1.3. [6] The Laplace transform of the Riemann-Liouville derivative is given in the subsequent expression

$$L\left\{{}_0D_t^{\beta} g(t); s\right\} = s^{\beta} G(s) - \sum_{\nu=0}^{n-1} s^{\nu}\, {}^{RL}_{0}D_t^{\beta-\nu-1} g(0) \tag{1.31}$$

with $\beta \in \mathbb{R}^+$, $n-1 < \beta < n$, and $n \in \mathbb{N}$. □

Theorem 1.4. [6] The Laplace transform of the Caputo derivative is given in the expression that follows

$$L\left\{{}_0D_t^{\beta} g(t); s\right\} = s^{\beta} G(s) - \sum_{\nu=0}^{n-1} s^{\beta-\nu-1} g^{(\nu)}(0) \tag{1.32}$$

with $\beta \in \mathbb{R}^+$, $n-1 < \beta < n$ and $n \in \mathbb{N}$. □

Remark 1.1. For zero initial conditions, the Laplace transform of the two fractional-order derivatives (Riemann-Liouville and Caputo) are similar and can be reduced to [1,6]

$$L\left\{{}^{RL}_{0}D_t^{\beta} g(t); s\right\} = L\left\{{}^{C}_{0}D_t^{\beta} g(t); s\right\} = s^{\beta} G(s) \tag{1.33}$$

□

1.2.7 Initial Value Problems of Fractional Operators

Initial values typically refer to the states of a system at its starting point or a specific time instant. These values serve as the basis for solving and analyzing mathematical models that articulate the system's behavior over the course of time. Specifying such values when solving differential equations is necessary to obtain a unique solution. The Riemann-Liouville derivative has a major disadvantage; it could be observed in (1.15) that when using FODEs that are based on Riemann-Liouville's definition it is mandatory to impose zero initial conditions [1]. Nevertheless, there are cases where a zero initial

condition may not be reasonable. Moreover, the Laplace transform of the Riemann-Liouville derivative in (1.31) necessitates knowledge of the initial conditions of the function ${}^{RL}_{0}D_{t}^{\beta-\nu-1}g(t)$, which is quite challenging to quire in terms of a physical quantity [3]. In contrast, FODEs that employ the Caputo derivative have similar initial conditions to those of integer-order differential equations. This is advantageous for practical applications as real-world problems often require definitions of fractional derivatives that involve clear and straightforward interpretations of initial conditions [1,6]. Besides, it is clear in (1.32) that the Laplace transform of the Caputo derivative required only the knowledge of initial conditions of the function $g^{(\nu)}(t)$, which possess a clear physical interpretation [3]. For these reasons, in practical applications Caputo's definition is preferred, whereas Riemann-Liouville's definition is utilized more frequently in mathematical contexts. Following the aforementioned discussion, we choose to adopt the Caputo fractional-order derivative to describe FOSs and design FOCs. Therefore, throughout the remainder of this thesis, we will symbolize the Caputo fractional derivative with the notation D^{β} rather than ${}^{C}_{0}D_{t}^{\beta}$. This notation simplifies the presentation and improves the clarity of our investigation into fractional calculus and its applications to control theory.

1.3 Fractional-Order Systems

The preceding sections covered some of the essential definitions, concepts, and properties of fractional-order operators. In this section, the main focus shifts to a particular class of systems known as fractional-order dynamical systems.

1.3.1 Fractional-Order Linear Systems

Similar to integer-order calculus in control theory, the transfer function representation of FOLSs can be obtained through the Laplace transform of their FODEs.

1.3.1.1 Transfer Function Method

In general, the continuous-time dynamics of a linear fractional-order system can be defined using a fractional-order differentiation equation developed based on its first principle as follows [59]

$$\begin{aligned} b_m D^{\beta_m} y(t) + b_{m-1} D^{\beta_{m-1}} y(t) + \dots b_0 D^{\beta_0} y(t) = \\ a_n D^{\alpha_n} u(t) + a_{n-1} D^{\alpha_{n-1}} u(t) + \dots a_0 D^{\alpha_0} u(t) \end{aligned} \tag{1.34}$$

where $b_i, i = 0,1,\dots,m$ and $a_k, k = 0,1,\dots,n$ are constant values, $\beta_i, i = 0,1,\dots,m$, and $\alpha_k, k = 1,2,\dots,n$ are real numbers, with $\beta_m > \beta_{m-1} \dots > \beta_0$, and $\alpha_n > \alpha_{n-1} \dots > \alpha_0$. If the fractional-order of both sides of (1.34) are integer multiples of a mutual factor, then the equation is termed to be of commensurate order. Conversely, if no common factor exists among them, the equation is referred to as being of incommensurate order.

For the case of commensurate fractional-orders, i.e., $\beta_i, \alpha_k = j\beta$ and $\beta \in \mathbb{R}^+$, the equation (1.34) can be simplified to

$$\sum_{j=0}^{m} b_j D^{j\beta} y(t) = \sum_{j=0}^{n} a_j D^{j\beta} u(t) \tag{1.35}$$

with $m > n$. By employing the Laplace transform to equation (1.34) while assuming zero initial conditions, the input-output representation of the fractional-order system in the form of a transfer function can be found as follows [6]

$$H(s) = \frac{a_n s^{\alpha_n} + a_{n-1} s^{\alpha_{n-1}} + \dots a_0 s^{\alpha_0}}{b_m s^{\beta_m} + b_{m-1} s^{\beta_{m-1}} + \dots b_0 s^{\beta_0}} = \frac{Y(s)}{U(s)} \tag{1.36}$$

with $Y(s)$ and $U(s)$ denote the fractional-order polynomials of the numerator and the denominator, respectively. For the case of commensurate fractional-orders, the equation (1.36) is reduced to

$$H(s) = \frac{\sum_{j=0}^{n} a_j (s^\beta)^j}{\sum_{j=0}^{m} b_j (s^\beta)^j} = \frac{Q(s^\beta)}{P(s^\beta)} \tag{1.37}$$

1.3.1.2 State Space Method

FOLSs can also be expressed in the state space domain, with a representation that takes the subsequent form [62]

$$\begin{aligned} D^\beta x(t) &= Ax(t) + Bu(t) \\ y(t) &= Cx(t) + Du(t) \end{aligned} \tag{1.38}$$

where $x(t) = [x_1(t), x_2(t), \dots x_m(t)]^T \in \mathbb{R}^m$ is the stat vector, $u(t) = [u_1(t), u_2(t), \dots u_n(t)]^T \in \mathbb{R}^n$ and $y(t) = [y_1(t), y_2(t), \dots y_p(t)]^T \in \mathbb{R}^p$ are the input and output vectors, respectively. $A \in \mathbb{R}^{m \times m}$ is the system matrix, $B \in \mathbb{R}^{m \times n}$ is the input matrix, $C \in \mathbb{R}^{p \times m}$ is the output matrix, and $D \in \mathbb{R}^{p \times n}$ is the direct transmission matrix. The fractional-order is denoted as β where $\beta = [\beta_1(t), \beta_2(t), \dots \beta_m(t)]^T \in \mathbb{R}^m$. It is worth noting that the fractional-order operator D^β is exclusively applied to the elements of the pseudo state vector $x(t)$ in the first equation of (1.38), where the latter is known as the fractional-order state equation, whereas the second equation of (1.38) corresponds to the output equation.

1.3.2 Fractional-Order Nonlinear Systems

Generally, incommensurate FONLSs are represented with the following expression

$$D^{\beta_i} x_i(t) = g_i(x_1(t), x_2(t), \dots x_m(t)), x_i(0) = x_{0i} \tag{1.39}$$

with $x_{0i}, i = 1, 2, \dots, m$ are the initial conditions of the system and $\beta_i, i = 1, 2, \dots, m$ are the derivative orders. A reduced representation of the system (1.39) can take the following

vector form

$$D^{\beta} x(t) = G(x) \tag{1.40}$$

where $\beta = [\beta_1(t), \beta_2(t), \ldots \beta_m(t)]^T \in \mathbb{R}^m$, $x(t) = [x_1(t), x_2(t), \ldots x_m(t)]^T \in \mathbb{R}^m$ and $G(t) = [g_1(t), g_2(t), \ldots g_m(t)]^T \in \mathbb{R}^m$.

Remark 1.2. When dealing with incommensurate FOSs, it is worth noting that the orders under consideration are both distinct and arbitrary. This lack of correlation between the orders poses a significant challenge in analysis and control design. On the other hand, in commensurate systems, the orders of the FODEs are either identical or multiples of the base order, making them mathematically manageable.

1.4 Stability of Fractional-Order Systems

The concept of stability is a fundamental aspect when discussing dynamical systems and their behaviors. The very first Bounded-Input Bounded-Output (BIBO) stability definition was introduced by Matignon [60]. This foundational definition was subsequently employed in the control of FOSs. Subsequent research efforts explored frequency domain stability, including fractional-order Nyquist-based criterion [63]. Additional results regarding FOLSs were on the basis of linear matrix inequality such as found in the work of Sabatier [64]. The emergence of the Laplace transform of fractional-order operators played a crucial role in investigating the stability of FOLSs; this transform allows stability analysis by examining the roots of the characteristic equation derived from system's transfer function [60]. The approach was further extended in one hand, to the state space models of FOLSs [65, 66]. To demonstrate the stability of FONLSs. Oustaloup [67] proposed a power law stability based on the Mittag-Leffler function [68]. Indeed, the exponential stability proved to be not suitable for examining the stability of FONLSs [60], and the power law stability serves in this case as an alternative method. Further studies focused on extending the Lyapunov criterion [69] to FONLSs. Podlubny's work [70] employed the Mittag-Leffler function to investigate stability of FONLSs using a fractional-order Lyapunov method, delivered some interesting results. Later efforts further refined the application of the Lyapunov method within the fractional-order domain. As observed in the mentioned works [10, 71, 72].

This section will present the stability of FOSs. Initially, an overview of the stability of FOLSs will be provided, followed by an analysis of the stability of FONLSs.

1.4.1 Stability of Fractional-Order Linear Systems

The analytical method employed to determine the stability of a factional-order linear system involves examining the position of the roots on Riemann surfaces, which are one-dimensional sheets utilized in complex analysis [73]. Without loss of generality, the stability condition for FOLSs can be summarized in the following theorems

Theorem 1.5. [60] The commensurate fractional-order system described by the transfer function $G(s) = Q(s^{\beta})/P(s^{\beta})$ in (1.37) is stable if and only if the subsequent condition is satisfied

$$|arg(\lambda_i)| > \beta\frac{\pi}{2}, P(\lambda) = 0 \tag{1.41}$$

where $\beta \in \mathbb{R}$ with respect to $0 < \beta < 2$, and λ_i is the i^{th} root of the nominator $P(s^{\beta})$. □

Hence, the concept of pole location for integer-order stability can be seen as a special case of this theorem, i.e., the case when $\beta = 1$ implies that all poles must appear in the left half of the complex plan. Moreover, according to Theorem 1.5, the stability region tends to the whole plan once β tends to zero, and tends to the real negative axis when β tends to 2 [20]. The aforementioned idea is visually explained in Figure 1.1.

If the fractional-order system under consideration is represented in state space form, the stability condition should have a slight modification, which can be expressed through the following theorem

Theorem 1.6. [62] Let us consider the commensurate fractional-order described by the state space representation in (1.38) in the case of the matrices triplet A, B, and C is minimal. The system is stable if and only if the subsequent condition is satisfied

$$|arg(eig(A))| > \beta\frac{\pi}{2} \tag{1.42}$$

with $0 < \beta < 2$ and $eig(A)$ are the eigenvalues of matrix A. □

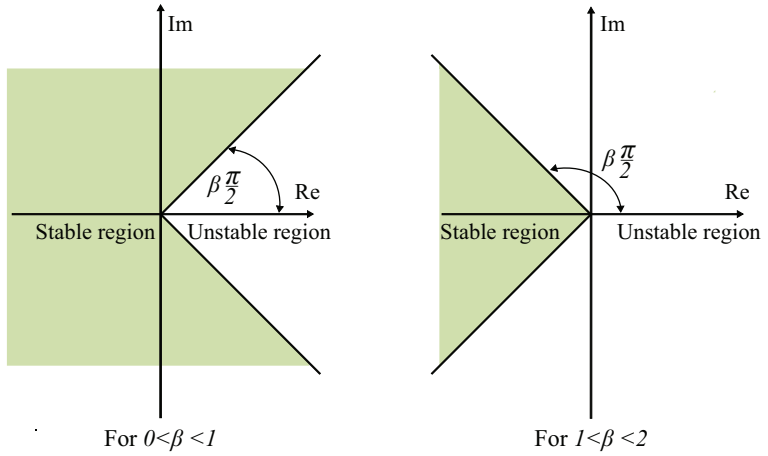

Figure 1.1: Stability regions for fractional-order linear systems.

1.4.2 Stability of Fractional-Order Nonlinear Systems

It was mentioned in [60] that exponential stability; which is commonly used to study the asymptotic stability of nonlinear systems, is not suitable for examining the stability of FONLSs. Consequently, alternative approaches must be considered. In that sense, a new definition of power law stability $t^{-\alpha}$ has been introduced by Oustaloup as follows

Definition 1.5. [67] The trajectory $x(t) = 0$ of the fractional-order system defined in (1.39) is $t^{-\alpha}$ asymptotically stable if there is a positive real α such that

$$\forall ||x(t)||, t \leq t_0, \ \exists J(x(t), t \leq t_0), \ such that \ \forall t \geq t_0, ||x(t)|| \leq J t^{-\alpha} \tag{1.43}$$

□

which implies that the trajectory of $x(t)$ gradually vanishes towards zero following $t^{-\alpha}$, which is, in fact, slower than the exponential decay rate of integer-order systems. Therefore, FOSs are occasionally called long memory systems [68]. The power law stability definition was subsequently used to establish a novel stability condition for FONLSs, referred to as Mittag-Leffler stability. This stability condition is expressed by the subsequent theorem

Theorem 1.7. [68] The fractional-order nonlinear system $D^{\beta}x(t) = G(t, x)$ is considered Mittag-Leffler stable if

$$||x(t)|| \leq \{\sigma[x(t_0)]E_{\beta}(-p(t - t_0)^{\beta})\}^b \tag{1.44}$$

where t_0 denotes the initial time, $0 < \beta < 1$, $p > 0$, $b > 0$, and E_{β} is the Mittag-Leffler function introduced in (1.8). The function $\sigma(x)$ is locally Lipschitz on $x \in \mathbb{B} \in \mathbb{R}^m$, which satisfies $\sigma(0) = 0$ and $\sigma(x) \geq 0$. □

Lyapunov's second method is widely recognized for its ability to study the stability of a system without the need to explicitly solve its differential equation. The work in [70] has expanded this method to FOSs in terms of Mittag-Leffler stability. The notions of the fractional-order Lyapunov stability are given in the following theorems

Theorem 1.8. [70] Let us consider $x = 0$ as an equilibrium point for the fractional-order autonomous systems $D^{\beta}x(t) = G(t, x)$ defined in (1.39), and $\mathbb{D}$ is a domain that contains the origin with $\mathbb{D} \subset \mathbb{R}^m$. Assuming the existence of a Lyapunov candidate function $V(t, x(t)) : [0, \infty) \times \mathbb{D} \rightarrow \mathbb{R}$, to be locally Lipschitz with respect to x and continuously differentiable such that

$$\beta_1 ||x||^a \leq V(t, x(t)) \leq \beta_2 ||x||^{ab} \tag{1.45}$$

and

$$D^{\beta}V(t, x(t)) \leq -\beta_3 ||x||^{ab} \tag{1.46}$$

with $t \geq 0$, $x \in \mathbb{D}$, $\beta \in \mathbb{R}$ with respect to $0 < \beta < 1$, β_1, β_2, β_3, a, and b are arbitrary positive constants. Then, the equilibrium point $x = 0$ is Mittag-Leffler stable. In the case where the considered assumptions hold globally on $\mathbb{R}^m$, then, the equilibrium point $x = 0$ is globally Mittag-Leffler stable. □

Theorem 1.9. [68] Let us consider $x = 0$ as an equilibrium point for the fractional-order autonomous systems $D^{\beta}x(t) = G(t, x)$ defined in (1.39). Assuming the existence of

a Lyapunov candidate function and $class-K$ functions $\beta_i, i = 1,2,3$ such that

$$\beta_1(||x||) \leq V(t,x(t)) \leq \beta_2(||x||) \tag{1.47}$$

and

$$D^{\beta}V(t,x(t)) \leq -\beta_3(||x||) \tag{1.48}$$

with $t \geq 0$, and $\beta \in \mathbb{R}$ with respect to $0 < \beta < 1$. Then, the equilibrium point $x = 0$ is asymptotically stable. Here, a $class-K$ function $\beta_i(t)$ is defined as a continuous function with $\beta_i : [0,t) \rightarrow [0,\infty)$ that is strictly increasing and satisfy $\beta_i(0) = 0$. □

Further details and aspects on the Lyapunov stability of FONLSs can be found in [3]. Other works such as in [65, 74], proposed an alternative approach to study the stability of FONLSs, which is based on the linearization of the systems via the Jacobian method. This approach is given below in the form of a theorem

Theorem 1.10. [65] Let us consider the Jacobian matrix $J = \frac{\partial G}{\partial x}$, evaluated at specific equilibrium point E^* where $G(t) = [g_1(t), g_2(t), \ldots g_m(t)]^T$. Then, the equilibrium point of the commensurate fractional-order system defined in (1.39) are asymptotically stable if

$$|arg(eig(J))| = |arg(eig(\lambda_i))| > \beta\frac{\pi}{2} \tag{1.49}$$

with $\lambda_i, i = 1,2,\ldots,m$ are the eigenvalues of the matrix J. □

1.5 Implementation of Fractional-Order Operators

In the previous sections, some basic definitions of FOSs and their stability theorems are addressed. Yet, the implementation of fractional-order operators remains unexplored. Indeed this aspect is straightforward for integer-order systems using traditional electrical elements, it is not the case for FOSs since their implementation necessitates unlimited amount of storage space. In fact, the fractional-order behavior can be exhibited via some recently introduced capacitors (fractances) and inductors (fractductors) [75]. However, these elements are currently in the development phase, and their availability is limited. As a result, alternative realization methods have been proposed using basic electrical elements. The R-C infinite ladder network [22] is a relevant example with an idea that is based on approximating the fractional-order behavior using a finite number of R-C elements. Hence, the major problem is the requirement of an approximation method to include any fractional-order operator in a practical realization or even an equivalent digital implementation. Theoretically, the main issue with the digital implementation is that a fractional-order operator requires an infinite amount of memory for the historical computational data; all past functions take place during the calculations of a fractional-order integral [76, 77]. For that particular reason, effective methods to represent a fractional-order operator in a finite-dimensional integer-order approximation are required [77]. Vari-

ous fractional-order approximation techniques have been designed for continuous time domains such as Carlson's method [78], Matsuda's method [79], and Oustaloup's method [80]. The Carlson's and the Matsuda's methods represent effective methods to approximate fractional-order operators. Despite this, several researchers [78, 81, 82] have highlighted major setbacks associated with the aforementioned. Carlson's method is limited to reduced orders of the fractional operator, and Matsuda's method results in improper approximations if its order is selected as an odd number. The approximation method proposed by Oustaloup relies on a recursive pole-zero distribution of the transfer function within a specific frequency range [83]. Of the available methods, Oustaloup's approximation has been established as the most suitable and stands out as popular and commonly used [20]. The strategy served as the foundation for the development of many software packages that assist fractional-order control design and system identification. A powerful computational software with a large set of tools for control design and system analysis as MATLAB/Simulink environment was eventually supported with some fractional-order packages such as the fractional-order robust control (Commande Robuste d'Ordre Non Entier (CRONE)) toolbox [83], Ninteger toolbox [84], the Fractional-Order Modeling and Control (FOMCON) toolbox [85], and the Fractional-Order Transfer Functions (FOTF) toolbox [86].

This section focuses on some of the most well-known approximation methods for fractional-order operators.

1.5.1 Carlson's Approximation

The method proposed by Carlson [78], which is derived from a regular Newton process used for iterative approximation of the β^{th} root. The method begins with the formulation of the subsequent relationships

$$H(s)^{\frac{1}{\beta}} - G(s) = 0,\ H(s) = G(s)^{\beta} \tag{1.50}$$

For each iteration we give $\beta = \frac{1}{\alpha}$ and $m = \frac{\alpha}{2}$, the starting from an initial value $H_0(s) = 1$, the approximated rational function is defined in the following form

$$H_i(s) = H_{i-1}(s)\frac{(\alpha - m) + H_{i-1}(s)(\alpha + m)G(s)}{(\alpha + m) + H_{i-1}(s)(\alpha - m)G(s)} \tag{1.51}$$

1.5.2 Matsuda's Approximation

The method proposed by Matsuda [79] involves approximating an irrational function with a rational one. This is achieved by using Continued Fraction Expansion and fitting the original function at a series of logarithmically spaced points. For N selected points given

as $s_k, k = 1,2,\ldots,N$, the approximation takes on the form

$$H(s) = a_0 + \frac{s-s_0}{a_1} + \frac{s-s_1}{a_2} + \frac{s-s_2}{a_3} + \ldots \tag{1.52}$$

with $a_i = v_i(s_i)$, $v_0(s) = H(s)$, and $v_{i+1}(s) = \frac{s-s_i}{v_i(s)-a_i}$.

1.5.3 Oustaloup's Approximation

Oustaloup's approximation, also known as Oustaloup's recursive filter, relies on the recursive pole-zero distribution of a transfer function within a specific frequency range (ω_b, ω_h). In other words, to approximate a fractional-order operator s^β by an integer-order transfer function, the poles and zeroes of the latter can be calculated using the equation that follows [80, 87]

$$H(s) = s^\beta \approx C \prod_{i=1}^{N} \frac{s+\omega_i'}{s+\omega_i} \tag{1.53}$$

where the filter gain C, poles, and zeros are evaluated using

$$\omega_i' = \omega_b \omega_u^{\frac{(2i-1-\beta)}{N}}, \omega_i = \omega_b \omega_u^{\frac{(2i-1+\beta)}{N}}, C = \omega_h^\beta \tag{1.54}$$

with $\omega_u = \sqrt{\frac{\omega_h}{\omega_b}}$ and N is the order of the filter.

In the case when $\beta \geq 1$ such as in the fractional-order transfer function (1.36), the operator s^β can be written as [88]

$$s^\beta = s^n s^\alpha \tag{1.55}$$

where $n = \beta - \alpha$ is the integer part of β. Therefore, only the fractional-order part s^α should be approximated. Hence, each operator found in (1.36) can be approximated based on (1.55), resulting in an integer-order transfer function.

1.6 Literature Review on Fractional-Order Adaptive Controllers

Due to the growing interest in FOSs and the challenges they present, many research efforts have focused on integrating fractional-order operators in adaptive control strategies. Notably, a fractional-order MRAC was designed in [89], introducing two methods to extend the conventional MRAC by incorporating fractional-order reference models and fractional-order adaptive laws. This work is considered one of the earliest research on this particular topic.

Research on fractional-order adaptive control remains a hot topic, with recent studies continuing to advance the field. For example, the work in [90] discussed the generalization of direct MRAC methodology, specifically tailored for FOLSs. On the other hand, [91] opts for an indirect MRAC to control a particular class of FOSs. A discussion on tuning

control and adaptive gains of a fractional-order MRAC using optimization algorithms was provided in [92]. Another example of locating the optimal values of the adaptive gains using a multi-objective genetic algorithm illustrated in [93]. The authors used fractional-order integral-type adaptation laws to accelerate the convergence and improve control signal efficiency. A fractional-order MRAC was suggested for the control of fractional-order multi-variable systems [32]. A composite fractional-order MRAC was developed including the estimation error parameter into the adaptation law [94]. A fractional-order MRAC design includes a feed-forward compensation to improve the stability behavior and the robustness of the closed-loop system [95].

In terms of improving the scheme of fractional-order adaptive controllers, an adaptive sliding mode controller was designed in [96]. The structure of this controller relies on a fractional-order switching control law and some adaptive laws to deal with uncertainties and external disturbances. Another adaptive sliding mode for control and synchronization of FOCSs is provided in [97]. The work in [98], offers a comparison between fractional-order adaptive sliding mode controllers. The study was based on two different sliding surfaces and the approaches used for chaos synchronization problems. A fractional-order adaptive backstepping controller was designed to deal with actuator faults, uncertainties, and disturbances, while achieving closed-loop stability for a considered fractional-order system [99]. In [38], a chaos synchronization strategy is presented, the former's purpose is to control an incommensurate system subject to input saturation using an adaptive controller with fractional-order adaptation laws.

The resulting improvements of incorporating intelligent algorithms as nonlinearity approximators can be observed for FOCs. As an example, the authors in [100, 101] used fuzzy system approximation in a fractional-order adaptive control scheme, while other works used Neural Networks (NN) approximators [102, 103]. To achieve a projective synchronization for two distinct FOCSs, besides employing a fuzzy adaptive controller, the authors in [104] used a fractional-order variable-structure technique to robustly deal with input nonlinearities within the system. The work in [105] discussed the use of the fuzzy adaptive mechanism in the synchronization of both uncertain and incommensurate FOCSs. The backstepping-based adaptive controller [106] benefited from a fuzzy system that treats fractional-order derivatives in the virtual command function as a part of the uncertain function. Authors in [107] have developed an adaptive resilient controller that was capable of ensuring the finite-time stability of the closed-loop system based on NN and fractional-order command-filtered backstepping methodology. The work in [108] proposed an adaptive NN control for a class of time-delayed FOSs. The controller uses a linear observer to estimate immeasurable tracking error components. An adaptive NN terminal sliding mode controller was established along with a commanded filtered backstepping approach to control a fractional-order synchronous motor in [109]. The adaptive NN controller in [110] relies on an event-triggered mechanism to achieve the stability of nonstrict-feedback FONLSs with input saturation. An adaptive controller based on a

fractional-order command filter and a Radial Basis Function Neural Network (RBFNN) is designed in [111] for FOCSs with uncertain input dead zones.

1.7 Conclusion

This chapter aims to offer a comprehensive insight into fractional calculus by focusing on its key aspects. Highlighting the fundamental definitions of fractional-order operators, including the fractional-order integral and two popular approaches for fractional-order derivatives. To facilitate further analysis, we explored the extension of the Laplace transform to fractional calculus. In addition, we examined several properties of fractional-order derivative definitions, thus, demonstrating the relevance and significance of the Caputo fractional-order derivative to this work. Outlining these fundamental definitions and exploring their properties, allow introducing a new class of systems known as fractional-order dynamical systems. These systems can be described using differential equations that involve fractional-order derivatives. The overall stability discussions reveal that the FOSs exhibit distinct behaviors compared to integer-order ones. Yet, it can be seen that the stability notations of the latter are rather special cases of the ones observed in FOSs. Moreover, the problem with the implementation of fractional-order operators has been discussed, showing that Oustaloup's recursive filter is a well-established method for finite-dimensional approximation of the fractional-order operator.

Chapter 2

$\mathscr{L}_1$ Adaptive Control

2.1 Introduction

Adaptive controllers are designed to handle the challenges posed by systems with uncertain dynamics, time-varying parameters, and external disturbances. Unlike traditional controllers, which rely on fixed parameters derived from precise mathematical models, adaptive controllers can modify their behavior in real-time to cope with changes in the system [41, 42]. $\mathscr{L}_1$ adaptive control represents a significant advancement in adaptive control methodologies, offering robust performance in the presence of system uncertainties and high adaptation gains [46, 56]. Distinguished by its fast adaptation capabilities, $\mathscr{L}_1$ adaptive control swiftly adjusts control parameters to maintain system stability and desired performance. This method stands out due to its ability ensures a predictable transient response while providing consistent performance even during adaptation [44]. $\mathscr{L}_1$ adaptive control is a new and promising technique that have been studied extensively in the last few years. The methodology of this controller, which is the foundation of this research, is relatively new and unique. Thus, this chapter will attempt to present the $\mathscr{L}_1$ adaptive controller, showcasing its structure and advantages. The rest of the chapter is divided into 4 sections and organized as follows. Section 2.2 shows the basic architecture of the $\mathscr{L}_1$ adaptive controller. Section 2.3 provides an analysis of the robustness and performance of the $\mathscr{L}_1$ adaptive controller. Section 2.4 offers a brief literature review on $\mathscr{L}_1$ adaptive control methodology. Section 2.5 concludes the chapter.

2.2 Basic Architecture of $\mathscr{L}_1$ Adaptive Controller

This section will provide an explanation of the theoretical principles behind the $\mathscr{L}_1$ adaptive controller, offering a comprehensive understanding that supports this research, noting that the following subsections adhere to the work stated in [44].

2.2.1 Mathematical Basis

2.2.1.1 Barbalat's lemma

Barbalat's lemma is a frequently employed mathematical concept in stability analysis and control theory. The lemma can be expressed within the scope of Lyapunov functions and their derivatives, under certain conditions, it can be utilized to establish the convergence of this functions to zero as time approaches infinity.

Lemma 2.1. [112] Let a function $g:\mathbb{R}\to\mathbb{R}$ be uniformly continuous on $[0,\infty)$. Then, if the term $\lim_{t\to\infty}\int_0^t g(\tau)d\tau$ exists and have a finite value, it holds that

$$\lim_{t\to\infty} g(t) = 0 \tag{2.1}$$

□

2.2.1.2 Projection Operator

The projection operator is frequently used to synthesize adaptation laws. Within the adaptive schemes, the utilization of the projection operator serves the purpose of avoiding parameter drifting, ensuring bounds to the estimated function, and guaranteeing the robustness of the controller. The application of the projection operator to adaptive schemes is detailed in [113]. In this part, we recall certain useful definitions and proprieties as stated in [44, 113].

Definition 2.1. $\Theta\subseteq\mathbb{R}^n$ is known as a convex set if for all $p,q\in\Theta$, we have

$$\varsigma p + (1-\varsigma)q \in \Theta \tag{2.2}$$

with $0\le\varsigma\le 1$. □

Definition 2.2. The function $g:\mathbb{R}^n\to\mathbb{R}$ is known as a convex function if for all $p,q\in\mathbb{R}^n$, we have

$$g(\varsigma p + (1-\varsigma)q) \le \varsigma g(p) + (1-\varsigma)g(q) \tag{2.3}$$

with $0\le\varsigma\le 1$. □

Definition 2.3. Let us consider a convex compact set Θ_k with a smooth boundary as

$$\Theta_k = \{p\in\mathbb{R}^{\mathrm{n}} \mid g(p)\le k\} \tag{2.4}$$

with $0\le k\le 1$, and $g:\mathbb{R}^n\to\mathbb{R}$ is the smooth convex function that follows

$$g(p) = \frac{(\epsilon_p+1)p^T p - p_{max}^2}{\epsilon_p p_{max}^2} \tag{2.5}$$

with p_{max} represents the imposed norm bound on the vector p and $\epsilon_p \in \mathbb{R}^+$ is the projection tolerance bound of the designer's choice. The definition of the projection operator $Proj(.,.)$ is given for any two vectors $p, q \in \mathbb{R}^n$ in the following form

$$Proj(p,q) = \begin{cases} q - \frac{\nabla g(p)(\nabla g(p))^T}{\|\nabla g(p)\|^2} q g(p), & if\, g(p) > 0\, and\, (\nabla g(p))^T q > 0 \\ q, & Otherwise \end{cases} \tag{2.6}$$

where $\nabla g(p) = (\frac{\partial g(p)}{\partial p_1} \dots \frac{\partial g(p)}{\partial p_n})^T$. □

Lemma 2.2. For a convex set Θ_0 defined as

$$\Theta_0 = \{p \in \mathbb{R}^n | g(p) \leq 0\} \tag{2.7}$$

and for a parameter $p(t)$ evolving according to the subsequent dynamics

$$\dot{p}(t) = Proj(p(t), q) \tag{2.8}$$

where $p(t_0) \in \Theta_k$. Then we have

$$p(t) \in \Theta_k \tag{2.9}$$

and for $p^* \in \Theta_0$, we have

$$(p - p^*)^T (Proj(p,q) - q) \leq 0 \tag{2.10}$$

□

2.2.2 Model Reference Adaptive control

In order to enhance comprehension of the $\mathscr{L}_1$ adaptive control theory, this part will provide a concise overview of the indirect MRAC, for that reason, let us consider the following class of linear time-invariant systems

$$\begin{cases} \dot{x}(t) = Ax(t) + B(u(t) + \theta^T(t)x(t)), x(0) = x_0 \\ y(t) = C^T x(t) \end{cases} \tag{2.11}$$

where $A \in \mathbb{R}^{n \times n}$ is a known matrix, B and $C \in \mathbb{R}^n$ are known constant vectors, such that the pair (A, B) is controllable, $x(t) = [x_1, \dots, x_n]^T \in \mathbb{R}^n$ is the measured state with $x_0 \in \mathbb{R}^n$ are the corresponding initial values, $y(t) \in \mathbb{R}$ is the system output, $\theta \in \mathbb{R}^n$ is a vector of unknown parameters, and $u \in \mathbb{R}$ is the control signal with the subsequent structure

$$u(t) = u_{ad}(t) + u_m(t) \tag{2.12}$$

where $u_{ad}(t)$ is the control law that incorporates the adaptive components and $u_m(t)$ is selected as follows

$$u_m(t) = -K^T x(t) \tag{2.13}$$

with $K \in \mathbb{R}^n$ is a feedback gain that yields in a Hurwitz matrix $A_m \in \mathbb{R}^{n\times n}$ defining the desired dynamics for the closed-loop system, where $A_m = A - BK^T$.

The objective of the controller is to achieve a bounded tracking response of the output signal $y(t)$ to a bounded reference signal $y_d(t)$. This can be achieved by using the nominal control signal that follows

$$u_{ad_{nom}}(t) = -\theta^T x(t) + K_g y_d(t) \tag{2.14}$$

with $K_g = -\frac{1}{C^T A_m^{-1} B}$ [115]. The choice of the control $u_{ad_{nom}}(t)$ provides a perfect cancellation of the uncertainties within the system (2.11), and leads to the subsequent reference system

$$\begin{cases} \dot{x}_m(t) = A_m x_m(t) + BK_g y_d(t), x(0) = x_0 \\ y(t) = C^T x(t) \end{cases} \tag{2.15}$$

However, due to the utilization of the unknown vector θ, the implementation of the control law (2.14) is not feasible. Hence, it is necessary to determine an appropriate control input $u_{ad}(t)$ as

$$u_{ad}(t) = -\hat{\theta}^T x(t) + K_g y_d(t) \tag{2.16}$$

where $\hat{\theta}(t) \in \mathbb{R}^n$ is the estimation of the unknown vector θ. Consequently, by denoting the tracking error as $e(t) = x_m(t) - x(t)$, one can have the following error dynamics

$$\dot{e}(t) = A_m e(t) + B\tilde{\theta}^T(t)x(t), e(0) = 0 \tag{2.17}$$

where $\tilde{\theta}(t) = \hat{\theta}(t) - \theta$ and $\hat{\theta}(t)$ follows the adaptation law given bellow

$$\dot{\hat{\theta}}(t) = -\Gamma x(t) e^T(t) PB, \hat{\theta}(0) = \hat{\theta}_0 \tag{2.18}$$

where $\Gamma > 0$ is the adaptation gain, and $P^T = P > 0$ is defined by solving the Lyapunov algebraic equation that follows

$$PA_m + A_m^T P = -Q \tag{2.19}$$

with $Q^T = Q > 0$ is an arbitrary symmetric matrix. With the choice of a Lyapunov candidate function as

$$V = e^T Pe + \frac{1}{\Gamma}\tilde{\theta}^T\tilde{\theta} \tag{2.20}$$

it is straightforward to find

$$\dot{V} = -e^T Qe \leq 0 \tag{2.21}$$

In other words, this means that the tracking error and the estimation error are Lyapunov stable. Furthermore, to prove that the tracking error converges asymptotically to zero, we calculate the second derivative of the Lyapunov function, hence

$$\ddot{V} = -2e^T Q\dot{e} \tag{2.22}$$

based on (2.17), it follows that $\dot{e}(t)$ and $\ddot{V}(t)$ are bounded which lead to the conclusion that $\dot{V}(t)$ is continuous. The previous discussion allows us to apply Barbalat's lemma (details are given in Lemma 2.1), which implies that $\lim_{t\to\infty} \dot{V}(t) = 0$ and $\lim_{t\to\infty} e(t) = 0$.

In the case of predictor-based MRAC, we consider the following state predictor dynamics

$$\begin{cases} \dot{\hat{x}}(t) = A_m\hat{x}(t) + B(u_{ad}(t) + \hat{\theta}^T(t)x(t)), \hat{x}(0) = x_0 \\ \hat{y}(t) = C^T\hat{x}(t) \end{cases} \tag{2.23}$$

where $\hat{x}(t) \in \mathbb{R}^n$ is the prediction of the state vector $x(t)$ and $\hat{y}(t) \in \mathbb{R}$ is the prediction of the output signal $y(t)$. By subtracting (2.11) from (2.23), i.e., $\tilde{x} = \hat{x}(t) - x(t)$, one can get the prediction error dynamics as follows

$$\dot{\tilde{x}}(t) = A_m\tilde{x}(t) + B\tilde{\theta}(t)x(t), \tilde{x}(0) = 0 \tag{2.24}$$

Applying the same adaptation law as in (2.18) results in the same analysis using Lyapunov function where $e(t)$ is replaced with $\tilde{x}(t)$. That is to say

$$\dot{V} = -\tilde{x}^T Q\tilde{x} \leq 0 \tag{2.25}$$

It is worth noting that the adaptive component in MRAC is derived by estimating the unknown parameter θ. Through the examination of the estimation error dynamics and the application of Lyapunov stability, it can be demonstrated that the estimation error is bounded but not necessarily convergent. It is important to note that without introducing the feedback signal $u(t)$, we cannot apply Barbalat's lemma to conclude the convergence of $\tilde{x}(t)$ to zero. Both $x(t)$ and $\hat{x}(t)$ can diverge at the same rate, keeping $\tilde{x}(t)$ uniformly bounded [115]. If we use the control law (2.16) in (2.23), we obtain

$$\begin{cases} \dot{\hat{x}}(t) = A_m\hat{x}(t) + BK_g y_d(t), \hat{x}(0) = x_0 \\ \hat{y}(t) = C^T\hat{x}(t) \end{cases} \tag{2.26}$$

which shows that the closed-loop state predictor replicates the bounded ideal system of (2.15). Hence, Barbalat's lemma can be invoked to conclude that $\lim_{t\to\infty} \tilde{x}(t) = 0$.

Furthermore, the Lyapunov analysis of the closed-loop system implies that the tracking error $e(t)$ (or the prediction error $\tilde{x}(t)$) is upper bounded for all $t \geq 0$ as

$$\|e(t)\| \leq \sqrt{\frac{V(t)}{\lambda_{min}(P)}} \leq \sqrt{\frac{V(0)}{\lambda_{min}(P)}} = \frac{\|\tilde{\theta}(0)\|}{\sqrt{\lambda_{min}(P)\Gamma}} \tag{2.27}$$

with $\lambda_{min}(P)$ is the minimum eigenvalue of the matrix P. This indicates that the tracking error can be arbitrarily reduced for higher adaptation gain Γ [114]. However, it follows from the representation of the control law (2.16) and the adaptation law (2.18) that large adaptation gains introduce high-gain feedback control, this can be seen through the presence of high-frequency oscillations in the control signal and a drop in the ability to

tolerate time delays [44].

2.2.3 $\mathscr{L}_1$ Adaptive Control

Just like the previous discussion of MRAC, we consider the system represented in (2.11) with the control structure defined by (2.12). According to the representation of $u_m(t)$, we can have the following representation of the system

$$\begin{cases} \dot{x}(t) = A_m x(t) + B(u_{ad}(t) + \theta^T(t)x(t)), x(0) = x_0 \\ y(t) = C^T x(t) \end{cases} \tag{2.28}$$

with the state predictor given by the representation bellow

$$\begin{cases} \dot{\hat{x}}(t) = A_m \hat{x}(t) + B(u_{ad}(t) + \hat{\theta}^T(t)x(t)), \hat{x}(0) = x_0 \\ \hat{y}(t) = C^T \hat{x}(t) \end{cases} \tag{2.29}$$

where the estimated values of the unknown vector $\theta(t)$ are governed by the subsequent projection-type adaptation law

$$\dot{\hat{\theta}}(t) = \Gamma Proj(\hat{\theta}(t), -\tilde{x}(t)PBx(t)), \hat{\theta}(0) = \hat{\theta}_0 \tag{2.30}$$

$Proj(.,.)$ is the Projection operator introduced in Definition 2.3. The control law u_{ad} is defined as

$$u_{ad} = -C(s)(\hat{\eta}(s) - K_g y_d(s)) \tag{2.31}$$

where $\hat{\eta}(s)$ and $y_d(s)$ are the transform functions of $\hat{\eta}(t) = \hat{\theta}(t)x(t)$ and $y_d(t)$, respectively, and $C(s)$ is a BIBO stable and strictly proper transfer function with the form

$$C(s) = \frac{\omega_c}{s + \omega_c} \tag{2.32}$$

which represents a filter with DC gain $C(0) = 1$.

Finally, the $\mathscr{L}_1$ adaptive controller given by equations (2.29), (2.30), and (2.31) is subject to the $\mathscr{L}_1$ norm condition in (2.33), with the filter $C(s)$ and the feedback gain K are chosen to fulfill it [44, 115]

$$\|G(s)\|_{\mathscr{L}_1} L < 1 \tag{2.33}$$

where $G(s) = H(s)(1 - C(s))$, $H(s) = (s\mathbb{I} + A_m)^{-1}B$ and $L = \underset{\theta \in \Theta}{max} \|\theta\|_1$, with Θ is a convex set.

We can examine both transient and steady-state performance by verifying that the prediction error remains uniformly bounded, regardless of the adaptive control signal. Additionally, we can prove that the control signal ensures that the prediction error converges to zero as time approaches infinity. To achieve this, let us start by defining the

prediction error dynamics using (2.28) and (2.29)

$$\dot{\tilde{x}}(t) = A_m\tilde{x}(t) + B\tilde{\theta}^T(t)x(t), \tilde{x}(0) = 0 \tag{2.34}$$

Next considering the Lyapunov candidate function as follows

$$V = \tilde{x}^T P\tilde{x} + \frac{1}{\Gamma}\tilde{\theta}^T\tilde{\theta} \tag{2.35}$$

with its derivative is given as

$$\dot{V} = -\tilde{x}^T Q\tilde{x} + 2\tilde{\theta}^T(Proj(\hat{\theta}, -x\tilde{x}^T PB) + x\tilde{x}^T PB) \tag{2.36}$$

according to Lemma 2.2, we can write the following inequality

$$\dot{V} \leq -\tilde{x}^T Q\tilde{x} \tag{2.37}$$

This implies that the prediction error and the estimation errors are bounded. Further analysis based on the Projection properties and the fact that $\tilde{x}(0) = 0$ yields in

$$\|\tilde{x}_\tau\|_{\mathscr{L}_\infty} \leq \sqrt{\frac{\theta_{max}}{\lambda_{min}(P)\Gamma}} \tag{2.38}$$

with $\theta_{max} = 4\underset{\theta\in\Theta}{max}\|\theta\|^2$. Moreover, as the bound on $\|\tilde{x}_\tau\|_{\mathscr{L}_\infty}$ was established regardless of the control signal, it implies that the signals $x(t)$ and $\hat{x}(t)$ can diverge at an equivalent rate, ensuring a uniformly bounded error. However, if the $\mathscr{L}_1$ norm condition given in (2.33) is satisfied, it is possible to prove that the prediction vector $\hat{x}(t)$ is uniformly bounded despite the presence of $u_{ad}(t)$ within its dynamics. Taking a step further, the asymptotic stability of the prediction error can be proved by the use of Barbalat's lemma, i.e., $\lim_{t\to\infty}\tilde{x}(t) = 0$.

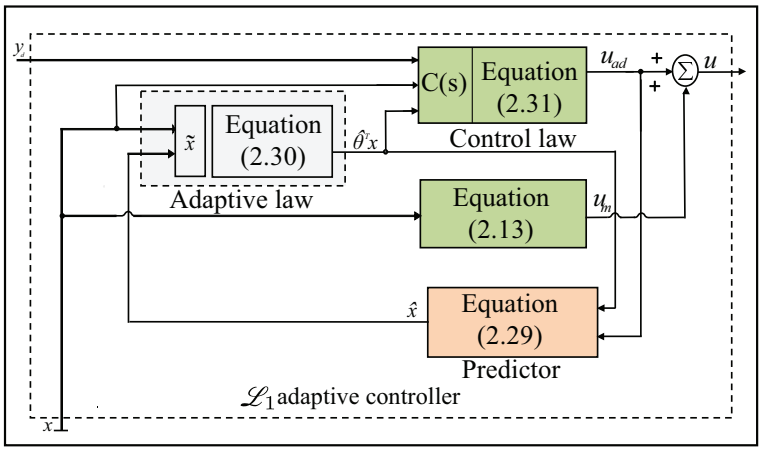

Figure 2.1: $\mathscr{L}_1$ adaptive control architecture.

In summary, the general form of the $\mathscr{L}_1$ adaptive controller is illustrated in Figure 2.1,

and it overall results can be outlined as follows [44]:

- The closed-loop system consists of two loops: The adaptation loop with the objective of estimating the unknown parameters, and the control loop that eliminates the effects of the unknown parameters.
- The system performance can be enhanced both in transient and steady-state response since fast adaptations can be accomplished by increasing the adaptation gain without compromising robustness.
- The high adaptation gains and low-pass filter complement each other. Separately, they might not be as effective. For instance, using high adaptation gains without the filter could result in high-gain feedback. Also, a low-pass filter without a high-gain could harm the system performance resulting in a sluggish response.

Detailed stability and performance analysis of $\mathscr{L}_1$ adaptive control theory can be found in [44].

2.3 Robustness and Performances Analysis

This subsection conducts a preliminary performance analysis of the $\mathscr{L}_1$ adaptive controller as introduced in (2.29), (2.30), and (2.31) compared to the MRAC outlined in (2.12), (2.16), and (2.18). To facilitate this comparison, we consider the scalar system that follows

$$\dot{x}(t) = -x(t) + u(t) + \theta, x(0) = x_0 \tag{2.39}$$

where θ is an unknown constant disturbance. The control objective is to stabilize the origin by effectively rejecting the disturbance θ. In this scenario, both the $\mathscr{L}_1$ adaptive controller and MRAC are reduced to linear model-following controllers [115]. Consequently, evaluating the performance of the closed-loop adaptive systems involves applying classical control theory tools like the Bode and Nyquist criteria. For the system described by (2.39), the MRAC architecture is presented by the integral controller that follows

$$u(t) = -\hat{\theta}(t) \tag{2.40}$$

where $\hat{\theta}(t)$ is the estimation of θ, which is given by

$$\dot{\hat{\theta}}(t) = -\Gamma e(t), \hat{\theta}(0) = \theta_0 \tag{2.41}$$

with $e(t) = x_m(t) - x(t)$ and x_m is generated by the subsequent reference model

$$\dot{x}_m(t) = -x_m(t), x_m(0) = x_0 \tag{2.42}$$

An illustrative block diagram of the closed-loop system is given in Figure 2.2. As it

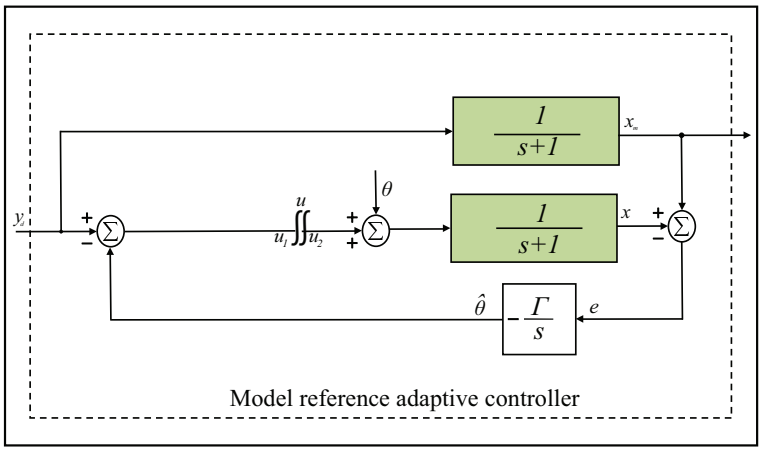

Figure 2.2: Closed-loop linear model-following model reference adaptive control.

can be seen, the adaptation gain Γ is positioned within the feedback loop of the control system. As a result, the loop gain and bandwidth of the closed-loop system are dependent on the value of Γ. Moreover, in the absence of the disturbance θ, the resulting closed-loop system is similar to the reference model in (2.42). Consequently, the robustness properties of MRAC can be examined through the stability margins of the loop transfer function, which can be computed utilizing the information provided in Figure 2.2 as

$$L_{u_1 u_2}(s) = \frac{\Gamma}{s(s+1)} \tag{2.43}$$

Figure 2.3 and Figure 2.4 depict Nyquist and Bode plots of this transfer function for different values of the adaptation gain. Figure 2.3 illustrates that Nyquist plots of $L_{u_1 u_2}(s)$ never crosses the negative part of the real line, signifying infinite gain margins ($g_m = \infty$) for the closed-loop system. Nevertheless, it is evident from Bode plots (Figure 2.4) that an increase in the adaptation gain results in a reduction of the phase margin, eventually leading to its disappearance. The gain crossover frequency ω_{gc} can be computed from [116] as

$$|L_{u_1 u_2}(j\omega_{gc})| = \frac{\Gamma}{\omega_{gc}\sqrt{\omega_{gc}+1}} \tag{2.44}$$

which results in

$$\omega_{gc} = \frac{\sqrt{\sqrt{4\Gamma^2+1}-1}}{2} \tag{2.45}$$

Finally, the phase margin is given by

$$\phi_m = \pi + \angle|L_{u_1 u_2}(j\omega_{gc})| = arctan(\frac{1}{\omega_{gc}}) \tag{2.46}$$

These equations imply that any increase in the adaptation gain Γ leads to a higher gain crossover frequency and consequently reduces the phase margin, which agrees with the results presented in Figure 2.3 and Figure 2.4. In other words, increasing Γ enhances closed-loop performance. However, it is evident that this improvement hurts its robust-

ness. Thus, the adaptation gain can be considered as the key in the balance between performance and robustness in the design of MRAC. Next, for the systems presented in

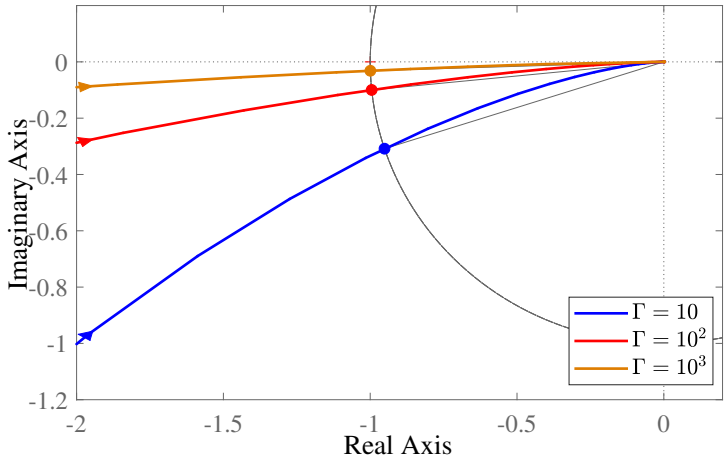

Figure 2.3: Nyquist plot for the loop transfer function $L_{u_1u_2}$.

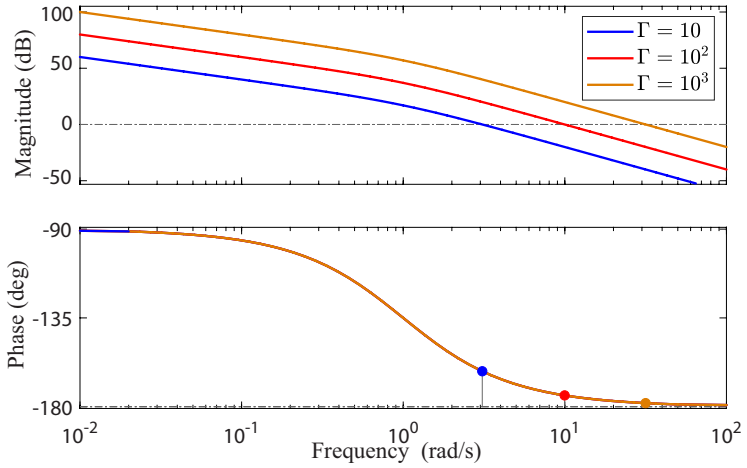

Figure 2.4: Bode plots for the loop transfer function $L_{u_1u_2}$.

(2.39), the state predictor of the $\mathscr{L}_1$ adaptive controller is given as

$$\dot{\hat{x}}(t) = -\hat{x}(t) + u(t) + \hat{\theta}(t), \hat{x}(0) = x_0 \tag{2.47}$$

which results in the following prediction error

$$\dot{\tilde{x}}(t) = -\tilde{x}(t) + \tilde{\theta}(t), \tilde{x}(0) = 0 \tag{2.48}$$

where the estimation $\hat{\theta}(t)$ is derived following the subsequent dynamics

$$\dot{\hat{\theta}}(t) = -\Gamma\tilde{x}(t), \dot{\theta}(0) = \theta_0 \tag{2.49}$$

Finally, the control signal is chosen as

$$u(t) = -C(s)\hat{\theta}(s) \tag{2.50}$$

with $C(s) = \frac{\omega_c}{s+\omega_c}$. An illustrative block diagram of the closed-loop system is provided in

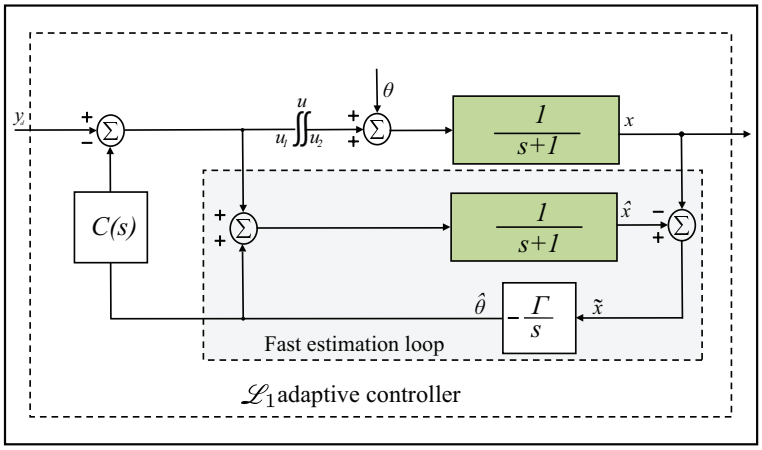

Figure 2.5: Closed-loop linear model-following $\mathscr{L}_1$ adaptive controller.

Figure 2.5, wherein it is evident that the adaptation gain Γ exclusively affects the fast estimation loop (depicted in Grey), whereas the bandwidth of the control loop is specified by the low-pass filter $C(s)$. In addition, according to this figure, we can deduce the loop transfer function that follows

$$H_{u_1 u_2}(s) = \frac{\Gamma C(s)}{s(s+1)\Gamma(1-C(s))} \tag{2.51}$$

Figure 2.6 illustrates Nyquist plot for this transfer function. This figure implies that the phase margin of the $\mathscr{L}_1$ adaptive controller approaches $\frac{\pi}{2}$ as the adaptation gain Γ increases. Hence, it is obvious that the phase and the gain margins of the $\mathscr{L}_1$ controller

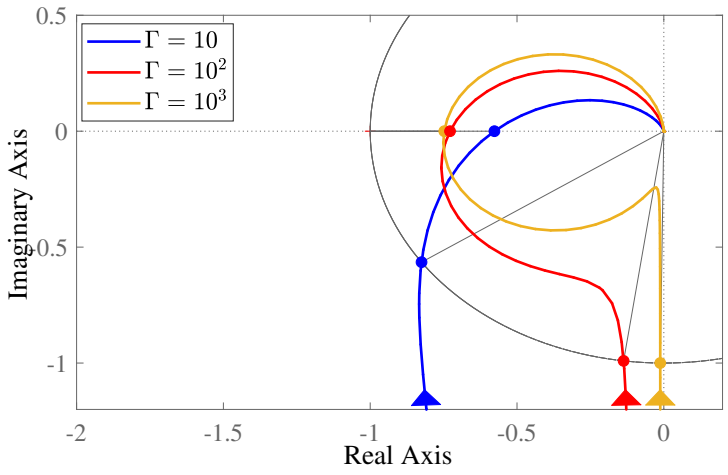

Figure 2.6: Nyquist plot for the loop transfer function $H_{u_1 u_2}$.

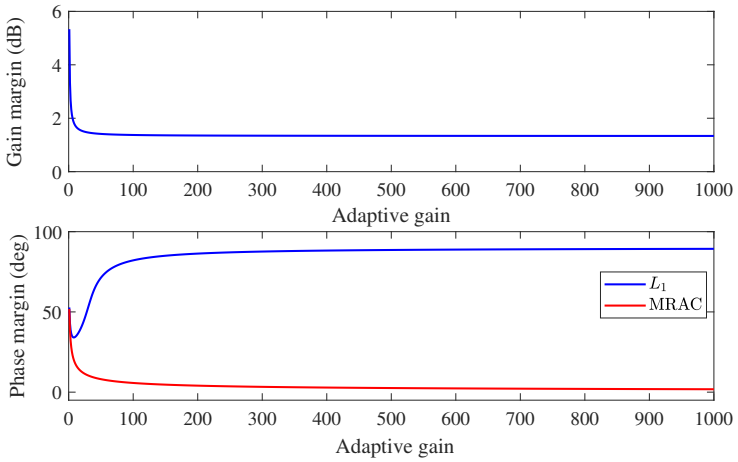

Figure 2.7: Effect of adaptation gain's value on gain and phase margins.

are not significantly affected by large values of Γ. The effect of the adaptive gain on the robustness margins of the two closed-loop systems is clearly presented in Figure 2.7. The figure shows that, while the MRAC has an infinite gain margin and a phase margin that diminishes as the adaptation gain increases, the $\mathscr{L}_1$ adaptive controller has a guaranteed bounded away from zero gain and phase margins in the presence of fast adaptation.

2.4 Literature Review on $\mathscr{L}_1$ Adaptive Control

Since introducing the concept of $\mathscr{L}_1$ adaptive control that proved its fast adaptation capabilities, extensive efforts have been dedicated to analyzing and elucidating its underlying principles. To further enrich theoretical understanding, Cao and Hovakimyan designed an $\mathscr{L}_1$ adaptive controller for a linear system with constant uncertainty [117]. Additional results [118] have explored a different system involving uncertain time-varying parameters and bounded disturbances. The work in [119] investigated a linear MIMO system considering unmatched uncertainties. Further findings on this subject are reported in [120]. The output-feedback concept was considered in the design of an $\mathscr{L}_1$ adaptive controller for a Single-Input Single-Output (SISO) system with time-varying disturbances [121]. The authors have also provided an in-depth discussion on the stability margins associated with the $\mathscr{L}_1$ methodology [122]. A comprehensive overview published in 2010 in a form of a book [44] consolidates most of the aforementioned results [46, 56, 117, 118, 121, 122] and provides detailed proofs, alongside structured design guidelines to solve the trade-off between closed-loop robustness, closed-loop performances, and system identification, taking into account various classes of linear and nonlinear systems.

In the area of practical systems, $\mathscr{L}_1$ adaptive control has undergone extensive validation, particularly in the field of flight control, especially before 2011. Notable examples include unmanned aerial vehicles [123], micro-air vehicles [124], flexible crew launch vehicle [125], and flexible aircraft (Sensorcraft) [126]. Importantly, $\mathscr{L}_1$ adaptive control is not exclusive to flight control; to this date it has found applications in other practical

systems requiring fast adaptations. Examples of such systems include parallel kinematic manipulators [127], electro-pneumatic actuators [58], and underwater vehicles [128].

Simultaneously, owing to the proven potential of $\mathscr{L}_1$ adaptive control, there pierced a surge of interest and several research works have been dedicated to extending its applicability to a wider range of systems and to introduce new aspects to the scheme. The work in [129] presents an extension to output feedback $\mathscr{L}_1$ adaptive control for a system with unknown time-varying and state-dependent nonlinearities, and also provides two filters for both matched and unmatched adaptive estimations. A nonlinear reference system based on $\mathscr{L}_1$ adaptive control was designed in [130]. The study demonstrated that the considered system follows the performance specifications imposed by the nonlinear ideal system both in transient and steady-state. However, this particular investigation was limited to affine systems in the presence of matched uncertainties. The challenge of controlling a system with unmatched disturbances has been addressed in several works [131,132]. Furthermore, researchers have discussed the application of the $\mathscr{L}_1$ adaptive control methodology to nonlinear uncertain non-affine systems, with investigations conducted on both SISO [58,133] and MIMO formulations [134].

In addition to these contributions, an $\mathscr{L}_1$ adaptive controller was designed for a class of nonlinear systems, taking into account the presence of an unknown time-varying hysteresis in the input [135]. This controller was also designed to address the presence of a dead-zone nonlinearity [136]. The subject of fault-tolerant control has been the focus of several works. For instance, the fault-dependent $\mathscr{L}_1$ adaptive backstepping controller [137] was designed to handle system uncertainties and to achieve a fault-tolerance control for nonlinear systems despite malfunctioning actuators. In another study [138], a sliding mode controller was used as an adaptive law and a virtual control within the $\mathscr{L}_1$ adaptive architecture, demonstrating promising results.

Interesting findings were presented in [139], showcasing the benefits of using NN as nonlinearity approximators in the $\mathscr{L}_1$ adaptive control structure. These findings hold practical significance and can be useful in real-world applications as the outcome of this architecture allows the relaxation of certain design parameters such as the adaptation gain, without compromising performances. Fuzzy Logic Systems (FLSs) have also demonstrated their advantages across various contexts. In one instance, a nonlinear system with an unknown backlash-like hysteresis was considered in [140], and the strategy involved the direct estimation of the nonlinear functions of the controlled system through the use of FLSs. The approach simplified controller implementation and reduced the required number of adaptive parameters. In [141], the authors introduced a modification to the $\mathscr{L}_1$ adaptive scheme by replacing the state predictor with a fuzzy predictor to control a disturbed nonlinear system. Feed-forward action, which is not fully provided by the $\mathscr{L}_1$ adaptive controller was also discussed and introduced to the scheme for a nonlinear system in the presence of unmodeled dynamics [142].

2.5 Conclusion

This chapter seeks to provide a general understanding of the $\mathscr{L}_1$ adaptive controller, elucidating its architecture in contrast to the MRAC. Through this comparison, it illustrates the major differences between the two schemes, while highlighting the ability of the $\mathscr{L}_1$ adaptive controller to deliver a satisfactory tracking response with faster adaptations in the presence of uncertainties. The architecture of the $\mathscr{L}_1$ adaptive controller consists of several key components, including a state predictor, a control law, a low-pass filter, and adaptation laws. The predictor is responsible for estimating the values of the time-varying uncertainties and the unknown external disturbances present in the system. These estimated values are then adjusted according to the adaptation laws, which are extracted via the Lyapunov stability criteria. Eventually, the adaptive estimates are incorporated into the control signal generated by the $\mathscr{L}_1$ adaptive controller. To achieve fast transient performance, high adaptation gains should be employed. However, a probable issue can arise from the high-frequency components introduced into the control channel through the adaptive estimates. These high-frequency components can lead to system instability. To resolve this problem and assure robust control, a low-pass filter is included in the control channel. Finally, a state feedback control signal is generated from the filtered control law and fed to the system under control.

Chapter 3

$\mathscr{L}_1$ Adaptive Control Design for Fractional-Order Uncertain Systems

3.1 Introduction

$\mathscr{L}_1$ adaptive control is a new promising technique introduced in [46, 56]. Regarded as an improvement to MRAC; both share state predictor architecture and a similar analysis approach. However, $\mathscr{L}_1$ adaptive control proves to deliver a satisfactory tracking response with faster adaptations in the presence of uncertainties and bounded external disturbances. The objective of this chapter is to design a new FOL1AC for a general class of FOSs with matched uncertainties and bounded time-varying external disturbances. Initially, a suitable form of a fractional-order sliding surface is selected to simplify the control design and the stability analysis of the considered class of FOSs. Besides the fractional-order sliding surface, the architecture of the controller is relatively based on the basic $\mathscr{L}_1$ adaptive controller. In the suggested control technique, a low-pass filter is incorporated in the control channel, which separates the estimation loop from the control loop. Besides, the proposed controller can ensure uniform performance bounds for system signals both in transient and steady-state. As a result, unlike conventional adaptive control methods, the proposed controller enables for fast adaptation without compromising robustness, making it an alternative controller for uncertain FOSs. The outline of the chapter is given as follows. Section 3.2 throws light on the problem. Section 3.3 introduces the proposed FOL1AC. Section 3.4 discusses the stability analysis of the proposed scheme. Section 3.5 investigates the validity of the controller via some simulation results. Section 3.6 concludes this chapter.

3.2 Problem Formulation

This section deals with the description of the class of systems under consideration and specifies the control objective. As a start, let us consider a class of SISO FOSs represented

in the following form

$$\begin{cases} D^{\beta}x(t) = Ax(t) + B(u(t) + \theta^{T}(t)x(t) + \sigma(t)), x(0) = x_0 \\ y(t) = C^{T}x(t) \end{cases} \tag{3.1}$$

where D^{β} is the Caputo fractional derivative, $0 < \beta < 1$ is the derivative order, $A \in \mathbb{R}^{n\times n}$ is a known matrix defined in (3.2), B and $C \in \mathbb{R}^{n}$ are known constant vectors, such that the pair (A, B) is controllable, $x(t) = [x_1(t), \ldots, x_n(t)]^{T} \in \mathbb{R}^{n}$ is the measured pseudo state vector of the fractional-order system, $x(0) = x_0$ is the corresponding vector of initial conditions, $u(t) \in \mathbb{R}$ is the control input, $y(t) \in \mathbb{R}$ is the system output, $\sigma(t) \in \mathbb{R}$ represent system external disturbances which is unknown, and $\theta(t) \in \mathbb{R}^{n}$ is a vector of unknown parameters

$$A = \begin{bmatrix} 0 & 1 & 0 & \ldots & 0 \\ 0 & 0 & 1 & \cdots & 0 \\ \vdots & \vdots & \vdots & \ddots & \vdots \\ 0 & 0 & 0 & \cdots & 1 \\ a_{1n} & a_{2n} & \ldots & \ldots & a_{nn} \end{bmatrix}, B = \begin{bmatrix} 0 \\ \vdots \\ 0 \\ B_n \end{bmatrix}, and\, C = \begin{bmatrix} 1 \\ 0 \\ \vdots \\ 0 \end{bmatrix} \tag{3.2}$$

According to (3.2), the system represented by the equation (3.1) can be written in the following form

$$\begin{cases} D^{\beta}x_1(t) = x_2(t) \\ D^{\beta}x_2(t) = x_3(t) \\ \vdots \\ D^{\beta}x_{n-1}(t) = x_n(t) \\ D^{\beta}x_n(t) = A_n x(t) + B_n(u(t) + \theta^{T}(t)x(t) + \sigma(t)) \\ y(t) = x_1(t) \end{cases} \tag{3.3}$$

with the vector $A_n = [a_{1n}\, a_{2n} \ldots a_{nn}] \in \mathbb{R}^{n}$ is the n^{th} row of the matrix A, and $B_n \in \mathbb{R}$ is the n^{th} value of the vector B.

The control objective is to synthesize an input signal $u(t)$ for the system represented in (3.3) in order to achieve a bounded tracking response of the output signal $y(t) = x_1(t)$ to a bounded reference signal $y_d(t)$ while compensating the unknown parameters and external disturbances and ensuring the boundedness of all other signals.

3.3 Fractional-Order $\mathscr{L}_1$ Adaptive Controller

In this section, the FOL1AC is developed based on a fractional-order sliding surface for the class of FOSs introduced in (3.3). To proceed with the control design, the following assumptions are necessary.

Assumption 3.1. The reference signal $y_d(t)$ and its successive fractional-order derivatives $D^{j\beta}y_d(t), j = 1, \ldots, n$ are assumed to exist, to be smooth and bounded. □

Assumption 3.2. The vector of unknown parameters $\theta(t)$ and external disturbances $\sigma(t)$ are upper bounded for all $t \geq 0$ as follows

$$\begin{aligned} &\theta(t) \in \Theta \\ &|\sigma(t)| < \Psi \end{aligned} \tag{3.4}$$

where $\Psi \in \mathbb{R}^+$ is a known constant and Θ is a known convex set with a definition given in Definition 2.1. □

Assumption 3.3. Let $\dot{\theta}(t)$ and $\dot{\sigma}(t)$ be the bounded derivatives of the continuous functions $\theta(t)$ and $\sigma(t)$, respectively, such that for all $t \geq 0$ we have

$$\begin{aligned} &\|\dot{\theta}(t)\| \leq d_\theta < \infty \\ &|\dot{\sigma}(t)| \leq d_\sigma < \infty \end{aligned} \tag{3.5}$$

where d_θ and d_σ are positive constants. □

3.3.1 Choice of an Appropriate Fractional-Order Sliding Surface

Let the error vector $E(t) = [e_1, e_2, \ldots, e_n]^T \in \mathbb{R}^n$ be defined as

$$E(t) = Y_d(t) - x(t) \tag{3.6}$$

where $e_1(t) = y_d(t) - x_1(t)$ is the tracking error and $Y_d(t) \in \mathbb{R}^n$ is a vector containing the reference signal $y_d(t)$ and its successive fractional-order derivatives. Therefore, one has the following representation of the error dynamics

$$\begin{cases} D^\beta e_1(t) = e_2(t) \\ D^\beta e_2(t) = e_3(t) \\ \vdots \\ D^\beta e_{n-1}(t) = e_n(t) \\ D^\beta e_n(t) = D^{n\beta} y_d(t) - D^\beta x_n(t) \end{cases} \tag{3.7}$$

To achieve the aforementioned objective, the design of this controller follows a two-step approach. The first step involves selecting the sliding surface function, denoted by $z(t)$, which ensures the convergence of the tracking errors. The second step focuses on synthesizing a suitable control law that forces the system states onto the predefined sliding surface in finite time.

Regarding the systems presented in (3.1) and the error dynamics in (3.7), we chose the form of a fractional-order sliding surface $z(t)$ as [104]

$$z(t) = D^{\beta-1} e_n(t) + \int_0^t \lambda^T E(t) d\tau = \begin{bmatrix} 1 & \lambda^T \end{bmatrix} \begin{bmatrix} D^{\beta-1} e_n(t) \\ \int_0^t E(t) d\tau \end{bmatrix} \tag{3.8}$$

with $\lambda = [\lambda_1, \lambda_2, \ldots \lambda_n]^T \in \mathbb{R}^n$ is a vector of adjustable design parameters to be determined by the designer in order to ensure the stability.

Remark 3.1. Integrating fractional-order sliding surfaces within fractional-order adaptive controllers is a well-established technique [97, 98, 104]. This approach simplifies the control architecture by offering reduced-order dynamics that are easier to handle. Notably, the specific form chosen in equation (3.8) presents a key advantage: it seamlessly accepts integer-order derivatives. This characteristic facilitates stability analysis and the derivation of adaptation laws in familiar integer-order forms. □

Once $z(t) = \dot{z}(t) = 0$, the system is known to operate in the sliding surface. Consequently, for a significantly small value of $\dot{z}(t)$, i.e., $\dot{z}(t) \approx 0$, and according to the property given in (1.26), one can have

$$D^{\beta} e_n(t) + \lambda^T E(t) = \begin{bmatrix} 1 & \lambda^T \end{bmatrix} \begin{bmatrix} D^{\beta} e_n(t) \\ E(t) \end{bmatrix} = 0 \tag{3.9}$$

which leads to

$$D^{\beta} e_n(t) = -\lambda^T E(t) \tag{3.10}$$

By replacing $D^{\beta} e_n(t)$ from equation (3.7) in (3.10), the state space representation of the errors dynamics in the case where $z(t) = \dot{z}(t) = 0$ can be written in the subsequent form

$$\underbrace{\begin{bmatrix} D^{\beta} e_1(t) \\ D^{\beta} e_2(t) \\ \vdots \\ D^{\beta} e_{n-1}(t) \\ D^{\beta} e_n(t) \end{bmatrix}}_{D^{\beta} E(t)} = \underbrace{\begin{bmatrix} 0 & 1 & 0 & \ldots & 0 \\ 0 & 0 & 1 & \cdots & 0 \\ \vdots & \vdots & \vdots & \ddots & \vdots \\ 0 & 0 & 0 & \cdots & 1 \\ -\lambda_1 & -\lambda_2 & -\lambda_3 & \cdots & -\lambda_n \end{bmatrix}}_{A_e} \underbrace{\begin{bmatrix} e_1(t) \\ e_2(t) \\ \vdots \\ e_{n-1}(t) \\ e_n(t) \end{bmatrix}}_{E(t)} \tag{3.11}$$

Thus, the design parameters $\lambda_i, i = 1, \ldots, n$ must be selected strictly positive to satisfy the stability condition in (1.42), i.e., $|arg(eig(A_e))| > \beta\frac{\pi}{2}$. This case implies that the sliding surface dynamics are asymptotically stable which ensures that tracking error and its fractional-order derivatives converge to zero. Therefore, the purpose of FOL1AC is to guarantee that the system reaches in the fractional-order sliding surface, which is true by ensuring that $z(t)$ vanishes towards zero.

3.3.2 Control Structure

Considering (3.8) and (3.7), the sliding surface dynamics can be written in the following form

$$\begin{aligned} \dot{z}(t) &= D^{\beta} e_n(t) + \lambda^T E(t) \\ &= D^{n\beta} y_d(t) - D^{\alpha} x_n(t) + \lambda^T E(t) \end{aligned} \tag{3.12}$$

replacing $D^{\beta}x_n(t)$ from (3.3) in (3.12), one has

$$\dot{z}(t) = D^{n\beta}y_d(t) - A_n x(t) - B_n(u(t) + \theta^T(t)x(t) + \sigma(t)) + \lambda^T E(t) \tag{3.13}$$

Let us consider the control signal structure as

$$u(t) = u_m(t) + u_{ad}(t) \tag{3.14}$$

where

$$u_m(t) = \frac{1}{B_n}(D^{n\beta}y_d(t) - A_n x(t) + \lambda^T E(t) + \alpha z(t)) \tag{3.15}$$

with α is a positive constant.

Replacing (3.15) and (3.14) in (3.13) to obtain the following sliding surface dynamics

$$\dot{z}(t) = -\alpha z(t) - B_n(u_{ad}(t) + \theta^T(t)x(t) + \sigma(t)), z(0) = z_0 \tag{3.16}$$

We consider the following predictor that replicates the dynamics described by (3.16) with the unknown parameters are replaced with their estimated values

$$\dot{\hat{z}}(t) = -\alpha \hat{z}(t) - B_n(u_{ad}(t) + \hat{\theta}^T(t)x(t) + \hat{\sigma}(t)), \hat{z}(0) = z_0 \tag{3.17}$$

where $\hat{z}(t) \in \mathbb{R}$ is the prediction of $z(t)$, $\hat{\theta}(t) \in \mathbb{R}^n$ and $\hat{\sigma}(t) \in \mathbb{R}$ are the projection-type adaptive estimations values of the unknown parameters $\theta(t)$ and $\sigma(t)$, respectively. These values are governed by the following projection-type adaptation laws

$$\begin{aligned} \dot{\hat{\theta}}(t) &= \Gamma Proj(\hat{\theta}(t), \tilde{z}(t)x(t)) \\ \dot{\hat{\sigma}}(t) &= \Gamma Proj(\hat{\sigma}(t), \tilde{z}(t)) \end{aligned} \tag{3.18}$$

where $\tilde{z}(t) = \hat{z}(t) - z(t) \in \mathbb{R}$ is the prediction error, $\Gamma > 0$ is the adaptation gain, and $Proj(.,.)$ is the projection operator introduced in Definition 2.3.

The control law u_{ad} is defined as

$$u_{ad}(s) = -C(s)\hat{\eta}(s) \tag{3.19}$$

where $\hat{\eta}(s)$ is the Laplace transform of $\hat{\eta}(t) = \hat{\theta}(t)x(t) + \hat{\sigma}(t)$, and $C(s)$ is a BIBO stable and strictly proper transfer function with the form

$$C(s) = \frac{\omega_c}{s + \omega_c} \tag{3.20}$$

which represents a filter with DC gain $C(0) = 1$. Finally, an illustrative block diagram of the proposed FOL1AC is given in Figure 3.1.

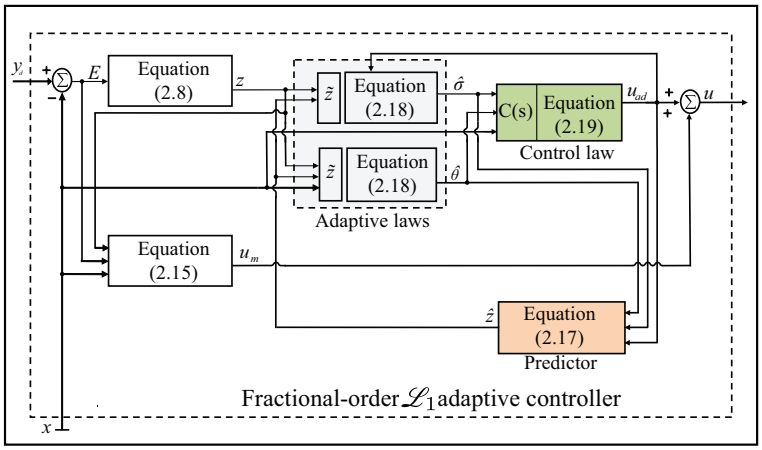

Figure 3.1: Diagram block of the proposed fractional-order $\mathscr{L}_1$ adaptive controller.

3.4 Stability and Performances Analysis

This section analyzes the performances and the stability of the developed controller, for that reason the subsequent assumptions are necessary

Assumption 3.4. The sliding surface form in (3.8) ensures that the two signals $z(t)$ and $x(t)$ share the same stability behaviors, using the facts that $\theta(t)$ is bounded in Assumption 3.2 and $\hat{\theta}(t) \in \Theta$ according to Lemma 2.2, the following bounds are acceptable

$$|\theta^T(t)x(t)| \leq L|z(t)| + L_0 \tag{3.21}$$

$$|\hat{\theta}^T(t)x(t)| \leq L|z(t)| + L_0 \tag{3.22}$$

where L and L_0 are positive constants. □

The controller proposed in (3.14), (3.17), (3.18), and (3.19) is subject to the $\mathscr{L}_1$ norm condition in (3.23), with the filter $C(s)$ and the design parameter α are chosen to fulfill it

$$\|G(s)\|_{\mathscr{L}_1} L < 1 \tag{3.23}$$

where $G(s) = H(s)(1 - C(s))$, $H(s) = -(s+\alpha)^{-1}B_n$ and $L > 0$ is introduced in Assumption 3.4.

Remark 3.2. Using the fact that $\alpha > 0$ and $C(s)$ is a BIBO stable and strictly proper transfer function we can easily conclude that $G(s)$ and $H(s)$ are also BIBO stable and proper transfer functions. □

3.4.1 Closed-loop Ideal Reference System

We consider now the non-adaptive form of the controller proposed in (3.14), (3.17), (3.18), and (3.19) to represent the closed-loop ideal reference system as follows

$$\begin{cases} \dot{z}_{ref}(t) = -\alpha z_{ref}(t) - B_n(u_{ad_{ref}}(t) + \theta^T(t)x_{ref}(t) + \sigma(t)), z_{ref}(0) = z_0 \\ u_{ad_{ref}}(s) = -C(s)(\eta_{ref}(s)) \end{cases} \tag{3.24}$$

where $\eta_{ref}(s)$ is the Laplace transform of $\eta_{ref}(t) = \theta^T(t)x_{ref}(t) + \sigma(t)$.

Remark 3.3. The control signal $u_{ad_{ref}}(t)$ depends on the unknown terms $\sigma(t)$ and $\theta(t)$ which is not practical. We mention that this is not the case for the actual control law $u_{ad}(t)$, and the signal $u_{ad_{ref}}(t)$ is used for analysis purposes only. □

Lemma 3.1. Let us consider that the design parameter α and the filter $C(s)$ satisfy the condition in (3.23), also regarding the representation of the closed-loop reference system in (3.24), we have the following bound

$$\|z_{ref\tau}\|_{\mathscr{L}_\infty} \leq \rho \tag{3.25}$$

where

$$\rho = \frac{\|G(s)\|_{\mathscr{L}_1}}{1 - L\|G(s)\|_{\mathscr{L}_1}}(L_0 + \Psi) + \frac{1}{1 - L\|G(s)\|_{\mathscr{L}_1}}\|z_{in\tau}\|_{\mathscr{L}_\infty} \tag{3.26}$$

with $z_{in} = (p + \alpha)^{-1}z_0$. □

Proof. From the representation of the closed-loop reference system (3.24), and using the Laplace transform formulation, one has

$$\begin{aligned} sz_{ref}(s) - z_0 &= -\alpha z_{ref}(s) - B_n(u_{ad_{ref}}(s) + \eta_{ref}(s)) \\ &= -\alpha z_{ref}(s) - B_n((1 - C(s))\eta_{ref}(s)) \end{aligned} \tag{3.27}$$

then

$$\begin{aligned} z_{ref}(s) &= -(s + \alpha)^{-1}B_n(1 - C(s))(\eta_{ref}(s)) + (s + \alpha)^{-1}z_0 \\ &= G(s)\eta_{ref}(s) + z_{in} \end{aligned} \tag{3.28}$$

Recalling that $G(s)$, $H(s)$, and $C(s)$ are BIBO stable and proper transfer functions, and since z_{in} is uniformly bounded. Then, for all $\tau > 0$ we have the following upper bound

$$\|z_{ref\tau}\|_{\mathscr{L}_\infty} \leq \|G(s)\|_{\mathscr{L}_1}\|\eta_{ref\tau}\|_{\mathscr{L}_\infty} + \|z_{in\tau}\|_{\mathscr{L}_\infty} \tag{3.29}$$

From the representation of $\eta_{ref}(t)$, and based on Assumption 3.2 and Assumption 3.4, we can conclude that

$$\|\eta_{ref\tau}\|_{\mathscr{L}_\infty} \leq L\|z_{ref\tau}\|_{\mathscr{L}_\infty} + L_0 + \Psi \tag{3.30}$$

Replacing (3.30) in (3.29), it results

$$\|z_{ref\tau}\|_{\mathscr{L}_\infty} \leq \|G(s)\|_{\mathscr{L}_1} L \|z_{ref\tau}\|_{\mathscr{L}_\infty} + \|G(s)\|_{\mathscr{L}_1} (L_0 + \Psi) + \|z_{in\tau}\|_{\mathscr{L}_\infty} \tag{3.31}$$

Solving (3.31) for $\|z_{ref\tau}\|_{\mathscr{L}_\infty}$, we get

$$\|z_{ref\tau}\|_{\mathscr{L}_\infty} \leq \frac{\|G(s)\|_{\mathscr{L}_1}}{1 - L\|G(s)\|_{\mathscr{L}_1}} (L_0 + \Psi) + \frac{1}{1 - L\|G(s)\|_{\mathscr{L}_1}} \|z_{in\tau}\|_{\mathscr{L}_\infty} \tag{3.32}$$

We know that L_0 and Ψ are finite positive values and z_{in} is uniformly bounded. Hence, if the condition in (3.23) is fulfilled, one obtains that $\|z_{ref\tau}\|_{\mathscr{L}_\infty}$ is uniformly bounded, that completes the proof. □

3.4.2 Transient and Steady-state Analysis

In this subsection, we analyze the performances bound between the closed-loop ideal reference system represented in (3.24) and the system (3.1) with the proposed controller defined in (3.14), (3.17), (3.18), and (3.19), both in transient and steady-state.

According to the Laplace transform formulation, the equations represented in (3.16) and (3.17) can be represented in the frequency domain by equations (3.33) and (3.34), respectively

$$\begin{aligned} z(s) &= -(s+\alpha)^{-1} B_n (u_{ad} + \eta(s)) + z_{in} \\ &= H(s)(-C(s)\hat{\eta}(s) + \eta(s) + C(s)\eta(s) - C(s)\eta(s)) + z_{in} \\ &= G(s)\eta(s) - C(s)H(s)\tilde{\eta}(s) + z_{in} \end{aligned} \tag{3.33}$$

and

$$\begin{aligned} \hat{z}(s) &= -(s+\alpha)^{-1} B_n (u_{ad} + \hat{\eta}(s)) + z_{in} \\ &= G(s)\hat{\eta}(s) + z_{in} \end{aligned} \tag{3.34}$$

where $\eta(s)$ and $\tilde{\eta}(s) = \hat{\eta}(s) - \eta(s)$ is the Laplace transforms of $\eta(t) = \theta^T(t)x(t) + \sigma(t)$ and $\tilde{\eta}(t) = \tilde{\theta}^T(t)x(t) + \tilde{\sigma}(t)$, respectively, with $\tilde{\theta}^T(t) = \hat{\theta}(t) - \theta(t) \in \mathbb{R}^n$ and $\tilde{\sigma}(t) = \hat{\sigma}(t) - \sigma(t) \in \mathbb{R}$ are the estimation errors.

Since the prediction error $\tilde{z}(t)$ is defined in (3.18) as $\tilde{z}(t) = \hat{z}(t) - z(t)$, it is easy to find $\tilde{z}(s)$ by subtracting (3.33) from (3.34), hence

$$\tilde{z}(s) = H(s)\tilde{\eta}(s) \tag{3.35}$$

Lemma 3.2. Consider the system presented in (3.16) with the controller proposed in (3.14), (3.17), (3.18), and (3.19), if the low-pass filter $C(s)$ and the design parameter α fulfill the condition in (3.23), we have the bounds that follow

$$\|\tilde{z}_\tau\|_{\mathscr{L}_\infty} \leq \sqrt{2\varphi} \tag{3.36}$$

and

$$\|\hat{z}_\tau\|_{\mathscr{L}_\infty} \leq \omega \tag{3.37}$$

where

$$\varphi = \frac{B_n}{2\Gamma}(4\underset{\theta\in\Theta}{max}\|\theta\|^2 + 4\Psi^2) + \frac{B_n}{\alpha\Gamma}(\underset{\theta\in\Theta}{max}\|\theta\| d_\theta + \Psi d_\sigma) \tag{3.38}$$

and

$$\omega = \frac{\|G(s)\|_{\mathscr{L}_1}(L\sqrt{2\varphi} + L_0 + \Psi)}{1 - \|G(s)\|_{\mathscr{L}_1} L} + \frac{\|z_{in\tau}\|_{\mathscr{L}_\infty}}{1 - \|G(s)\|_{\mathscr{L}_1} L} \tag{3.39}$$

□

Proof. Let us consider the candidate Lyapunov function for stability analysis purpose as follows

$$V(\tilde{z},\tilde{\theta},\tilde{\sigma}) = \frac{1}{2}\tilde{z}^2 + \frac{B_n}{2\Gamma}\tilde{\theta}^2 + \frac{B_n}{2\Gamma}\tilde{\sigma}^2 \tag{3.40}$$

The time derivative of $V(\tilde{z},\tilde{\theta},\tilde{\sigma})$ in (3.40) is given as

$$\dot{V}(\tilde{z},\tilde{\theta},\tilde{\sigma}) = \tilde{z}\dot{\tilde{z}} + \frac{B_n}{\Gamma}\tilde{\theta}^T\dot{\tilde{\theta}} + \frac{B_n}{\Gamma}\tilde{\sigma}\dot{\tilde{\sigma}} \tag{3.41}$$

Recalling (3.16) and (3.17), we can write

$$\dot{V}(\tilde{z},\tilde{\theta},\tilde{\sigma}) = -\alpha\tilde{z}^2 - \tilde{z}B_n\tilde{\eta} + \frac{B_n}{\Gamma}\tilde{\theta^T}\dot{\tilde{\theta}} + \frac{B_n}{\Gamma}\tilde{\sigma}\dot{\tilde{\sigma}} \tag{3.42}$$

or

$$\dot{V}(\tilde{z},\tilde{\theta},\tilde{\sigma}) = -\alpha\tilde{z}^2 + B_n\tilde{\theta^T}(\frac{1}{\Gamma}\dot{\hat{\theta}} - x\tilde{z}) + B_n\tilde{\sigma}(\frac{1}{\Gamma}\dot{\hat{\sigma}} - \tilde{z}) - \frac{B_n}{\Gamma}\tilde{\theta^T}\dot{\theta} - \frac{B_n}{\Gamma}\tilde{\sigma}\dot{\sigma} \tag{3.43}$$

Replacing the adaptation laws (3.18) in (3.43), one can have

$$\begin{aligned}\dot{V}(\tilde{z},\tilde{\theta},\tilde{\sigma}) \leq -\alpha\tilde{z}^2 + B_n\tilde{\theta}(Proj(\hat{\theta},x\tilde{z}) - x\tilde{z}) + B_n\tilde{\sigma}(Proj(\hat{\sigma},\tilde{z}) - \tilde{z}) \\ + \frac{B_n}{\Gamma}(|\,\tilde{\theta^T}\dot{\theta}\,| + |\,\tilde{\sigma}\dot{\sigma}\,|)\end{aligned} \tag{3.44}$$

Lemma 2.2 implies that

$$B_n\tilde{\theta}(Proj(\hat{\theta},x\tilde{z}) - x\tilde{z}) + B_n\tilde{\sigma}(Proj(\hat{\sigma},\tilde{z}) - \tilde{z}) \leq 0 \tag{3.45}$$

then

$$\dot{V}(\tilde{z},\tilde{\theta},\tilde{\sigma}) \leq -\alpha\tilde{z}^2 + \frac{B_n}{\Gamma}(|\,\tilde{\theta^T}\dot{\theta}\,| + |\,\tilde{\sigma}\dot{\sigma}\,|) \tag{3.46}$$

The projection operator ensures that $\hat{\theta}(t) \in \Theta$ and $|\hat{\sigma}| \leq \Psi$, hence

$$\underset{t\geq 0}{max}(\tilde{\theta}^2(t) + \tilde{\sigma}^2(t)) \leq (4\underset{\theta\in\Theta}{max}\|\theta\|^2 + 4\Psi^2) \tag{3.47}$$

Also, using the upper bounds in Assumption 3.3, the following inequality holds

$$\frac{B_n}{\Gamma}(|\,\tilde{\theta}^T\dot{\theta}\,|+|\,\tilde{\sigma}\dot{\sigma}\,|)\leq\frac{2B_n}{\Gamma}(\underset{\theta\in\Theta}{max}\|\theta\|d_\theta+\Psi d_\sigma) \tag{3.48}$$

Consequently, if there exists a time $t_1>0$, one has $V(t_1)>\varphi$. Then, from (3.38), (3.40), and (3.47), we can deduce that

$$\frac{1}{2}\tilde{z}^2>\frac{B_n}{\alpha\Gamma}(\underset{\theta\in\Theta}{max}\|\theta\|d_\theta+\Psi d_\sigma) \tag{3.49}$$

or

$$\alpha\tilde{z}^2>\frac{2B_n}{\Gamma}(\underset{\theta\in\Theta}{max}\|\theta\|d_\theta+\Psi d_\sigma) \tag{3.50}$$

Hence, from (3.46) and (3.50) it is easy to conclude that $\dot{V}(t_1)<0$. Moreover, since $z(0)=\hat{z}(0)$ we can verify that for all $t>0$, we have

$$\frac{1}{2}\|\tilde{z}\|^2\leq V(t)\leq V(0)<\frac{B_n}{2\Gamma}(4\underset{\theta\in\Theta}{max}\|\theta\|^2+4\Psi^2)<\varphi \tag{3.51}$$

which results in $\|\tilde{z}\|^2\leq 2\varphi$. Consequently, the fact that $\|.\|_\infty\leq\|.\|$ leads to the bound in (3.36).

Next, using the inequality (3.36) and since $\tilde{z}(t)=\hat{z}(t)-z(t)$, one can have

$$|\,\|\hat{z}_\tau\|_{\mathscr{L}_\infty}-\|z_\tau\|_{\mathscr{L}_\infty}|\leq\sqrt{2\varphi} \tag{3.52}$$

or

$$\|z_\tau\|_{\mathscr{L}_\infty}\leq(\|\hat{z}_\tau\|_{\mathscr{L}_\infty}+\sqrt{2\varphi}) \tag{3.53}$$

Using the frequency domain representation of the predictor dynamics (3.34) and recalling that $G(s)$, $H(s)$, and $C(s)$ are BIBO stable and proper transfer functions. Then, for all $\tau>0$ we have the following upper bound

$$\|\hat{z}_\tau\|_{\mathscr{L}_\infty}\leq\|G(s)\|_{\mathscr{L}_1}\|\hat{\eta}\|_{\mathscr{L}_\infty}+\|z_{in\tau}\|_{\mathscr{L}_\infty} \tag{3.54}$$

Based on Assumption 3.2 and Assumption 3.4, we can conclude that $\hat{\eta}(t)\leq L|z(t)|+L_0+\Psi$. Therefore, we have the upper bound that follows

$$\|\hat{z}_\tau\|_{\mathscr{L}_\infty}\leq\|G(s)\|_{\mathscr{L}_1}L\|z_\tau\|_{\mathscr{L}_\infty}+\|G(s)\|_{\mathscr{L}_1}(L_0+\Psi)+\|z_{in\tau}\|_{\mathscr{L}_\infty} \tag{3.55}$$

Replacing (3.53) in (3.55), we get

$$\|\hat{z}_\tau\|_{\mathscr{L}_\infty}\leq\|G(s)\|_{\mathscr{L}_1}(L(\|\hat{z}_\tau\|_{\mathscr{L}_\infty}+\sqrt{2\varphi})+L_0+\Psi)+\|z_{in\tau}\|_{\mathscr{L}_\infty} \tag{3.56}$$

or by solving for $\|\hat{z}_\tau\|_{\mathscr{L}_\infty}$

$$\|\hat{z}_\tau\|_{\mathscr{L}_\infty} \leq \frac{\|G(s)\|_{\mathscr{L}_1}(L\sqrt{2\varphi}+L_0+\Psi)}{1-\|G(s)\|_{\mathscr{L}_1}L} + \frac{\|z_{in\tau}\|_{\mathscr{L}_\infty}}{1-\|G(s)\|_{\mathscr{L}_1}L} \tag{3.57}$$

We know that L, $\sqrt{2\varphi}$, L_0, Ψ are finite values and z_{in} is uniformly bounded. Then, if the condition in (3.23) is fulfilled, one obtains that $\|\hat{z}_\tau\|_{\mathscr{L}_\infty}$ is uniformly bounded, that completes the proof. □

Proposition 3.1. For the system in (3.1) and the controller defined via (3.14), (3.17), (3.18), and (3.19), if the low-pass filter $C(s)$ and the design parameter α fulfill the condition in (3.23), we have

$$\begin{aligned} &\|(z_{ref}(s)-z(s))_\tau\|_{\mathscr{L}_\infty} \leq \delta_1 \\ &\|(u_{ad_{ref}}(s)-u_{ad}(s))_\tau\|_{\mathscr{L}_\infty} \leq \delta_2 \end{aligned} \tag{3.58}$$

and

$$\begin{aligned} &\lim_{\Gamma\to\infty}(z_{ref}(t)-z(t)) = 0 \\ &\lim_{\Gamma\to\infty}(u_{ad_{ref}}(t)-u_{ad}(t)) = 0 \end{aligned} \tag{3.59}$$

where

$$\delta_1 = \frac{\|C(s)\|_{\mathscr{L}_1}}{1-\|G(s)\|_{\mathscr{L}_1}L}\sqrt{2\varphi} \tag{3.60}$$

and

$$\delta_2 = \|C(s)\|_{\mathscr{L}_1}L\delta_1 + \|H_1(s)\|_{\mathscr{L}_1}\sqrt{2\varphi} \tag{3.61}$$

with $H_1(s) = \frac{C(s)}{H(s)}$ is a stable and proper transfer function. □

Proof. From (3.28) and (3.33), one can have

$$z_{ref}(s)-z(s) = G(s)\eta_e(s) + C(s)H(s)\tilde{\eta}(s) \tag{3.62}$$

where $\eta_e(s)$ is the Laplace transform of $\eta_e(t) = \theta^T(t)(x_{ref}(t)-x(t))$, which can be bounded based on Assumption 3.4 as

$$\|\eta_{e\tau}\|_{\mathscr{L}_\infty} \leq L\|(z_{ref}(s)-z(s))_\tau\|_{\mathscr{L}_\infty} \tag{3.63}$$

Replacing (3.35) in (3.62), one can have

$$z_{ref}(s)-z(s) = G(s)\eta_e(s) + C(s)\tilde{z}(s) \tag{3.64}$$

Since $G(s)$, $H(s)$, and $C(s)$ are BIBO stable and proper transfer functions. Then, for all $\tau > 0$ we have the following upper bound

$$\|(z_{ref}(s)-z(s))_\tau\|_{\mathscr{L}_\infty} \leq \|G(s)\|_{\mathscr{L}_1}L\|(z_{ref}(s)-z(s))_\tau\|_{\mathscr{L}_\infty} + \|C(s)\|_{\mathscr{L}_1}\|\tilde{z}_\tau\|_{\mathscr{L}_\infty} \tag{3.65}$$

Solving for $\|(z_{ref}(s)-z(s))_\tau\|_{\mathscr{L}_\infty}$, results in

$$\|(z_{ref}(s)-z(s))_\tau\|_{\mathscr{L}_\infty} \leq \frac{\|C(s)\|_{\mathscr{L}_1}}{1-\|G(s)\|_{\mathscr{L}_1}L}\sqrt{2\varphi} \tag{3.66}$$

We know that $\sqrt{2\varphi}$ is a finite value and $C(s)$ is uniformly bounded, then if the condition in (3.23) is fulfilled, one obtains that $\|(z_{ref}(s)-z(s))_\tau\|_{\mathscr{L}_\infty}$ is uniformly bounded.

To demonstrate the second bound of (3.58), we can deduce the subsequent relation from (3.19) and (3.24)

$$u_{ad_{ref}}(s)-u_{ad}(s) = -C(s)\eta_{ref}(s)+C(s)\hat{\eta}(s) \tag{3.67}$$

Adding and subtracting $C(s)\eta(s)$, yields in

$$u_{ad_{ref}}(s)-u_{ad}(s) = -C(s)\eta_e(s)+C(s)\tilde{\eta}(s) \tag{3.68}$$

According to the work in [44] and using (3.35), we can write $C(s)\tilde{\eta}(s)$ in the following form

$$C(s)\tilde{\eta}(s) = \frac{C(s)}{H(s)}H(s)\tilde{\eta}(s) \tag{3.69}$$

or

$$C(s)\tilde{\eta}(s) = H_1(s)\tilde{z}(s) \tag{3.70}$$

Consequently, the equation (3.68) can be written as

$$u_{ad_{ref}}(s)-u_{ad}(s) = -C(s)\eta_e(s)+H_1(s)\tilde{z}(s) \tag{3.71}$$

According to the fact that $C(s)$ is BIBO stable and strictly proper transfer function, $H_1(s)$ is a proper and stable system. Therefore, we have the following upper bound for all $\tau > 0$

$$\|(u_{ad_{ref}}(s)-u_{ad}(s))_\tau\|_{\mathscr{L}_\infty} \leq \|C(s)\|_{\mathscr{L}_1}\|\eta_{e\tau}\|_{\mathscr{L}_\infty}+\|H_1(s)\|_{\mathscr{L}_1}\|\tilde{z}_\tau\|_{\mathscr{L}_\infty} \tag{3.72}$$

using the bounds $\|\eta_{e\tau}\|_{\mathscr{L}_\infty} \leq L\|(z_{ref}(s)-z(s))_\tau\|_{\mathscr{L}_\infty}$ and $\|\tilde{z}_\tau\|_{\mathscr{L}_\infty} \leq \sqrt{2\varphi}$ to deduce that

$$\|(u_{ad_{ref}}(s)-u_{ad}(s))_\tau\|_{\mathscr{L}_\infty} \leq \|C(s)\|_{\mathscr{L}_1}L\frac{\|C(s)\|_{\mathscr{L}_1}}{1-\|G(s)\|_{\mathscr{L}_1}L}\sqrt{2\varphi}+\|H_1(s)\|_{\mathscr{L}_1}\sqrt{2\varphi} \tag{3.73}$$

Since $\sqrt{2\varphi}$ and L are finite values and based on the fact that $C(s)$ and $H_1(s)$ are uniformly bounded. Then, if the condition in (3.23) is fulfilled, one obtains that $\|(u_{ad_{ref}}(s)-u_{ad}(s))_\tau\|_{\mathscr{L}_\infty}$ is uniformly bounded.

Next, for the second part of the proof we can easily confirm that φ defined in (3.38) is subject to the following limit $\lim_{\Gamma\to\infty}\varphi = 0$ which leads to conclude that $\lim_{\Gamma\to\infty}\delta_1 = 0$ and $\lim_{\Gamma\to\infty}\delta_2 = 0$. Since $\|(z_{ref}(s)-z(s))_\tau\|_{\mathscr{L}_\infty} \leq \delta_1$ and $\|(u_{ad_{ref}}(s)-u_{ad}(s))_\tau\|_{\mathscr{L}_\infty} \leq \delta_2$, we can confirm that $\lim_{\Gamma\to\infty}(z_{ref}(t)-z(t)) = 0$ and $\lim_{\Gamma\to\infty}(u_{ad_{ref}}(t)-u_{ad}(t)) = 0$, which completes the proof. □

Remark 3.4. The representation of φ Lemma 3.2 a proves that the prediction error can

be improved arbitrarily by increasing the adaptation gain Γ and the design parameter α. In addition, the closed-loop ideal reference system in (3.24) is able to deliver the optimal performance of the proposed controller since its architecture depends on the unknown terms $\sigma(t)$ and $\theta(t)$; this system is the result of eliminating the uncertainties within a specific frequency. Hence, according to Proposition 3.1, this optimal performance can be archived by the proposed controller since it can derive the signals $z(t)$ and $u(t)$ to track those of the reference signal. □

Remark 3.5. The proposed FOL1AC can be used to control a general class of uncertain FOSs. Compared with the existing adaptive control schemes in [143–145], rapid adaptation is possible without losing robustness since the estimation and control loops are separated. In contrast to the sliding mode controllers in [146, 147], the resulting control signal in the presented controller is smooth and bounded. Contrary to the backstepping control methods in [148, 149], which are afflicted by the issue of explosion of complexity, the structure of the controller in this work is easy to implement in real time. □

3.5 Simulation Results

In this section, we will perform a numerical simulation to confirm the validity and effectiveness of the proposed FOL1AC. The simulation will be based on the designed controller, including a control law in the form of (3.19) with adaptation laws as in (3.18), and a predictor in the form of (3.17). Towards this end, let us consider a system in the form of (3.1) such that

$$A = \begin{bmatrix} 0 & 1 \\ 1 & 1.5 \end{bmatrix}, B = \begin{bmatrix} 0 \\ 1 \end{bmatrix}, C = \begin{bmatrix} 1 \\ 0 \end{bmatrix} \text{ and } \beta = 0.95 \tag{3.74}$$

where the convex set Θ and the positive constant Ψ considered in Assumption 3.2 are defined within this simulation study by $\Theta = \{\rho = [r_1, r_2]^T \in \mathbb{R}^2 : r_i \in [-6, 6], i = 1, 2\}$ and $\Psi = 50$. The design parameters Γ, λ, and α are chosen to reach the best performances, and their values are set based on trial and error as $\Gamma = 100000$, $\lambda = [11.5, 4.3]^T$ and $\alpha = 100$. In addition, the designed low-pass filter $C(p)$ introduced in (3.20) is selected as $C(s) = \frac{16}{p+16}$. The initial conditions of the system are set as $x_0 = [2, 0]^T$. Finally, the dynamics of the systems are simulated for $25s$, and the parameters of Oustaloup's filter are fixed as $\omega_b = 10^{-3}$, $\omega_h = 10^3$, and the approximation order $N = 5$. Two simulation cases will be illustrated, each one is performed for two reference signals $y_{d1} = 5$ and $y_{d2} = 5sin(0.5t)$. The first case is when both uncertainties and external disturbances are constants, i.e., $\theta_1 = [4, -3.5]^T$ and $\sigma_1 = 2$. Secondly, we examine the ability of the controller under time-varying uncertainties and external disturbances, i.e., $\theta_2 = \left[2 + cos(\frac{\pi}{2}t), 2 + 0.4sin(\pi t) + 0.3cos(2t)\right]^T$ and $\sigma_2 = cos(\frac{\pi}{2}t)$.

3.5.1 Case of Constant Uncertainties

Figures 3.2-3.11 present system responses to constant uncertainties and external disturbances. Figure 3.2 illustrates the actual output y for the reference signal y_{d1} and Figure 3.7 for the reference signal y_{d2}. The resulting errors e_1 and e_2 for y_{d1} and y_{d2} are reported in Figure 3.4 and Figure 3.9, respectively. These results confirm that, for both reference signals, the controlled system follows its references with satisfactory transient behaviors and small response times, about $t_r = 1.5s$ for y_{d1} and $t_r = 1s$ for y_{d2}. Besides, the time evolution of the fractional-order sliding surface z presented in Figure 3.5 and Figure 3.10 show that z rapidly converges to its prediction $\hat{z}$. The curves of the control input u are smooth as illustrated in Figure 3.3 and Figure 3.8. From Figure 3.6 and Figure 3.11, one can conclude that the controller is able to achieve a good estimation $\hat{\eta}$ of the bounded uncertain quantity η, which minimizes its effects on overall control performances.

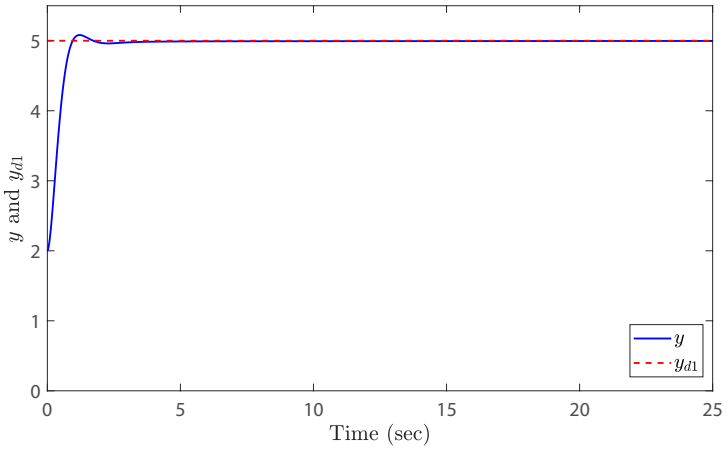

Figure 3.2: Actual output y and reference signal y_{d1} in the case of constant uncertainties and disturbances.

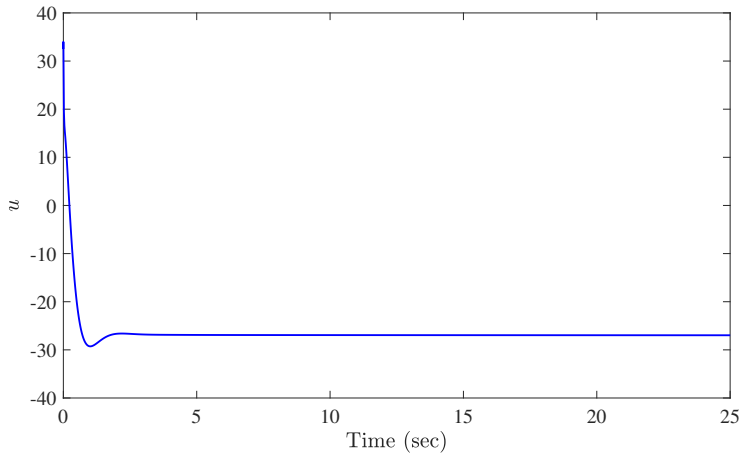

Figure 3.3: Control signal u for reference signal y_{d1} in the case of constant uncertainties and disturbances.

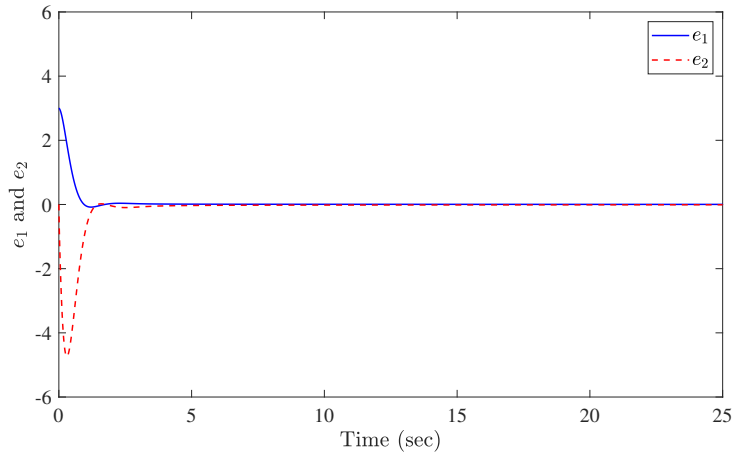

Figure 3.4: Tracking errors e_1 and e_2 for reference signal y_{d1} in the case of constant uncertainties and disturbances.

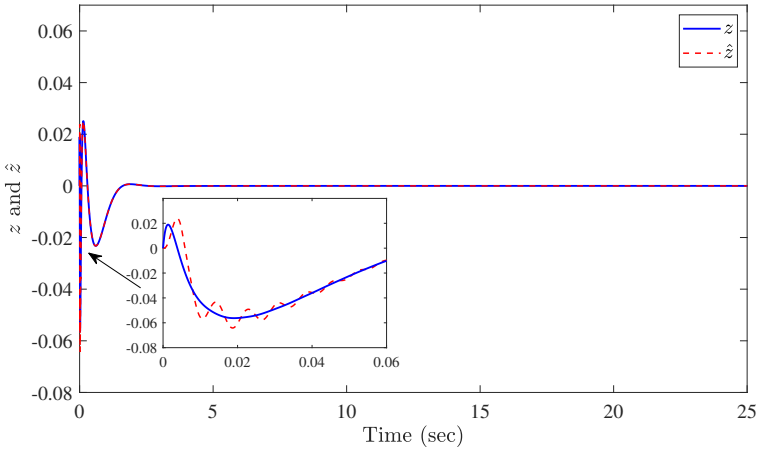

Figure 3.5: Sliding surface z and its predictor $\hat{z}$ for reference signal y_{d1} in the case of constant uncertainties and disturbances.

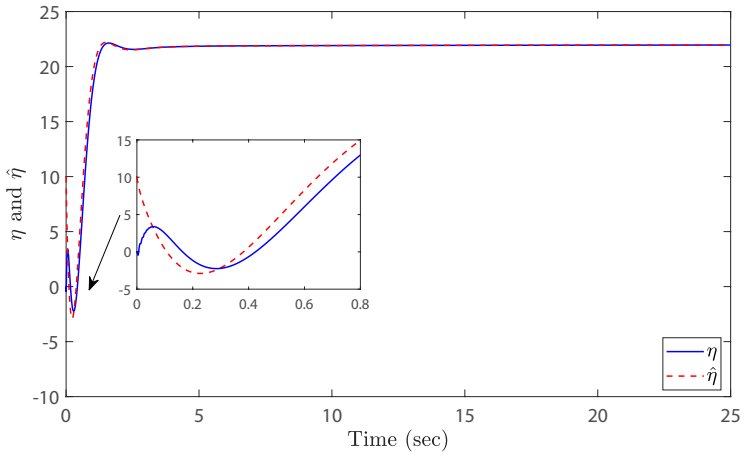

Figure 3.6: Uncertain quantity η and its estimation $\hat{\eta}$ for reference signal y_{d1} in the case of constant uncertainties and disturbances.

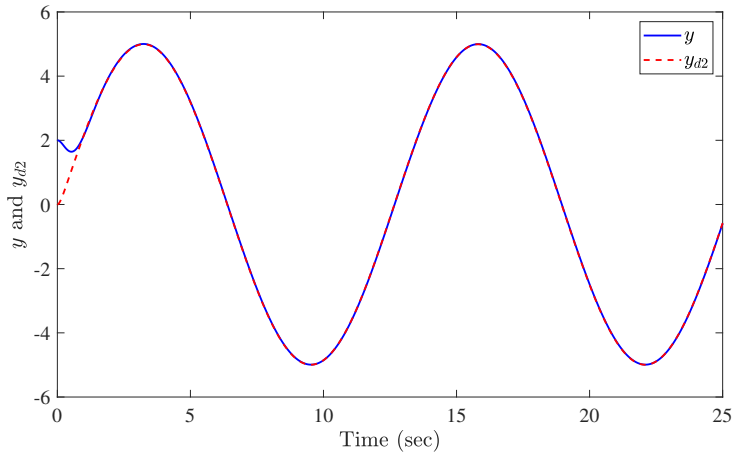

Figure 3.7: Actual output y and reference signal y_{d2} in the case of constant uncertainties and disturbances.

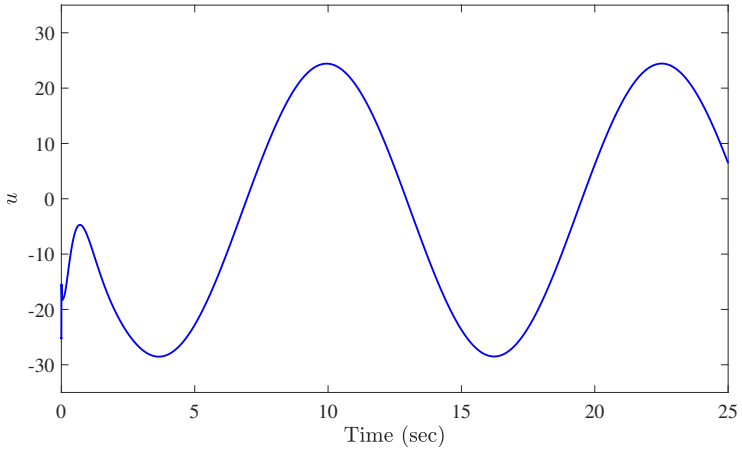

Figure 3.8: Control signal u for reference signal y_{d2} in the case of constant uncertainties and disturbances.

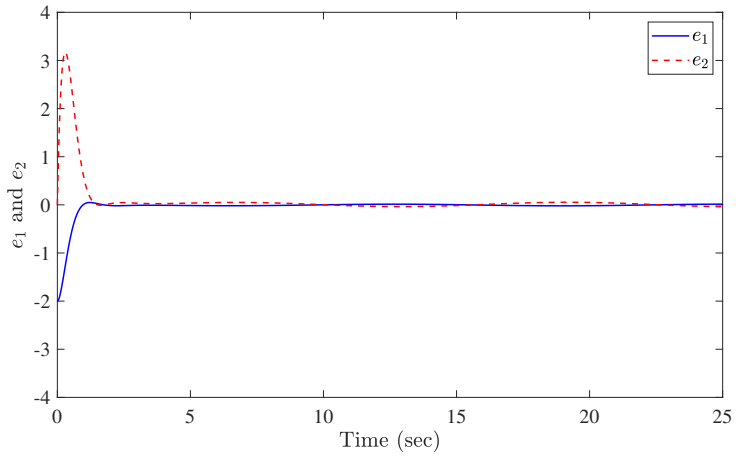

Figure 3.9: Tracking errors e_1 and e_2 for reference signal y_{d2} in the case of constant uncertainties and disturbances.

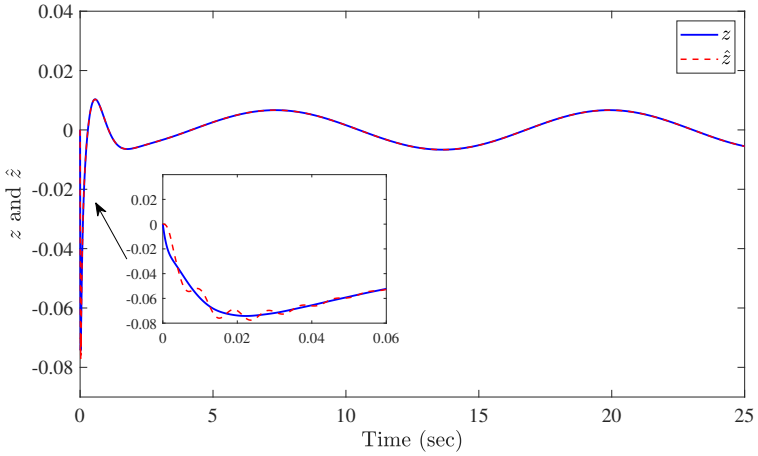

Figure 3.10: Sliding surface z and its predictor $\hat{z}$ for reference signal y_{d2} in the case of constant uncertainties and disturbances.

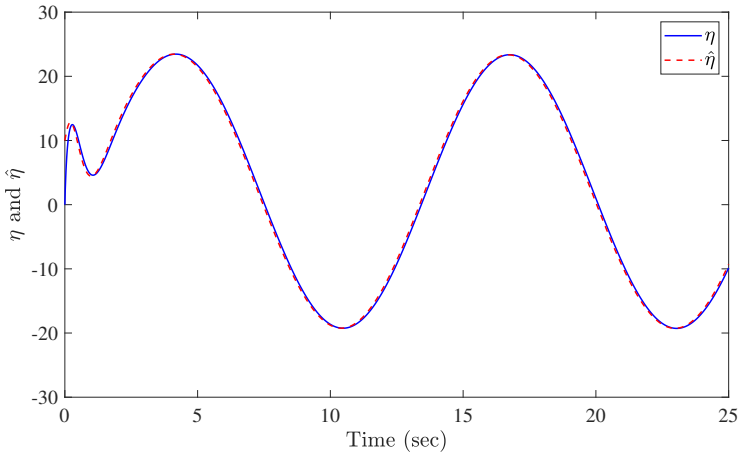

Figure 3.11: Uncertain quantity η and its estimation $\hat{\eta}$ for reference signal y_{d2} in the case of constant uncertainties and disturbances.

3.5.2 Case of Time-varying Uncertainties

System responses for time-varying uncertainties and external disturbance are reported in Figures 3.12-3.21. System actual responses y for the reference signals y_{d1} and y_{d2} are represented in Figure 3.12 and Figure 3.17, respectively. Figure 3.14 illustrates both tracking errors e_1 and e_2 for the reference signal y_{d1}, and Figure 3.19 plots these errors for y_{d2}. The overall results affirm that, even in the presence of time-varying uncertainties and external disturbance, the controller is able to achieve a satisfactory tracking response while maintaining decent transient performances.

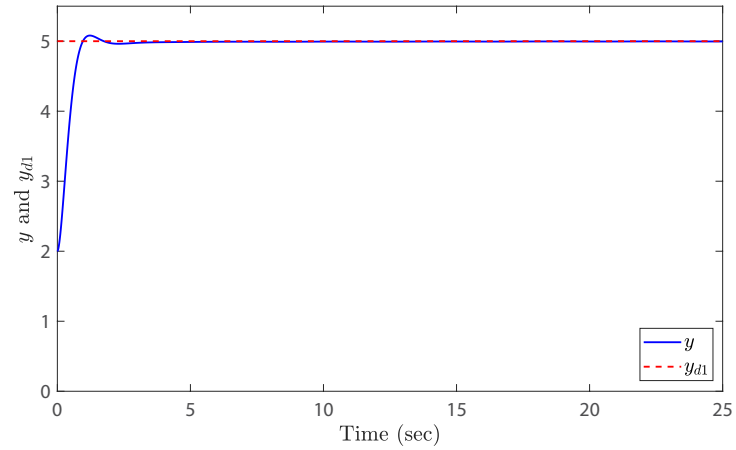

Figure 3.12: Actual output y and reference signal y_{d1} in the case of time-varying uncertainties and disturbances.

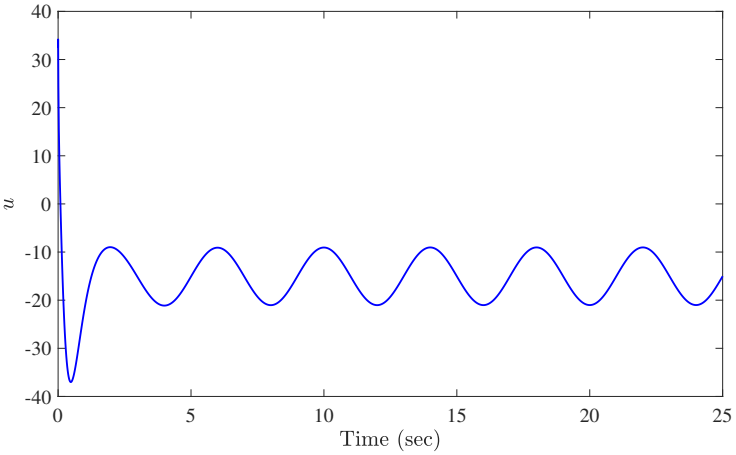

Figure 3.13: Control signal u for reference signal y_{d1} in the case of time-varying uncertainties and disturbances.

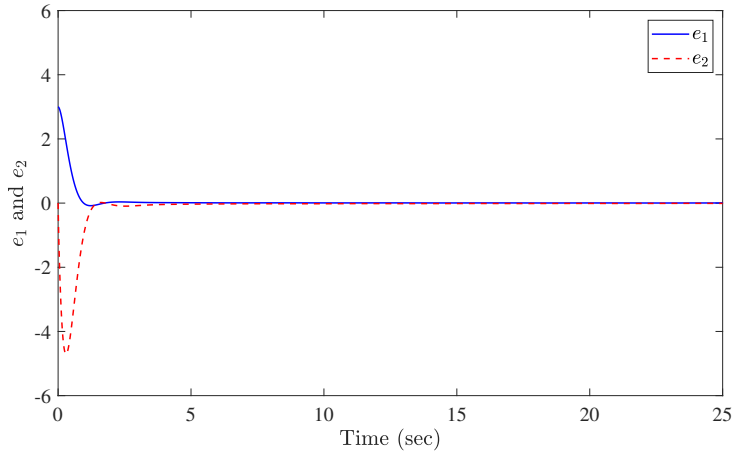

Figure 3.14: Tracking errors e_1 and e_2 for reference signal y_{d1} in the case of time-varying uncertainties and disturbances.

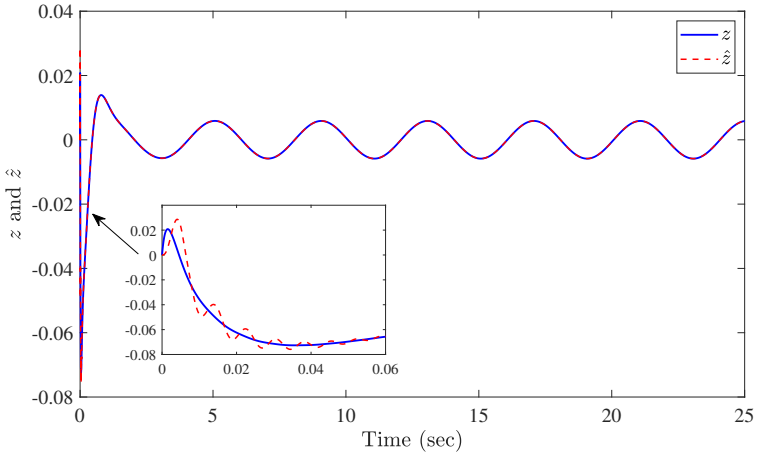

Figure 3.15: Sliding surface z and its predictor $\hat{z}$ for reference signal y_{d1} in the case of time-varying uncertainties and disturbances.

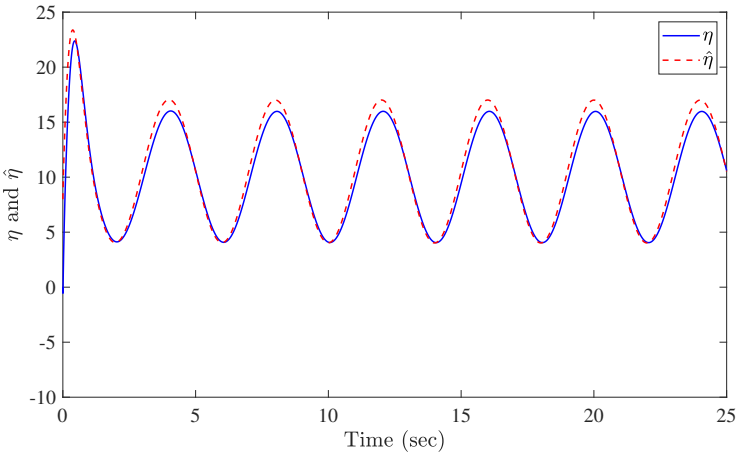

Figure 3.16: Uncertain quantity η and its estimation $\hat{\eta}$ for reference signal y_{d1} in the case of time-varying uncertainties and disturbances.

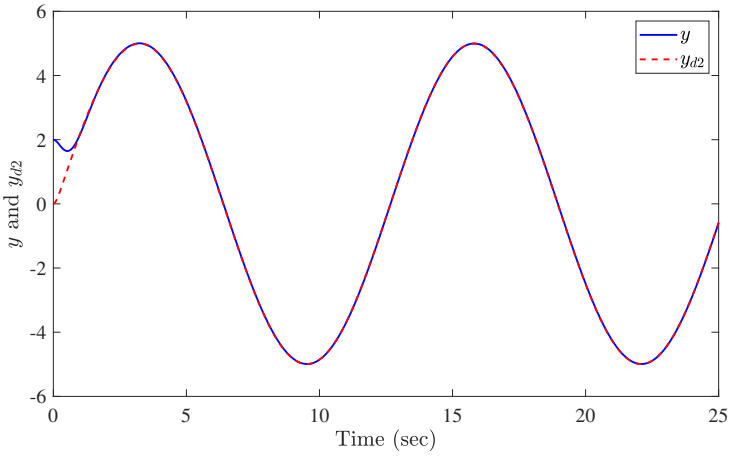

Figure 3.17: Actual output y and reference signal y_{d2} in the case of time-varying uncertainties and disturbances.

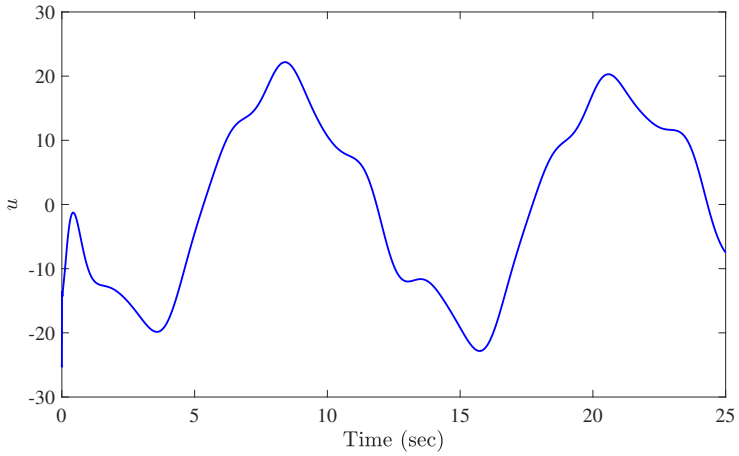

Figure 3.18: Control signal u for reference signal y_{d2} in the case of time-varying uncertainties and disturbances.

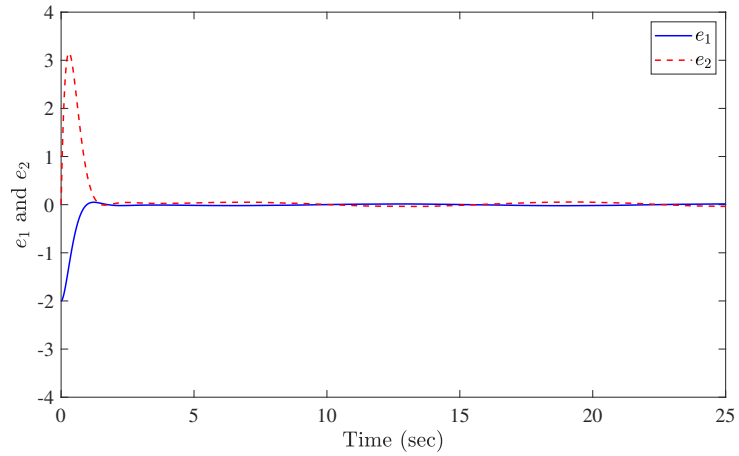

Figure 3.19: Tracking errors e_1 and e_2 for reference signal y_{d2} in the case of time-varying uncertainties and disturbances.

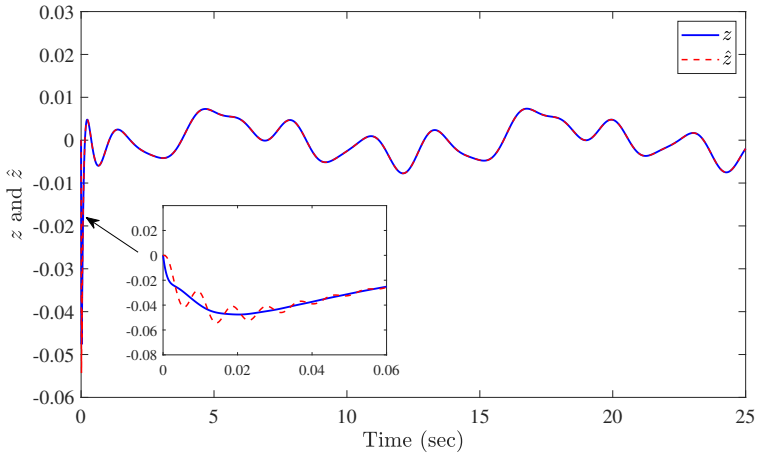

Figure 3.20: Sliding surface z and its predictor $\hat{z}$ for reference signal y_{d2} in the case of time-varying uncertainties and disturbances.

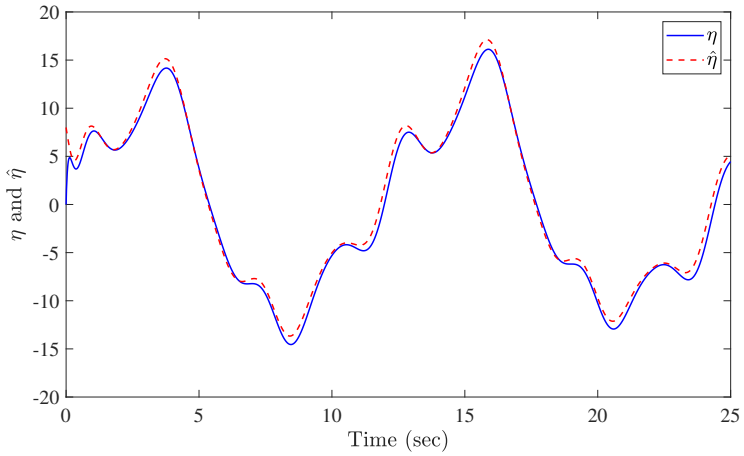

Figure 3.21: Uncertain quantity η and its estimation $\hat{\eta}$ for reference signal y_{d2} in the case time-varying uncertainties and disturbances.

Furthermore, Figure 3.13 and Figure 3.18 show a smooth bounded plot of the control signal u for both $y_{d1}$and y_{d2}. Moreover, In Figure 3.15 and Figure 3.20, we can see a fast tracking response of the fractional-order sliding surface z to its stable predictor $\hat{z}$. Finally, good estimations of the uncertain quantity η are depicted in Figure 3.16 and Figure 3.21, which confirm the robustness of the proposed controller and its ability to handle the considered uncertainties.

3.5.3 Comparative Study

To further assess the benefits of the proposed controller, a comparative study of the FOL1AC against the FOSMC suggested in [146] is executed under the same conditions and for the two reference signals $y_{d1}$and y_{d2}. We consider the case of time-varying uncertainties and external disturbances where $\theta_3 = \left[2 + cos(\frac{\pi}{2}t), 2 + 0.4sin(\pi t) + 0.3cos(2t)\right]^T$ and $\sigma_3 = \frac{1}{2} + \frac{3}{2}cos(\frac{\pi}{2}t)$.

In order to emphasize the control performances of the suggested method, we examine the characteristic of the tracking error e_1 resulting from the FOL1AC and FOSMC in the duration between $t_1 = 5s$ and $t_2 = 25s$ of the simulation. The resulting average absolute value of e_1 over the considered amount of test time, the range of e_1, and its Standard Deviation (STD) can be seen in Table 3.1 and Table 3.2 for the two reference signals y_{d1} and y_{d2}, respectively. The collected results confirm that the proposed FOL1AC yields in a faster response time (see Figure 3.22 and Figure 3.24) with better tracking performances (see Table 3.1 and Table 3.2). In addition, unlike the resulting smooth control signals of FOL1AC depicted in Figure 3.23 (top) and Figure 3.25 (top), the time evolution of the fractional-order sliding mode control signals which are illustrated in Figure 3.23 (bottom) and Figure 3.25 (bottom) suffer from the undesirable chattering problem. Besides, the FOSMC requires the knowledge of the uncertain quantity $\theta^T X$ for its implementation which is not the case for the proposed controller.

Table 3.1: Precision comparisons between the proposed fractional-order $\mathscr{L}_1$ adaptive control and the fractional-order sliding mode controller for the reference signal y_{d1}.

Control method	$Avg(abs(e_1)) \times 10^{-3}$	Range of $e_1 \times 10^{-3}$	STD of $e_1 \times 10^{-3}$
FOL1AC	5.40	$(2.73, 10.79)$	1.69
FOSMC [146]	7.33	$(3.95, 18.51)$	2.95

Table 3.2: Precision comparisons between the proposed fractional-order $\mathscr{L}_1$ adaptive control and the fractional-order sliding mode controller for the reference signal y_{d2}.

Control method	$Avg(abs(e_1)) \times 10^{-3}$	Range of $e_1 \times 10^{-3}$	STD of $e_1 \times 10^{-3}$
FOL1AC	11.45	$(-21.01, 15.48)$	12.18
FOSMC [146]	13.49	$(-23.87, 16.02)$	14

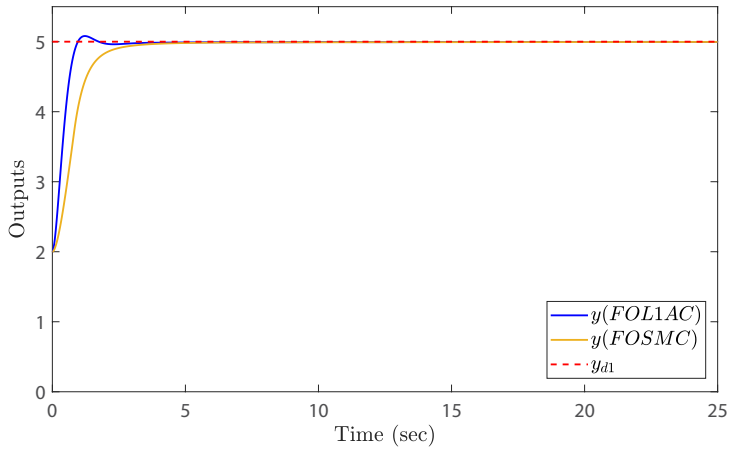

Figure 3.22: Comparative study for the reference signal y_{d1} in the case of time-varying uncertainties and disturbances θ_3 and σ_3.

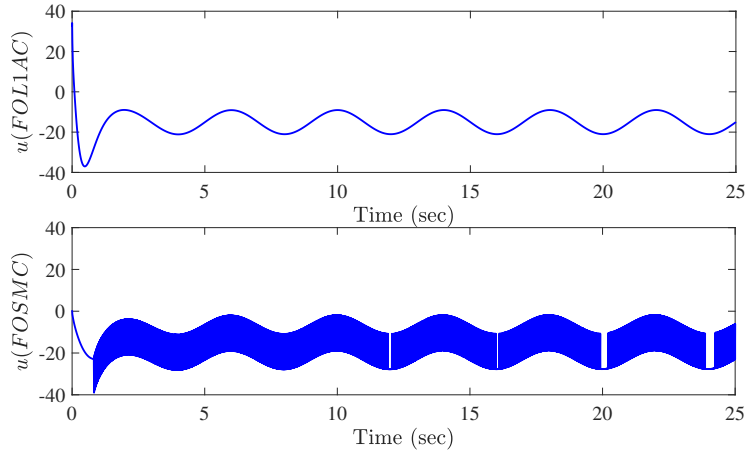

Figure 3.23: Comparative study for the reference signal y_{d1}. Top. fractional-order $\mathscr{L}_1$ adaptive control signal. Bottom. fractional-order sliding mode control signal.

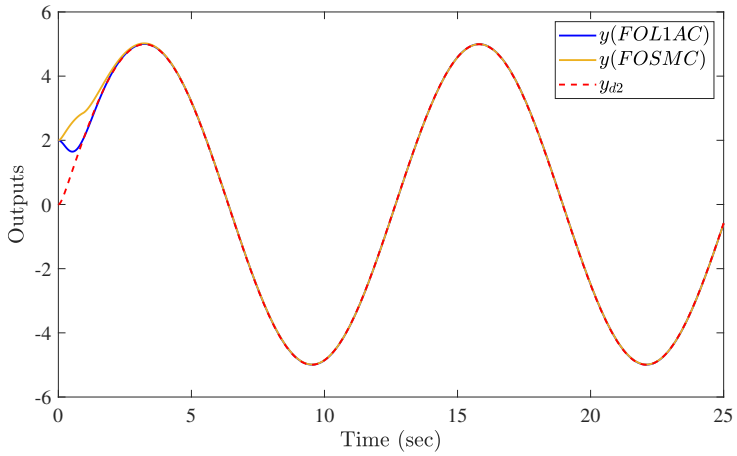

Figure 3.24: Comparative study for the reference signal y_{d2} in the case of time-varying uncertainties and disturbances θ_3 and σ_3.

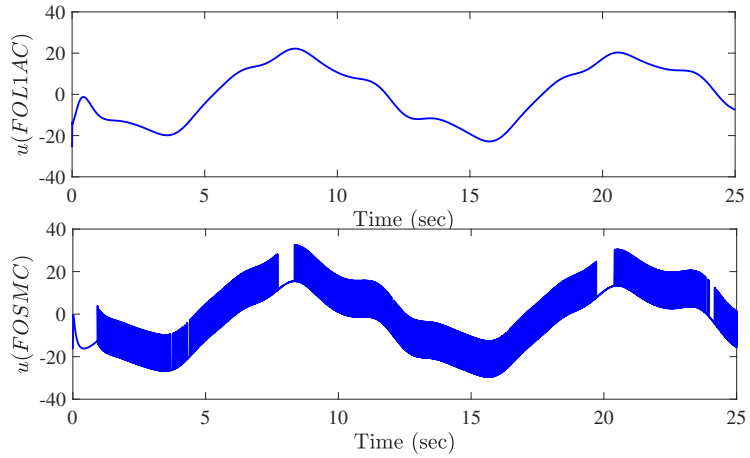

Figure 3.25: Comparative study for the reference signal y_{d2}. Top. fractional-order $\mathscr{L}_1$ adaptive control signal. Bottom. fractional-order sliding mode control signal.

3.6 Conclusion

This chapter presents the development of a FOL1AC strategy for a class of FOSs, subject to uncertainties and external disturbances. The architecture of the controller comprises several components, namely a fractional-order sliding surface, a control law, an adaptive mechanism, and a predictor. Theoretical findings indicate that both input and output system signals converge to those of a stable closed-loop reference system. Furthermore, the controller has the capability to perform a fast tracking response with satisfactory transient performances. The low-pass filter integrated into the control structure guarantees a fast adaptation without losing robustness. Numerical simulations illustrate that the controller is able to robustly deal with constant and time-varying uncertainties and external disturbances, which agrees with the theoretical finding and confirms the effectiveness and validity of the proposed controller.

Chapter 4

Multivariable $\mathscr{L}_1$ Adaptive Control Design for Fractional-Order Systems with Constant Input Gain

4.1 Introduction

In the previous chapter, the $\mathscr{L}_1$ adaptive methodology has been effectively expanded to encompass the control of FOSs that are subject to matched uncertainties and bounded time-varying external disturbances. Notably, the aforementioned investigations did not study the case of incommensurate systems with unknown input gain. Thus, the objective of this chapter is to broaden the scope of the proposed FOL1AC by introducing a novel MFOL1AC. The latter is designed for a large class of uncertain systems with constant input gain that have not been discussed in this thesis. Examples of such include fractional-order hyper-chaotic systems, MIMO, and incommensurate FOSs. Furthermore, the designed MFOL1AC does not rely on the structure of the system under consideration, where the uncertainties are estimated through some projective-type adaptation laws. Finally, Similar to previous studies on $\mathscr{L}_1$ adaptive control, the proposed approach can deliver a fast and robust response with decent transient performance despite model uncertainties, external disturbances, unknown input gain, and fast adaptations. The outline of the chapter is given as follows. Section 4.2 throws light on the problem. Section 4.3 introduces the proposed MFOL1AC. Section 4.4 discusses the stability analysis of the proposed scheme. Section 4.5 investigates the validity of the controller via some simulation results. Section 4.6 concludes this chapter.

4.2 Problem Formulation

This section deals with the description of the class of systems under consideration and specifies the control objective. To begin, let us consider a class of MIMO incommensurate

FOSs represented in the subsequent form

$$D^{\beta_i} x_i(t) = f_{xi}(x) + \Delta F_{xi}(x,t) + \sigma_i u_i(t) \tag{4.1}$$

where $i = 1,2,\ldots,n$, D^{β_i} is the Caputo fractional derivative, $0 < \beta_i < 1$ is the derivative order, $x(t) = [x_1(t), x_2(t), \ldots, x_n(t)]^T \in \mathbb{R}^n$ is the pseudo states vector of the system, $f_{xi}(x)$ and $\Delta F_{xi}(x,t)$ are unknown continuous nonlinear functions that represent model uncertainties and external disturbances, respectively, $\sigma_i, i = 1,2,\ldots,n$ are the input gains with respect to $0 < \omega_{li} < \sigma_i < \omega_{ui}$, here, ω_{li}, ω_{ui} are positive constants, and $u(t) = [u_1(t), u_2(t), \ldots, u_n(t)]^T \in \mathbb{R}^n$ is the vector of control signals.

The objective of this chapter is to synthesize a control law $u_i(t)$ based on a fractional-order $\mathscr{L}_1$ adaptive controller to successfully achieve a bounded tracking response of the pseudo states vector $x(t)$ to a bounded vector of reference signals $y_d(t) = [y_{d1}(t), y_{d2}(t), \ldots, y_{dn}(t)]^T \in \mathbb{R}^n$ while compensating the model uncertainties, external disturbances, and input gains, as well as ensuring the boundedness of all other signals.

4.3 Multivariable Fractional-Order $\mathscr{L}_1$ Adaptive Controller

This section discussed the structure of the MFOL1AC, which is developed based on a fractional-order sliding surface for the class of FOSs introduced in (4.1). To proceed with the control design, the following assumption is necessary

Assumption 4.1. The Caputo fractional derivatives $D^{\beta_i} y_{di}(t)$ of the given reference signals are assumed to exist, to be smooth and bounded. □

4.3.1 Choice of an Appropriate Fractional-Order Sliding Surface

Let the tracking errors vector $e(t) = [e_1(t), e_2(t), \ldots, e_n(t)]^T \in \mathbb{R}^n$ be defined as

$$e(t) = x(t) - y_d(t) \tag{4.2}$$

where $e_i(t) = x_i(t) - y_{di}(t)$. Therefore, the error dynamics can be written according to (4.1) as

$$D^{\beta_i} e_i(t) = f_{xi}(x) + \Delta F_{xi}(x,t) + \sigma_i u_i(t) - D^{\beta_i} y_{di} \tag{4.3}$$

Regarding the systems presented in (4.1) and the error dynamics in (4.3), we chose a fractional-order sliding surface as follows

$$z_i(t) = D^{\beta_i - 1} e_i(t) + \int_0^t \lambda_i e_i(t) d\tau \tag{4.4}$$

where $z(t) = [z_1(t), z_2(t), \ldots z_n(t)]^T \in \mathbb{R}^n$, and $\lambda = [\lambda_1, \lambda_2, \ldots, \lambda_n]^T$ is a vector positive design parameters. According to the property given in (1.26), the time derivative of (4.4) is given

as

$$\dot{z}_i(t) = D^{\beta_i} e_i(t) + \lambda_i e_i(t) \tag{4.5}$$

Once $z_i(t) = \dot{z}_i(t) = 0$, the system is known to operate in the sliding surface. Consequently, for a significantly small value of $\dot{z}_i(t)$, i.e., $\dot{z}_i(t) \approx 0$, one can have

$$D^{\beta_i} e_i(t) + \lambda_i e_i(t) = 0 \tag{4.6}$$

we know that $0 < \beta_i < 1$, hence, it is sufficient to fix $\lambda_i > 0$ for all $i = 1, 2, \ldots, n$ to ensure the stability of the sliding mode dynamics in (4.6) . In other words, $\lambda_i > 0$ satisfies the stability condition applied for linear fractional-order systems give in (1.42), i.e., $|arg(-\lambda_i)| > \beta_i \frac{\pi}{2}$.

The above discussion implies that in the case of $z_i(t) = \dot{z}_i(t) = 0$ the sliding surface dynamics are asymptotically stable which ensures that tracking errors converge to zero. Therefore, the purpose of MFOL1AC is to guarantee that the system reaches the fractional-order sliding surface which is true by ensuring that $z_i(t)$ vanishes towards zero.

4.3.2 Control Structure

Replacing $D^{\beta_i} e_i(t)$ from (4.3) in (4.5) to get the following expression

$$\dot{z}_i(t) = f_{xi}(x) + \Delta F_{xi}(x, t) + \sigma_i u_i(t) + \lambda_i e_i(t) - D^{\beta_i} y_{di} \tag{4.7}$$

For simplicity, let us denote a function $h_i(y_d, x)$ as

$$h_i(y_d, x) = \alpha_i z_i(t) + f_{xi}(x) + \Delta F_{xi}(x, t) + \lambda_i e_i(t) - D^{\beta_i} y_{di} \tag{4.8}$$

hence, we can have

$$\dot{z}_i(t) = -\alpha_i z_i(t) + \sigma_i u_i(t) + h_i(y_d, x), z_i(0) = z_{i0} \tag{4.9}$$

with $\alpha = [\alpha_1, \alpha_2, \ldots, \alpha_n]^T$ is a vector of positive constants.

The predictor represented in (4.10) replicates the dynamics described by (4.9) with the unknown function $h_i(y_d, x)$ and the gain σ_i are replaced with their estimated functions $\hat{h}_i(t)$ and $\hat{\sigma}_i(t)$.

$$\dot{\hat{z}}_i(t) = -\alpha_i \hat{z}_i(t) + \hat{\sigma}_i(t) u_i(t) + \hat{h}_i(t), \hat{z}_i(0) = z_{i0} \tag{4.10}$$

where $\hat{z}_i(t) \in \mathbb{R}$ is the prediction of $z_i(t)$. The estimations $\hat{h}_i(t)$ and $\hat{\sigma}_i(t)$ are conducted by the following projection-type adaptation law

$$\begin{aligned} \dot{\hat{\sigma}}_i(t) &= \Gamma_i Proj(\hat{\sigma}_i(t), -\tilde{z}(t)_i u_i(t)) \\ \dot{\hat{h}}_i(t) &= \Gamma_i Proj(\hat{h}_i(t), -\tilde{z}_i(t)) \end{aligned} \tag{4.11}$$

where $\tilde{z}(t) = \hat{z}(t) - z(t) \in \mathbb{R}^n$ is the vector of prediction errors, $\Gamma_i \in \mathbb{R}^+$ is the adaptation

gain, and $Proj(.,.)$ is the projection operator introduced in Definition 2.3.

The control law u_i is employed as

$$u_i(s) = -K_i D(s)\hat{\eta}_i(s) \tag{4.12}$$

where $\hat{\eta}_i(s)$ is the Laplace transform of $\hat{\eta}(t) = \hat{\sigma}_i(t)u_i(t) + \hat{h}_i(t)$, $K = [K_1, K_2, \ldots, K_n]^T$ is a vector of positive feedback gains, and $D(s)$ is a strictly proper transfer function, which is included in the expression of a stable proper closed-loop filter as

$$\hat{C}_i(s) = \frac{\hat{\sigma}_i K_i D(s)}{1 + \hat{\sigma}_i K_i D(s)} \tag{4.13}$$

consequently, the resulting form of the filter $\hat{C}_i(s)$ in (4.13) can represent a low-pass first-order filter with the choice of the transfer function $D(s)$ as $D(s) = \frac{1}{s}$, which gives

$$\hat{C}_i(s) = \frac{\hat{\sigma}_i K_i}{s + \hat{\sigma}_i K_i} \tag{4.14}$$

where $\hat{C}_i(0) = 1$.

4.4 Stability and Performances Analysis

This section analyzes the performances and the stability of the developed controller, for that reason the subsequent assumptions are necessary

Assumption 4.2. The nonlinear function $h_i(y_d, x)$ is assumed to accept the following bound

$$|h_i(y_d, x)| \leq L|z_i(t)| + L_0 \tag{4.15}$$

with L and L_0 are positive constants. □

Assumption 4.3. The derivative of nonlinear function $h_i(y_d, x)$ can be bounded as

$$|\dot{h}_i(y_d, x)| \leq d_{hi} < \infty \tag{4.16}$$

□

The controller proposed in (4.10), (4.11), and (4.12) is subject to the $\mathscr{L}_1$ norm condition given by (4.17) are chosen to fulfill it

$$\|G_i(s)\|_{\mathscr{L}_1} L < 1 \tag{4.17}$$

where $G_i(s) = H_i(s)(1 - C_i(s))$, $H_i(s) = (s + \alpha_i)^{-1}$, $C_i(s) = \frac{\sigma_i K_i}{s + \sigma_i K_i}$ is a low pass filter, and $L > 0$ is introduced in Assumption 4.2. Therefore, the design parameter α_i and the filter $C(s)_i$ are selected to fulfill it.

Remark 4.1. Using the fact that $\alpha_i > 0$ and $C_i(s)$ is a BIBO stable and strictly proper transfer function we can easily conclude that $G_i(s)$ and $H_i(s)$ are also BIBO stable and proper transfer functions. □

4.4.1 Closed-loop Ideal Reference System

Let us consider now a well-behaving reference system that stands for the closed-loop non-adaptive description of the system in (4.1) with the controller given by (4.10), (4.11), and (4.12). This system is given as

$$\begin{cases} \dot{z}_{iref}(t) = -\alpha_i z_{iref}(t) + \sigma_i u_{iref}(t) + h_i(x_{ref}) \\ u_{iref}(s) = -\dfrac{C_i(s)}{\sigma_i}\eta_{iref}(s) \end{cases} \tag{4.18}$$

where $z_{iref}(0) = z_{i0}$ and $\eta_{iref}(s)$ is the Laplace transform of $\eta_{iref}(t) = h_i(x_{ref})$.

Remark 4.2. The reference system in (4.18) is able to deliver the best achievable performance of the proposed controller since its architecture depends on the unknown function h_i and input gain σ_i. However, its utilization is limited to stability and performance analysis only. □

Lemma 4.1. Let us consider that both the design parameter α_i and the filter $C_i(s)$ satisfy the $\mathscr{L}_1$ norm condition in (4.17), then with regards to the closed-loop reference system representation in (4.18), the bound given bellow holds

$$\|z_{iref\tau}\|_{\mathscr{L}_\infty} \leq \rho_i \tag{4.19}$$

where

$$\rho_i = \frac{\|G_i(s)\|_{\mathscr{L}_1}}{1 - L\|G_i(s)\|_{\mathscr{L}_1}} L_0 + \frac{1}{1 - L\|G_i(s)\|_{\mathscr{L}_1}} \|\overline{z}_{i\tau}\|_{\mathscr{L}_\infty} \tag{4.20}$$

with $\overline{z}_i = (s + \alpha_i)^{-1} z_{i0}$. □

Proof. From the representation of the closed-loop reference system (4.18), and using the Laplace transform formulation, one has

$$sz_{iref}(s) - z_{i0} = -\alpha_i z_{iref}(s) + \sigma_i u_{iref}(s) + \eta_{iref}(s) \tag{4.21}$$

by replacing $u_{iref}(s)$, we can have

$$z_{iref}(s) = G_i(s)\eta_{iref}(s) + \overline{z}_i \tag{4.22}$$

It is obvious that $\overline{z}_i$ is uniformly bounded and according to Remark 4.1, the following upper bound is valid for all $\tau > 0$

$$\|z_{iref\tau}\|_{\mathscr{L}_\infty} \leq \|G_i(s)\|_{\mathscr{L}_1} \|\eta_{iref\tau}\|_{\mathscr{L}_\infty} + \|\overline{z}_{i\tau}\|_{\mathscr{L}_\infty} \tag{4.23}$$

Using Assumption 4.2, we can conclude that $\|\eta_{iref\tau}\|_{\mathscr{L}_\infty} \leq L\|z_{iref\tau}\|_{\mathscr{L}_\infty} + L_0$. Hence

$$\|z_{iref\tau}\|_{\mathscr{L}_\infty} \leq \frac{\|G_i(s)\|_{\mathscr{L}_1}}{1 - L\|G_i(s)\|_{\mathscr{L}_1}} L_0 + \frac{1}{1 - L\|G_i(s)\|_{\mathscr{L}_1}} \|\overline{z}_{i\tau}\|_{\mathscr{L}_\infty} \tag{4.24}$$

We know that L_0 is a finite positive value and $\overline{z}_i$ is uniformly bounded. Hence, if the condition in (4.17) is fulfilled, one obtains that $\|z_{iref\tau}\|_{\mathscr{L}_\infty}$ is uniformly bounded, which completes the proof. □

4.4.2 Transient and Steady-state Analysis

In this subsection, we analyze the performances bound between the closed-loop ideal reference system represented in (4.18) and the system (4.1) with the controller given by (4.10), (4.11), and (4.12), both in transient and steady-state.

Let denote $\eta_i(s)$ as the Laplace transform of $\eta_i(t) = h_i(y_d, x)$. Then, the control law given in (4.12) can expanded as

$$u_i(s) = -K_i D(s)(\tilde{\eta}_i(s) + \eta_i(s) + \sigma_i u_i(s)) \tag{4.25}$$

where $\tilde{\eta}_i(s)$ is the Laplace transform of $\tilde{\eta}_i(t) = \tilde{\sigma}_i(t)u_i(t) + \tilde{h}_i(t)$ with $\tilde{\sigma}_i(t)$ and $\tilde{h}_i(t)$ are the estimation errors. Therefore, one can have

$$u_i(s) = -\frac{C_i}{\sigma_i}(\tilde{\eta}_i(s) + \eta_i(s)) \tag{4.26}$$

Consequently, the expression (4.9) can be written in the frequency domain as

$$sz_i(s) - z_{i0} = -\alpha_i z_i(s) - C_i(s)(\tilde{\eta}_i(s) + \eta_i(s)) + \eta_i(s) \tag{4.27}$$

or

$$z_i(s) = G_i(s)\eta_i(s) - C_i(s)H_i(s)\tilde{\eta}_i(s) + \overline{z}_i \tag{4.28}$$

Next, it is easy to find $\tilde{z}_i(t)$ from (4.9) and (4.10) since we have $\tilde{z}_i(t) = \hat{z}_i(t) - z_i(t)$, hence

$$\dot{\tilde{z}}_i(t) = -\alpha_i \tilde{z}_i(t) + \tilde{\sigma}_i(t)u_i(t) + \tilde{h}_i(t), \tilde{z}_i(0) = 0 \tag{4.29}$$

Consequently, it is straightforward to deduce the expression of $\tilde{z}_i(s)$ as

$$\tilde{z}_i(s) = H_i(s)\tilde{\eta}_i(s) \tag{4.30}$$

Lemma 4.2. Regarding the system in (4.9) with the controller presented by (4.10), (4.11), and (4.12), if the low-pass filter $C_i(s)$ and the design parameter α_i fulfill the condition in (4.17), we have the bound that follows

$$\|\tilde{z}_{i\tau}\|_{\mathscr{L}_\infty} \leq \sqrt{2\varphi_i} \tag{4.31}$$

where

$$\varphi_i = \frac{1}{2\Gamma_i}(4\underset{h_i\in\Theta}{max}\|h_i\|^2 + (\omega_{ui}-\omega_{li})^2) + \frac{1}{\alpha_i\Gamma_i}\underset{h_i\in\Theta}{max}\|h_i\|d_{hi} \tag{4.32}$$

□

Proof. Consider the following Lyapunov candidate function

$$V_i(\tilde{z}_i,\tilde{h}_i,\tilde{\sigma}_i) = \frac{1}{2}\tilde{z}_i^2 + \frac{1}{2\Gamma_i}\tilde{h}_i^2 + \frac{1}{2\Gamma_i}\tilde{\sigma}_i^2 \tag{4.33}$$

the time derivative of $V_i(\tilde{z}_i,\tilde{h}_i,\tilde{\sigma}_i)$ in (4.33) is given as

$$\dot{V}_i(\tilde{z}_i,\tilde{h}_i,\tilde{\sigma}_i) = \tilde{z}_i\dot{\tilde{z}}_i + \frac{1}{\Gamma_i}\tilde{h}_i\dot{\tilde{h}}_i + \frac{1}{\Gamma_i}\tilde{\sigma}_i\dot{\tilde{\sigma}}_i \tag{4.34}$$

Since σ_i is a constant and by recalling (4.29), we can have

$$\dot{V}_i(\tilde{z}_i,\tilde{h}_i,\tilde{\sigma}_i) = -\alpha\tilde{z}_i^2 + \tilde{z}_i\tilde{h}_i + \tilde{z}_i\tilde{\sigma}_i u_i + \frac{1}{\Gamma_i}\tilde{h}_i\dot{\hat{h}}_i - \frac{1}{\Gamma_i}\tilde{h}_i\dot{h}_i + \frac{1}{\Gamma_i}\tilde{\sigma}_i\dot{\tilde{\sigma}} \tag{4.35}$$

or

$$\dot{V}_i(\tilde{z}_i,\tilde{h}_i,\tilde{\sigma}_i) = -\alpha\tilde{z}_i^2 + \tilde{h}_i(\frac{1}{\Gamma_i}\dot{\hat{h}}_i + \tilde{z}_i) + \tilde{\sigma}_i(\frac{1}{\Gamma_i}\dot{\hat{\sigma}}_i + \tilde{z}_i u_i) - \frac{1}{\Gamma_i}\tilde{h}_i\dot{h}_i \tag{4.36}$$

according to the adaptation law in (4.11) we can deduce that

$$\dot{V}_i(\tilde{z}_i,\tilde{h}_i,\tilde{\sigma}_i) \le -\alpha\tilde{z}_i^2 + \tilde{h}_i(Proj(\hat{h}_i,-\tilde{z}_i)+\tilde{z}_i) + \tilde{\sigma}_i(Proj(\hat{\sigma}_i,-\tilde{z}_i u_i)+\tilde{z}_i u_i) + \frac{1}{\Gamma_i}\mid\tilde{h}_i\dot{h}_i\mid \tag{4.37}$$

besides, Lemma 2.2 implies that

$$\tilde{h}_i(Proj(\hat{h}_i,-\tilde{z}_i)+\tilde{z}_i) + \tilde{\sigma}_i(Proj(\hat{\sigma}_i,-\tilde{z}_i u_i)+\tilde{z}_i u_i) \le 0 \tag{4.38}$$

that is to say that

$$\dot{V}_i(\tilde{z}_i,\tilde{h}_i,\tilde{\sigma}_i) \le -\alpha\tilde{z}_i^2 + \frac{1}{\Gamma_i}\mid\tilde{h}_i\dot{h}_i\mid \tag{4.39}$$

The projection operator ensures that the estimated value $\hat{h}_i$ remain within the compact set Θ and $|\hat{\sigma}_i| \le \chi$, with $\chi \in [\omega_{li},\omega_{ui}]$. Hence

$$\underset{t\ge 0}{max}(\tilde{h}_i^2 + \tilde{\sigma}_i^2) \le (4\underset{h_i\in\Theta}{max}\|h_i\|^2 + (\omega_{ui}-\omega_{li})^2) \tag{4.40}$$

consequently, the upper bound in Assumption 4.3 implies that

$$\frac{1}{\Gamma_i}\mid\tilde{h}_i\dot{h}_i\mid \le \frac{2}{\Gamma_i}\underset{h_i\in\Theta}{max}\|h_i\|d_{hi} \tag{4.41}$$

For any given time $t_1 > 0$, supposing that $V_i(t_1) > \varphi_i$. Then, based on representation of φ_i and V_i we can write

$$\frac{1}{2}\tilde{z}_i^2 > \frac{1}{\alpha_i\Gamma_i}\underset{h_i\in\Theta}{max}\|h_i\|d_{hi} \tag{4.42}$$

or

$$\alpha_i \tilde{z}_i^2 > \frac{2}{\Gamma_i} \underset{h_i \in \Theta}{max} \|h_i\| d_{hi} \tag{4.43}$$

which also means that $\dot{V}_i(t) < 0$. Moreover, the bound $\|\tilde{z}_\tau\|^2 \leq 2\varphi_i$ can be obtained based on the fact $\tilde{z}(0) = 0$ as

$$\|\tilde{z}\|^2 \leq V(t) \leq V(0) < \frac{1}{2\Gamma_i}(4 \underset{h_i \in \Theta}{max} \|h_i\|^2 + (\omega_{ui} - \omega_{li})^2) < \varphi_i \tag{4.44}$$

Finally, since $\|.\|_\infty \leq \|.\|$, we can have $\|\tilde{z}_\tau\|_{\mathscr{L}_\infty} \leq \sqrt{2\varphi_i}$, that completes the proof. □

Remark 4.3. Lemma 4.2 and the representation of φ_i prove that the prediction error can be improved arbitrarily by increasing the adaptation gain Γ_i and the design parameter α_i. □

Proposition 4.1. Regarding the systems in equations (4.9) and (4.18) with the controller presented by (4.10), (4.11), and (4.12), if the filter $C_i(s)$ and the parameter α_i are chosen to fulfill the condition in (4.17), then, we have the following

$$\begin{aligned} &\|(z_{iref}(s) - z_i(s))_\tau\|_{\mathscr{L}_\infty} \leq \delta_{1i} \\ &\|(u_{iref}(s) - u_i(s))_\tau\|_{\mathscr{L}_\infty} \leq \delta_{2i} \end{aligned} \tag{4.45}$$

$$\begin{aligned} &\lim_{\Gamma_i \to \infty} (z_{iref}(t) - z_i(t)) = 0 \\ &\lim_{\Gamma_i \to \infty} (u_{iref}(t) - u_i(t)) = 0 \end{aligned} \tag{4.46}$$

where

$$\delta_{1i} = \frac{\|C_i(s)\|_{\mathscr{L}_1}}{1 - \|G_i(s)\|_{\mathscr{L}_1} L} \sqrt{2\varphi_i} \tag{4.47}$$

and

$$\delta_{2i} = \|\frac{C_i(s)}{\sigma_i}\|_{\mathscr{L}_1} L\delta_{1i} + \|\frac{H_{1i}(s)}{\sigma_i}\|_{\mathscr{L}_1} \sqrt{2\varphi_i} \tag{4.48}$$

with $H_{1i}(s) = \frac{C_i(s)}{H_i(s)}$ is a stable and proper transfer function. □

Proof. By subtracting (4.28) from (4.22), one can have

$$z_{iref}(s) - z_i(s) = G_i(s)(\eta_{iref}(s) - \eta_i(s)) + C_i(s)H_i(s)\tilde{\eta}_i(s) \tag{4.49}$$

denoting $\eta_{ei}(s) = \eta_{iref}(s) - \eta_i(s)$ and according to (4.30), we can write

$$z_{iref}(s) - z_i(s) = G_i(s)\eta_{ei}(s) + C_i(s)\tilde{z}_i(s) \tag{4.50}$$

The expression of $\eta_{ei}(s)$ can be bounded according to Assumption 4.2 as

$$\|\eta_{ie}(s)_\tau\|_{\mathscr{L}_\infty} \leq L\|(z_{iref}(s) - z_i(s))_\tau\|_{\mathscr{L}_\infty} \tag{4.51}$$

therefore, for all $\tau > 0$ we have the following upper bound

$$\|(z_{iref}(s) - z_i(s))_\tau\|_{\mathscr{L}_\infty} \leq \|G_i(s)\|_{\mathscr{L}_1} L \|(z_{iref}(s) - z_i(s))_\tau\|_{\mathscr{L}_\infty} + \|C_i(s)\|_{\mathscr{L}_1} \sqrt{2\varphi_i} \tag{4.52}$$

solving for $\|(z_{iref}(s) - z_i(s))_\tau\|_{\mathscr{L}_\infty}$, yields in

$$\|(z_{iref}(s) - z_i(s))_\tau\|_{\mathscr{L}_\infty} \leq \frac{\|C_i(s)\|_{\mathscr{L}_1}}{1 - \|G_i(s)\|_{\mathscr{L}_1} L} \sqrt{2\varphi_i} \tag{4.53}$$

We know that $\sqrt{2\varphi_i}$ is a finite value and $C_i(s)$ is uniformly bounded, which means that if $\|G_i(s)\|_{\mathscr{L}_1} L < 1$, then, for all $\tau > 0$ we have that $\|(z_{iref}(s) - z_i(s))_\tau\|_{\mathscr{L}_\infty}$ is uniformly bounded.

Similarly, by subtracting (4.26) from (4.18), one can have

$$u_{iref}(s) - u_i(s) = -\frac{C_i(s)}{\sigma_i} \eta_{ie}(s) + \frac{C_i(s)}{\sigma_i} \tilde{\eta}_i(s) \tag{4.54}$$

The work in [44] and the expression in (4.30) confirm that

$$C_i(s)\tilde{\eta}_i(s) = H_{1i}(s)\tilde{z}_i(s) \tag{4.55}$$

Consequently, the bound $\|\eta_{e\tau}\|_{\mathscr{L}_\infty} \leq L\|(z_{ref}(s) - z(s))_\tau\|_{\mathscr{L}_\infty}$ gives

$$\|(u_{iref}(s) - u_i(s))_\tau\|_{\mathscr{L}_\infty} \leq \|\frac{C_i(s)}{\sigma_i}\|_{\mathscr{L}_1} L\delta_{1i} + \|\frac{H_{1i}(s)}{\sigma_i}\|_{\mathscr{L}_1} \sqrt{2\varphi_i} \tag{4.56}$$

Recalling the facts that $C_i(s)$ and $H_{1i}(s)$ are uniformly bounded transfer functions which means that if $\|G_i(s)\|_{\mathscr{L}_1} L < 1$, then, for all $\tau > 0$ we have that $\|(u_{iref}(s) - u_i(s))_\tau\|_{\mathscr{L}_\infty}$ is uniformly bounded.

Next, for the second part of the proof, it is easy to establish that $\lim_{\Gamma_i \to \infty} \varphi_i = 0$, which implies that $\lim_{\Gamma_i \to \infty} \delta_{1i} = 0$ and $\lim_{\Gamma_i \to \infty} \delta_{2i} = 0$. In addition, we have $\|(z_{iref}(s) - z_i(s))_\tau\|_{\mathscr{L}_\infty} \leq \delta_{1i}$ and $\|(u_{iref}(s) - u_i(s))_\tau\|_{\mathscr{L}_\infty} \leq \delta_{2i}$, that is to say $\lim_{\Gamma_i \to \infty} (z_{iref}(t) - z_i(t)) = 0$ and $\lim_{\Gamma_i \to \infty} (u_{iref}(t) - u_i(t)) = 0$, that completes the proof. □

Remark 4.4. Proposition 4.1 admits that the proposed controller can drive $z_i(t)$ to track the best achievable performances delivered by the reference system (4.18), that is when the value of the adaptation gain Γ_i is large enough. □

4.5 Simulation Results

In this section, we will test the effectiveness and confirm the above theoretical results found on the proposed controller presented by (4.10), (4.11), and (4.12). To this end, two simulation cases are considered along with a comparative study. First, we suggest controlling chaos of the incommensurate fractional-order Hopfield neural chaotic network

[150, 151] which is subject to model uncertainties, external disturbances, and unknown input gain. The second case of simulation is concerned with the chaos suppression of a 4-dimensional fractional-order hyper-chaotic system. The latter is also considered in a comparative study of the MFOL1AC against another fractional-order controller.

4.5.1 Case of Incommensurate Orders

Let us consider the representation of the incommensurate fractional-order Hopfield neural chaotic network, which is given in [150, 151] as

$$\begin{cases} D^{\beta_1} x_1(t) = -x_1(t) + 2tanh(x_1) - 1.2tanh(x_2) + \Delta F_{x1}(x,t) + \sigma_1 u_1(t) \\ D^{\beta_2} x_2(t) = -x_2(t) + 2tanh(x_1) - 1.71tanh(x_2) + 1.15tanh(x_3) + \Delta F_{x2}(x,t) + \sigma_2 u_2(t) \\ D^{\beta_3} x_3(t) = -x_1(t) - 4.75tanh(x_1) + 1.1tanh(x_2) + \Delta F_{x2}(x,t) + \sigma_3 u_3(t) \end{cases} \tag{4.57}$$

with $\Delta F_{x1}(x,t) = 0.2cos(\pi x_2 x_3) \times cos(\pi x_1) \times sin(100t)$, $\Delta F_{x2}(x,t) = 0.2cos(\pi x_1 x_3) \times cos(\pi x_2) \times sin(100t)$, $\Delta F_{x3}(x,t) = -0.2cos(\pi x_2 x_1) \times cos(\pi x_3) \times sin(100t)$, and $\sigma_i = 2, i = 1,2,3$. The fractional-orders are fixed as $\beta = [0.96, 0.97, 0.98]^T$ to ensure that the considered system behaves chaotically [151]. The dynamics of the closed-loop system are simulated for $5s$ with the initial conditions and reference signals are fixed as $x(0) = [2.5, 2, 2.5]^T$ and $y_d(t) = [3cos(2t), 1.5cos(t), 3cos(2t)]^T$, respectively. The initial values of $\hat{h}$ are set to be zero and $\hat{\sigma}(0) = 0.01$ with their bounds in the projection operator are $\hat{\sigma} \in [0.01, 6]$ and $\hat{h} \in [6, -6]$. To reach the best performances, the simulation was executed using the following design parameters acquired through trial and error: $\alpha = [12, 11, 13]^T$, $\Gamma = [4000, 8500, 4500]^T$, and $\lambda_i = 10, i = 1,2,3$. For the filter $C_i(s)$ we chose the feedback gain $K_i = 20, i = 1,2,3$. Finally, the parameters of the Oustaloup's filter are fixed as $\omega_b = 10^{-3}$, $\omega_h = 10^3$, and the approximation order $N = 5$.

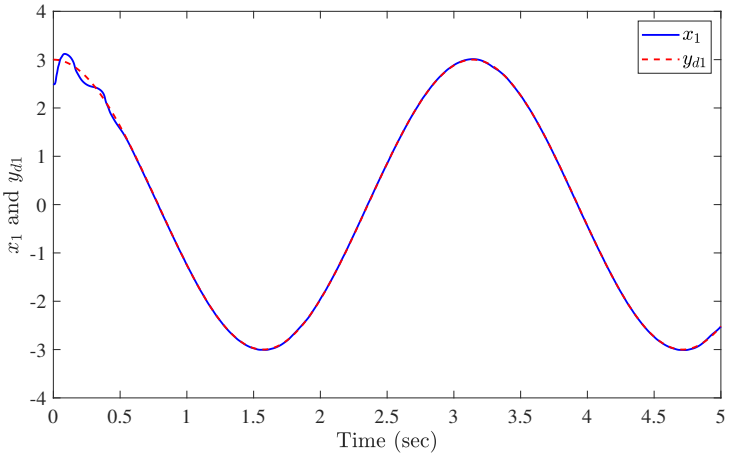

Figure 4.1: Evolution of the state x_1 and y_{d1} in the case of incommensurate orders.

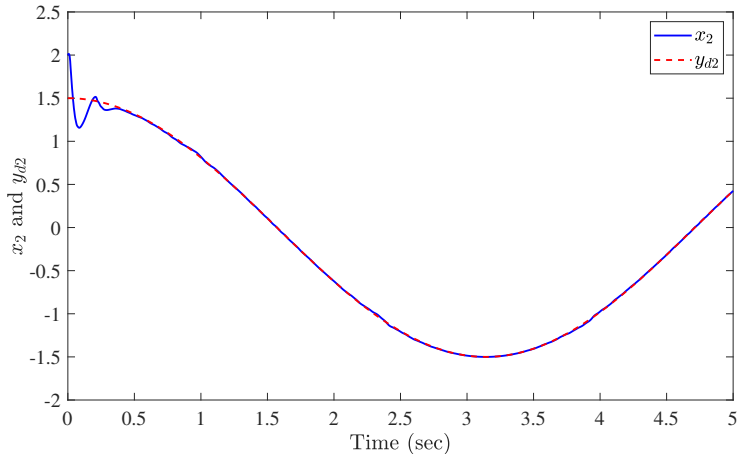

Figure 4.2: Evolution of the state x_2 and y_{d2} in the case of incommensurate orders.

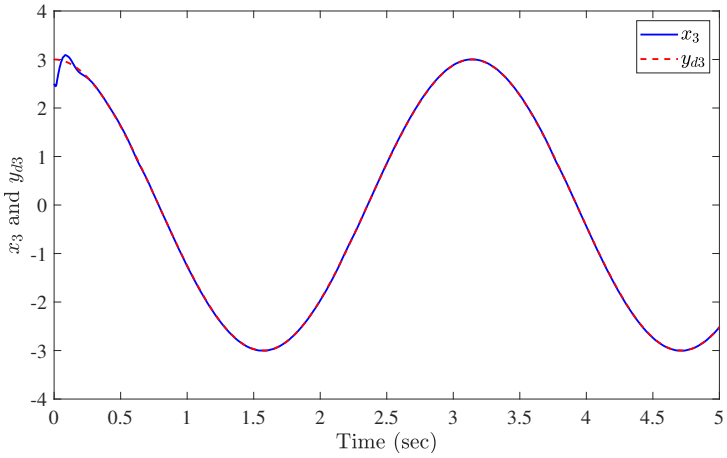

Figure 4.3: Evolution of the state x_3 and y_{d3} in the case of incommensurate orders.

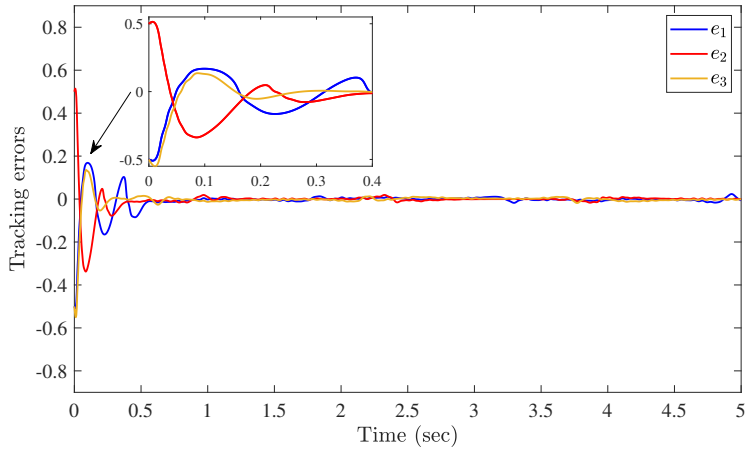

Figure 4.4: Tracking errors e_1, e_2, and e_3 in the case of incommensurate orders.

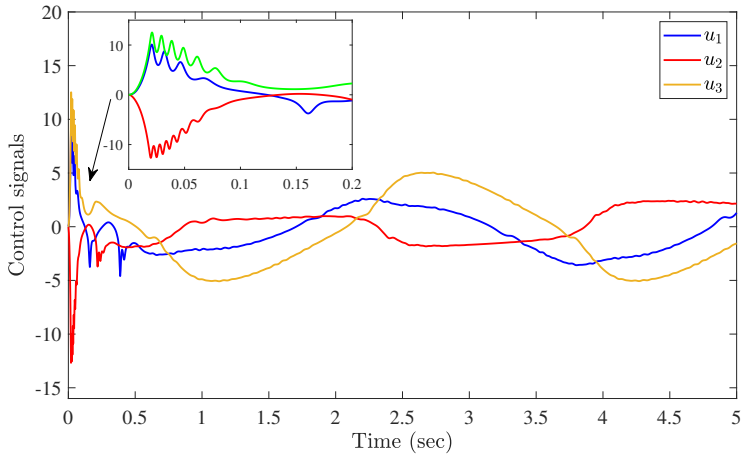

Figure 4.5: Control signals u_1, u_2, and u_3 in the case of incommensurate orders.

Figures 4.1-4.5 show closed-loop system responses in the case of incommensurate orders. Figure 4.1, Figure 4.2, and Figure 4.3 illustrate the tracking trajectories of the states x_1, x_2, and x_3, respectively, to their corresponding reference signals. The evolution of the tracking errors e_1, e_2, and e_3 are represented in Figure 4.4. Besides, the resulting control signals u_1, u_2, and u_3 are smooth and bounded as it can be seen in Figure 4.5. It is obvious from the mentioned results that the states track their desired reference signals, performing a fast response and decent transient behavior maintaining smooth and bounded control signals. Besides, this simulation confirms that the closed-loop stability of the system is acquired and the MFOL1AC can behave robustly against model uncertainties, external disturbances, and unknown input gain, which confirms the theoretical findings in previous sections.

4.5.2 Case of Hyper-chaos Suppression

This subsection considers chaos suppression of a 4-dimensional fractional-order hyper-chaotic systems, which is represented in the state space as [152]

$$\begin{cases} D^{\beta_1} x_1(t) = 5(x_3 - x_1 + x_4) + \Delta G_{x1}(x,t) + u_1(t) \\ D^{\beta_2} x_2(t) = (1 - 10 x_1 x_3) + \Delta G_{x2}(x,t) + u_2(t) \\ D^{\beta_3} x_3(t) = (-6 + 10 x_1 x_2) + \Delta G_{x3}(x,t) + u_3(t) \\ D^{\beta_4} x_4(t) = (-10 x_2) + \Delta G_{x4}(x,t) + u_4(t) \end{cases} \tag{4.58}$$

with $\Delta G_{x1}(x,t) = 0.65sin(3x_4) - 0.55cos(3t)$, $\Delta G_{x2}(x,t) = -0.65cos(5x_1) + 0.55sin(3t)$, $\Delta G_{x3}(x,t) = -0.6cos(3x_2) + 0.55sin(3.5t)$, and $\Delta G_{x4}(x,t) = 0.65sin(1.5y_3) - 0.55cos(2t)$. The fractional-orders are selected as $\beta_i = 0.95, i = 1,2,\ldots,4$ to confirm the existence of chaos phenomena [152]. The initial conditions of the systems are set as $x(0) = [0.7, 0.6, 0.8, 0.5]^T$. The initial values of $\hat{h}_i$ are set to be zero and $\hat{\sigma}_i(0) = 0.01$ with their bounds in the projection operator are $\hat{\sigma}_i \in [0.01, 6]$ and $\hat{h}_i \in [6, -6]$. The parameters α_i, Γ_i, and λ_i are selected

to achieve the best performances possible and their values are set as $\alpha = [27,53,28,22]^T$, $\Gamma = [64636,48084,48704,108592]^T$, and $\lambda_i = 10, i = 1,2,\ldots,4$. For the filter $C_i(s)$ we chose the feedback gain $K_i = 35, i = 1,2,\ldots,4$. Finally, the dynamics of the chaos suppression are simulated for $6s$, and with the parameters of the Oustaloup's filter are fixed as $\omega_b = 10^{-3}$, $\omega_h = 10^3$, and the approximation order $N = 5$.

Figures 4.6-4.11 illustrate the simulation results in the case of hyper-chaos suppression. Figures 4.6-4.9 show the trajectories of the states x_1, x_2, x_3, and x_4. The tracking errors $e_i(t), i = 1,2,\ldots,4$ are presented in Figure 4.10. These figures demonstrate that the suppression objective is achieved since the states x_1, x_2, x_3, and x_4 quickly converge near the origin (about $t_r = 0.4s$). Finally, the evolution of the control signals $u_i(t), i = 1,2,\ldots,4$ can be seen in Figure 4.11. Based on the mentioned figure, it is clear that the resulted control signals are bounded and relatively smooth. Therefore, this simulation example agrees that the proposed control can ensure a fast response maintaining decent transient performances and smooth control signals despite model uncertainties and external disturbances presented by the systems, which affirms the obtained theoretical results.

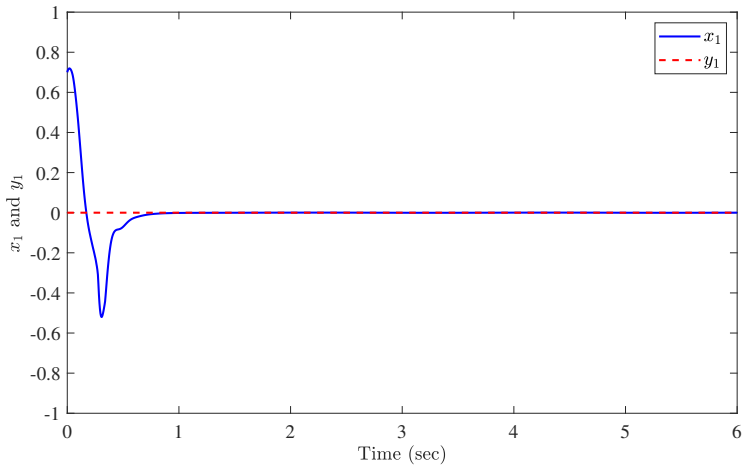

Figure 4.6: Evolution of the state x_1 and y_{d1} in the case of hyper-chaos suppression.

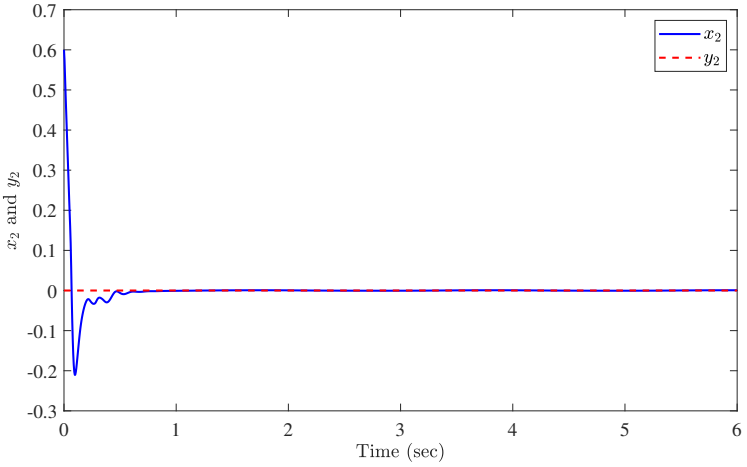

Figure 4.7: Evolution of the state x_2 and y_{d2} in the case of hyper-chaos suppression.

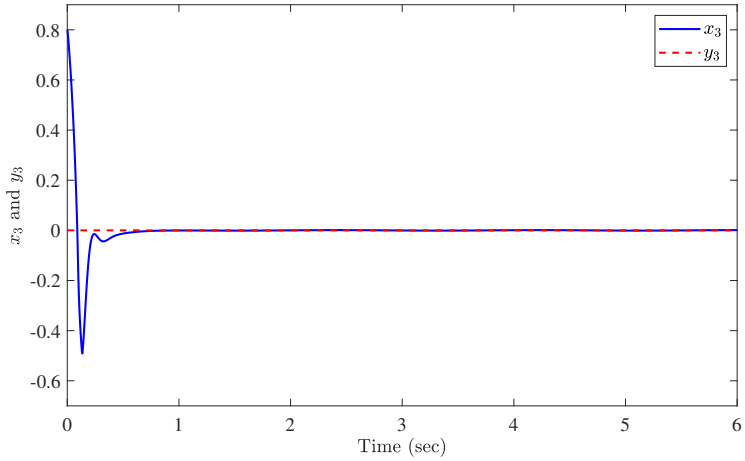

Figure 4.8: Evolution of the state x_3 and y_{d3} in the case of hyper-chaos suppression.

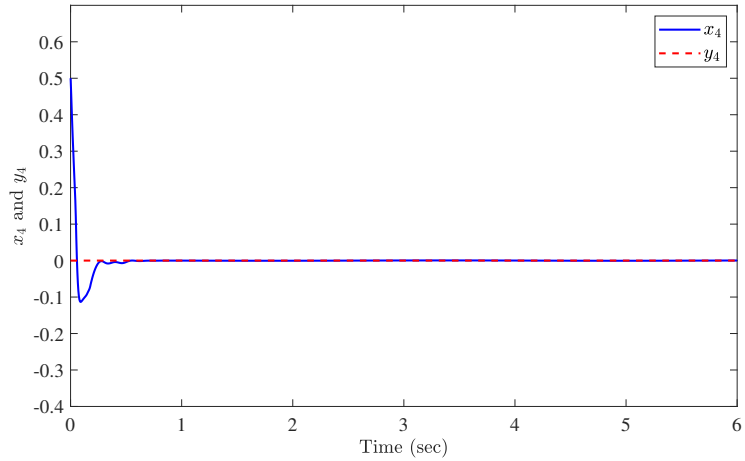

Figure 4.9: Evolution of the state x_4 and y_{d4} in the case of hyper-chaos suppression.

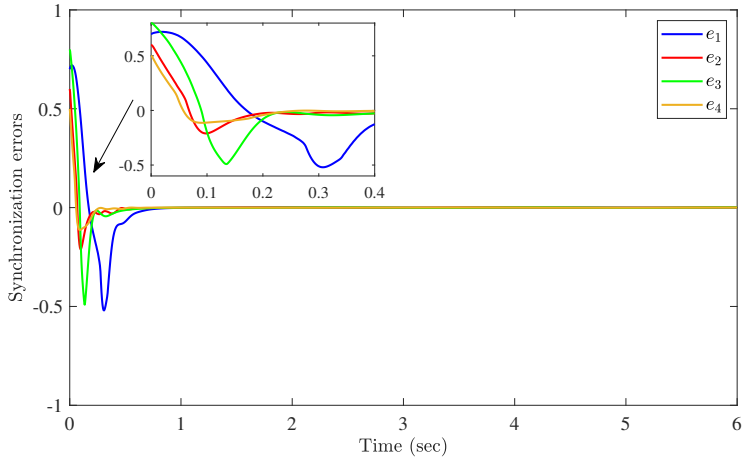

Figure 4.10: Tracking errors e_1, e_2, e_3, and e_4 in the case of hyper-chaos suppression.

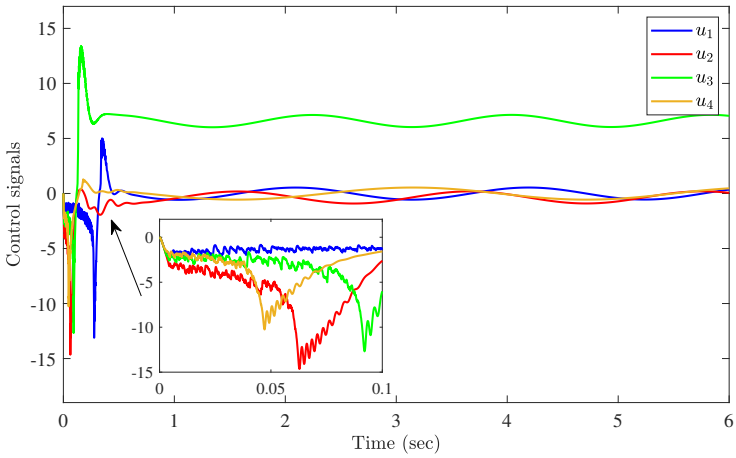

Figure 4.11: Resulting control signals u_1, u_2, u_3, and u_4 in the case of hyper-chaos suppression.

4.5.3 Comparative Study

To further assess the benefits of the proposed controller, a comparative study of the MFOL1AC against the Adaptive Sliding Mode Control (ASMC) suggested in [152] is executed under the same conditions for the case of hyper-chaos suppression. The control precision in this comparative study was inspected based on the errors $e_i, i = 1,2,\ldots,4$, delivered by the two controllers over a period of time (focusing on steady-state performances). These characteristics are presented in Table 4.1, which includes the range, the STD, and the average absolute value of the tracking errors.

Figure 4.12 and Figure 4.13 illustrate the resulting tracking errors $e_i(t), i = 1,2,\ldots,4$ for both controllers. These figures demonstrate clearly the faster response delivered by the MFOL1AC, it also illustrates the enhanced steady-state preference which can be translated to better robustness.

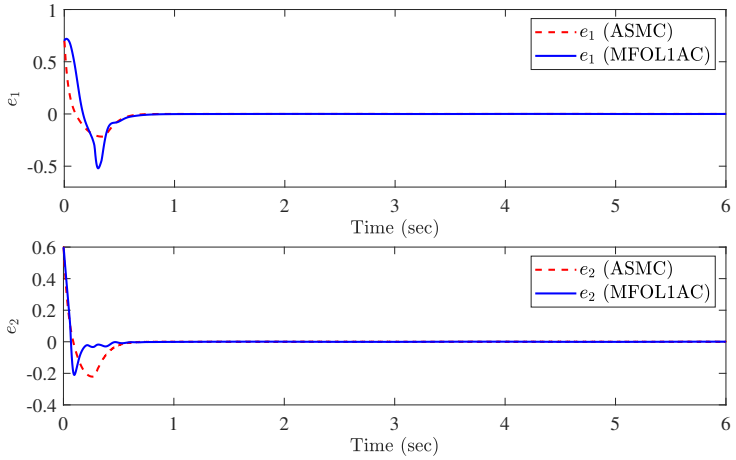

Figure 4.12: Comparative study in the case of hyper-chaotic systems. Tracking errors. Top. e_1. Bottom. e_2.

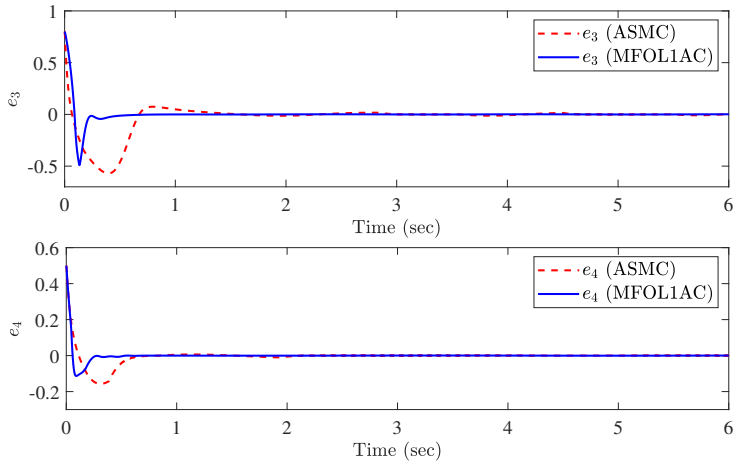

Figure 4.13: Comparative study in the case of hyper-chaotic systems. Tracking errors. Top. e_3. Bottom. e_4

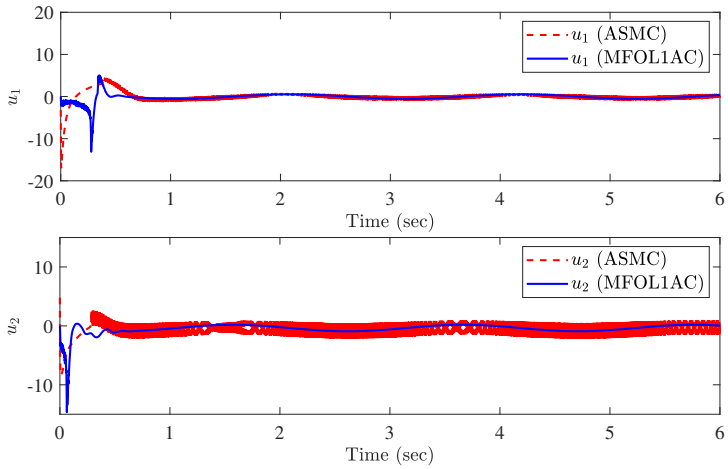

Figure 4.14: Comparative study in the case of hyper-chaotic systems. Resulting control signals. Top. u_1. Bottom. u_2.

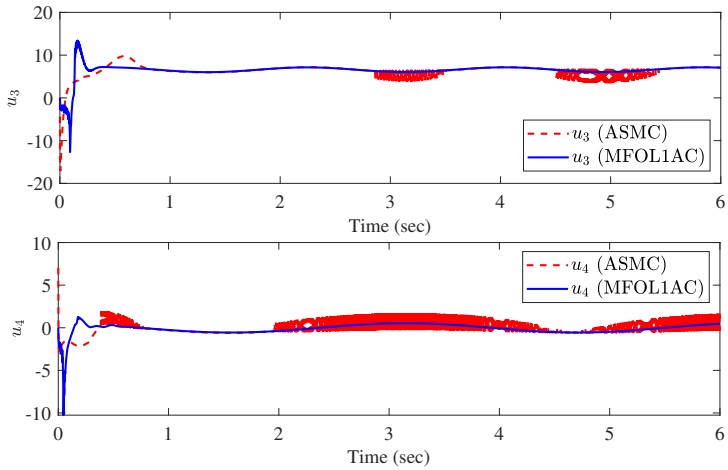

Figure 4.15: Comparative study in the case of hyper-chaotic systems. Resulting control signals. Top. u_3. Bottom. u_4.

Table 4.1: Precision comparisons between the proposed multivariable fractional-order $\mathscr{L}_1$ adaptive control and the adaptive sliding mode control.

Controller	Errors	$Avg(abs(e_i) \times 10^{-3}$	Range of $e_i \times 10^{-3}$	STD of $e_i \times 10^{-3}$
MFOL1AC	e_1	0.29	$(-0.44, 0.43)$	0.31
	e_2	0.39	$(-0.53, 0.66)$	0.44
	e_3	0.62	$(-0.96, 0.54)$	0.68
	e_4	0.30	$(-0.74, 0.45)$	0.33
ASMC [152]	e_1	0.32	$(-0.72, 0.71)$	0.37
	e_2	0.80	$(-1.50, 1.23)$	0.90
	e_3	5.70	$(-17.5, 19.1)$	8.02
	e_4	0.51	$(-1.20, 1.13)$	0.64

The control signals are depicted in Figure 4.14 and Figure 4.15, in which it is obvious that the resulting control signals of MFOL1AC do not suffer from the undesirable chattering problem. Finally, the overall results affirm the main advantage of the $\mathscr{L}_1$ adaptive controller which is faster responses with a decent transient response. Besides, Table 4.1 reveals the very satisfactory results of the proposed method in the steady-state regime in comparison with those of the ASMC.

4.6 Conclusion

In this chapter, an MFOL1AC is proposed to control a class of MIMO FOSs. The design begins by selecting a fractional-order sliding surface, followed by the synthesis of a control law based on the $\mathscr{L}_1$ adaptive control methodology. The latter ensures the existence of the sliding motion and eventually the convergence of the tracking errors. Theoretical findings demonstrate that the controller can deliver a fast and robust response with decent transient performance for a large class of systems in the presence of high adaptation gains, model uncertainties, external disturbances, and unknown input gains. Finally, two simulation cases were considered to investigate the ability of the proposed scheme: chaos control of an incommensurate FOCSs, and a hyper-chaos suppression for fractional-order hyper-chaotic system. The simulation discussion revealed that the results are satisfactory for both cases and approve the theoretical discussions.

Chapter 5

Neural network $\mathscr{L}_1$ Adaptive Control Design for Fractional-Order Systems with Time-varying Input Gain

5.1 Introduction

The aim of this chapter is to design a NNFOL1AC for a class of uncertain FONLSs that are subject to model uncertainties and unknown time-varying input gain. In the previous chapters, the objective of controlling FOSs is achieved using the $\mathscr{L}_1$ adaptive control methodology. Here, the control architecture integrates an RBFNN as an uncertainty estimator. This allows the implementation of the controller without any prior knowledge of the controlled system model. NN are known for their universal approximation property; they can approximate continuous nonlinear functions to any desired precision [153]. The principle is to incorporate the approximated function delivered by a neural network estimator in the control architecture, which plays a key role in handling of the uncertain nonlinearities of the system, results in small prediction errors, and significantly improves control accuracy. Finally, the developed controller can also ensure uniform performance bounds for system signals both in transient and steady-state. The rest of this chapter is arranged in 5 sections as follows. Section 5.2 describes the main problem. Section 5.3 introduces the structure of the NNFOL1AC. Section 5.4 shows the stability analysis of the proposed closed-loop scheme. Section 5.5 investigates the effectiveness and efficiency of the proposed controller on two FONLSs via some numerical simulations and comparative studies. Section 5.6 represents a conclusion to this chapter.

5.2 Problem Formulation

This section focuses on the characterization of the class of FOSs under consideration alongside the nomination of the control objective. To begin, we consider a class of SISO

uncertain FONLSs described as follows

$$\begin{cases} D^{\beta}x_1(t) = x_2(t), D^{\beta}x_2(t) = x_3(t), \ldots, D^{\beta}x_{n-1}(t) = x_n(t) \\ D^{\beta}x_n(t) = f(x) + g(x)u(t) \\ y(t) = x_1(t) \end{cases} \tag{5.1}$$

where D^{β} is the Caputo fractional derivative, β is the corresponding derivative order with respect to $0 < \beta < 1$, $x(t) = [x_1(t), \ldots, x_n(t)]^T \in \mathbb{R}^n$ is the pseudo states vector which is supposed to be measurable, $u(t) \in \mathbb{R}$ is the control signal, $y(t) \in \mathbb{R}$ is the output signal, $f(.)$ and $g(.)$ are continuous unknown smooth functions that represent system uncertain dynamics and unknown input gain, respectively.

The main objective of this chapter is to design an NNFOL1AC for the considered system (5.1) in order to achieve a bounded tracking response of the output signal $y(t) = x_1(t)$ to a bounded reference signal $y_d(t) \in \mathbb{R}$ while maintaining the boundedness for all system signals.

5.3 Neural Network Fractional-Order $\mathscr{L}_1$ Adaptive controller

This part will discuss the structure of the closed-loop system, which is based on a fractional-order sliding surface, an RBFNN, an $\mathscr{L}_1$ adaptive controller and the systems introduced in (5.1).

To proceed with the control design and with regard to the system in (5.1), the following assumptions are essential.

Assumption 5.1. For all $x(t) \in \mathbb{R}$ we assume that the nonlinear function $g(x)$ is bounded and strictly positive with respect to $0 < \theta_1 < g(x) < \theta_2$, where θ_1 and θ_2 are positive constants. It is worth noting that $g(x)$ can be assumed strictly negative as $-\theta_2 < g(x) < -\theta_1 < 0$, while the controller can be obtained similarly. □

Assumption 5.2. The reference signal $y_d(t)$ and its successive fractional-order derivatives $D^{j\beta}y_d(t), j = 1, \ldots, n$ are assumed to exist, to be smooth and bounded. □

5.3.1 Choice of an Appropriate Fractional-Order Sliding Surface

Let the vector $E(t) = [e_1(t), e_2(t), \ldots, e_n(t)]^T \in \mathbb{R}^n$ be defined as

$$E(t) = Y_d(t) - x(t) \tag{5.2}$$

such as $e_1(t) = y_d(t) - x_1(t)$ is the tracking error and $Y_d(t)$ is the vector of the reference signal and its successive fractional-order derivatives defined in Assumption 5.2. Conse-

quently, the error dynamics can be evaluated in the following form

$$\begin{cases} D^{\beta}e_1(t) = e_2(t), D^{\beta}e_2(t) = e_3(t), \ldots, D^{\beta}e_{n-1}(t) = e_n(t) \\ D^{\beta}e_n(t) = D^{n\beta}y_d(t) - D^{\beta}x_n(t) \end{cases} \tag{5.3}$$

regarding the error dynamics in (5.3) and the considered system in (5.1), the suitable form of the fractional-order sliding surface to design the controller is the following

$$z(t) = D^{\beta-1}e_n(t) + \int_0^t \lambda^T E(\tau)d\tau \tag{5.4}$$

where $\lambda = [\lambda_1, \lambda_2, \ldots \lambda_n]^T \in \mathbb{R}^n$ is a vector of adjustable design parameters, their values will be discussed further in this chapter.

The time derivative of the fractional-order sliding surface is given according to the property in (1.26) as

$$\dot{z}(t) = D^{\beta}e_n(t) + \lambda^T E(t) \tag{5.5}$$

In the case where the system reaches in the fractional-order sliding surface, one can have $z(t) = \dot{z}(t) = 0$. Thus, for $\dot{z}(t)$ significantly small, i.e., $\dot{z}(t) \approx 0$, it results

$$D^{\beta}e_n(t) + \lambda^T E(t) = 0 \tag{5.6}$$

or

$$D^{\beta}e_n(t) = -\lambda^T E(t) \tag{5.7}$$

Furthermore, in this case, and by replacing the resulted equation (5.7) in (5.3), one can extend the representation of the error dynamics to the subsequent form

$$\underbrace{\begin{bmatrix} D^{\beta}e_1(t) \\ D^{\beta}e_2(t) \\ \vdots \\ D^{\beta}e_{n-1}(t) \\ D^{\beta}e_n(t) \end{bmatrix}}_{D^{\beta}E(t)} = \underbrace{\begin{bmatrix} 0 & 1 & 0 & \ldots & 0 \\ 0 & 0 & 1 & \cdots & 0 \\ \vdots & \vdots & \vdots & \ddots & \vdots \\ 0 & 0 & 0 & \cdots & 1 \\ -\lambda_1 & -\lambda_2 & -\lambda_3 & \cdots & -\lambda_n \end{bmatrix}}_{A} \underbrace{\begin{bmatrix} e_1(t) \\ e_2(t) \\ \vdots \\ e_{n-1}(t) \\ e_n(t) \end{bmatrix}}_{E(t)} \tag{5.8}$$

Particularly, $D^{\beta}E(t) = AE(t)$, where $A \in \mathbb{R}^{n\times n}$ is a constant matrix, the stability condition in Theorem 1.6, i.e., $|arg(eig(A))| > \beta\frac{\pi}{2}$, implies that the design parameters $\lambda_i, i = 1, 2, \ldots, n$, must be strictly positive in order the guarantee that the sliding surface dynamics are asymptotically stable. In addition, these conditions confirm that the tracking error and its fractional-order derivatives converge towards zero. Therefore, the purpose of the NNFOL1AC is to guarantee that the system reaches in the fractional-order sliding surface by controlling $z(t)$ toward zero.

Next step, replacing $D^{\beta}e_n(t)$ from (5.3) in (5.5), which results in

$$\dot{z}(t) = D^{n\beta}y_d(t) - D^{\beta}x_n(t) + \lambda^T E(t) \tag{5.9}$$

this form can be extended using $D^{\beta}x_n(t)$ from (5.1) to the form that follows

$$\dot{z}(t) = D^{n\beta}y_d(t) - f(x) - g(x)u(t) + \lambda^T E(t) \tag{5.10}$$

Let define a function v as

$$v(t,z) = D^{n\beta}y_d(t) + \lambda^T E(t) + \alpha z(t) \tag{5.11}$$

with α is a positive constant.

From (5.11), and by subtracting and adding αz in (5.10), one can have the following equation

$$\dot{z}(t) = -\alpha z(t) - f(x) - g(x)u(t) + v(t,z) \tag{5.12}$$

For the unknown nonlinear expression $g(x)u(t)$ in (5.12), there exist always σ and $\Delta(x,u)$, such that

$$g(x)u(t) = \sigma u(t) - \Delta(x,u) \tag{5.13}$$

where Δ is the mismatch between $g(x)u(t)$ and $\sigma u(t)$, σ is a positive unknown constant with respect to $0 < \omega_1 < \sigma < \omega_2$, with ω_1 and ω_2 are positive constants.

Now, by replacing (5.13) in (5.12), one can have

$$\dot{z}(t) = -\alpha z(t) - f(x) - \sigma u(t) + \Delta(x,u) + v(t,z) \tag{5.14}$$

denoting $H(x,u,v) = \Delta(x,u) - f(x) + v(t,z)$, hence

$$\dot{z}(t) = -\alpha z(t) - \sigma u(t) + H(x,u,v) \tag{5.15}$$

Given its definition, the nonlinear function $H(x,v,u)$ is obscured by the uncertain terms $\Delta(x,u)$ and $f(x)$. Consequently, the subsequent section will focus on approximating $H(x,v,u)$ by employing an RBFNN.

5.3.2 Neural Network Approximation

RBFNN are usually considered as two layers networks; a hidden layer that delivers a nonlinear transformation of the inputs, and an output layer that linearly combines the output of the previous layer. These networks can approximate any given continuous nonlinear function $H(\vartheta) : \mathbb{R}^n \to \mathbb{R}$ into the following [102, 107, 154]

$$H(\vartheta) = w^T \phi(\vartheta) + \epsilon(\vartheta), |\epsilon(\vartheta)| \leq \varepsilon \tag{5.16}$$

where $\vartheta = [\vartheta_1, \vartheta_2, \ldots, \vartheta_n]^T \in \Omega_\vartheta \subset \mathbb{R}^n$ is the input vector, $w = [w_1, \ldots, w_l]^T \in \mathbb{R}^l$ is the weight vector, $l > 1$ is the network nodes number and $\phi(\vartheta) = [\phi_1(\vartheta), \ldots, \phi_l(\vartheta)]^T \in \mathbb{R}^l$ is the output of the hidden layer with $\phi_m(\vartheta)$ is given by the Gaussian radial basis function that follows

$$\phi_m(\vartheta) = exp(-\frac{(\vartheta - \zeta_m)^T(\vartheta - \zeta_m)}{\kappa_m^2}), m = 1, \ldots, l \tag{5.17}$$

with the parameters $\zeta_m = [\zeta_{m1}, \zeta_{m2}, \ldots, \zeta_{mn}]^T$ and κ_m are the center of the receptive vector and the width of the Gaussian function, receptively. □

According to (5.16), the function $H(x, u, v)$ can be approximated by an RBFNN over a compact set as

$$H(\vartheta) = w^T(t)\phi(\vartheta) + \epsilon(\vartheta), |\epsilon(\vartheta)| \leq \varepsilon \tag{5.18}$$

with $\epsilon(\vartheta)$ is the approximation error, and ε is a uniform bound for $\epsilon(\vartheta)$.

Replacing (5.18) in (5.15) gives

$$\dot{z}(t) = -\alpha z(t) - \sigma u(t) + w^T(t)\phi(\vartheta) + \epsilon(\vartheta), z(0) = z_0 \tag{5.19}$$

5.3.3 Control Structure

Let us consider the following form of the predictor, which replicates the dynamics described by (5.19) with the unknown parameters σ and $w(t)$ are replaced with their estimations $\hat{\sigma}(t)$ and $\hat{w}(t)$, respectively

$$\dot{\hat{z}}(t) = -\alpha \hat{z}(t) - \hat{\sigma} u(t) + \hat{w}^T(t)\phi(\vartheta), \hat{z}(0) = z_0 \tag{5.20}$$

where $\hat{z}(t) \in \mathbb{R}$ is the prediction of the sliding surface $z(t)$. The values of $\hat{\sigma}(t)$ and $\hat{w}(t)$ are governed by the following projection-type adaptation laws

$$\begin{aligned} \dot{\hat{\sigma}}(t) &= \Gamma Proj(\hat{\sigma}(t), \tilde{z}(t)u(t)) \\ \dot{\hat{w}}(t) &= \Gamma Proj(\hat{w}(t), -\tilde{z}(t)\phi(\vartheta)) \end{aligned} \tag{5.21}$$

where $\tilde{z}(t) = \hat{z}(t) - z(t) \in \mathbb{R}$ represents the prediction error, Γ is a positive value that denotes the adaptation gain, and $Proj(.,.)$ is the projection operator given by Definition 2.3.

Let us consider the following control law

$$u(s) = KD(s)\hat{\eta}(s) \tag{5.22}$$

with $\hat{\eta}(s)$ is the Laplace transform of $\hat{\eta}(t) = -\hat{\sigma}(t)u(t) + \hat{w}^T(t)\phi(\vartheta)$, $D(s)$ is a strictly proper transfer function, and $K \in \mathbb{R}^+$ is a positive feedback gain, which results in a stable proper transfer function

$$\hat{C}(s) = \frac{\hat{\sigma}KD(s)}{1 + \hat{\sigma}KD(s)} \tag{5.23}$$

The choice of $D(s) = \frac{1}{s}$ introduces $\hat{C}(s)$ in the form of the first-order low-pass filter in

(5.24) with DC gain $\hat{C}(0) = 1$

$$\hat{C}(s) = \frac{\hat{\sigma}K}{s + \hat{\sigma}K} \tag{5.24}$$

Finally, an illustrative block diagram of the proposed NNFOL1AC is given in Figure 5.1.

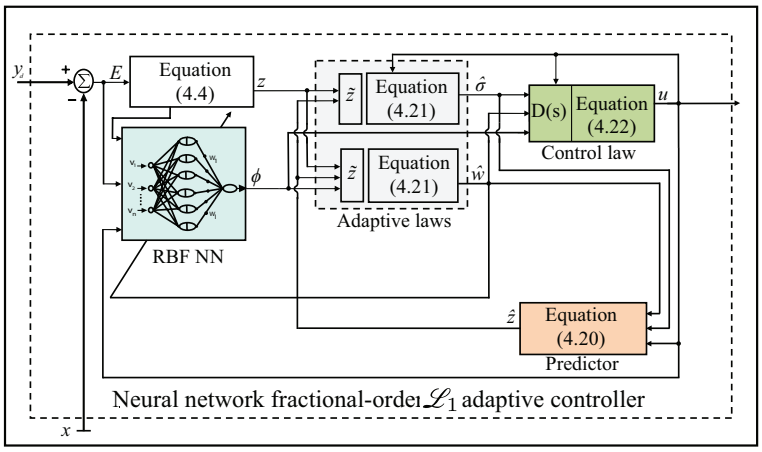

Figure 5.1: Diagram block of the proposed neural network fractional-order $\mathscr{L}_1$ adaptive controller.

5.4 Stability and Performances Analysis

This section analyzes the performances and the stability of the developed controller. For that reason, the following assumptions are required

Assumption 5.3. Since the pseudo state vector $x(t)$ shares a similar behavior with $z(t)$ in terms of stability and boundedness, then the following bound is justifiable

$$|H(x,u,v)| \leq L|z(t)| + L_0 \tag{5.25}$$

where L and L_0 are positive constants. □

Assumption 5.4. Let $w(t)$ be continuously derivable and its derivative $\dot{w}(t)$ is bounded for all $t \geq 0$ as follows

$$\|\dot{w}\| \leq d_w < \infty \tag{5.26}$$

□

The controller proposed in (5.20), (5.21), and (5.22) is subject to the $\mathscr{L}_1$ norm condition in (5.27)

$$\|G(s)\|_{\mathscr{L}_1} L < 1 \tag{5.27}$$

where $G(s) = H(s)(1 - C(s))$, $H(s) = (s+\alpha)^{-1}$, $C(s) = \frac{\sigma K}{s+\sigma K}$ is a low pass filter, and L is given in (5.25). Therefore, the design parameter α and the filter $C(s)$ are selected to fulfill it.

Remark 5.1. Since $C(s)$ is a BIBO stable and strictly proper transfer function and $\alpha > 0$, we can find that $H(s)$ and $G(s)$ are also BIBO stable and proper transfer functions. □

Remark 5.2. The design parameters $\lambda_i, i = 1,2,\ldots,n$ and α are utilized in this approach to specify the desired closed-loop dynamics and the feedback gain K can be used to adjust the bandwidth-limited filter $C(s)$. In a given frequency range, this filter serves a critical role in maintaining good tracking of the reference signals and enhancing robustness against uncertainties. □

5.4.1 Closed-loop Ideal Reference System

In this subsection, we consider a well-behaved reference system that represents the non-adaptive description of the system (5.1) and the proposed controller in (5.20), (5.21), and (5.22)

$$\begin{cases} \dot{z}_{ref}(t) = -\alpha z_{ref}(t) - \sigma u_{ref}(t) + w^T(t)\phi(\vartheta_{ref}) + \epsilon(\vartheta_{ref}), z_{ref}(0) = z_0 \\ u_{ref}(s) = \dfrac{C(s)}{\sigma}\eta_{ref}(s) \end{cases} \tag{5.28}$$

with $\eta_{ref}(s)$ is the Laplace transform of $\eta_{ref}(t) = w^T(t)\phi(\vartheta_{ref})$.

Remark 5.3. The control signal $u_{ref}(t)$ depends on the unknown terms σ and $w(t)$ which is not practical. We mention that this is not the case for the actual control law $u(t)$ and the signal $u_{ref}(t)$ is used for analysis purposes only. □

Lemma 5.1. Let us consider that the design parameter α and the filter $C(s)$ satisfy the condition in (5.27), also regarding the representation of the closed-loop reference system in (5.28), we have the following bound

$$\|z_{ref\tau}\|_{\mathscr{L}_\infty} \leq \rho \tag{5.29}$$

where

$$\rho = \frac{\|G(s)\|_{\mathscr{L}_1}}{1 - L\|G(s)\|_{\mathscr{L}_1}}(L_0 + \varepsilon) + \frac{\|H(s)\|_{\mathscr{L}_1}}{1 - L\|G(s)\|_{\mathscr{L}_1}}\varepsilon + \frac{1}{1 - L\|G(s)\|_{\mathscr{L}_1}}\|z_{in\tau}\|_{\mathscr{L}_\infty} \tag{5.30}$$

with $z_{in} = (s+\alpha)^{-1}z_0$ □

Proof. The closed-loop reference system in (5.28) can be expressed in the frequency domain as follows

$$\begin{aligned} sz_{ref}(s) - z_0 &= -\alpha z_{ref}(s) - \sigma u_{ref}(s) + \eta_{ref}(s) + \epsilon_{ref} \\ &= -\alpha z_{ref}(s) - C(s)\eta_{ref}(s) + \eta_{ref}(s) + \epsilon_{ref} \end{aligned} \tag{5.31}$$

where ϵ_{ref} is the Laplace transform of $\epsilon(\vartheta_{ref})$. Consequently

$$\begin{aligned} z_{ref}(s) &= (s+\alpha)^{-1}(1 - C(s))\eta_{ref}(s) + (s+\alpha)^{-1}\epsilon_{ref} + (s+\alpha)^{-1}z_0 \\ &= G(s)\eta_{ref}(s) + H(s)\epsilon_{ref} + z_{in} \end{aligned} \tag{5.32}$$

Since $G(s)$, $H(s)$, and $C(s)$ are BIBO stable transfer functions and z_{in} is known and

uniformly bounded, then, for all $\tau > 0$ the expression in (5.32) yields in

$$\|z_{ref\tau}\|_{\mathscr{L}_\infty} \leq \|G(s)\|_{\mathscr{L}_1} \|\eta_{ref\tau}\|_{\mathscr{L}_\infty} + \|H(s)\|_{\mathscr{L}_1} \varepsilon + \|z_{in\tau}\|_{\mathscr{L}_\infty} \tag{5.33}$$

Next, based on the representations of $H(x,u,v)$ and $\eta_{ref}(t)$ in (5.18) and (5.28), respectively, we can deduce that

$$\|\eta_{ref\tau}\|_{\mathscr{L}_\infty} = \|H(z_{ref}) - \epsilon(z_{ref})\|_{\mathscr{L}_\infty} \tag{5.34}$$

In addition, regarding Assumption 5.3 and using the bound of $\epsilon(\vartheta)$ in (5.18), one can obtain

$$\|\eta_{ref\tau}\|_{\mathscr{L}_\infty} \leq L\|z_{ref\tau}\|_{\mathscr{L}_\infty} + L_0 + \varepsilon \tag{5.35}$$

Replacing (5.35) in (5.33), it results

$$\|z_{ref\tau}\|_{\mathscr{L}_\infty} \leq \|G(s)\|_{\mathscr{L}_1} (L\|z_{ref\tau}\|_{\mathscr{L}_\infty} + L_0 + \varepsilon) + \|H(s)\|_{\mathscr{L}_1} \varepsilon + \|z_{in\tau}\|_{\mathscr{L}_\infty} \tag{5.36}$$

Finally, solving for $\|z_{ref\tau}\|_{\mathscr{L}_\infty}$, we obtain

$$\begin{aligned} \|z_{ref\tau}\|_{\mathscr{L}_\infty} \leq \frac{\|G(s)\|_{\mathscr{L}_1}}{1 - L\|G(s)\|_{\mathscr{L}_1}} (L_0 + \varepsilon) + \frac{\|H(s)\|_{\mathscr{L}_1}}{1 - L\|G(s)\|_{\mathscr{L}_1}} \varepsilon \\ + \frac{1}{1 - L\|G(s)\|_{\mathscr{L}_1}} \|z_{in\tau}\|_{\mathscr{L}_\infty} \end{aligned} \tag{5.37}$$

It is evident that L_0, ε are finite values, and z_{in} is known and uniformly bounded. Consequently, the bound in (5.37) implies that if the condition in (5.27) is satisfied, then, $\|z_{ref\tau}\|_{\mathscr{L}_\infty}$ is uniformly bounded, this completes the proof. □

5.4.2 Transient and Steady-state Analysis

In this subsection, we present a performance analysis in both the transient and steady-state of the system (5.1) and the proposed controller in (5.20), (5.21), and (5.22) in relation to the well-behaved closed-loop reference system represented in (5.28).

In order to describe the prediction error dynamics $\tilde{z}(t)$, we subtract (5.19) from (5.20), which results in

$$\dot{\tilde{z}}(t) = -\alpha \tilde{z}(t) - \tilde{\sigma}(t)u(t) + \tilde{w}^T(t)\phi(\vartheta) - \epsilon(\vartheta) \tag{5.38}$$

with $\hat{\sigma}(t) = \hat{\sigma}(t) - \sigma$ and $\tilde{w}(t) = \hat{w}(t) - w(t)$ represent the estimation errors.

Thus, the frequency domain expression of the prediction error dynamics is the following

$$\tilde{z}(s) = H(s)(\tilde{\eta}(s) - \epsilon(s)) \tag{5.39}$$

where $\tilde{\eta}(s)$ is the Laplace transform of $\tilde{\eta}(t) = -\tilde{\sigma}u(t) + \tilde{w}^T(t)\phi(\vartheta)$.

Lemma 5.2. Consider the system presented in (5.19) with the controller proposed in (5.20), (5.21), and (5.22), if the low-pass filter $C(s)$ and the design parameter α fulfill the condition in (5.27), we have the bound that follow

$$\|\tilde{z}_\tau\|_{\mathscr{L}_\infty} \leq \sqrt{\varphi} \tag{5.40}$$

where

$$\varphi = \frac{1}{\Gamma}(4 \underset{w\in\Theta}{max}\|w\|^2 + (\omega_2 - \omega_1)^2) + \frac{\Upsilon^{-1}}{\Gamma} 4 \underset{w\in\Theta}{max}\|w\| d_w + \Upsilon^{-1}\varepsilon^2 \tag{5.41}$$

with $\Upsilon = (2\alpha - 1)$ and $\alpha > \frac{1}{2}$. □

Proof. In order to study the stability, we consider the following Lyapunov candidate function

$$V(\tilde{z}, \tilde{w}, \tilde{\sigma}) = \tilde{z}^2 + \frac{1}{\Gamma}\tilde{w}^T\tilde{w} + \frac{1}{\Gamma}\tilde{\sigma}^2 \tag{5.42}$$

The time derivative $\dot{V}$ of (5.42) is given as

$$\dot{V}(\tilde{z}, \tilde{w}, \tilde{\sigma}) = 2\tilde{z}\dot{\tilde{z}} + \frac{2}{\Gamma}\tilde{w}^T\dot{\tilde{w}} + \frac{2}{\Gamma}\tilde{\sigma}\dot{\tilde{\sigma}} \tag{5.43}$$

Replacing (5.38) in (5.43), results in

$$\dot{V}(\tilde{z}, \tilde{w}, \tilde{\sigma}) = 2\tilde{z}(-\alpha\tilde{z} - \tilde{\sigma}u + \tilde{w}^T\phi - \epsilon) + \frac{2}{\Gamma}\tilde{w}^T\dot{\tilde{w}} + \frac{2}{\Gamma}\tilde{\sigma}\dot{\tilde{\sigma}} - \frac{2}{\Gamma}\tilde{w}^T\dot{w} \tag{5.44}$$

or

$$\dot{V}(\tilde{z}, \tilde{w}, \tilde{\sigma}) = -2\alpha\tilde{z}^2 + 2\tilde{w}^T(\frac{1}{\Gamma}\dot{\tilde{w}} + \tilde{z}\phi) + 2\tilde{\sigma}(\frac{1}{\Gamma}\dot{\tilde{\sigma}} - \tilde{z}u) - \frac{2}{\Gamma}\tilde{w}^T\dot{w} - 2\tilde{z}\epsilon \tag{5.45}$$

where $\dot{\tilde{w}}$ and $\dot{\tilde{\sigma}}$ are given in the adaptation laws (5.21). Thus

$$\begin{aligned}\dot{V}(\tilde{z}, \tilde{w}, \tilde{\sigma}) = -\alpha\tilde{z}^2(t) + 2\tilde{w}^T(Proj(\hat{w}, -\tilde{z}\phi) + \tilde{z}\phi) + 2\tilde{\sigma}(Proj(\hat{\sigma}, \tilde{z}u) - \tilde{z}u) \\ - \frac{2}{\Gamma}\tilde{w^T}\dot{w} - 2\tilde{z}\epsilon\end{aligned} \tag{5.46}$$

Lemma 2.2 suggests that

$$2\tilde{w}^T(Proj(\hat{w}, -\tilde{z}\phi) + \tilde{z}\phi) + 2\tilde{\sigma}(Proj(\hat{\sigma}, \tilde{z}u) - \tilde{z}u) \leq 0 \tag{5.47}$$

which can give a bound to $\dot{V}$ as follows

$$\dot{V}(\tilde{z}, \tilde{w}, \tilde{\sigma}) \leq -2\alpha\tilde{z}^2 + \frac{2}{\Gamma}\mid \tilde{w}^T\dot{w} \mid + 2 \mid \tilde{z} \mid \varepsilon \tag{5.48}$$

It is easy to prove that $2\tilde{z}\varepsilon \leq \tilde{z}^2 + \varepsilon^2$, which leads to

$$\dot{V}(\tilde{z}, \tilde{w}, \tilde{\sigma}) \leq -\Upsilon\tilde{z}^2 + \frac{2}{\Gamma}\mid \tilde{w}^T\dot{w} \mid + \varepsilon^2 \tag{5.49}$$

According to Lemma 2.2, the projection operator used in (5.21) ensures that $\hat{w} \in \Theta$

and $|\hat{\sigma}| \leq \chi, \chi \in [\omega_1, \omega_2]$, that is to say

$$\underset{t\geq 0}{max}(\tilde{w}^T\tilde{w} + \tilde{\sigma}^2) \leq (4\underset{w\in\Theta}{max}\|w\|^2 + (\omega_2 - \omega_1)^2) \tag{5.50}$$

In addition, the upper bound in Assumption 5.4 implies that

$$\frac{2}{\Gamma} \mid \tilde{w}^T\dot{w} \mid \leq \frac{4}{\Gamma}(\underset{w\in\Theta}{max}\|w\|d_w) \tag{5.51}$$

which leads to

$$\dot{V}(\tilde{z}, \tilde{w}, \tilde{\sigma}) \leq -\Upsilon\tilde{z}^2 + \frac{4}{\Gamma}\underset{w\in\Theta}{max}\|w\|d_w + \varepsilon^2 \tag{5.52}$$

Adding and subtracting $\frac{\Upsilon}{\Gamma}\tilde{w}^T\tilde{w} + \frac{\Upsilon}{\Gamma}\tilde{\sigma}^2$ in (5.52), gives

$$\dot{V}(\tilde{z}, \tilde{w}, \tilde{\sigma}) \leq -\Upsilon\tilde{z}^2 - \frac{\Upsilon}{\Gamma}\tilde{w}^T\tilde{w} - \frac{\Upsilon}{\Gamma}\tilde{\sigma}^2 + \frac{\Upsilon}{\Gamma}\tilde{w}^T\tilde{w} + \frac{\Upsilon}{\Gamma}\tilde{\sigma}^2 + \frac{4}{\Gamma}\underset{w\in\Theta}{max}\|w\|d_w + \varepsilon^2 \tag{5.53}$$

or

$$\begin{aligned}\dot{V}(\tilde{z}, \tilde{w}, \tilde{\sigma}) \leq -\Upsilon V(\tilde{z}, \tilde{w}, \tilde{\sigma}) + \Upsilon(\frac{1}{\Gamma}(4\underset{w\in\Theta}{max}\|w\|^2 + (\omega_2 - \omega_1)^2) \\ + \frac{\Upsilon^{-1}}{\Gamma}4\underset{w\in\Theta}{max}\|w\|d_w + \Upsilon^{-1}\varepsilon^2)\end{aligned} \tag{5.54}$$

In conclusion

$$\dot{V}(\tilde{z}, \tilde{w}, \tilde{\sigma}) \leq -\Upsilon V(\tilde{z}, \tilde{w}, \tilde{\sigma}) + \Upsilon\varphi \tag{5.55}$$

Therefore, if at any time $t_1 > 0$, one has $V(t_1) > \varphi$, the inequality in (5.55) leads to conclude that $\dot{V}(t_1) < 0$. Also using the fact that $z(0) = \hat{z}(0)$, we obtain

$$V(0) < \frac{1}{\Gamma}(4\underset{w\in\Theta}{max}\|w\|^2 + (\omega_2 - \omega_1)^2) < \varphi \tag{5.56}$$

Hence, $V(t) < \varphi$ for all $t > 0$. In addition, since $\tilde{z}^2 \leq V(t)$ and $\|.\|_\infty \leq \|.\|$, the bound $\|\tilde{z}_\tau\|_{\mathscr{L}_\infty} \leq \sqrt{\varphi}$ is acquired and the proof is completed. □

Proposition 5.1. Let us consider that the design parameter α and the filter $C(s)$ satisfy the condition in (5.27), then for the system represented in (5.1) and the controller defined via (5.20), (5.21), and (5.22), we have

$$\begin{aligned}\|(z_{ref}(s) - z(s))_\tau\|_{\mathscr{L}_\infty} \leq \delta_1 \\ \|(u_{ref}(s) - u(s))_\tau\|_{\mathscr{L}_\infty} \leq \delta_2\end{aligned} \tag{5.57}$$

and

$$\begin{aligned}\lim_{\Gamma\to\infty, \varepsilon\to 0}(z_{ref}(t) - z(t)) = 0 \\ \lim_{\Gamma\to\infty, \varepsilon\to 0}(u_{ref}(t) - u(t)) = 0\end{aligned} \tag{5.58}$$

where

$$\delta_1 = \frac{\|C(s)\|_{\mathscr{L}_1}}{1 - \|G(s)\|_{\mathscr{L}_1}L}\sqrt{\varphi} + \frac{3\|G(s)\|_{\mathscr{L}_1} + \|H(s)\|_{\mathscr{L}_1}}{1 - \|G(s)\|_{\mathscr{L}_1}L}\varepsilon \tag{5.59}$$

and

$$\delta_2 = \|\frac{C(s)}{\sigma}\|_{\mathscr{L}_1}(L\delta_1 + 3\varepsilon) + \|\frac{H_1(s)}{\sigma}\|_{\mathscr{L}_1}\sqrt{\varphi} \tag{5.60}$$

with $H_1(s) = \frac{C(s)}{H(s)}$. □

Proof. First, adding and subtracting $\sigma u(s) + \eta(s)$ in (5.22), that is to say

$$u(s) = KD(s)(\hat{\eta}(s) + \sigma u(s) + \eta(s) - \eta(s) - \sigma u(s)) \tag{5.61}$$

where we denote $\eta(t) = w^T(t)\phi(\vartheta)$. Consequently, according to the definition of $\hat{\eta}(s)$ and $\tilde{\eta}(s)$ we can rewrite the control law as

$$u(s) = KD(s)(\tilde{\eta}(s) + \eta(s) - \sigma u(s)) \tag{5.62}$$

or by choosing $D(s) = \frac{1}{s}$

$$u(s) = \frac{K}{s + K\sigma}(\tilde{\eta}(s) + \eta(s)) \tag{5.63}$$

which results in

$$u(s) = \frac{C(s)}{\sigma}(\tilde{\eta}(s) + \eta(s)) \tag{5.64}$$

Replacing (5.64) in (5.19) and according to the Laplace transform, one can have

$$\begin{aligned} z(s) =& H(s)((1 - C(s))\eta(s) - C(s)\tilde{\eta}(s) + \epsilon(s)) + z_{in} \\ =& G(s)\eta(s) - H(s)C(s)\tilde{\eta}(s) + H(s)\epsilon(s) + z_{in} \\ =& G(s)\eta(s) - C(s)\tilde{z}(s) + G(s)\epsilon(s) + z_{in} \end{aligned} \tag{5.65}$$

Now, by subtracting (5.65) from (5.32), we can have

$$z_{ref}(s) - z(s) = G(s)\eta_e(s) + C(s)\tilde{z}(s) - G(s)\epsilon(s) + H(s)\epsilon_{ref} \tag{5.66}$$

where $\eta_e(s) = \eta_{ref}(s) - \eta(s)$, which can be bounded based on Assumption 5.3 and the bound of $\epsilon(\vartheta)$ in (5.18) as follows

$$\|\eta_{e\tau}\|_{\mathscr{L}_\infty} \leq L\|(z_{ref}(s) - z(s))_\tau\|_{\mathscr{L}_\infty} + 2\varepsilon \tag{5.67}$$

We know that $G(s)$, $H(s)$, and $C(s)$ are BIBO stable transfer functions and z_{in} is known and uniformly bounded. Therefore, using the bound of η_e, we can conclude that

$$\begin{aligned} \|(z_{ref}(s) - z(s))_\tau\|_{\mathscr{L}_\infty} \leq& \|G(s)\|_{\mathscr{L}_1}(L\|(z_{ref}(s) - z(s))_\tau\|_{\mathscr{L}_\infty} + 2\varepsilon) \\ &+ \|C(s)\|_{\mathscr{L}_1}\sqrt{\varphi} + \|G(s) + H(s)\|_{\mathscr{L}_1}\varepsilon \end{aligned} \tag{5.68}$$

Solving (5.68) for $\|(z_{ref}(s) - z(s))_\tau\|_{\mathscr{L}_\infty}$, leads to

$$\|(z_{ref}(s) - z(s))_\tau\|_{\mathscr{L}_\infty} \leq \frac{\|C(s)\|_{\mathscr{L}_1}}{1 - \|G(s)\|_{\mathscr{L}_1}L}\sqrt{\varphi} + \frac{3\|G(s)\|_{\mathscr{L}_1} + \|H(s)\|_{\mathscr{L}_1}}{1 - \|G(s)\|_{\mathscr{L}_1}L}\varepsilon \tag{5.69}$$

Consequently, the bound in (5.69) implies that if the condition in (5.27) is satisfied then $\|(z_{ref}(s)-z(s))_\tau\|_{\mathscr{L}_\infty}$ is uniformly bounded.

On the other hand, from (5.64) and (5.28), one can have

$$u_{ref}(s)-u(s)=\frac{C(s)}{\sigma}\eta_e(s)-\frac{C(s)}{\sigma}\tilde{\eta}(s) \tag{5.70}$$

According to the work in [44], we can write $\frac{C(s)}{\sigma}\tilde{\eta}(s)$ as follows

$$\begin{aligned}\frac{C(s)}{\sigma}(\tilde{\eta}(s)-\epsilon(s)) &= \frac{1}{\sigma}\frac{C(s)}{H(s)}H(s)(\tilde{\eta}(s)-\epsilon(s))\\ &= \frac{1}{\sigma}H_1(s)\tilde{z}(s)\end{aligned} \tag{5.71}$$

or

$$\frac{C(s)}{\sigma}\tilde{\eta}(s)=\frac{1}{\sigma}H_1(s)\tilde{z}(s)+\frac{C(s)}{\sigma}\epsilon(s) \tag{5.72}$$

Using the fact that $C(s)$ is represented by a proper transfer function, $H_1(s)$ is proper and stable. Consequently, the following bound holds

$$\|(u_{ref}(s)-u(s))_\tau\|_{\mathscr{L}_\infty}\leq\|\frac{C(s)}{\sigma}\|_{\mathscr{L}_1}(L\|(z_{ref}(s)-z(s))_\tau\|_{\mathscr{L}_\infty}+3\varepsilon)+\|\frac{H_1(s)}{\sigma}\|_{\mathscr{L}_1}\sqrt{\varphi} \tag{5.73}$$

Also, we use (5.69) to conclude the subsequent bound

$$\|(u_{ref}(s)-u(s))_\tau\|_{\mathscr{L}_\infty}\leq\|\frac{C(s)}{\sigma}\|_{\mathscr{L}_1}(L\delta_1+3\varepsilon)+\|\frac{H_1(s)}{\sigma}\|_{\mathscr{L}_1}\sqrt{\varphi} \tag{5.74}$$

Next, for the second part of the proof, it is evident that φ defined in (5.40) is subject to the following limit $\lim_{\Gamma\to\infty,\varepsilon\to 0}\varphi=0$, which leads to easily conclude that $\lim_{\Gamma\to\infty,\varepsilon\to 0}\delta_1=0$ and $\lim_{\Gamma\to\infty,\varepsilon\to 0}\delta_2=0$. It is proven that $\|(z_{ref}(s)-z(s))_\tau\|_{\mathscr{L}_\infty}\leq\delta_1$ and $\|(u_{ref}(s)-u(s))_\tau\|_{\mathscr{L}_\infty}\leq\delta_2$, thus, $\lim_{\Gamma\to\infty,\varepsilon\to 0}(z_{ref}(t)-z(t))=0$ and $\lim_{\Gamma\to\infty,\varepsilon\to 0}(u_{ref}(t)-u(t))=0$. That completes the proof. □

Remark 5.4. Regarding the representation of φ in Lemma 5.2, it is clear that any augmentation in the values of the design parameter α or the adaptation gain Γ can reduce arbitrary the prediction error. Besides, Proposition 5.1 affirms that if the chosen adaptation gain Γ is large enough and the approximation error ε delivered by the RBFNN is sufficiently small, the signals $z(t)$ and $u(t)$ can track those of the reference signal which reflect the optimal non-adaptive performances of the proposed controller. □

Remark 5.5. Unlike $\mathscr{L}_1$ adaptive control approaches that rely solely on fast projection-type adaptive laws, the use of an RBFNN can relax some design parameters, dependent on the adaptation rate, while still achieving high performance. □

5.5 Simulation Results

In this section, we will test the effectiveness and efficiency of the proposed NNFOL1AC. To this end, two simulation cases are considered alongside a comparative study. First, we suggest controlling the chaos of the fractional-order uncertain Genesio system with an unknown constant input gain [155]. In the second case, we will test the capability of the proposed controller for FONLSs with unknown time-varying input gain. Lastly, a comparative study of the NNFOL1AC is executed against two other FOCs and for the two considered FOSs. This simulation study includes a control law as in (5.22) with its adaptation laws as in (5.21), the predictor form is selected as in (5.20), and the RBFNN introduced in (5.16) and (5.17) is used in the control architecture as an estimator.

5.5.1 Case of Constant Input gain

Let us consider the fractional-order Genesio system [155] which takes the form of (5.1) as follows

$$\begin{cases} D^{\beta}x_1(t) = x_2(t) \\ D^{\beta}x_2(t) = x_3(t) \\ D^{\beta}x_3(t) = f_1(x) + u(t) + d_1(t) \\ \quad y(t) = x_1(t) \end{cases} \tag{5.75}$$

where $x(t) = [x_1(t), x_2(t), x_3(t)]^T$ is the system pseudo states vector which is considered as measurable, $f_1(x) = x_1^2 - 6x_1 - 2.92x_2 - 1.2x_3$ represent system uncertainties, $d_1(t) = 0.1cos(5t)x_3 - 0.1sin(t)$ is the unknown external disturbances, $y(t)$ and $u(t)$ are the output and input signals, respectively, the fractional-order β is fixed as $\beta = 0.98$, and the initial conditions considered for the system are $x(0) = [3,1,1]^T$.

This simulation example is performed for a reference signal $y_d(t) = sin(t)$, where the values of the design parameters are fixed as $\Gamma = 1000$, $\lambda = [7.5, 9, 5]^T$, and $\alpha = 5$, which fulfill the $\mathscr{L}_1$ norm condition in (5.27) and the stability condition in Theorem 1.6, and lead to reach the best performances. The initial values of $\hat{w}$ are set to be zero and $\hat{\sigma}(0) = 0.01$ with their bounds in the projection operator are $\hat{\sigma} \in [0.01, 12]$ and $\hat{w} \in [12, -12]$. The feedback gain K and $D(s)$ mentioned in the control law (5.22) are chosen as $K = 40$ and $D(s) = \frac{1}{s}$. For the RBFNN nodes number $l = 200$, where the center of the receptive vector $\zeta_m \in [-3, 3]$ with an increment of 0.0302, the input vector is $\vartheta = [e_1, e_2, e_3, u]^T$ and the width of the Gaussian function is $\kappa_m = 4, m = 1, 2, \ldots, l$. Finally, the dynamics of the closed-loop system are simulated for $30s$, and the parameters of the Oustaloup's filter are fixed as $\omega_b = 10^{-3}$, $\omega_h = 10^3$, and the approximation order $N = 5$.

Figures 5.2-5.8 show system responses in the case of constant input gain. Figure 5.2 illustrates the tracking response of the system output y to the desired signal y_d. The time evolution of x_2 and x_3 are illustrated in Figure 5.3 and Figure 5.4, respectively. Moreover, the control input is represented in Figure 5.6. It can be seen from the mentioned results

that the system pseudo state vectors track their desired reference signals, performing a fast response and decent transient behavior with a smooth and bounded control signal. Figure 5.5 represents the time evolution of the sliding surface z and its prediction $\hat{z}$. Indeed, this figure affirms that z tracks $\hat{z}$ across the origin. Finally, Figure 5.7 and Figure 5.8, show bounded values of the estimations $\| \hat{w} \|$ and $\hat{\sigma}$, respectively. As a result, it is clear that this simulation confirms that the closed-loop stability of the system is acquired and the NNFOL1AC can behave robustly against system uncertain dynamics and unknown external disturbances.

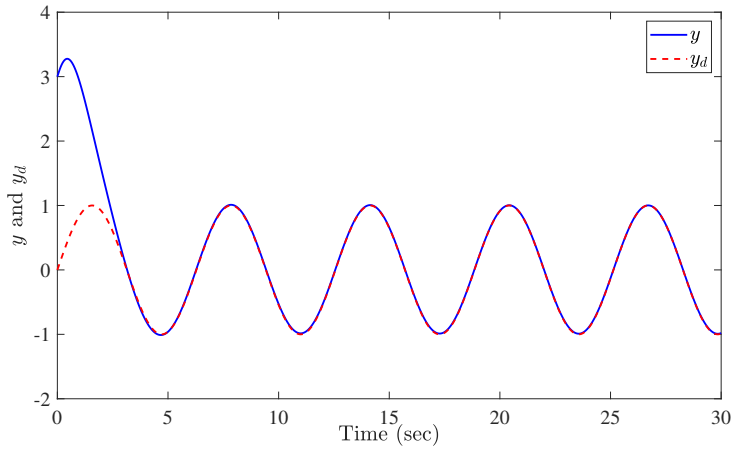

Figure 5.2: Actual output y and reference signal y_d in the case of constant input gain.

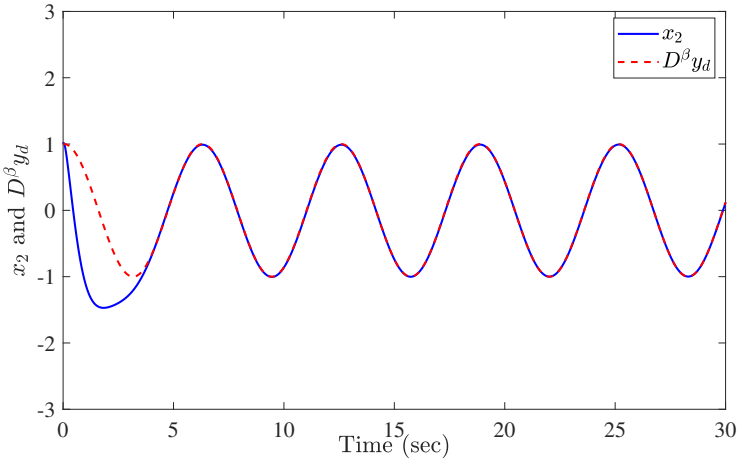

Figure 5.3: Evolution of the state $x_2 = D^\beta x_1$ and $D^\beta y_d$ in the case of constant input gain.

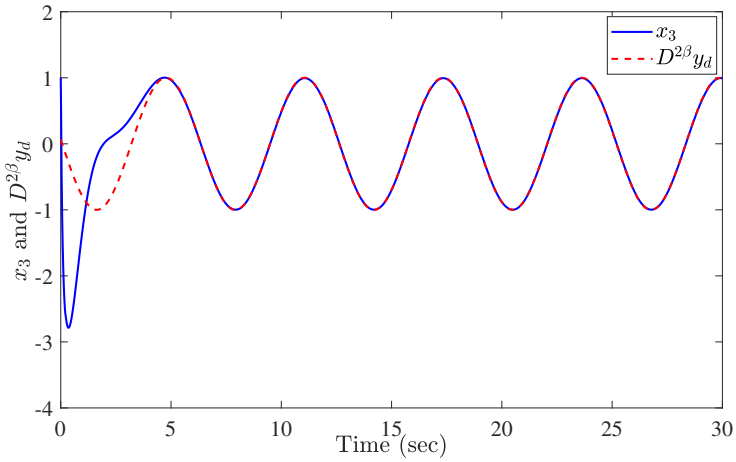

Figure 5.4: Evolution of the state $x_3 = D^{2\beta}x_1$ and $D^{2\beta}y_d$ in the case of constant input gain.

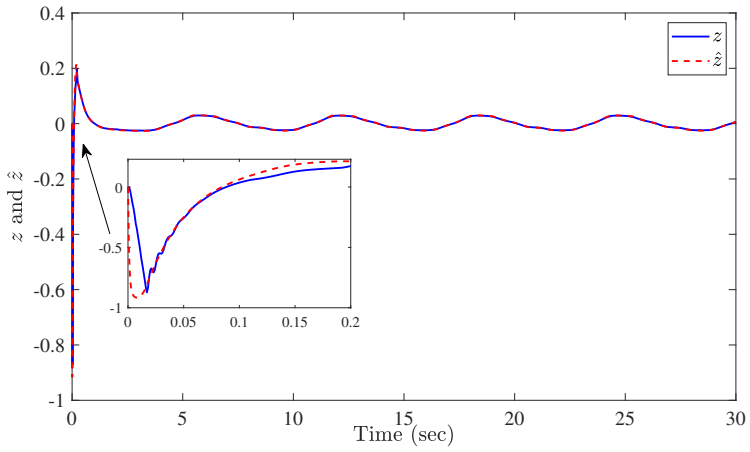

Figure 5.5: Sliding surface z and its prediction $\hat{z}$ in the case of constant input gain.

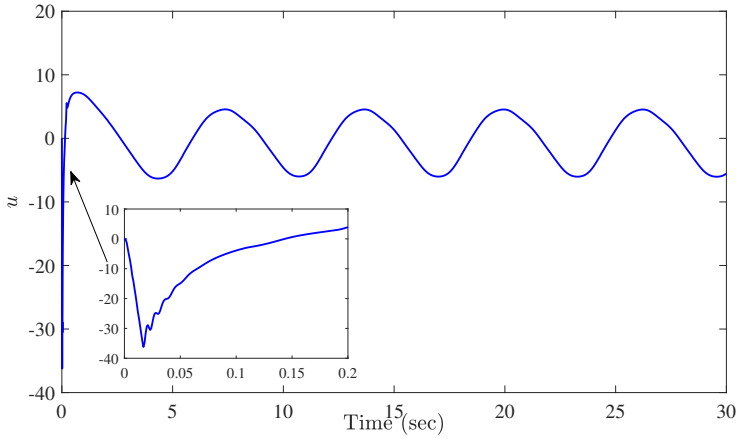

Figure 5.6: Control signal u in the case of constant input gain.

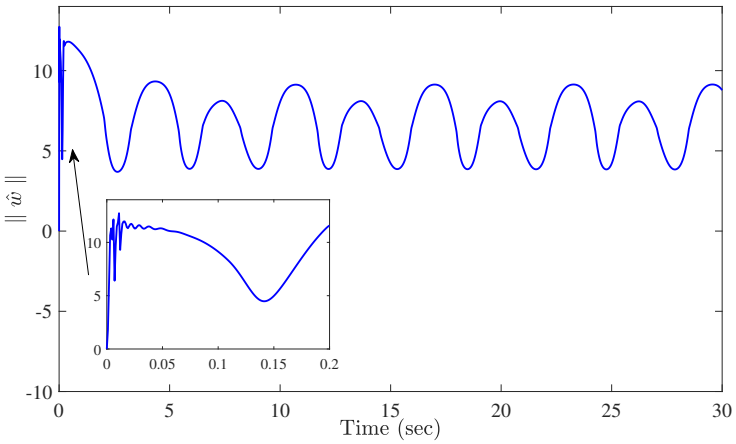

Figure 5.7: Evolution of the Euclidean norm of the estimation $\hat{w}$ in the case of constant input gain.

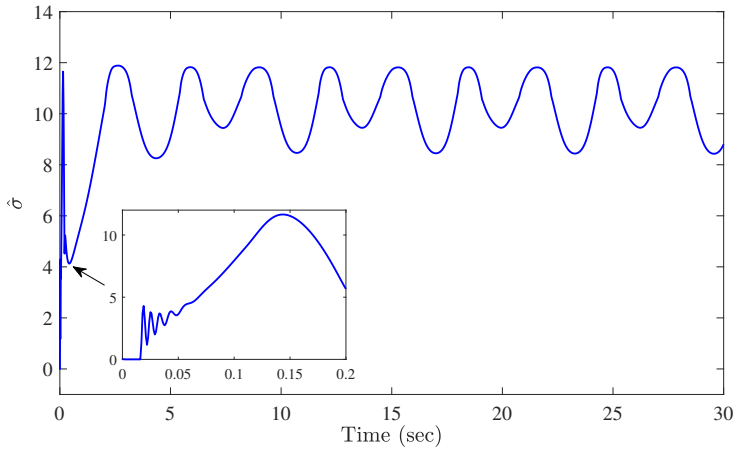

Figure 5.8: Evolution of the estimated value $\hat{\sigma}$ in the case of constant input gain.

5.5.2 Case of Time-varying Input Gain

In this part of the simulation, we consider the uncertain nonlinear fractional-order system (5.76) which is in the form of (5.1)

$$\begin{cases} D^{\beta} x_1(t) = x_2(t) \\ D^{\beta} x_2(t) = f_2(x) + g_2(x)u(t) + d_2(t) \\ \quad y(t) = x_1(t) \end{cases} \tag{5.76}$$

where D^{β} is the Caputo fractional derivative, $\beta = 0.95$ is the corresponded order, $x(t) = [x_1(t), x_2(t)]^T$ represents the overall pseudo states vector which is considered as measurable, $y(t)$ and $u(t)$ are the output and input signals, respectively. $f_2(x)$, $g_2(x)$, and $d_2(t)$ are considered as continuous unknown nonlinear functions, these functions represent system uncertain dynamics, unknown input gain, and external disturbances, respectively. These

functions are given as

$$f_2(x) = \frac{gsinx_1 - m_t m_p q x_2^2 cosx_1 sinx_1}{q(4/3 - m_t m_p cos^2 x_1)} \tag{5.77}$$

$$g_2(x) = \frac{m_t cosx_1}{q(4/3 - m_t m_p cos^2 x_1)} \tag{5.78}$$

$$d_2(t) = 0.1sin(2t)e^{-0.1t} \tag{5.79}$$

The numerical values of $m_t, m_p, g,$ and q are selected as $m_t = 0.909$, $m_p = 0.1$, $g = 9.8$, and $q = 0.5$. It is important to mention that the functions $f_2(x), g_2(x)$ and $d_2(t)$ are used only for simulation purposes. Indeed, these functions are assumed to be unknown, that is to say, the NNFOL1AC does not rely on their values.

The RBFNN estimator introduced in (5.16) is used in the control architecture, where the network nodes number is fixed as $l = 200$, the width of the Gaussian function $\tau_m = 5; m = 1, 2, \ldots, l$, the center of the receptive vector $\zeta_m \in [-6.5, 6.5]$ with an increment of 0.0653, and the input vector $z = [e_1, e_2, u]^T$. In order to achieve the best performances, the design parameters are selected as $\Gamma = 5000$, $\lambda = [25, 5.8]^T$, and $\alpha = 75$. The bounds of the projection operator are $\hat{\sigma} \in [0.01, 12]$ and $\hat{w} \in [12, -12]$ with the initial values of $\hat{w}(0) = 0$ and $\hat{\sigma}(0) = 0.01$. The simulation results are obtained for a reference signal $y_d = 0.5sin(t)$ and initial conditions $x(0) = [0.2, 0]^T$. For the control law introduced in (5.22), we select the feedback gain $K = 34$ and $D(s) = \frac{1}{s}$. Finally, the dynamics of the closed-loop system are simulated for $15s$, and the parameters of the Oustaloup's filter are fixed as $\omega_b = 10^{-3}$, $\omega_h = 10^3$, and the approximation order $N = 5$. Figures 5.9-5.14 show system responses in the case of time-varying input gain. Figure 5.9 represents the tracking trajectory of the actual system output y in response to the reference signal y_d. The time evolution of x_2 and $D^\beta y_d$ are reported in Figure 5.10. In addition, the resulting control signal u is illustrated in Figure 5.12. These mentioned results affirm that the closed-loop system tracks its reference signal with a fast response time, about $t_r = 0.5s$, and a decent transient behavior maintaining a smooth and bounded control signal.

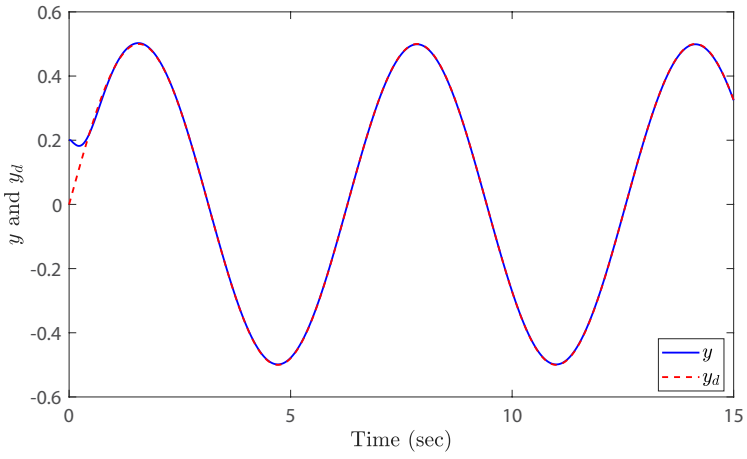

Figure 5.9: Actual output y and reference signal y_d in the case of time-varying input gain.

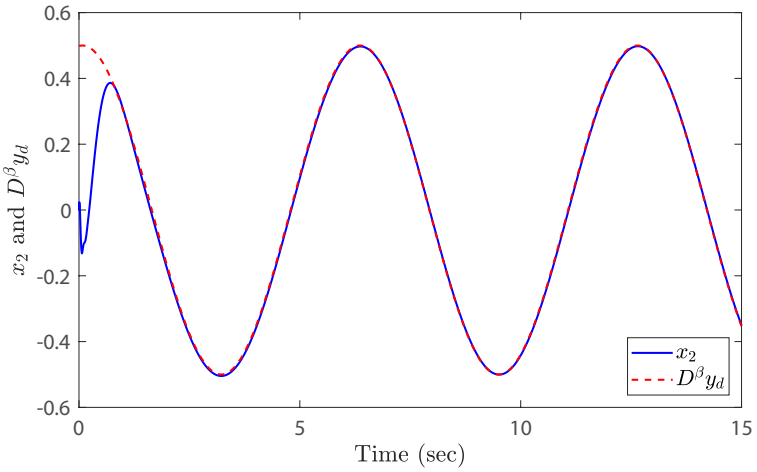

Figure 5.10: Evolution of the state $x_2 = D^\beta x_1$ and $D^\beta y_d$ in the case of time-varying input gain.

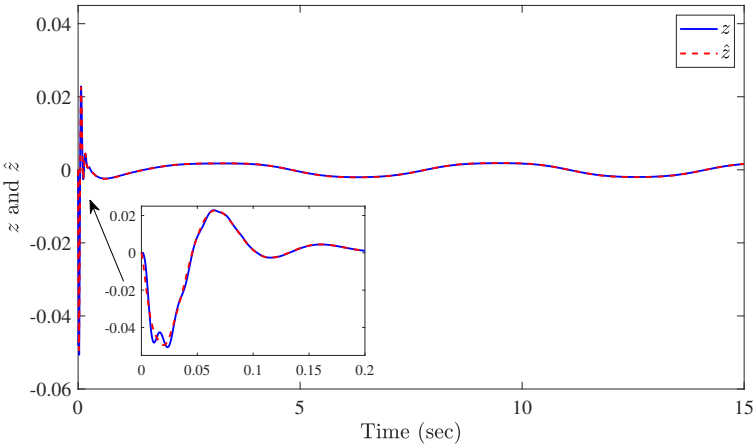

Figure 5.11: Sliding surface z and its prediction $\hat{z}$ in the case of time-varying input gain.

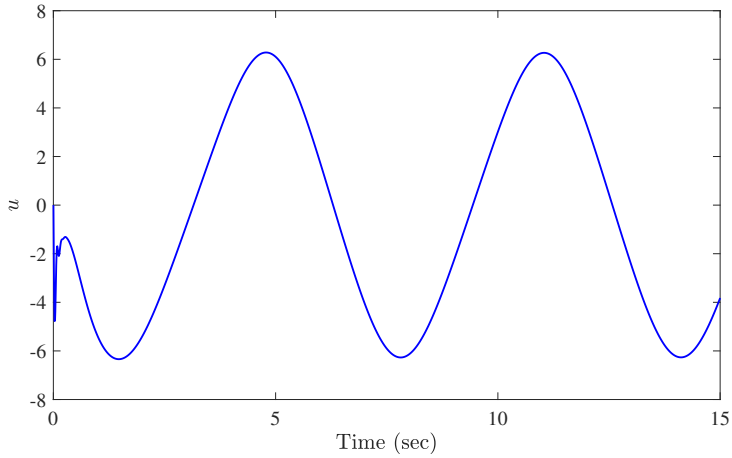

Figure 5.12: Control signal u in the case of time-varying input gain.

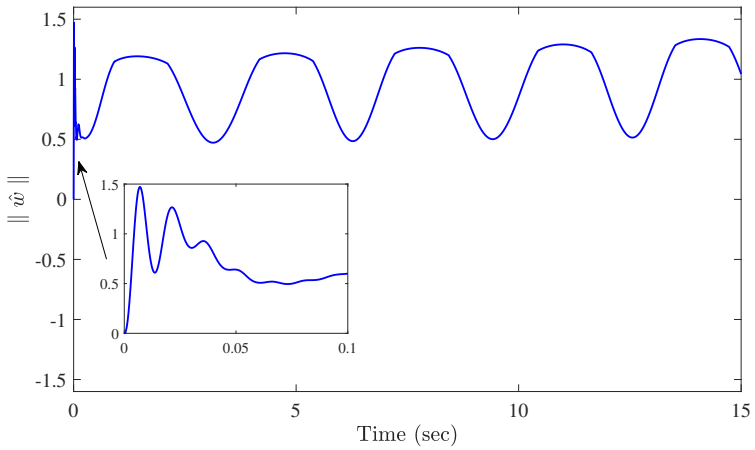

Figure 5.13: Evolution of the Euclidean norm of the estimation $\hat{w}$ in the case of time-varying input gain.

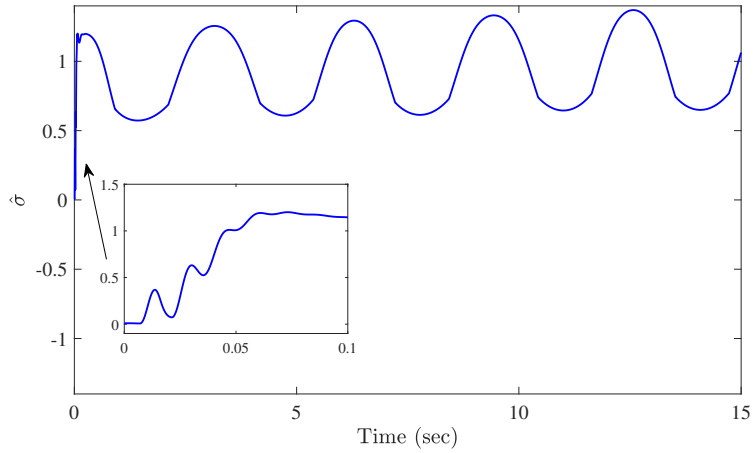

Figure 5.14: Evolution of the estimated value $\hat{\sigma}$ in the case of time-varying input gain.

Moreover, Figure 5.11 shows that the sliding surface z converges to its corresponding prediction $\hat{z}$ across the origin. In Figure 5.13 and Figure 5.14, one can clearly see bounded values of the estimations $\| \hat{w} \|$ and $\hat{\sigma}$, respectively. Thereby, the closed-loop stability of the system and the robust behaviors of the controller against uncertain dynamics, unknown input gain, and external disturbances, are confirmed by these simulation results.

5.5.3 Comparative study

In order to highlight the advantages and the performances of the proposed NNFOL1AC, two comparative studies have been performed of the proposed strategy against the Sliding Mode Active Disturbance Rejection Controller (SMADRC) suggested in [156] and the FOSMC designed in [146] for the systems (5.75) and (5.76), respectively. The same conditions as the previous simulations have been considered for the NNFOL1AC.

The performances of the controllers on each comparative simulation were examined based on the characteristics of the resulted tracking error e_1 for a considered interval of

time; the average absolute value of e_1, its range, and its STD, alongside the sum of the absolute value of u over the whole time of simulation. The above characteristics for both NNFOL1AC and SMADRC for an interval of time $t \in [15, 30]$ are listed in Table 5.1 and for both NNFOL1AC and FOSMC for an interval of time $t \in [5, 15]$ are listed in Table 5.2. Figure 5.15, Figure 5.16, and Figure 5.17 illustrate the tracking responses of the system (5.75) to their reference signals for the NNFOL1AC and SMADRC. Figure 5.18 (Top) and Figure 5.18 (Bottom) show the time evolution of the control signal u delivered by the NNFOL1AC and SMADRC, respectively. Figure 5.19 depicts the tracking responses of the system (5.76) to their reference signals for the NNFOL1AC and FOSMC. Figure 5.20 (Top) and Figure 5.20 (Bottom) show the time evolution of the control signal u delivered by the NNFOL1AC and FOSMC. From these results, it is clear that for each case both control strategies can achieve closed-loop stability. However, the NNFOL1AC is capable to deliver a faster response with better transient performances and smaller tracking errors alongside a smaller sum of the absolute value of the control signal.

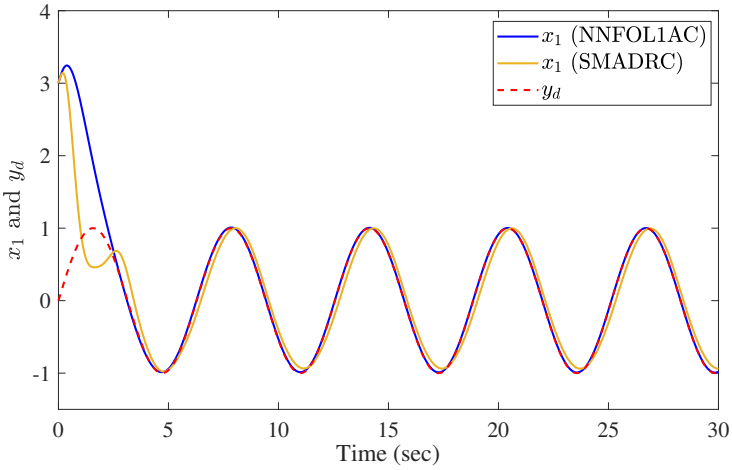

Figure 5.15: Comparative study in the case of constant input gain. Actual output $y = x_1$ and reference signal y_d.

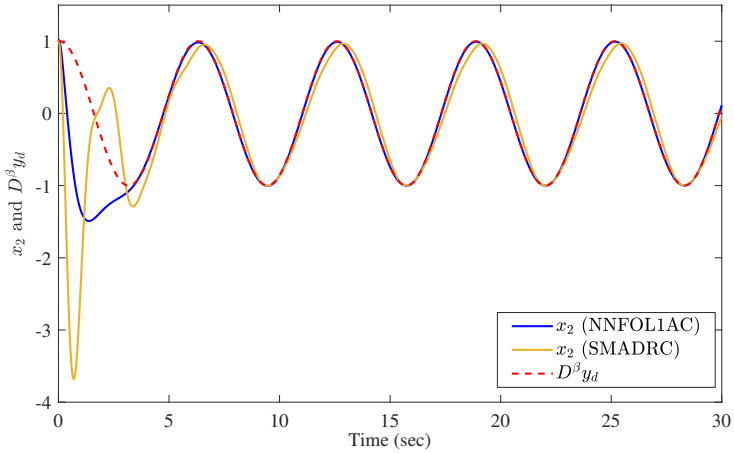

Figure 5.16: Comparative study in the case of constant input gain. Evolution of the state $x_2 = D^\beta x_1$ and $D^\beta y_d$.

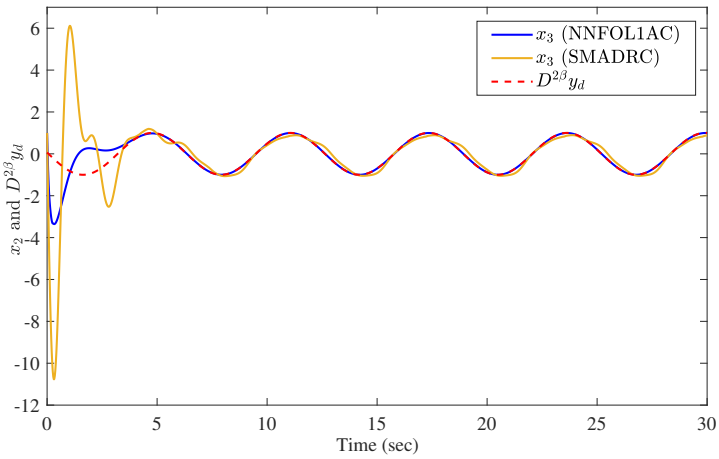

Figure 5.17: Comparative study in the case of constant input gain. Evolution of the state $x_3 = D^{2\beta}x_1$ and $D^{2\beta}y_d$.

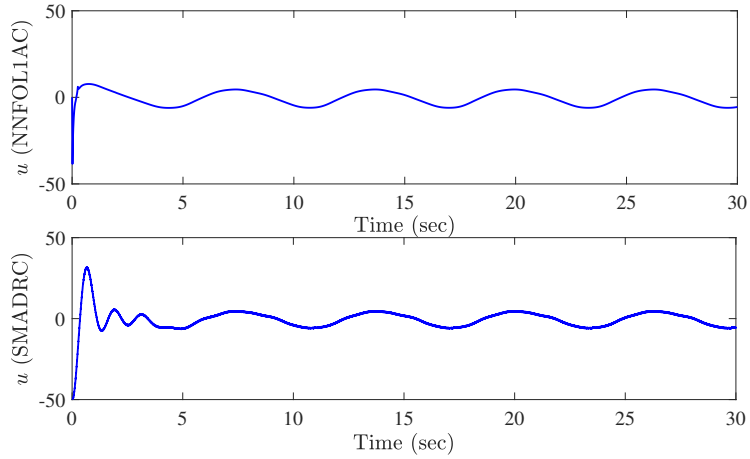

Figure 5.18: Comparative study in the case of constant input gain. Top. Neural network fractional-order $\mathscr{L}_1$ adaptive control signal. Bottom. Sliding mode active disturbance rejection control signal.

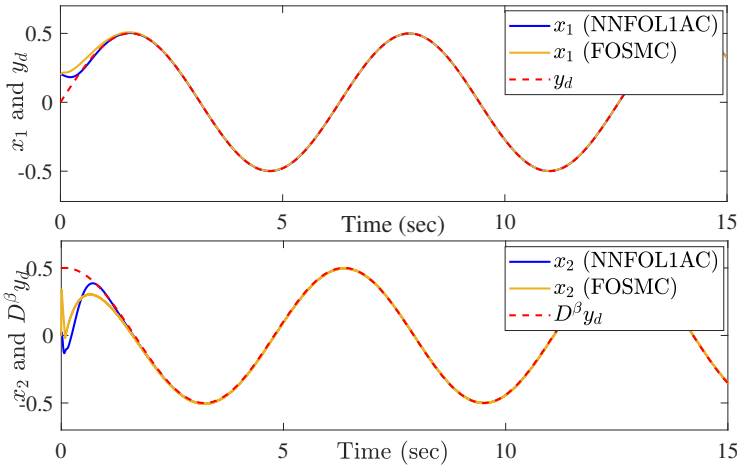

Figure 5.19: Comparative study in the case of time-varying input gain. Actual state vectors and reference signals.

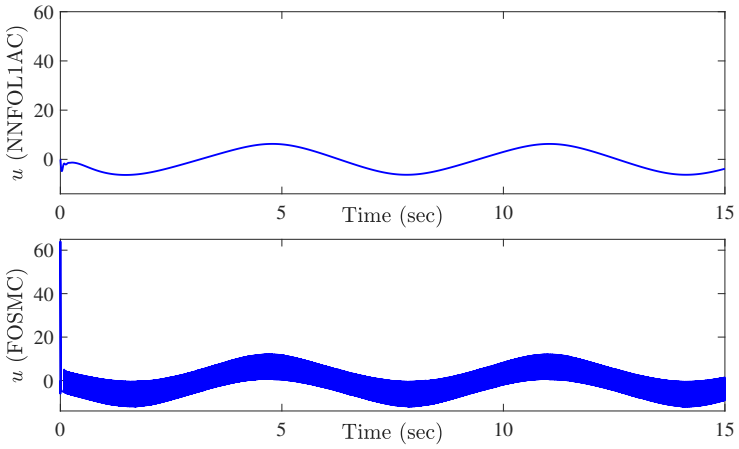

Figure 5.20: Comparative study in the case of time-varying input gain. Top. Neural network fractional-order $\mathscr{L}_1$ adaptive control signal. Bottom. Fractional-order sliding mode control signal.

It is important to mention that the main advantage of the proposed NNFOL1AC (in addition to the tracking performance) is that the control signal does not rely on the values of $f_i(x)$ and $g_i(x)$, $i = 1,2$, where the SMADRC is designed for a constant and known input gain σ and the FOSMC requires the values $f_2(x)$ and $g_2(x)$ in the control design. Besides, the control signal of the latter is suffering from the chartering phenomena which is unfavorable for the controller and the system.

Table 5.1: Precision comparisons between the proposed neural network fractional-order $\mathscr{L}_1$ adaptive control and the sliding mode active disturbance rejection controller.

Control method	$Avg(abs(e_1)) \times 10^{-2}$	Range of $e_1 \times 10^{-2}$	STD of $e_1 \times 10^{-2}$	$\sum(abs(u))$
NNFOL1AC	0.56	$(-0.59, -0.13)$	0.28	1.07×10^5
SMADRC [156]	11.13	$(-13.79, 19.71)$	11.69	1.22×10^5

Table 5.2: Precision comparisons between the proposed neural network fractional-order $\mathscr{L}_1$ adaptive control and the fractional-order sliding mode controller.

Control method	$Avg(abs(e_1)) \times 10^{-3}$	Range of $e_1 \times 10^{-3}$	STD of $e_1 \times 10^{-3}$	$\sum(abs(u))$
NNFOL1AC	0.741	$(-1.37, 1.005)$	0.83	5.94×10^5
FOSMC [146]	0.973	$(-2.35, 1.009)$	1.04	8.08×10^5

5.6 Conclusion

This chapter presents the design of an NNFOL1AC for a considered class of uncertain FONLSs. The proposed controller is based on $\mathscr{L}_1$ adaptive control architecture and incorporates a fractional-order sliding surface and an RBFNN. Theoretical demonstrations prove that the controller is capable of achieving closed-loop stability with improvable

performance bounds in relation to a stable virtual reference system. The low-pass filter placed in the control channel plays a central role in the separation of the estimation loop from the control loop, which leads to preserving the robustness during the improvement of the transient performances in contrast to the conventional adaptive control methods. Besides, the control law has an integral structure which results in a smooth control signal. The simulation results in this chapter were obtained from the application of the proposed controller to an uncertain fractional-order chaotic system, having complex dynamics and unpredictable behavior. Further simulations, have been presented for a nonlinear fractional-order system in the case of unknown time-varying input gain. The simulation discussion revealed that the results are satisfactory for both cases and approve with the theoretical discussions.

Chapter 6

Fuzzy $\mathscr{L}_1$ Adaptive Control Design for Fractional-Order Uncertain Systems with Input Nonlinearity

6.1 Introduction

The main goal of this chapter is to explore and investigate the control of FOSs that are subject to unknown structure, perturbations, and input nonlinearities (dead-zone and sector nonlinearities). The parametric uncertainties and disturbances have a significant impact on the performance of a control scheme. Moreover, the presence of unknown input nonlinearities further complicates the achievement of tracking responses for FOSs. Since real-world applications of FOSs often involve input nonlinearities, it is more convenient to consider these nonlinearities in control schemes. If not, it may end up in poor performances and eventually system instability [104]. Towards controlling such a class of systems, an alternative control scheme is developed, based on $\mathscr{L}_1$ adaptive control strategy and FLSs. The latter serves as an online estimator, aiding in the manipulation and approximation of system uncertainties and unknown input nonlinearities. The developed FFOL1AC in this chapter can be seen as a model-free controller that can control all system states with one controller while delivering a fast response, decent transient performances, a smooth control signal, and a bound to all closed-loop signals. The rest of the chapter is divided into 5 sections and organized as follows. Section 6.2 introduces the problem formulation and the main control objective. Section 6.3 develops and explains the control architecture. Section 6.4 investigates the closed-loop stability of the system. Section 6.5 presents two simulation examples and a comparative study. Section 6.6 concludes the chapter.

6.2 Problem Formulation

This section deals with the description of the class of systems under consideration and specifies the control objective. Towards this end, let us consider the following class of

SISO n-dimensional uncertain FONLSs

$$\begin{cases} D^{\beta}x_j(t) = x_{j+1}(t), j = 1,2,\ldots,n-1 \\ D^{\beta}x_n(t) = f(x) + \mu(u(t)) + d(x,t) \\ y(t) = x_1(t) \end{cases} \tag{6.1}$$

where β is the derivative order with respect to $0 < \beta < 1$, $x(t) = [x_1(t),\ldots,x_n(t)]^T \in \mathbb{R}^n$ is the system pseudo states vector which is supposed to be measurable, $f(.)$ is an unknown continuous nonlinear function, $u(t) \in \mathbb{R}$ is the control signal, $\mu(u(t))$ is the input nonlinearity that will be defined later, and $d(x,t)$ represents system perturbations.

Input nonlinearity $\mu(u(t))$ includes both dead-zone and sector nonlinearities which can be described as [104]

$$\mu(u(t)) = \begin{cases} \kappa_1(u)(u - u_{max}), & u > u_{max} \\ 0, & -u_{min} \le u \le u_{max} \\ \kappa_2(u)(u + u_{min}), & u < -u_{min} \end{cases} \tag{6.2}$$

with $\kappa_1(u) > 0$ and $\kappa_2(u) > 0$ are unknown nonlinear functions, u_{max} and u_{min} are strictly positive and unknown values. The objective of this chapter is to design an FFOL1AC to achieve a robust tracking response of the output signal $y(t)$ to a bounded reference signal $y_d(t) \in \mathbb{R}$, despite the presence of uncertain dynamics, unknown perturbations, and input nonlinearities.

6.3 Fuzzy Fractional-Order $\mathscr{L}_1$ Adaptive Controller

This section will introduce the structure of the proposed control scheme, which is based on a fractional-order sliding surface, a fuzzy logic system, and an $\mathscr{L}_1$ adaptive controller. Therefore, the following assumption is essential.

Assumption 6.1. The reference signal $y_d(t)$ and its successive fractional-order derivatives $D^{j\beta}y_d(t), j = 1,\ldots,n$ are assumed to exist, to be smooth and bounded. □

6.3.1 Choice of an Appropriate Fractional-Order Sliding Surface

To begin, let us select a fractional-order sliding surface in the subsequent form

$$z(t) = D^{\beta-1}e_n(t) + \int_0^t \lambda^T E(\tau)d\tau \tag{6.3}$$

where $z(t) \in \mathbb{R}$, $\lambda^T = [\lambda_1, \lambda_2, \ldots \lambda_n] \in \mathbb{R}^n$ is a vector of design parameters that will be defined later to ensure the stability, and $E(t) = [e_1(t), e_2(t),\ldots,e_n(t)]^T \in \mathbb{R}^n$ is the vector of tracking

errors defined as

$$E(t) = x(t) - Y_d(t) \tag{6.4}$$

with $e_1(t) = x_1(t) - y_d(t)$ is the tracking error and $Y_d(t)$ is the vector of the reference signal and its successive fractional-order derivatives. From (6.4), the tracking errors dynamics can be described as follows

$$\begin{cases} D^{\beta} e_j(t) = e_{j+1}(t), j = 1, 2, \ldots, n-1 \\ D^{\beta} e_n(t) = D^{\beta} x_n(t) - D^{n\beta} y_d(t) \end{cases} \tag{6.5}$$

According to the property in (1.26), the time derivative of (6.3) is given as

$$\dot{z}(t) = D^{\beta} e_n(t) + \lambda^T E(t) \tag{6.6}$$

In the case where the system reaches in the fractional-order sliding surface, one can have $z(t) = \dot{z}(t) = 0$. Hence, for a significantly small value of the resulted $\dot{z}(t)$, i.e., $\dot{z}(t) \approx 0$, one has

$$D^{\beta} e_n(t) = -\lambda^T E(t) \tag{6.7}$$

As a generalization from equations (6.5) and (6.7), the state space representation of the error dynamics can be written as

$$\underbrace{\begin{bmatrix} D^{\beta} e_1(t) \\ D^{\beta} e_2(t) \\ \vdots \\ D^{\beta} e_{n-1}(t) \\ D^{\beta} e_n(t) \end{bmatrix}}_{D^{\beta} E} = \underbrace{\begin{bmatrix} 0 & 1 & 0 & \ldots & 0 \\ 0 & 0 & 1 & \cdots & 0 \\ \vdots & \vdots & \vdots & \ddots & \vdots \\ 0 & 0 & 0 & \cdots & 1 \\ -\lambda_1 & -\lambda_2 & -\lambda_3 & \cdots & -\lambda_n \end{bmatrix}}_{A} \underbrace{\begin{bmatrix} e_1(t) \\ e_2(t) \\ \vdots \\ e_{n-1}(t) \\ e_n(t) \end{bmatrix}}_{E} = AE \tag{6.8}$$

or $D^{\beta} E = AE$ where $A \in \mathbb{R}^{n \times n}$ is a constant matrix. The well-known stability condition that is applied to FOLSs and summarized in Theorem 1.6, i.e., $|arg(eig(A))| > \beta \frac{\pi}{2}$, requires that the design parameters λ_i, $i = 1, 2, \ldots, n$, must be chosen strictly positive. This case implies that the sliding surface dynamics are asymptotically stable which ensures that tracking error and its fractional-order derivatives converge to zero. Therefore, the purpose of the controller can be fulfilled by controlling $z(t)$ and $\dot{z}(t)$ toward zero.

To acquire a dynamical representation of the sliding surface $z(t)$, we begin by replacing (6.5) in (6.6), hence

$$\dot{z}(t) = D^{\beta} x_n(t) - D^{n\beta} y_d(t) + \lambda^T E(t) \tag{6.9}$$

replacing $D^{\beta} x_n(t)$ from (6.1) in (6.9), one has

$$\dot{z}(t) = f(x) + \mu(u(t)) + d(x, t) - D^{n\beta} y_d(t) + \lambda^T E(t) \tag{6.10}$$

Let us define a function v as

$$v(t,z) = \lambda^T E(t) + \alpha z(t) \tag{6.11}$$

with $\alpha \in \mathbb{R}^+$. Adding and subtracting αz in (6.10) and considering (6.11), we have the subsequent expression

$$\dot{z}(t) = -\alpha z(t) + v(t,z) + f(x) + \mu(u(t)) + d(x,t) - D^{n\beta} y_d(t) \tag{6.12}$$

For the input nonlinearity $\mu(u(t))$ defined by (6.2), there is always a positive unknown constant σ and an unknown function $\Delta(x,u)$, such that

$$\mu(u(t)) = \sigma u(t) - \Delta(x,u) \tag{6.13}$$

where $0 < \omega_1 < \sigma < \omega_2$, with ω_1 and ω_2 are some positive constants, and $\Delta(x,u)$ represents the mismatch between $\mu(u(t))$ and $\sigma u(t)$. Hence

$$\dot{z}(t) = -\alpha z(t) + v(t,z) + f(x) + \sigma u(t) - \Delta(x,u) + d(x,t) - D^{n\beta} y_d(t) \tag{6.14}$$

Now, by introducing a function $h(x,v,u)$ as

$$h(x,v,u) = v(t,z) + f(x) + d(x,t) - \Delta(x,u) - D^{n\beta} y_d(t) \tag{6.15}$$

one obtains

$$\dot{z}(t) = -\alpha z(t) + \sigma u(t) + h(x,v,u) \tag{6.16}$$

Note that the nonlinear function $h(x,v,u)$ remains uncertain due to its unknown terms. In the subsequent section, we introduce and employ a fuzzy logic system for the purpose of approximating this function.

6.3.2 Fuzzy Logic System Approximation

A fuzzy logic system is commonly used as an estimator in the control architecture. Basically, FLSs includes a fuzzifier, a rule base, a fuzzy inference system, and a defuzzifier. In this chapter, we consider a zero-order Takagi–Sugeno fuzzy logic system that employs a set of fuzzy $IF-THEN$ rules to define a mapping from the input vector $\vartheta^T = [\vartheta_1, \vartheta_2, \ldots, \vartheta_m] \in \Omega_\vartheta \subset \mathbb{R}^{\mathrm{m}}$ to a scalar output $\hat{h} \in \mathbb{R}$, where the $i^{th}\, If-THEN$ fuzzy rule is defined for m fuzzy sets $N_k^i, k = 1, \ldots, m$ as follows [104, 105, 157]

$$if\ \vartheta_1\ is\ N_1^i\ and \ldots, and\ \vartheta_m\ is\ N_m^i\ Then\ \hat{h}\ is\ h^i, i = 1, \ldots, M \tag{6.17}$$

with h^i is a fuzzy singleton of the output in the corresponding rule.

The use of a production inference system and a singleton fuzzifier lead to the equation

of the fuzzy logic system output

$$\hat{h}(\vartheta) = \frac{\sum_{i=1}^{M} h^i(\prod_{k=1}^{m} \psi_{N_k^i}(\vartheta_k))}{\sum_{i=1}^{M}(\prod_{k=1}^{m} \psi_{N_k^i}(\vartheta_k))} = w^T(\vartheta)\phi \tag{6.18}$$

with $\psi_{N_k^i}(\vartheta_k)$ represents the membership degree of the corresponding input ϑ_k, M is the number of fuzzy rules defined by (6.17), ϕ is a vector containing all adjustable elements in the resulting part of the fuzzy rule and $w^T(\vartheta) = [w_1(\vartheta), \ldots, w_M(\vartheta)] \in \mathbb{R}^M$ is the basis functions vector with

$$w_i(\vartheta) = \frac{\prod_{k=1}^{m} \psi_{N_k^i}(\vartheta_k)}{\sum_{i=1}^{M}(\prod_{k=1}^{m} \psi_{N_k^i}(\vartheta_k))} \tag{6.19}$$

As mentioned before, FLSs are commonly used as online estimators in the control architecture. Based on the universal approximation results presented by [158], this fuzzy system demonstrates the capability to approximate any nonlinear smooth function $h(\vartheta)$ within a compact operating space with a high degree of accuracy. Hence, according to (6.18), the function $h(x, v, u)$ can be approximated as follows

$$h(\vartheta) = w^T(\vartheta)\phi(t) + \epsilon(\vartheta), |\epsilon(\vartheta)| \leq \varepsilon \tag{6.20}$$

with $\epsilon(\vartheta)$ is the approximation error, and ε is a uniform bound for $\epsilon(\vartheta)$. It is worth noting that (6.20) is true assuming that the structure and parameters of the fuzzy system are properly predefined.

Now, replacing (6.20) in (6.16), one can acquire the following representation of the sliding surface dynamics

$$\dot{z}(t) = -\alpha z(t) + \sigma u(t) + w^T(\vartheta)\phi(t) + \epsilon(\vartheta),\ z(0) = z_0 \tag{6.21}$$

Remark 6.1. The control input $u(t)$ is used as an input for the fuzzy system approximator employed to estimate the unknown function $h(x, v, u)$. It is worth noting that there is no algebraic loop problem since the control law has an integral structure as can be observed throughout the rest of this chapter. □

6.3.3 Control Structure

The following predictor (6.22) replicates the dynamics described by (6.21) with the unknown parameters σ and $\phi(t)$ are replaced with their estimations $\hat{\sigma}(t)$ and $\hat{\phi}(t)$, respectively.

$$\dot{\hat{z}}(t) = -\alpha \hat{z}(t) + \hat{\sigma}(t)u(t) + w^T(\vartheta)\hat{\phi}(t),\ \hat{z}(0) = z_0 \tag{6.22}$$

where $\hat{z}(t) \in \mathbb{R}$ represents the prediction of the sliding surface $z(t)$. The values of $\hat{\sigma}(t)$ and

$\hat{\phi}(t)$ are governed by the following projection-type adaptation laws

$$\begin{aligned}\dot{\hat{\sigma}}(t) &= \Gamma Proj(\hat{\sigma}(t), -\tilde{z}(t)u(t)) \\ \dot{\hat{\phi}}(t) &= \Gamma Proj(\hat{\phi}(t), -\tilde{z}(t)w(\vartheta))\end{aligned} \tag{6.23}$$

where $\Gamma \in \mathbb{R}^+$ is the adaptation gain, $Proj(.,.)$ is introduced in Definition 2.3 as the projection operator, and $\tilde{z}(t)$ is the prediction error that is defined as $\tilde{z}(t) = \hat{z}(t) - z(t)$.

The control law is defined as

$$u(s) = -KD(s)\hat{\eta}(s) \tag{6.24}$$

with $\hat{\eta}(s)$ is the Laplace transform of $\hat{\eta}(t) = \hat{\sigma}(t)u(t) + w^T(\vartheta)\hat{\phi}(t)$, K is a feedback gain, and $D(s)$ is a strictly proper transfer function, which is included in the expression of a stable proper closed-loop filter as

$$\hat{C}(s) = \frac{\hat{\sigma}KD(s)}{1 + \hat{\sigma}KD(s)} \tag{6.25}$$

consequently, the resulting form of the filter $\hat{C}(s)$ in (6.25) can represent a low-pass first-order filter with the choice of the transfer function $D(s)$ as $D(s) = \frac{1}{s}$, which gives

$$\hat{C}(s) = \frac{\hat{\sigma}K}{s + \hat{\sigma}K} \tag{6.26}$$

where $\hat{C}(0) = 1$. Finally, an illustrative block diagram of the proposed FFOL1AC is given in Figure 6.1.

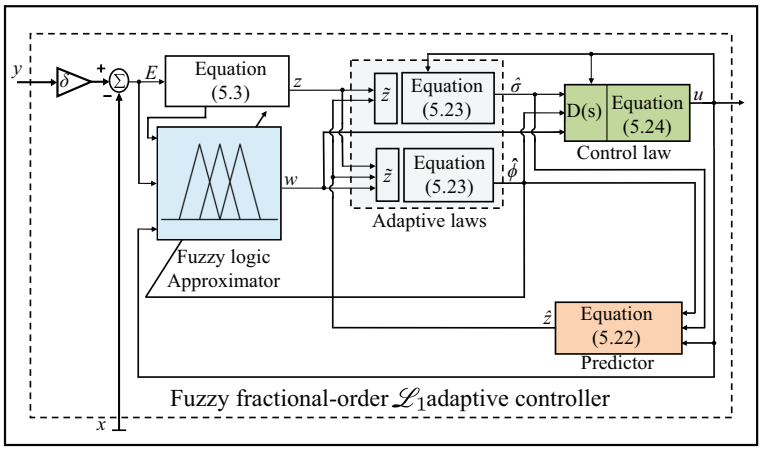

Figure 6.1: Diagram block of the proposed fuzzy fractional-order $\mathscr{L}_1$ adaptive controller.

6.4 Stability and Performances Analysis

This part focuses on the performance and the stability analysis of the developed controller. Hence, we consider that the following assumptions are necessary

Assumption 6.2. In the description of the above system (6.1), the perturbation $d(x,t)$ is assumed to accept a bound $d^* \in \mathbb{R}^+$ as follows

$$|d(x,t)| \leq d^* \tag{6.27}$$

□

Assumption 6.3. Assuming that $h(x,v,u)$ in (6.15) accepts the following bound

$$|h(x,v,u)| \leq L|z(t)| + L_0 \tag{6.28}$$

where L and L_0 are some positive constants. □

Assumption 6.4. Let $\dot{\phi}$ be the bounded derivative of the continuous function $\phi(t)$ such as for all $t \geq 0$

$$\|\dot{\phi}\| \leq d_\phi < \infty \tag{6.29}$$

□

Remark 6.2. The fractional-order sliding surface (6.3) ensures that $x(t)$ shares the same stability behavior with $z(t)$, using the fact that $v(t,z)$ is known and $d(x,t)$ is bounded as suggested in Assumption 6.2. We can assume that the uncertain quantity $h(x,v,u)$ is upper bounded by a functional bound. Hence, with regards to the bound in (6.28), it is obvious that the latter is not constant and it grows as the sliding surface $z(t)$ grows to infinity, which makes it physically acceptable. □

The control architecture defined via (6.22), (6.23), and (6.24), is subject to the $\mathscr{L}_1$ norm condition that follows

$$\|G(s)\|_{\mathscr{L}_1} L < 1 \tag{6.30}$$

where $G(s) = H(s)(1-C(s))$, $H(s) = (s+\alpha)^{-1}$, $C(s) = \frac{\sigma K}{s+\sigma K}$ is a low pass filter, and L is given in (6.28). Therefore, the design parameter α and the filter $C(s)$ are selected to fulfill it.

Remark 6.3. Using the fact that $\alpha > 0$ and $C(s)$ is a strictly proper and BIBO stable transfer function, we can easily conclude that both $G(s)$ and $H(s)$ are BIBO stable and proper transfer functions. □

6.4.1 Closed-Loop Ideal Reference System

We consider now a well-behaving reference system that stands for the closed-loop non-adaptive description of the system (6.21) with the control architecture defined via (6.22), (6.23), and (6.24), this system is defined as

$$\begin{cases} \dot{z}_{ref}(t) = -\alpha z_{ref}(t) + \sigma u_{ref}(t) + w^T(\vartheta_{ref})\phi(t) + \epsilon(\vartheta_{ref}), z_{ref}(0) = z_0 \\ u_{ref}(s) = -\dfrac{C(s)}{\sigma}\eta_{ref}(s) \end{cases} \tag{6.31}$$

with $\eta_{ref}(s)$ denotes the Laplace transform of $\eta_{ref}(t) = w^T(\vartheta_{ref})\phi(t)$.

Remark 6.4. Unlike the proposed control law $u(s)$ in (6.24), the representation of $u_{ref}(s)$ relies on the unknown terms σ and $\phi(t)$ which does not reflect the purpose of this work. However, we mention that $u_{ref}(s)$ is used for analytical purposes only. □

Lemma 6.1. Let us consider that both the design parameter α and the filter $C(s)$ satisfy the $\mathscr{L}_1$ norm condition in (6.30), then with regards to the closed-loop reference system representation in (6.31), the bound that follows holds

$$\|z_{ref\tau}\|_{\mathscr{L}_\infty} \leq \rho \tag{6.32}$$

where

$$\rho = \frac{\|G(s)\|_{\mathscr{L}_1}}{1 - L\|G(s)\|_{\mathscr{L}_1}}(\varepsilon + L_0) + \frac{\|H(s)\|_{\mathscr{L}_1}}{1 - L\|G(s)\|_{\mathscr{L}_1}}\varepsilon + \frac{1}{1 - L\|G(s)\|_{\mathscr{L}_1}}\|z_{in\tau}\|_{\mathscr{L}_\infty} \tag{6.33}$$

with $z_{in} = (s+\alpha)^{-1}z_0$. □

Proof. The closed-loop reference system expression in (6.31) can be represented in the frequency domain as

$$sz_{ref}(s) - z_0 = -\alpha z_{ref}(s) + \sigma u_{ref}(s) + \eta_{ref}(s) + \epsilon_{ref} \tag{6.34}$$

where ϵ_{ref} is the Laplace transform of $\epsilon(\vartheta_{ref})$. Thus, replacing $u_{ref}(s)$ with its expressions, it results

$$z_{ref}(s) = (s+\alpha)^{-1}(1 - C(s))\eta_{ref}(s) + (s+\alpha)^{-1}\epsilon_{ref} + (s+\alpha)^{-1}z_0 \tag{6.35}$$

or

$$z_{ref}(s) = G(s)\eta_{ref}(s) + H(s)\epsilon_{ref} + z_{in} \tag{6.36}$$

Since z_{in} is known and the transfer functions $G(s)$ and $H(s)$ are BIBO stable and proper, it follows from (6.36) that the next upper bound is valid for all $\tau > 0$

$$\|z_{ref\tau}\|_{\mathscr{L}_\infty} \leq \|G(s)\|_{\mathscr{L}_1}\|\eta_{ref\tau}\|_{\mathscr{L}_\infty} + \|H(s)\|_{\mathscr{L}_1}\varepsilon + \|z_{in\tau}\|_{\mathscr{L}_\infty} \tag{6.37}$$

Next, based on the expression (6.20) and replacing $w^T(\vartheta_{ref})\phi(t)$ with $\eta_{ref}(t)$, we can easily obtain

$$\|\eta_{ref\tau}\|_{\mathscr{L}_\infty} = \|h(\vartheta_{ref}) - \epsilon(\vartheta_{ref})\|_{\mathscr{L}_\infty} \tag{6.38}$$

Furthermore, Assumption 6.3 and the bound of $\epsilon(\vartheta)$ in (6.20) suggest the following bound

$$\|\eta_{ref\tau}\|_{\mathscr{L}_\infty} \leq L\|z_{ref\tau}\|_{\mathscr{L}_\infty} + \varepsilon + L_0 \tag{6.39}$$

replacing (6.39) in (6.37), yields in

$$\|z_{ref\tau}\|_{\mathscr{L}_\infty} \leq \|G(s)\|_{\mathscr{L}_1}(L\|z_{ref\tau}\|_{\mathscr{L}_\infty} + \varepsilon + L_0) + \|H(s)\|_{\mathscr{L}_1}\varepsilon + \|z_{in\tau}\|_{\mathscr{L}_\infty} \tag{6.40}$$

solving for $\|z_{ref\tau}\|_{\mathscr{L}_\infty}$, we deduce that

$$\|z_{ref\tau}\|_{\mathscr{L}_\infty} \leq \frac{\|G(s)\|_{\mathscr{L}_1}}{1-L\|G(s)\|_{\mathscr{L}_1}}(\varepsilon + L_0) + \frac{\|H(s)\|_{\mathscr{L}_1}}{1-L\|G(s)\|_{\mathscr{L}_1}}\varepsilon + \frac{1}{1-L\|G(s)\|_{\mathscr{L}_1}}\|z_{in\tau}\|_{\mathscr{L}_\infty} \tag{6.41}$$

It is clear that z_{in} is known and uniformly bounded, also both L_0 and ε have finite values. By considering that the condition in (6.30) is satisfied, it follows from (6.41) that the boundedness of $\|z_{ref\tau}\|_{\mathscr{L}_\infty}$ holds for all $\tau > 0$, which completes the proof. □

6.4.2 Transient and Steady-state Analysis

In this subsection, we discuss the transient and steady-state performances of the system (6.1) and the control architecture defined via (6.22), (6.23), and (6.24) with respect to the well-behaving reference system represented in (6.31).

Since we have $\tilde{z}(t) = \hat{z}(t) - z(t)$, the prediction error dynamics can be described by subtracting (6.21) from (6.22) as

$$\dot{\tilde{z}}(t) = -\alpha\tilde{z}(t) + \tilde{\sigma}(t)u(t) + w^T(\vartheta)\tilde{\phi}(t) - \epsilon(\vartheta) \tag{6.42}$$

where $\tilde{\sigma}(t) = \hat{\sigma}(t) - \sigma$ and $\tilde{\phi}(t) = \hat{\phi}(t) - \phi(t)$ are the estimation errors.

Consequently, expanding (6.42) to the frequency domain, one has

$$\tilde{z}(s) = H(s)(\tilde{\eta}(s) - \epsilon(s)) \tag{6.43}$$

with $\tilde{\eta}(s)$ is the Laplace transform of $\tilde{\eta}(t) = \tilde{\sigma}(t)u(t) + w^T(\vartheta)\tilde{\phi}(t)$.

Lemma 6.2. Let us consider that both the design parameter α and the filter $C(s)$ satisfy the $\mathscr{L}_1$ norm condition in (6.30), then with regards to the prediction error dynamics representation in (6.43), the following bound is valid

$$\|\tilde{z}_\tau\|_{\mathscr{L}_\infty} \leq \sqrt{\varphi} \tag{6.44}$$

where

$$\varphi = (\frac{1}{\Gamma}(4\underset{\phi\in\Theta}{max}\|\phi\|^2 + (\omega_2 - \omega_1)^2) + \frac{\Upsilon^{-1}}{\Gamma}4\underset{\phi\in\Theta}{max}\|\phi\|d_\phi + \Upsilon^{-1}\varepsilon^2 \tag{6.45}$$

with $\Upsilon = (2\alpha - 1)$ and $\alpha > \frac{1}{2}$. □

Proof. In view of studying the stability, we consider the candidate Lyapunov function that follows

$$V(\tilde{z}, \tilde{\phi}, \tilde{\sigma}) = \tilde{z}^2 + \frac{1}{\Gamma}\tilde{\phi}^T\tilde{\phi} + \frac{1}{\Gamma}\tilde{\sigma}^2 \tag{6.46}$$

where its time derivative $\dot{V}$ is given as

$$\dot{V}(\tilde{z}, \tilde{\phi}, \tilde{\sigma}) = 2\tilde{z}\dot{\tilde{z}} + \frac{2}{\Gamma}\tilde{\phi}^T\dot{\tilde{\phi}} + \frac{2}{\Gamma}\tilde{\sigma}\dot{\tilde{\sigma}} \tag{6.47}$$

replacing (6.42) in (6.47), it results in

$$\dot{V}(\tilde{z},\tilde{\phi},\tilde{\sigma}) = 2\tilde{z}(-\alpha\tilde{z}+\tilde{\sigma}u+w^T\tilde{\phi}-\epsilon)+\frac{2}{\Gamma}\tilde{\phi^T}\dot{\hat{\phi}}-\frac{2}{\Gamma}\tilde{\phi^T}\dot{\phi}+\frac{2}{\Gamma}\tilde{\sigma}\dot{\hat{\sigma}} \tag{6.48}$$

or

$$\begin{aligned}\dot{V}(\tilde{z},\tilde{\phi},\tilde{\sigma}) = -2\alpha\tilde{z}^2(t)+2\tilde{\phi^T}(\frac{1}{\Gamma}\dot{\hat{\phi}}+\tilde{z}w)+2\tilde{\sigma}(\frac{1}{\Gamma}\dot{\hat{\sigma}}+\tilde{z}u)\\ -\frac{2}{\Gamma}\tilde{\phi^T}\dot{\phi}-2\tilde{z}\epsilon\end{aligned} \tag{6.49}$$

Consequently, from (6.23), one has

$$\begin{aligned}\dot{V}(\tilde{z},\tilde{\phi},\tilde{\sigma}) = -2\alpha\tilde{z}^2(t)-\frac{2}{\Gamma}\tilde{\phi^T}\dot{\phi}-2\tilde{z}\epsilon+2\tilde{\phi^T}(Proj(\hat{\phi},-\tilde{z}w)+\tilde{z}w)\\ +2\tilde{\sigma}(Proj(\hat{\sigma},-\tilde{z}u)+\tilde{z}u)\end{aligned} \tag{6.50}$$

It follows from Lemma 2.2 that

$$2\tilde{\phi^T}(Proj(\hat{\phi},-\tilde{z}w)+\tilde{z}w)+2\tilde{\sigma}(Proj(\hat{\sigma},-\tilde{z}u)+\tilde{z}u)\leq 0 \tag{6.51}$$

hence

$$\dot{V}(\tilde{z},\tilde{\phi},\tilde{\sigma}) \leq -2\alpha\tilde{z}^2+\frac{2}{\Gamma}\mid\tilde{\phi^T}\dot{\phi}\mid+2\mid\tilde{z}\mid\varepsilon \tag{6.52}$$

It is straightforward to establish that $2\tilde{z}\varepsilon\leq\tilde{z}^2+\varepsilon^2$, that is to say

$$\dot{V}(\tilde{z},\tilde{\phi},\tilde{\sigma}) \leq -\Upsilon\tilde{z}^2+\frac{2}{\Gamma}\mid\tilde{\phi^T}\dot{\phi}\mid+\varepsilon^2 \tag{6.53}$$

Letting Θ be a convex set, with $\hat{\phi}\in\Theta$ follows from Lemma 2.2, the latter also ensures that $|\hat{\sigma}|\leq\chi,\chi\in[\omega_1,\omega_2]$, hence

$$\underset{t\geq 0}{max}(\tilde{\phi}^T\tilde{\phi}+\tilde{\sigma}^2)\leq(4\underset{\phi\in\Theta}{max}\|\phi\|^2+(\omega_2-\omega_1)^2) \tag{6.54}$$

Similarly, based on the upper bound in Assumption 6.4, we get

$$\frac{2}{\Gamma}\mid\tilde{\phi^T}\dot{\phi}\mid\leq\frac{4}{\Gamma}(\underset{\phi\in\Theta}{max}\|\phi\|d_\phi) \tag{6.55}$$

as a result

$$\dot{V}(\tilde{z},\tilde{\phi},\tilde{\sigma}) \leq -\Upsilon\tilde{z}^2+\frac{4}{\Gamma}\underset{\phi\in\Theta}{max}\|\phi\|d_\phi+\varepsilon^2 \tag{6.56}$$

adding and subtracting $\frac{\Upsilon}{\Gamma}\tilde{\phi}^T\tilde{\phi}+\frac{\Upsilon}{\Gamma}\tilde{\sigma}^2$ in (6.56), yields in

$$\dot{V}(\tilde{z},\tilde{\phi},\tilde{\sigma}) \leq -\Upsilon\tilde{z}^2-\frac{\Upsilon}{\Gamma}\tilde{\phi}^T\tilde{\phi}-\frac{\Upsilon}{\Gamma}\tilde{\sigma}^2+\frac{\Upsilon}{\Gamma}\tilde{\phi}^T\tilde{\phi}+\frac{\Upsilon}{\Gamma}\tilde{\sigma}^2+\frac{4}{\Gamma}\underset{\phi\in\Theta}{max}\|\phi\|d_\phi+\varepsilon^2 \tag{6.57}$$

or

$$\begin{aligned}\dot{V}(\tilde{z},\tilde{\phi},\tilde{\sigma}) \leq -\Upsilon V(\tilde{z},\tilde{\phi},\tilde{\sigma}) + \Upsilon((\frac{1}{\Gamma}(4\underset{\phi\in\Theta}{max}\|\phi\|^2 + (\omega_2-\omega_1)^2) \\ + \frac{\Upsilon^{-1}}{\Gamma}4\underset{\phi\in\Theta}{max}\|\phi\|d_\phi + \Upsilon^{-1}\varepsilon^2)\end{aligned} \tag{6.58}$$

Finally, one can conclude that

$$\dot{V}(\tilde{z},\tilde{\phi},\tilde{\sigma}) \leq -\Upsilon V(\tilde{z},\tilde{\phi},\tilde{\sigma}) + \Upsilon\varphi \tag{6.59}$$

Thus, for any given time $t_1 > 0$, if we have $V(t_1) > \varphi$, it follows from (6.59) that $\dot{V}(t_1) < 0$. Besides, since $z(0) = \hat{z}(0)$, it is obvious that $V(0) < \frac{1}{\Gamma}(4\underset{\phi\in\Theta}{max}\|\phi\|^2 + (\omega_2-\omega_1)^2) < \varphi$. Therefore, we can conclude that $V(t) < \varphi$ for all $t > 0$. Finally, the bound $\|\tilde{z}_\tau\|_{\mathscr{L}_\infty} \leq \sqrt{\varphi}$ can be acquired based on the facts that $\tilde{z}^2 < V(t)$ and $\|.\|_\infty \leq \|.\|$, that completes the proof. □

Proposition 6.1. Let us consider that both design parameter α and the filter $C(s)$ satisfy the $\mathscr{L}_1$ norm condition in (6.30), then for the system represented in (6.1), we have

$$\begin{aligned}\|(z_{ref}(s) - z(s))_\tau\|_{\mathscr{L}_\infty} \leq \delta_1 \\ \|(u_{ref}(s) - u(s))_\tau\|_{\mathscr{L}_\infty} \leq \delta_2\end{aligned} \tag{6.60}$$

and

$$\begin{aligned}\lim_{\Gamma\to\infty,\varepsilon\to 0}(z_{ref}(t) - z(t)) = 0 \\ \lim_{\Gamma\to\infty,\varepsilon\to 0}(u_{ref}(t) - u(t)) = 0\end{aligned} \tag{6.61}$$

where

$$\delta_1 = \frac{\|C(s)\|_{\mathscr{L}_1}}{1-\|G(s)\|_{\mathscr{L}_1}L}\sqrt{\varphi} + \frac{3\|G(s)\|_{\mathscr{L}_1} + \|H(s)\|_{\mathscr{L}_1}}{1-\|G(s)\|_{\mathscr{L}_1}L}\varepsilon \tag{6.62}$$

and

$$\delta_2 = \|\frac{C(s)}{\sigma}\|_{\mathscr{L}_1}(L\delta_1 + 3\varepsilon) + \|\frac{H_1(s)}{\sigma}\|_{\mathscr{L}_1}\sqrt{\varphi} \tag{6.63}$$

with $H_1(s) = \frac{C(s)}{H(s)}$. □

Proof. First, adding and subtracting $\sigma u(s) + \eta(s)$ which allows us to rewrite the control law in (6.24) as

$$u(s) = -KD(s)(\hat{\eta}(s) + \sigma u(s) + \eta(s) - \sigma u(s) - \eta(s)) \tag{6.64}$$

by letting $\eta(t) = w^T(\vartheta)\phi(t)$, we can have

$$u(s) = -KD(s)(\tilde{\eta}(s) + \eta(s) + \sigma u(s)) \tag{6.65}$$

consequently, by choosing $D(s) = \frac{1}{s}$, we can deduce

$$u(s) = -\frac{K}{s+\sigma K}(\tilde{\eta}(s) + \eta(s)) \tag{6.66}$$

recalling the representation of the filter $C(p)$ from (6.25), that is to say

$$u(s) = -\frac{C(s)}{\sigma}(\tilde{\eta}(s) + \eta(s)) \tag{6.67}$$

The expression in (6.21) can be expressed in the frequency domain as

$$z(s) = (s+\alpha)^{-1}(\sigma u(s) + \eta(s) + \epsilon(s)) + z_{in} \tag{6.68}$$

replacing (6.67) in (6.68), leads to

$$z(s) = G(s)\eta(s) - H(s)C(s)\tilde{\eta}(s) + H(s)\epsilon(s) + z_{in} \tag{6.69}$$

using the representation of $\tilde{z}(s)$ in (6.43) to deduce that

$$z(s) = G(s)\eta(s) - C(s)\tilde{z}(s) + G(s)\epsilon(\vartheta) + z_{in} \tag{6.70}$$

Next, letting $\eta_e(t) = \eta_{ref}(t) - \eta(t)$ and subtracting (6.70) from (6.36), results in

$$z_{ref}(s) - z(s) = G(s)\eta_e(s) + C(s)\tilde{z}(s) + H(s)\epsilon_{ref} - G(s)\epsilon(s) \tag{6.71}$$

According to Assumption 6.3 and using the bound of $\epsilon(\vartheta)$ in (6.20), η_e can be bounded as

$$\|\eta_{e\tau}\|_{\mathscr{L}_\infty} \leq L\|(z_{ref}(s) - z(s))_\tau\|_{\mathscr{L}_\infty} + 2\varepsilon \tag{6.72}$$

Since the transfer functions $C(s)$, $G(s)$, and $H(s)$ are BIBO stable and proper, with regards to (6.71), we deduce that the next upper bound holds for all $\tau > 0$

$$\begin{aligned}\|(z_{ref}(s) - z(s))_\tau\|_{\mathscr{L}_\infty} \leq \|G(s)\|_{\mathscr{L}_1}(L\|(z_{ref}(s) - z(s))_\tau\|_{\mathscr{L}_\infty} + 2\varepsilon) \\ + \|C(s)\|_{\mathscr{L}_1}\|\tilde{z}_\tau\|_{\mathscr{L}_\infty} + \|G(s) + H(s)\|_{\mathscr{L}_1}\varepsilon\end{aligned} \tag{6.73}$$

solving for $\|(z_{ref}(s) - z(s))_\tau\|_{\mathscr{L}_\infty}$, results in

$$\|(z_{ref}(s) - z(s))_\tau\|_{\mathscr{L}_\infty} \leq \frac{\|C(s)\|_{\mathscr{L}_1}}{1 - \|G(s)\|_{\mathscr{L}_1}L}\sqrt{\varphi} + \frac{3\|G(s)\|_{\mathscr{L}_1} + \|H(s)\|_{\mathscr{L}_1}}{1 - \|G(s)\|_{\mathscr{L}_1}L}\varepsilon \tag{6.74}$$

Similarly, in the second part of the proof, from (6.67) and (6.31), one can have

$$u_{ref}(s) - u(s) = -\frac{C(s)}{\sigma}\eta_e(s) + \frac{C(s)}{\sigma}\tilde{\eta}(s) \tag{6.75}$$

It follows from the work in [44] that $\frac{C(s)}{\sigma}\tilde{\eta}(s)$ can be written as

$$\begin{aligned}\frac{C(s)}{\sigma}(\tilde{\eta}(s) - \epsilon(s)) &= \frac{1}{\sigma}\frac{C(s)}{H(s)}H(s)(\tilde{\eta}(s) - \epsilon(s)) \\ &= \frac{1}{\sigma}H_1(s)\tilde{z}(s)\end{aligned} \tag{6.76}$$

consequently

$$\frac{C(s)}{\sigma}\tilde{\eta}(s) = \frac{1}{\sigma}H_1(s)\tilde{z}(s) + \frac{C(s)}{\sigma}\epsilon(s) \tag{6.77}$$

$H_1(s)$ is a stable and proper transfer function according to the fact that $C(s)$ is BIBO stable and strictly proper. Thus, replacing (6.77) in (6.75) leads to conclude that the next upper bound is valid for all $\tau > 0$

$$\|(u_{ref}(s) - u(s))_\tau\|_{\mathscr{L}_\infty} \leq \|\frac{C(s)}{\sigma}\|_{\mathscr{L}_1}(L\|(z_{ref}(s) - z(s))_\tau\|_{\mathscr{L}_\infty} + 3\varepsilon) + \|\frac{H_1(s)}{\sigma}\|_{\mathscr{L}_1}\sqrt{\varphi} \tag{6.78}$$

or

$$(u_{ref}(s) - u(s))_\tau\|_{\mathscr{L}_\infty} \leq \|\frac{C(s)}{\sigma}\|_{\mathscr{L}_1}(L\delta_1 + 3\varepsilon) + \|\frac{H_1(s)}{\sigma}\|_{\mathscr{L}_1}\sqrt{\varphi} \tag{6.79}$$

Next, it is obvious that φ defined in Lemma 6.2 agrees with the following limit $\lim_{\Gamma\to\infty,\varepsilon\to 0}\varphi = 0$ that leads to easily deduce that $\lim_{\Gamma\to\infty,\varepsilon\to 0}\delta_1 = 0$ and $\lim_{\Gamma\to\infty,\varepsilon\to 0}\delta_2 = 0$. In addition, it was proven that $\|(z_{ref}(s) - z(s))_\tau\|_{\mathscr{L}_\infty} \leq \delta_1$ and $\|(u_{ad}(s) - u_{ad}(s))_\tau\|_{\mathscr{L}_\infty} \leq \delta_2$, hence, $\lim_{\Gamma\to\infty,\varepsilon\to 0}(z_{ref}(t) - z(t)) = 0$ and $\lim_{\Gamma\to\infty,\varepsilon\to 0}(u_{ref}(t) - u(t)) = 0$, that completes the proof. □

Remark 6.5. Lemma 6.2 admits that the prediction error can be significantly reduced by increasing the design parameter α and the adaptation gain Γ. Further results can be seen in Proposition 6.1 since it affirms that if the chosen adaptation gain Γ is large enough and the approximation error ε delivered by the fuzzy system is sufficiently small, the proposed controller represented via (6.22), (6.23), and (6.24) can drive the signals $z(t)$ and $u(t)$ to track those of the well-behaving reference system (6.31). □

6.5 Simulation results

In this section, we discuss the synchronization of different 2-dimensional and 3-dimensional FOCSs to assess the effectiveness of the suggested FFOL1AC. These systems are subject to uncertain dynamic terms, unknown perturbations, and input nonlinearities. For synchronization purposes the structure of the FFOL1AC must have a slight modification. To begin, let us consider the following class of n-dimensional uncertain FOCSs

$$\begin{cases} D^\beta x_j(t) = x_{j+1}(t), j = 1,2,\ldots,n-1 \\ D^\beta x_n(t) = f_x(x) \end{cases} \tag{6.80}$$

where β is the derivative order with respect to $0 < \beta < 1$, $x(t) = [x_1(t),\ldots,x_n(t)]^T \in \mathbb{R}^n$ is the system pseudo states vector which is supposed to be measurable, $f_x(.)$ is an unknown continuous nonlinear function. Model (6.80) is considered as the master system. Thus, the controlled slave system that is related to (6.80) is given by

$$\begin{cases} D^\beta y_j(t) = y_{j+1}(t), j = 1,2,\ldots,n-1 \\ D^\beta y_n(t) = f_y(y) + \mu(u(t)) + d(y,t) \end{cases} \tag{6.81}$$

where $y(t) = [y_1(t), \ldots, y_n(t)]^T \in \mathbb{R}^n$ is the system pseudo states vector which is assumed to be measurable, $u(t) \in \mathbb{R}$ is the control signal, $\mu(u)$ is the input nonlinearity, $d(y,t)$ represents system perturbations, and $f_y(.)$ is an unknown continuous nonlinear function. The vector of tracking error given by (6.4) must be replaced with the vector of synchronization errors given bellow

$$E(t) = y(t) - \varrho x(t) \tag{6.82}$$

with ϱ is a scaling factor. Hence, the function $h(x,v,u)$ defined in (6.15) must be selected as

$$h(x,y,v,u) = v(t,z) + f_y(y) + d(y,t) - \Delta(y,u) - \varrho f_x(x) \tag{6.83}$$

The resulting sliding surface dynamics are the same as (6.21). Besides, the numerical simulations were performed for a scaling factor $\varrho = 1$ and based on the designed controller in the previous sections, including a control law in the form of (6.24) with adaptation laws as in (6.23), a predictor in the form of (6.22), and a fuzzy logic system as described by (6.17), (6.18), and (6.19). We mention that, since the modifications only affects the function $h(x,v,u)$, which is approximated using FLSs, the structure of the controller and its stability analysis remain the same while the vector of the reference signal and its successive derivatives $Y_d(t)$ is replaces with the pseudo states vector $x(t)$ of the master system.

6.5.1 Case of 2-dimensional Chaotic Systems

This example considers two different Duffing-Holmes FOCSs. The master and slave descriptions can be represented in the forms of (6.84) and (6.85), respectively

$$Master \begin{cases} D^\beta x_1(t) = x_2(t) \\ D^\beta x_2(t) = x_1(t) - a_{11}x_2(t) - x_1^3(t) + a_{12}cos(t) \end{cases} \tag{6.84}$$

$$Slave \begin{cases} D^\beta y_1(t) = y_2(t) \\ D^\beta y_2(t) = y_1(t) - a_{21}y_2(t) - y_1^3(t) + a_{22}cos(t) + f_{1y}(x,t) + d_1(t) + \mu_1(u(t)) \end{cases} \tag{6.85}$$

where $a_{11} = 0.25$, $a_{12} = 0.3$, $a_{21} = 0.3$, $a_{22} = 0.35$, $d_1(t) = 0.8sin(t) + 0.45cos(3t)$, and $f_{1y}(x,t) = 0.1sin(t)\sqrt{y_1^2 + y_2^2}$. According to the work in [37], chaotic behavior of the considered systems appears for $\beta = 0.98$.

The initial conditions are chosen as $x(0) = [0.2, 0.1]^T$ and $y(0) = [-0.15, 0.25]^T$. To reach the best performances, the simulation was executed using the following design parameters acquired through trial and error: $\lambda = [6.2, 5.6]^T$, $\alpha = 10.5$, and $\Gamma = 85000$. The parameters of the low-pass filter (6.25) are selected here as $K = 35$ and $D(s) = \frac{1}{s}$. For the estimations $\hat{\sigma}(t)$ and $\hat{\phi}(t)$, we chose their initial values as $\hat{\sigma}(0) = 0.01$ and $\hat{\phi}(0) = 0$ with projection bounds $\hat{\sigma} \in [0.01, 6]^T$and $\hat{\phi} \in [-6, 6]^T$. The input vector of the fuzzy logic system is fixed

as $\vartheta = [e_1, e_2, u, z]^T$ and three membership functions $\psi_{N_k^i}(\vartheta_k)$ set for each input $\vartheta_k, k = 1,2,\ldots,4$ as follows

$$\begin{cases} \psi_{N_k^1}(\vartheta_k) = \dfrac{1}{2}(1 + tanh(-\dfrac{\vartheta_k + \xi_{1k}}{\varsigma_k})) \\ \psi_{N_k^2}(\vartheta_k) = exp(-\dfrac{1}{2}(\dfrac{\vartheta_k + \xi_{2k}}{\varsigma_{kj}})) \\ \psi_{N_k^3}(\vartheta_k) = \dfrac{1}{2}(1 + tanh(\dfrac{\vartheta_k + \xi_{3k}}{\varsigma_k})) \end{cases} \tag{6.86}$$

with the variances $\varsigma_k = [0.2, 0.2, 2.9, 0.03]^T$ and the centers $\xi_{i1} = [0.5, 0, -0.5]$, $\xi_{i2} = [0.5, 0, -0.5]$, $\xi_{i3} = [7, 0, -7]$, and $\xi_{i4} = [0.08, 0, -0.08]$. Furthermore, the input nonlinearity $\mu_1(u)$ is fixed in this case as

$$\mu_1(u) = \begin{cases} (0.5 - 0.2e^{0.1sin(u)})(u - 0.7), & u > 0.7 \\ 0, & -0.7 \leq u \leq 0.7 \\ (0.5 - 0.2e^{0.2cos(u)})(u + 0.7), & u < -0.7 \end{cases} \tag{6.87}$$

Finally, the dynamics of the chaos synchronization between the systems (6.84) and (6.85) are simulated for $100s$, and with the parameters of the Oustaloup's filter are fixed as $\omega_b = 10^{-3}$, $\omega_h = 10^3$, and the approximation order $N = 5$.

Figures 6.2-6.6 display simulation results in the case of 2-dimensional chaotic systems. Figure 6.2 and Figure 6.3 illustrate the master and slave synchronization trajectories of the states (x_1, y_1) and (x_2, y_2), respectively. The synchronization errors e_1 and e_2 are represented in Figure 6.4. These figures affirm that the slave system (6.85) states trajectories are synchronized in a short time to those of the master system (6.84). The control signal u is relatively smooth and bounded as it can be seen in Figure 6.5. Figure 6.6 shows that the sliding surface z converges to its expected values along with its prediction $\hat{z}$.

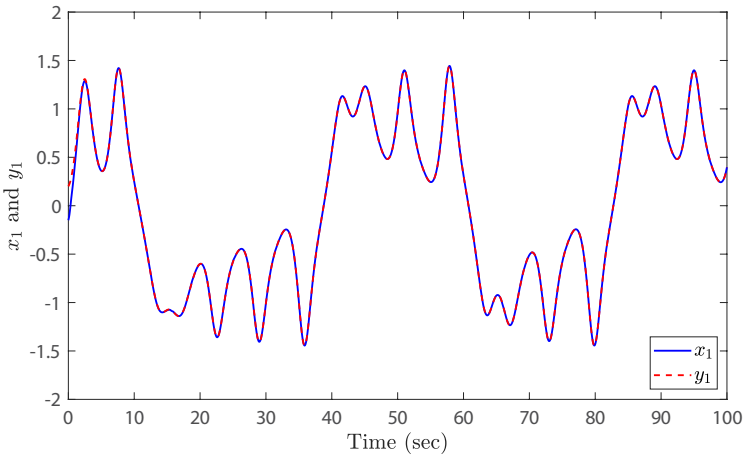

Figure 6.2: Master-slave synchronization trajectories of x_1 and y_1 in the case of 2-dimensional chaotic systems.

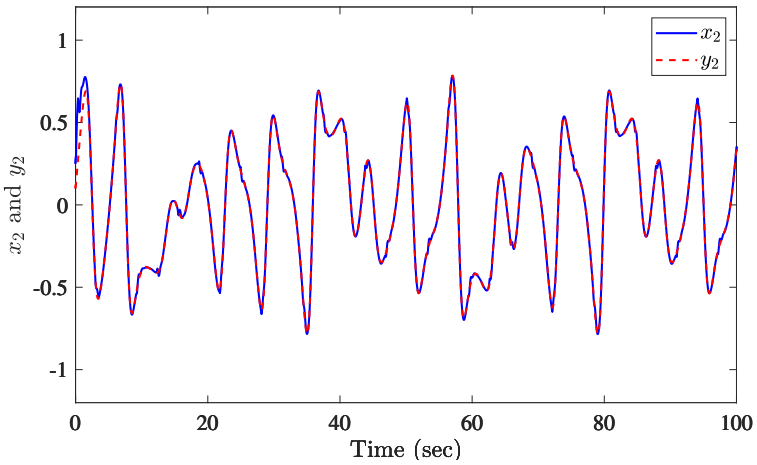

Figure 6.3: Master-slave synchronization trajectories of x_2 and y_2 in the case of 2-dimensional chaotic systems.

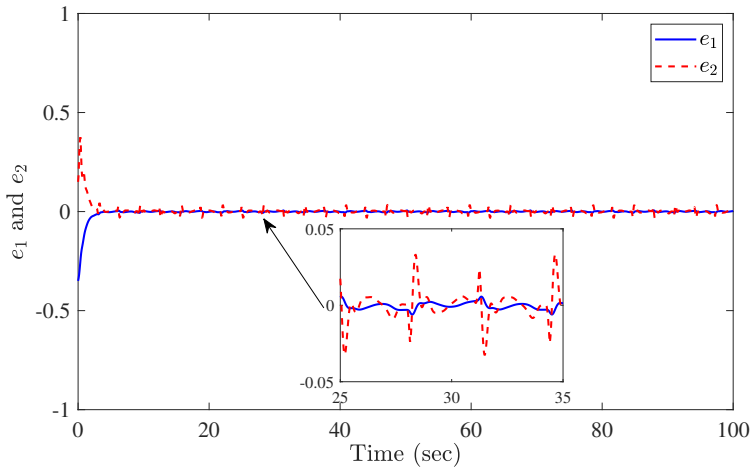

Figure 6.4: Master-slave synchronization errors e_1 and e_2 in the case of 2-dimensional chaotic systems.

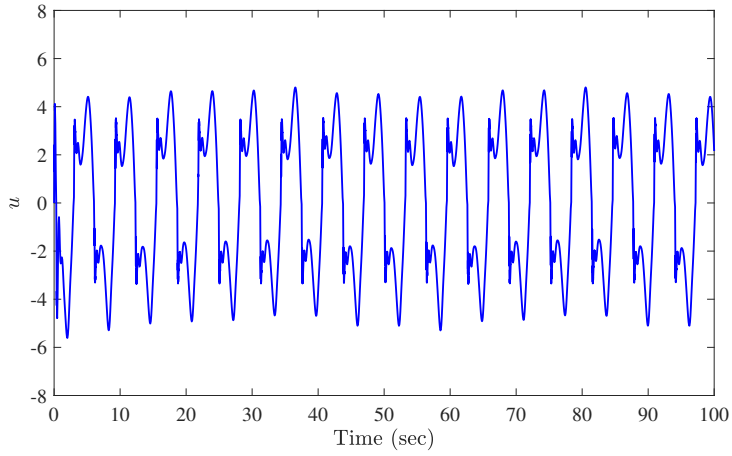

Figure 6.5: Control signal u in the case of 2-dimensional chaotic systems.

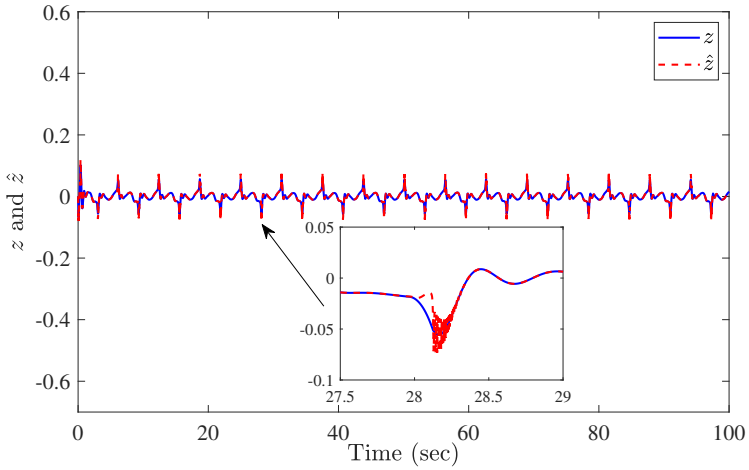

Figure 6.6: Evolution of the sliding surface z and its prediction $\hat{z}$ in the case of 2-dimensional chaotic systems.

Finally, the overall results confirm that the proposed controller ensures the boundedness of all closed-loop signals with fast convergence of the synchronization errors e_1 and e_2 to zero, despite the control complexity due to the considered uncertain models, unknown perturbations, and input nonlinearities.

6.5.2 Case of 3-dimensional Chaotic Systems

This subsection considers the synchronization of two different 3-dimensional FOCSs. As a start, let us consider the fractional-order hybrid optical system [111] as the master system with its description that takes the form of (6.80) as follows

$$Master \begin{cases} D^{\beta} x_1(t) = x_2(t) \\ D^{\beta} x_2(t) = x_3(t) \\ D^{\beta} x_3(t) = -0.326 x_3(t) - x_2(t) + 0.761 x_1(t)(1 - x_1(t)) \end{cases} \tag{6.88}$$

The corresponding slave system is the fractional-order Genesio-Tesi system. Its description is given by (6.89) in the form of (6.81)

$$Slave \begin{cases} D^{\beta} y_1(t) = y_2(t) \\ D^{\beta} y_2(t) = y_3(t) \\ D^{\beta} y_3(t) = -6 y_1(t) - 2.29 y_2(t) - 1.2 y_3(t) + y^2(t) + d_2(t) + \mu_2(u(t)) \end{cases} \tag{6.89}$$

For the fractional-order $\beta = 0.99$, the master system and slave systems behave chaotically [111,159]. The simulation was performed for the initial conditions $x(0) = [0.5, 0.25, 0.12]^T$ and $y(0) = [1.6, -0.05, -0.55]^T$. The external perturbations introduced in (6.89) are chosen as $d_2(t) = 0.45 sin(\pi t) y_1 + 1.1 cos(2t)$. To achieve satisfactory projective synchronization performance, the following design parameters were chosen using the trial and error method: $\lambda = [3.12, 4.6, 2.8]^T$, $\alpha = 95$, and $\Gamma = 16000$. For the low-pass filter (6.25), we

select $K = 45$ and $D(s) = \frac{1}{s}$. The projection bounds are set as $\hat{\sigma} \in [0.01, 6]^T$ and $\hat{\phi} \in [-6, 6]^T$, with the initial values are selected as $\hat{\sigma}(0) = 0.01$ and $\hat{\phi}(0) = 0$. For the applied fuzzy logic system, the input vector is fixed as $\vartheta = [e_1, e_2, e_{3,} u, z]^T$. As in the previous example, three membership functions $\psi_{N_k^i}(\vartheta_k)$ are fixed for each input ϑ_k, $k = 1, 2, \ldots, 5$. Their forms are already presented in (6.86), with the variances $\varsigma_k = [0.3, 0.25, 0.6, 1.5, 0.09]^T$ and the centers $\xi_{i1} = [1, 0.25, -0.5]$, $\xi_{i2} = [0.3, 0.25, -0.8]$, $\xi_{i3} = [1, -0.25, -1.5]$, $\xi_{i4} = [-3, -6.5, -10]$, and $\xi_{i5} = [0.2, 0, -0.2]$. Besides, this case considers the following input nonlinearity

$$\mu_2(u) = \begin{cases} (1 - 0.3sin(u))(u-3), & u > 3 \\ 0, & -3 \le u \le 3 \\ (0.8 - 0.3cos(u))(u+3), & u < -3 \end{cases} \tag{6.90}$$

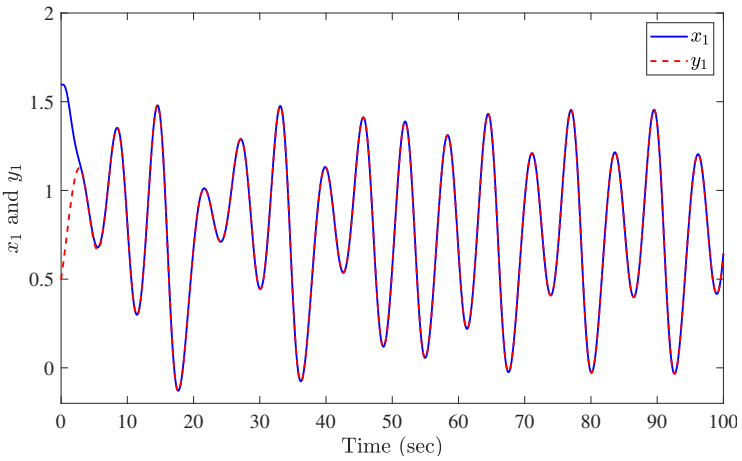

Figure 6.7: Master-slave synchronization trajectories of x_1 and y_1 in the case of 3-dimensional chaotic systems.

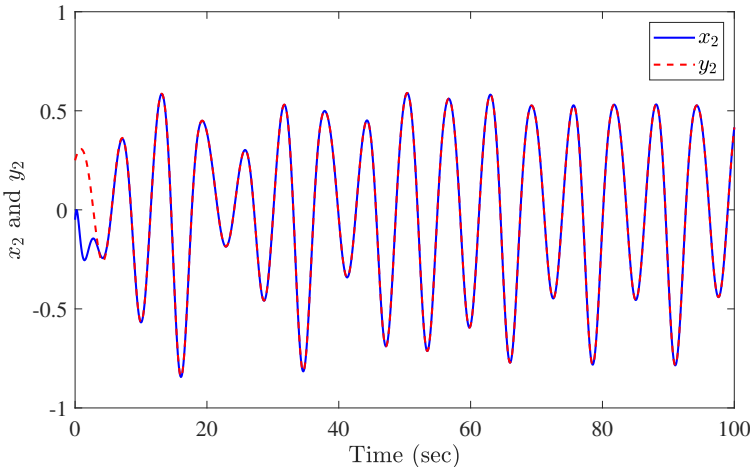

Figure 6.8: Master-slave synchronization trajectories of x_2 and y_2 in the case of 3-dimensional chaotic systems.

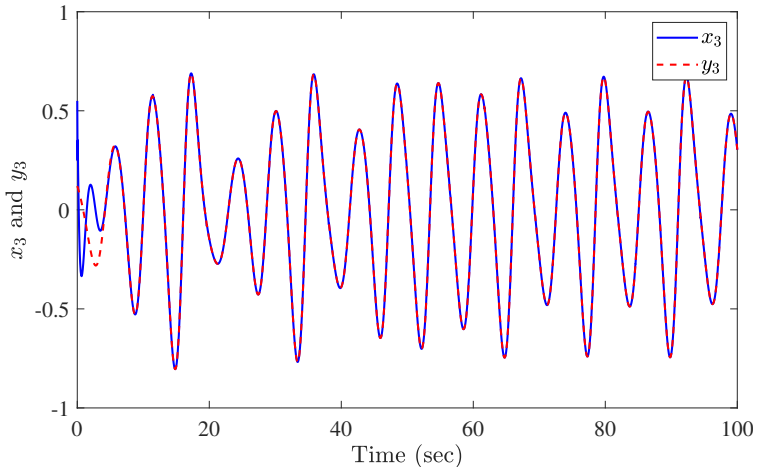

Figure 6.9: Master-slave synchronization trajectories of x_3 and y_3 in the case of 3-dimensional chaotic systems.

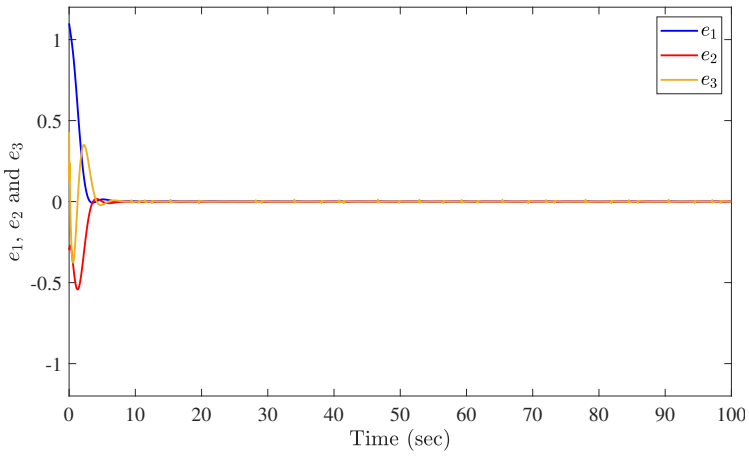

Figure 6.10: Master-slave synchronization errors e_1, e_2, and e_3 in the case of 3-dimensional chaotic systems.

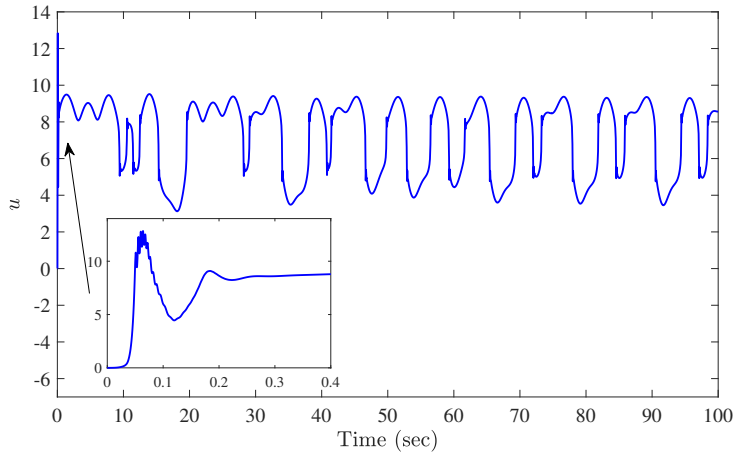

Figure 6.11: Control signal u in the case of 3-dimensional chaotic systems.

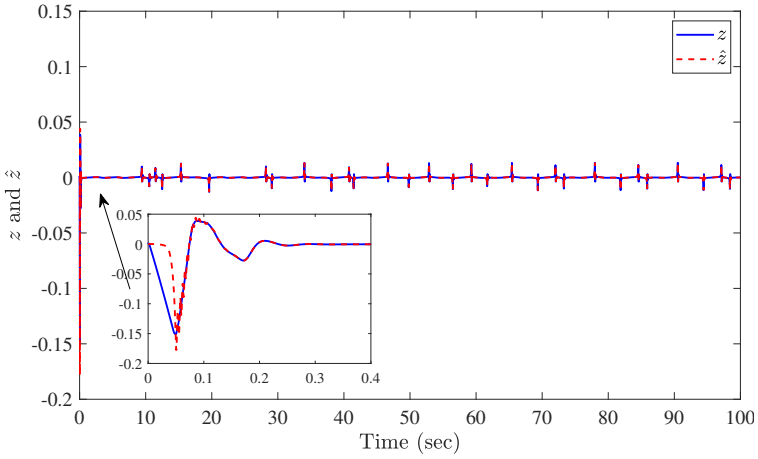

Figure 6.12: Evolution of the sliding surface z and its prediction $\hat{z}$ in the case of 3-dimensional chaotic systems.

Finally, the dynamics of the chaos synchronization between the systems (6.88) and (6.89) are simulated for $100s$, and with the parameters of the Oustaloup's filter are fixed as: $\omega_b = 10^{-3}$,$\omega_h = 10^3$, and the approximation order $N = 5$.

Figures 6.7-6.12 illustrate simulation results in the case of 3-dimensional chaotic systems. Figure 6.7, Figure 6.8, and Figure 6.9 depict the master and slave synchronization trajectories of the states (x_1, y_1), (x_2, y_2), and (x_3, y_3), respectively. Figure 6.10 shows the synchronization errors e_1, e_2, and e_3. Based on the mentioned figures, it is clear that a fast synchronization response is achieved between the slave system (6.89) and the master system (6.88). Figure 6.11 reveals that the control signal u is also smooth and bounded for this example. Figure 6.12 shows that the sliding surface z quickly converges towards its prediction $\hat{z}$.

6.5.3 Comparative Study

To further highlight the advantages of the proposed FFOL1AC, a comparative study has been carried out between the FFOL1AC and the CFANNC suggested in [111] for the master-slave synchronization of the systems (6.88) and (6.89). The same conditions as the previous simulation have been considered for the NNFOL1AC. However, this case considers the following input nonlinearity

$$\mu_2(u) = \begin{cases} 2.1(u-1), & u > 1 \\ 0, & -1 \leq u \leq 1 \\ 2(u+1), & u < -1 \end{cases} \tag{6.91}$$

The synchronization precision in this comparative study was inspected based on the errors e_1, e_2, and e_3 delivered by the two synchronization methods over a period of time (focusing on steady-state performances). Three main characteristics are presented in Table 6.1, the range, the STD, and the average absolute value of the synchronization errors.

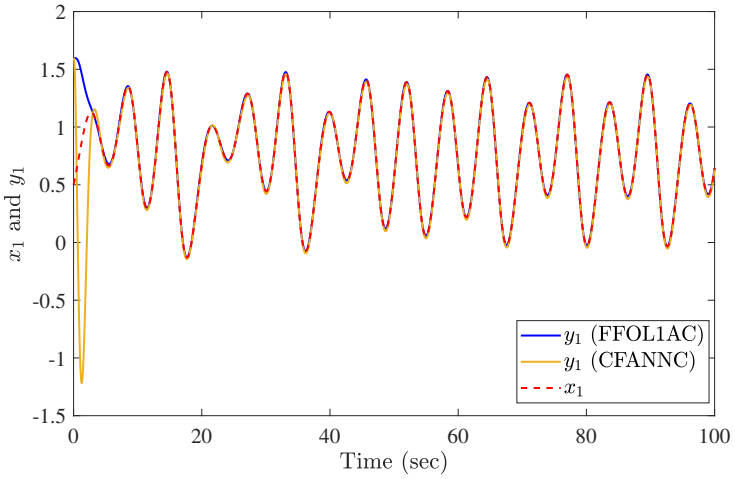

Figure 6.13: Comparative study in the case of 3-dimensional chaotic systems. Master-slave synchronization trajectories of x_1 and y_1.

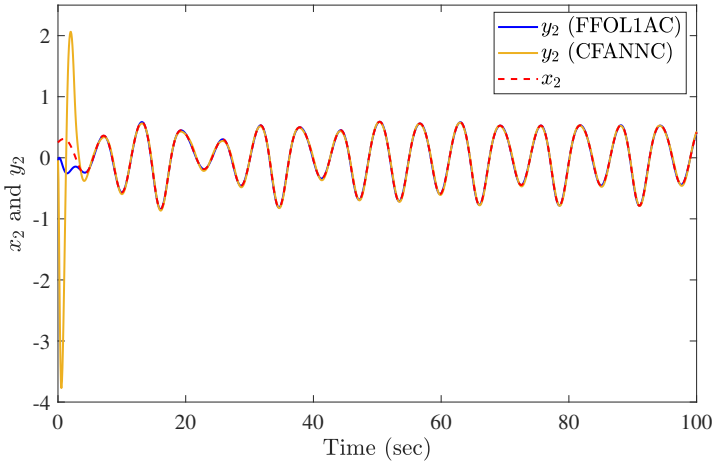

Figure 6.14: Comparative study in the case of 3-dimensional chaotic systems. Master-slave synchronization trajectories of x_2 and y_2.

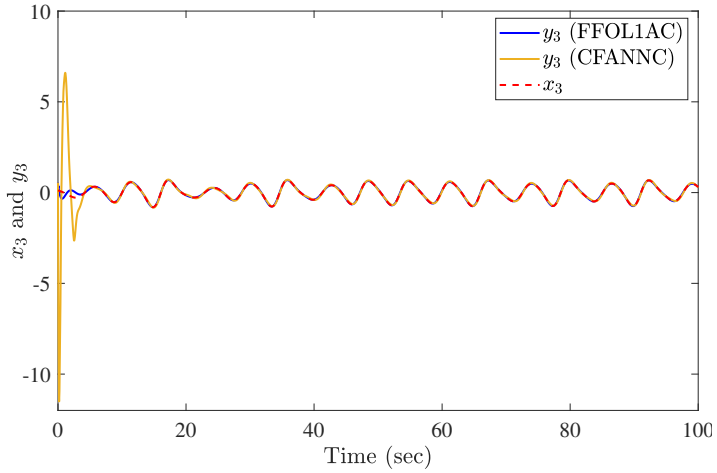

Figure 6.15: Comparative study in the case of 3-dimensional chaotic systems. Master-slave synchronization trajectories of x_3 and y_3.

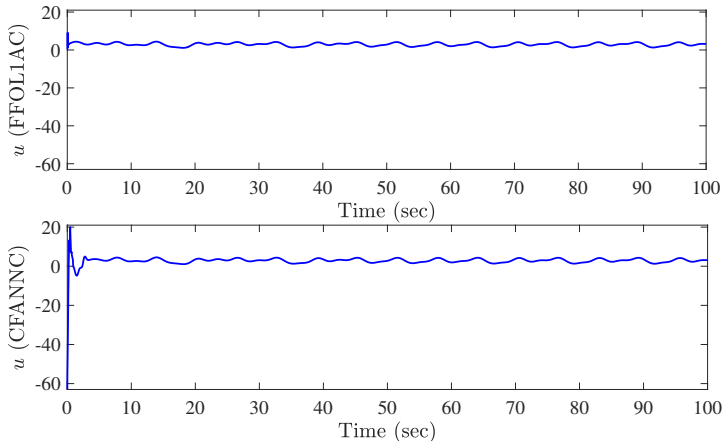

Figure 6.16: Comparative study in the case of 3-dimensional chaotic systems. Top. Fuzzy fractional-order $\mathscr{L}_1$ adaptive control signal. Bottom. Command-filtered adaptive neural network control.

Table 6.1: Precision comparisons between the proposed fuzzy fractional-order $\mathscr{L}_1$ adaptive control and the command-filtered adaptive neural network control.

Controller	Errors	$Avg(abs(e_i) \times 10^{-2}$	Range of $e_i \times 10^{-2}$	STD of $e_i \times 10^{-2}$
FFOL1AC	e_1	0.20	$(0.16, 0.23)$	0.03
	e_2	0.12	$(-0.25, -0.07)$	0.04
	e_3	0.11	$(-0.04, -0.47)$	0.15
CFANNC [111]	e_1	1.40	$(-3.34, -0.82)$	1.50
	e_2	2.60	$(-2.84, 3.76)$	2.90
	e_3	4.53	$(-6.42, 6.62)$	4.86

Figure 6.13, Figure 6.14, and Figure 6.15 illustrates master-slave synchronization trajectories of the states (x_1, y_1), (x_2, y_2), and (x_3, y_3) for both controllers. The resulting control signals by the FFOL1AC and CFANNC are depicted in Figure 6.16 (top) and Figure 6.16 (bottom), respectively. These figures affirm the main advantage of the $\mathscr{L}_1$ adaptive controller which is fast adaptation with decent transient response. Besides, Table 6.1 reveals the very satisfactory results of the steady-state regime.

In summary, it is obvious that the simulation results agree with the theoretical and analytical results and demonstrate the effectiveness of the designed FFOL1AC.

6.6 Conclusion

In this chapter, a FFOL1AC is designed to control a general class of FOSs that are subject to uncertain models, unknown perturbations, and input nonlinearities. The controller is derived based on a fractional-order sliding surface and includes a control law, an adaptive mechanism, and a predictor. Besides, a fuzzy logic system is used in this control method to efficiently handle system uncertainties and input nonlinearities. The estimation loop

is decoupled from the control loop thanks to the low-pass filter placed within the input channel. Thereby, the controller can achieve tracking response and preserve robustness along with improving transient performances, which offers an efficient and robust control strategy for the class of FOSs considered in this chapter. The conducted simulations in this work focused on projective synchronization problems for different FOCSs. The results are provided from two numerical simulation examples that demonstrate the applicability and efficacy of the proposed synchronization approach, as well as the theoretical debates.

General Conclusion

Conclusion

This thesis explores the extension of $\mathscr{L}_1$ adaptive architecture and its implementation in controlling several classes of fraction-order systems. The main contribution of the work is to design new control schemes, accompanied by their theoretical demonstrations of stability and validations through numerical simulations. With multiple architectures proposed, this work can be summarized with 4 different parts: The 1^{st} part is the development of a fractional-order $\mathscr{L}_1$ adaptive controller for a class of fractional-order systems that are subject to uncertainties and external disturbances. The architecture of the controller comprises several components, namely a fractional-order sliding surface, a control law, an adaptive mechanism, and a predictor. The use of the fractional-order sliding surface is the key to apply the $\mathscr{L}_1$ adaptive methodology to a fractional-order system. It helps to study the stability and derive integer-order forms of the adaptation laws. The 2^{nd} part addresses the problem of multiple-input multiple-output fractional-order systems. The developed multivariable fractional-order $\mathscr{L}_1$ adaptive controller in this part is designed to deal with model uncertainties and unknown input gain, where it was proven to encompass the control of different classes of systems such as multiple-input multiple-output, incommensurate, and hyper-chaotic systems. The 3^{rd} part focuses on extending further the idea by incorporating a radial basis function neural network approximator into its architecture. The latter is used to approximate and handle nonlinear uncertain dynamics of the system alongside the unknown time-varying input gain, which helps in relaxing some design parameters and results in small tracking errors that significantly improves control accuracy. The 4^{th} part further extends the developed controller to the case fractional-order systems that are subject to unknown input nonlinearity. The latter further complicates the achievement of closed-loop stability. Thereby, the suggested controller includes a fuzzy system, which helps in the manipulation of the uncertain dynamics, external disturbances, and input nonlinearity posed by the structure of the system. The overall discussions on the developed controllers demonstrate that both input and output system signals converge to those of a stable closed-loop reference system, which indicates that the controller is able to achieve closed-loop stability while performing a fast tracking response with sat-

isfactory transient performances. The conducted simulations illustrate the applicability of the $\mathscr{L}_1$ adaptive controller for different classes of fractional-order systems, holding the key advantages of the methodology and robustly dealing with several challenges posed by system uncertainties.

Future Perspectives

The various extensions and controllers discussed in this thesis are relatively new and promising for further studies. However, similar to other fields of research, certain challenges still exist. In this section, we will present a variety of potential research scopes that can be derived from our research.

- The designed fractional-order $\mathscr{L}_1$ adaptive controllers so far are still not beyond simulations. Thus, a real-world implementation is necessary in order to fully validate the effectiveness of such controllers.
- Applying the developed controller to other classes of systems. For example, systems with unknown fractional-order and time-delayed systems.
- Extending the methodology to output feedback formulation and suggesting improvements to the scheme by introducing a state observer.
- Incorporating an online estimator in the architecture of the multivariable fractional-order $\mathscr{L}_1$ adaptive controller developed in Chapter 4, which could help in enhancing the control accuracy and the overall performances.
- Investigating the effects of using a fractional-order low-pass filter in the control channel, alongside developing projection-type adaptation laws of fractional-order.

Bibliography

[1] Ivo Petráš. *Fractional-order nonlinear systems: Modeling, analysis and simulation*. Springer Science & Business Media, 2011.

[2] Mou Chen, Shuyi Shao, and Peng Shi. *Robust adaptive control for fractional-order systems with disturbance and saturation*. John Wiley & Sons, 2017.

[3] Bijnan Bandyopadhyay and Shyam Kamal. *Stabilization and control of fractional order systems: A sliding mode approach*, volume 317. Springer, 2015.

[4] Rudolf Gorenflo. Abel integral equations with special emphasis on applications. *(No Title)*, 1996.

[5] Indranil Pan and Saptarshi Das. *Intelligent fractional order systems and control: An introduction*, volume 438. Springer, 2012.

[6] Igor Podlubny. *Fractional differential equations: An introduction to fractional derivatives, fractional differential equations, to methods of their solution and some of their applications*. Elsevier, 1998.

[7] Ricardo Almeida, Shakoor Pooseh, and Delfim FM Torres. *Computational methods in the fractional calculus of variations*. World Scientific Publishing Company, 2015.

[8] Changpin Li and Weihua Deng. Remarks on fractional derivatives. *Applied mathematics and computation*, 187(2):777–784, 2007.

[9] Dingyü Xue. FOTF toolbox for fractional-order control systems. *Applications in control*, 6:237–266, 2019.

[10] Manuel A Duarte-Mermoud, Norelys Aguila-Camacho, Javier A Gallegos, and Rafael Castro-Linares. Using general quadratic Lyapunov functions to prove Lyapunov uniform stability for fractional order systems. *Communications in Nonlinear Science and Numerical Simulation*, 22(1-3):650–659, 2015.

[11] Michele Caputo. Linear models of dissipation whose Q is almost frequency independent–II. *Geophysical Journal International*, 13(5):529–539, 1967.

[12] Rudolf Hilfer. *Applications of fractional calculus in physics*. World scientific, 2000.

[13] Maria da Graça Marcos, Fernando BM Duarte, and JA Tenreiro Machado. Fractional dynamics in the trajectory control of redundant manipulators. *Communications in Nonlinear Science and Numerical Simulation*, 13(9):1836–1844, 2008.

[14] Chien-Cheng Tseng. Design of FIR and IIR fractional order Simpson digital integrators. *Signal Processing*, 87(5):1045–1057, 2007.

[15] Tom T Hartley, Carl F Lorenzo, and H Killory Qammer. Chaos in a fractional order Chua's system. *IEEE Transactions on Circuits and Systems I: Fundamental Theory and Applications*, 42(8):485–490, 1995.

[16] Clara Mihaela Ionescu. *The human respiratory system: An analysis of the interplay between anatomy, structure, breathing and fractal dynamics*. Springer Science & Business Media, 2013.

[17] Andrew W Lo. Long-term memory in stock market prices. *Econometrica: Journal of the Econometric Society*, pages 1279–1313, 1991.

[18] Stephen W Wheatcraft and Mark M Meerschaert. Fractional conservation of mass. *Advances in Water Resources*, 31(10):1377–1381, 2008.

[19] Abdon Atangana and Necdet Bildik. The use of fractional order derivative to predict the groundwater flow. *Mathematical Problems in Engineering*, 2013, 2013.

[20] Concepción A Monje, YangQuan Chen, Blas M Vinagre, Dingyu Xue, and Vicente Feliu-Batlle. *Fractional-order systems and controls: Fundamentals and applications*. Springer Science & Business Media, 2010.

[21] Igor Podlubny. Fractional-order systems and fractional-order controllers. *Institute of Experimental Physics, Slovak Academy of Sciences, Kosice*, 12(3):1–18, 1994.

[22] Igor Podlubny, Ivo Petráš, Blas M Vinagre, Paul O'Leary, and L' Dorčák. Analogue realizations of fractional-order controllers. *Nonlinear dynamics*, 29:281–296, 2002.

[23] Igor Podlubny. Fractional-order systems and $PI^{\lambda}D^{\mu}$ controllers. *IEEE Trans Autom Control*, 44(1):208–214, 1999.

[24] YangQuan Chen, Ivo Petras, and Dingyu Xue. Fractional order control-a tutorial. In *2009 American control conference*, pages 1397–1411. IEEE, 2009.

[25] Martin Cech and Milos Schlegel. The fractional-order PID controller outperforms the classical one. *Process control*, pages 1–6, 2006.

[26] Parvesh Kumar and Jetesh Raheja. Optimal design of robust FOPID for the flight control system using multi-objective differential evolution. In *2015 2nd International Conference on Recent Advances in Engineering & Computational Sciences (RAECS)*, pages 1–4. IEEE, 2015.

[27] Bo Yang, Jingbo Wang, Junting Wang, Hongchun Shu, Danyang Li, Chunyuan Zeng, Yijun Chen, Xiaoshun Zhang, and Tao Yu. Robust fractional-order PID control of supercapacitor energy storage systems for distribution network applications: A perturbation compensation based approach. *Journal of Cleaner Production*, 279:123362, 2021.

[28] Pritesh Shah and Sudhir Agashe. Review of fractional PID controller. *Mechatronics*, 38:29–41, 2016.

[29] Saptarshi Das, Suman Saha, Shantanu Das, and Amitava Gupta. On the selection of tuning methodology of FOPID controllers for the control of higher order processes. *ISA transactions*, 50(3):376–388, 2011.

[30] Ying Luo and YangQuan Chen. Stabilizing and robust fractional order PI controller synthesis for first order plus time delay systems. *Automatica*, 48(9):2159–2167, 2012.

[31] Hai-Peng Ren, Xuan Wang, Jun-Tao Fan, and Okyay Kaynak. Fractional order sliding mode control of a pneumatic position servo system. *Journal of the Franklin Institute*, 356(12):6160–6174, 2019.

[32] Fang Yan, Xiaorong Hou, and Tingting Tian. Fractional-order multivariable adaptive control based on a nonlinear scalar update law. *Mathematics*, 10(18):3385, 2022.

[33] Ivo Petráš. Novel fractional-order model predictive control: State-space approach. *IEEE Access*, 9:92769–92775, 2021.

[34] Boris Andrievskii and Alexander Fradkov. Control of chaos: Methods and applications. II. applications. *Automation and remote control*, 65:505–533, 2004.

[35] Jun Guo Lu. Chaotic dynamics and synchronization of fractional-order Arneodo's systems. *Chaos, Solitons & Fractals*, 26(4):1125–1133, 2005.

[36] Yongguang Yu, Han-Xiong Li, Sha Wang, and Junzhi Yu. Dynamic analysis of a fractional-order Lorenz chaotic system. *Chaos, Solitons & Fractals*, 42(2):1181–1189, 2009.

[37] Hassan Hosseinnia, Reza Ghaderi, Mohammad Mahmoudian, and Shaher Momani. Sliding mode synchronization of an uncertain fractional order chaotic system. *Computers & Mathematics with Applications*, 59(5):1637–1643, 2010.

[38] Yan Zhou, Hongxing Wang, and Heng Liu. Generalized function projective synchronization of incommensurate fractional-order chaotic systems with inputs saturation. *International Journal of Fuzzy Systems*, 21:823–836, 2019.

[39] Tiedong Ma, Wei Luo, Zhengle Zhang, and Zhenyu Gu. Impulsive synchronization of fractional-order chaotic systems with actuator saturation and control gain error. *IEEE Access*, 8:36113–36119, 2020.

[40] Abolhassan Razminia and Dumitru Baleanu. Complete synchronization of commensurate fractional order chaotic systems using sliding mode control. *Mechatronics*, 23(7):873–879, 2013.

[41] Petros A Ioannou and Jing Sun. *Robust adaptive control*, volume 1. PTR Prentice-Hall Upper Saddle River, NJ, 1996.

[42] Gang Tao. *Adaptive control design and analysis*, volume 37. John Wiley & Sons, 2003.

[43] Philip Gregory. *Proceedings of the Self Adaptive Flight Control Systems Symposium*, volume 59. Wright Air Development Center, Air Research and Development Command, United, 1959.

[44] Naira Hovakimyan and Chengyu Cao. $\mathscr{L}_1$ *adaptive control theory: Guaranteed robustness with fast adaptation*. SIAM, 2010.

[45] Eli Mishkin, Ludwig Braun, and John G Truxal. *Adaptive Control Systems: Brooklyn Polytechnic Institute Series*. Literary Licensing, LLC, 2013.

[46] Chengyu Cao and Naira Hovakimyan. Design and analysis of a novel $\mathscr{L}_1$ adaptive controller, part I: Control signal and asymptotic stability. In *2006 American Control Conference*, pages 3397–3402. IEEE, 2006.

[47] Brian DO Anderson and Arvin Dehghani. Challenges of adaptive control–past, permanent and future. *Annual reviews in control*, 32(2):123–135, 2008.

[48] Zhuquan Zang and Robert R Bitmead. Transient bounds for adaptive control systems. In *29th IEEE conference on decision and control*, pages 2724–2729. IEEE, 1990.

[49] Petros A Ioannou and Petar Kokotovic. Robust redesign of adaptive control. *IEEE Transactions on Automatic Control*, 29(3):202–211, 1984.

[50] Kumpatis Narendra and Anuradham Annaswamy. A new adaptive law for robust adaptation without persistent excitation. *IEEE Transactions on Automatic control*, 32(2):134–145, 1987.

[51] Jean-Jacques Slotine and Weiping Li. *Applied nonlinear control*, volume 199. Prentice hall Englewood Cliffs, NJ, 1991.

[52] Daniel E Miller and Edward J Davison. An adaptive controller which provides an arbitrarily good transient and steady-state response. *IEEE Transactions on Automatic Control*, 36(1):68–81, 1991.

[53] Aniruddha Datta and Petros A Ioannou. Performance analysis and improvement in model reference adaptive control. *IEEE Transactions on Automatic Control*, 39(12):2370–2387, 1994.

[54] Kumpati S Narendra and Jeyendran Balakrishnan. Improving transient response of adaptive control systems using multiple models and switching. *IEEE Transactions on automatic control*, 39(9):1861–1866, 1994.

[55] Jing Sun. A modified model reference adaptive control scheme for improved transient performance. *IEEE Transactions on Automatic Control*, 38(8):1255–1259, 1993.

[56] Chengyu Cao and Naira Hovakimyan. Design and analysis of a novel $\mathscr{L}_1$ adaptive controller, part II: Guaranteed transient performance. In *2006 American Control Conference*, pages 3403–3408. IEEE, 2006.

[57] Roshni Maiti, Kaushik Das Sharma, and Gautam Sarkar. *Hybrid $\mathscr{L}_1$ Adaptive Control: Applications of Fuzzy Modeling, Stochastic Optimization and Metaheuristics*, volume 422. Springer Nature, 2022.

[58] Ahsene Boubakir, Toufik Souanef, Salim Labiod, Franck Plestan, and Fares Boudjema. An $\mathscr{L}_1$ fuzzy adaptive controller for a class of SISO nonaffine nonlinear systems: Application to the control of an electropneumatic actuator. *Proceedings of the Institution of Mechanical Engineers, Part I: Journal of Systems and Control Engineering*, 230(8):736–748, 2016.

[59] Nicole Heymans and Igor Podlubny. Physical interpretation of initial conditions for fractional differential equations with riemann-liouville fractional derivatives. *Rheologica Acta*, 45:765–771, 2006.

[60] Denis Matignon. Stability results for fractional differential equations with applications to control processing. In *Computational engineering in systems applications*, volume 2, pages 963–968. Citeseer, 1996.

[61] Anatoliy Aleksandrovich Kilbas, Hari M Srivastava, and Juan J Trujillo. *Theory and applications of fractional differential equations*, volume 204. elsevier, 2006.

[62] Denis Matignon. Stability properties for generalized fractional differential systems. In *ESAIM: proceedings*, volume 5, pages 145–158. EDP Sciences, 1998.

[63] Jun Zhou. Nyquist-like stability criteria for fractional-order linear dynamical systems. *Control Theory in Engineering*, page 31, 2019.

[64] Jocelyn Sabatier, Mathieu Moze, and Christophe Farges. LMI stability conditions for fractional order systems. *Computers & Mathematics with Applications*, 59(5):1594–1609, 2010.

[65] Mohammad Saleh Tavazoei and Mohammad Haeri. A necessary condition for double scroll attractor existence in fractional-order systems. *Physics Letters A*, 367(1-2):102–113, 2007.

[66] Mohammad Saleh Tavazoei and Mohammad Haeri. Chaotic attractors in incommensurate fractional order systems. *Physica D: Nonlinear Phenomena*, 237(20):2628–2637, 2008.

[67] Alain Oustaloup, Jocelyn Sabatier, Patrick Lanusse, Rachid Malti, Pierre Melchior, Xavier Moreau, and Mathieu Moze. An overview of the CRONE approach in system analysis, modeling and identification, observation and control. *IFAC Proceedings Volumes*, 41(2):14254–14265, 2008.

[68] Yan Li, YangQuan Chen, and Igor Podlubny. Mittag–Leffler stability of fractional order nonlinear dynamic systems. *Automatica*, 45(8):1965–1969, 2009.

[69] Aleksandr Mikhailovich Lyapunov. The general problem of the stability of motion. *International journal of control*, 55(3):531–534, 1992.

[70] Yan Li, YangQuan Chen, and Igor Podlubny. Stability of fractional-order nonlinear dynamic systems: Lyapunov direct method and generalized Mittag–Leffler stability. *Computers & Mathematics with Applications*, 59(5):1810–1821, 2010.

[71] Weisheng Chen, Hao Dai, Yanfei Song, and Zhengqiang Zhang. Convex Lyapunov functions for stability analysis of fractional order systems. *IET Control Theory & Applications*, 11(7):1070–1074, 2017.

[72] AnPing Li, GuoRong Liu, YiPing Luo, and XiaoLiang Yang. An indirect Lyapunov approach to robust stabilization for a class of linear fractional-order system with positive real uncertainty. *Journal of Applied Mathematics and Computing*, 57:39–55, 2018.

[73] Hermann Weyl and Gerald R MacLane. *The concept of a Riemann surface*. Courier Corporation, 2009.

[74] Mohammad Saleh Tavazoei and Mohammad Haeri. Limitations of frequency domain approximation for detecting chaos in fractional order systems. *Nonlinear Analysis: Theory, Methods & Applications*, 69(4):1299–1320, 2008.

[75] Ahmed S Elwakil. Fractional-order circuits and systems: An emerging interdisciplinary research area. *IEEE Circuits and Systems Magazine*, 10(4):40–50, 2010.

[76] Krzysztof Oprzedkiewicz, Marek Chochol, Waldemar Bauer, and Tomasz Meresinski. Modeling of elementary fractional order plants at PLC SIEMENS platform. In *Advances in Modelling and Control of Non-integer-Order Systems: 6th Conference on Non-integer Order Calculus and Its Applications, 2014 Opole, Poland*, pages 265–273. Springer, 2015.

[77] Zhuo Li, Lu Liu, Sina Dehghan, YangQuan Chen, and Dingyü Xue. A review and evaluation of numerical tools for fractional calculus and fractional order controls. *International journal of control*, 90(6):1165–1181, 2017.

[78] Aleksei Tepljakov, Eduard Petlenkov, and Juri Belikov. Application of Newton's method to analog and digital realization of fractional-order controllers. *International Journal of Microelectronics and Computer Science*, 3(2):45–52, 2012.

[79] Duarte Valério, Juan J Trujillo, Margarita Rivero, JA Tenreiro Machado, and Dumitru Baleanu. Fractional calculus: A survey of useful formulas. *The European Physical Journal Special Topics*, 222(8):1827–1846, 2013.

[80] Alain Oustaloup, Francois Levron, Benoit Mathieu, and Florence M Nanot. Frequency-band complex noninteger differentiator: Characterization and synthesis. *IEEE Transactions on Circuits and Systems I: Fundamental Theory and Applications*, 47(1):25–39, 2000.

[81] Hu Sheng, YangQuan Chen, and TianShuang Qiu. *Fractional processes and fractional-order signal processing: Techniques and applications*. Springer Science & Business Media, 2011.

[82] Ali Yüce, Furkan N Deniz, and Nusret Tan. A new integer order approximation table for fractional order derivative operators. *IFAC-PapersOnLine*, 50(1):9736–9741, 2017.

[83] Alain Oustaloup, Pierre Melchior, Patrick Lanusse, O Cois, and F Dancla. The CRONE toolbox for Matlab. In *CACSD. Conference Proceedings. IEEE International Symposium on Computer-Aided Control System Design (Cat. No. 00TH8537)*, pages 190–195. IEEE, 2000.

[84] Duarte Valerio and José Sá Da Costa. Ninteger: A non-integer control toolbox for Matlab. *Proceedings of fractional differentiation and its applications, Bordeaux*, 2004.

[85] Aleksei Tepljakov, Eduard Petlenkov, and Juri Belikov. FOMCOM: a Matlab toolbox for fractional-order system identification and control. *International Journal of Microelectronics and computer science*, 2(2):51–62, 2011.

[86] Dingyü Xue, YangQuan Chen, and Derek P Atherton. *Linear feedback control: Analysis and design with MATLAB*. SIAM, 2007.

[87] Alain Oustaloup. *La commande CRONE: Commande robuste d'ordre non entier*. Hermes Science Publications, 1991.

[88] Aleksei Tepljakov. *Fractional-order modeling and control of dynamic systems*. Springer, 2017.

[89] Blas M Vinagre, Ivo Petráš, Igor Podlubny, and YangQuan Chen. Using fractional order adjustment rules and fractional order reference models in model-reference adaptive control. *Nonlinear Dynamics*, 29:269–279, 2002.

[90] Hanane Balaska, Samir Ladaci, and Abdelbaki Djouambi. Direct fractional order MRAC adaptive control design for a class of fractional order commensurate linear systems. *Journal of Control and Decision*, 8(3):363–371, 2021.

[91] Yuquan Chen, Yiheng Wei, Shu Liang, and Yong Wang. Indirect model reference adaptive control for a class of fractional order systems. *Communications in Nonlinear Science and Numerical Simulation*, 39:458–471, 2016.

[92] Marco E Ortiz-Quisbert, Manuel A Duarte-Mermoud, Freddy Milla, Rafael Castro-Linares, and Gastón Lefranc. Optimal fractional order adaptive controllers for AVR applications. *Electrical Engineering*, 100:267–283, 2018.

[93] Shengzheng Kang, Hongtao Wu, Xiaolong Yang, Yao Li, and Yaoyao Wang. Fractional-order robust model reference adaptive control of piezo-actuated active vibration isolation systems using output feedback and multi-objective optimization algorithm. *Journal of Vibration and Control*, 26(1-2):19–35, 2020.

[94] Songsong Cheng, Yiheng Wei, Yuquan Chen, Yong Wang, and Qing Liang. Fractional-order multivariable composite model reference adaptive control. *International Journal of Adaptive Control and Signal Processing*, 31(10):1467–1480, 2017.

[95] Keziz Bouziane, Abdelbaki Djouambi, and Samir Ladaci. Fractional-order model reference adaptive controller design using a modified MIT rule and a feed-forward action for a DC-DC boost converter stabilization. In *2017 5th International Conference on Electrical Engineering-Boumerdes (ICEE-B)*, pages 1–6. IEEE, 2017.

[96] Chun Yin, Yuhua Cheng, YangQuan Chen, Brandon Stark, and Shouming Zhong. Adaptive fractional-order switching-type control method design for 3D fractional-order nonlinear systems. *Nonlinear Dynamics*, 82(1-2):39–52, 2015.

[97] Yucheng Chen, Chunming Tang, and Majid Roohi. Design of a model-free adaptive sliding mode control to synchronize chaotic fractional-order systems with input saturation: An application in secure communications. *Journal of the Franklin Institute*, 358(16):8109–8137, 2021.

[98] Ayub Khan and Nasreen. A comparative study between two different adaptive sliding mode control techniques. *International Journal of Applied and Computational Mathematics*, 7:1–18, 2021.

[99] Zeeshan Anjum and Yu Guo. Finite time fractional-order adaptive backstepping fault tolerant control of robotic manipulator. *International Journal of Control, Automation and Systems*, 19:301–310, 2021.

[100] Wenshan Bi, Tong Wang, and Xinghu Yu. Fuzzy adaptive decentralized control for nonstrict-feedback large-scale switched fractional-order nonlinear systems. *IEEE Transactions on Cybernetics*, 52(9):8887–8896, 2021.

[101] Yongliang Zhan and Shaocheng Tong. Adaptive fuzzy output-feedback decentralized control for fractional-order nonlinear large-scale systems. *IEEE Transactions on Cybernetics*, 52(12):12795–12804, 2021.

[102] Juntao Fei and Cheng Lu. Adaptive fractional order sliding mode controller with neural estimator. *Journal of the Franklin Institute*, 355(5):2369–2391, 2018.

[103] Yifei Zhao and Zongxia Jiao. Fractional model reference adaptive control for electro-hydraulic servo system. In *2016 IEEE Chinese Guidance, Navigation and Control Conference (CGNCC)*, pages 2048–2052. IEEE, 2016.

[104] Amina Boubellouta, Farouk Zouari, and Abdesselem Boulkroune. Intelligent fuzzy controller for chaos synchronization of uncertain fractional-order chaotic systems with input nonlinearities. *International journal of general systems*, 48(3):211–234, 2019.

[105] Amel Bouzeriba, Abdesselem Boulkroune, Toufik Bouden, and Sundarapandian Vaidyanathan. Fuzzy adaptive synchronization of incommensurate fractional-order chaotic systems. *Advances and Applications in Chaotic Systems*, pages 363–378, 2016.

[106] Shumin Ha, Heng Liu, Shenggang Li, and Aijing Liu. Backstepping-based adaptive fuzzy synchronization control for a class of fractional-order chaotic systems with input saturation. *International Journal of Fuzzy Systems*, 21:1571–1584, 2019.

[107] Shuai Song, Ju H Park, Baoyong Zhang, and Xiaona Song. Adaptive NN finite-time resilient control for nonlinear time-delay systems with unknown false data injection

and actuator faults. *IEEE Transactions on Neural Networks and Learning Systems*, 33(10):5416–5428, 2021.

[108] Farouk Zouari, Asier Ibeas, Abdesselem Boulkroune, Jinde Cao, and Mohammad Mehdi Arefi. Adaptive neural output-feedback control for nonstrict-feedback time-delay fractional-order systems with output constraints and actuator nonlinearities. *Neural Networks*, 105:256–276, 2018.

[109] Senkui Lu, Xingcheng Wang, and Yanan Li. Adaptive neural network finite-time command filtered tracking control of fractional-order permanent magnet synchronous motor with input saturation. *Journal of the Franklin Institute*, 357(18):13707–13733, 2020.

[110] Boqiang Cao and Xiaobing Nie. Event-triggered adaptive neural networks control for fractional-order nonstrict-feedback nonlinear systems with unmodeled dynamics and input saturation. *Neural Networks*, 142:288–302, 2021.

[111] Shumin Ha, Liangyun Chen, and Heng Liu. Command filtered adaptive neural network synchronization control of fractional-order chaotic systems subject to unknown dead zones. *Journal of the Franklin Institute*, 358(7):3376–3402, 2021.

[112] Khalil Hassan. Nonlinear systems. *Departement of Electrical and computer Engineering, Michigan State University*, 2002.

[113] Jean-Baptiste Pomet and Laurent Praly. Adaptive nonlinear regulation: Estimation from the Lyapunov equation. *IEEE Transactions on automatic control*, 37(6):729–740, 1992.

[114] Miroslav Krstic, Petar V Kokotovic, and Ioannis Kanellakopoulos. *Nonlinear and adaptive control design*. John Wiley & Sons, Inc., 1995.

[115] Naira Hovakimyan, Chengyu Cao, Evgeny Kharisov, Enric Xargay, and Irene Gregory. $\mathscr{L}_1$ adaptive control for safety-critical systems. *IEEE Control Systems Magazine*, 31(5):54–104, 2011.

[116] Evgeny Kharisov, Naira Hovakimyan, and Karl J Åström. Comparison of architectures and robustness of model reference adaptive controllers and $\mathscr{L}_1$ adaptive controllers. *International Journal of Adaptive Control and Signal Processing*, 28(7-8):633–663, 2014.

[117] Chengyu Cao and Naira Hovakimyan. Design and analysis of a novel $\mathscr{L}_1$ adaptive control architecture with guaranteed transient performance. *IEEE Transactions on Automatic Control*, 53(2):586–591, 2008.

[118] Chengyu Cao and Naira Hovakimyan. Adaptive controller for systems with unknown time-varying parameters and disturbances in the presence of non-zero trajectory initialization error. *International Journal of Control*, 81(7):1147–1161, 2008.

[119] Chengyu Cao and Naira Hovakimyan. $\mathscr{L}_1$ adaptive controller for multi-input multi-output systems in the presence of unmatched disturbances. In *2008 American Control Conference*, pages 4105–4110. IEEE, 2008.

[120] Enric Xargay, Naira Hovakimyan, and Chengyu Cao. $\mathscr{L}_1$ adaptive controller for multi-input multi-output systems in the presence of nonlinear unmatched uncertainties. In *Proceedings of the 2010 American control conference*, pages 874–879. IEEE, 2010.

[121] Chengyu Cao and Naira Hovakimyan. $\mathscr{L}_1$ adaptive output feedback controller for systems of unknown dimension. *IEEE Transactions on Automatic Control*, 53(3):815–821, 2008.

[122] Chengyu Cao and Naira Hovakimyan. Stability margins of $\mathscr{L}_1$ adaptive control architecture. *IEEE Transactions on Automatic Control*, 55(2):480–487, 2010.

[123] Enric Xargay, Naira Hovakimyan, Vladimir Dobrokhodov, Issac Kaminer, Ioannis Kitsios, Chengyu Cao, Irene M Gregory, and Lena Valavani. Experimental validation of l1 adaptive control: Rohrs' counterexample in flight. Technical report, 2010.

[124] Randy Beard, Chengyu Cao, and Naira Hovakimyan. An $\mathscr{L}_1$ adaptive pitch controller for miniature air vehicles. In *AIAA guidance, navigation, and control conference and exhibit*, page 6777, 2006.

[125] Evgeny Kharisov, Irene Gregory, Chengyu Cao, and Naira Hovakimyan. L1 adaptive control for flexible space launch vehicle and proposed plan for flight validation. In *AIAA Guidance, Navigation and Control Conference and Exhibit*, page 7128, 2008.

[126] Irene Gregory, Chengyu Cao, Vijay Patel, and Naira Hovakimyan. Adaptive control laws for flexible semi-span wind tunnel model of high-aspect ratio flying wing. In *AIAA Guidance, Navigation and Control Conference and Exhibit*, page 6525, 2007.

[127] Moussab Bennehar, Ahmed Chemori, and François Pierrot. $\mathscr{L}_1$ adaptive control of parallel kinematic manipulators: Design and real-time experiments. In *2015 IEEE International Conference on Robotics and Automation (ICRA)*, pages 1587–1592. IEEE, 2015.

[128] Nicholas Rober, Maxwell Hammond, Venanzio Cichella, Juan E Martin, and Pablo Carrica. 3D path following and $\mathscr{L}_1$ adaptive control for underwater vehicles. *Ocean Engineering*, 253:110971, 2022.

[129] Jie Luo and Chengyu Cao. $\mathscr{L}_1$ adaptive output feedback controller for a class of nonlinear systems. In *2011 50th IEEE Conference on Decision and Control and European Control Conference*, pages 5425–5430. IEEE, 2011.

[130] Xiaofeng Wang and Naira Hovakimyan. $\mathscr{L}_1$ adaptive controller for nonlinear time-varying reference systems. *Systems & Control Letters*, 61(4):455–463, 2012.

[131] Hai-tao Song, Tao Zhang, and Guo-liang Zhang. $\mathscr{L}_1$ adaptive controller of nonlinear reference system in presence of unmatched uncertainties. *Journal of Central South University*, 23:834–840, 2016.

[132] Zhiyuan Li and Naira Hovakimyan. $\mathscr{L}_1$ adaptive controller for MIMO systems with unmatched uncertainties using modified piecewise constant adaptation law. In *2012 IEEE 51st IEEE conference on decision and control (CDC)*, pages 7303–7308. IEEE, 2012.

[133] Ronald Choe, Enric Xargay, and Naira Hovakimyan. $\mathscr{L}_1$ adaptive control for a class of nonaffine-in-control nonlinear systems. *IFAC Proceedings Volumes*, 46(11):477–482, 2013.

[134] Jie Luo, Chengyu Cao, and Qinmin Yang. $\mathscr{L}_1$ adaptive controller for a class of non-affine multi-input multi-output nonlinear systems. *international Journal of Control*, 86(2):348–359, 2013.

[135] Xiaotian Zou, Chengyu Cao, and Naira Hovakimyan. $\mathscr{L}_1$ adaptive controller for systems with hysteresis uncertainties. In *Proceedings of the 2010 American Control Conference*, pages 6662–6667. IEEE, 2010.

[136] Zongyu Zuo, Xiao Li, and Zhiguang Shi. $\mathscr{L}_1$ adaptive control of uncertain gear transmission servo systems with deadzone nonlinearity. *ISA transactions*, 58:67–75, 2015.

[137] Mikkel Eske Nørgaard Sørensen and Morten Breivik. UAV fault-tolerant control by combined $\mathscr{L}_1$ adaptive backstepping and fault-dependent control allocation. In *2015 IEEE Conference on Control Applications (CCA)*, pages 1880–1886. IEEE, 2015.

[138] Wang Chao, Xie Wujie, Dong Wenhan, and Jiao Jinyan. $\mathscr{L}_1$ fault tolerant control with sliding-mode based adaptive law for aircraft actuator fault. In *2017 5th International Conference on Mechanical, Automotive and Materials Engineering (CMAME)*, pages 259–264. IEEE, 2017.

[139] John Cooper, Jiaxing Che, and Chengyu Cao. The use of learning in fast adaptation algorithms. *International Journal of Adaptive Control and Signal Processing*, 28(3-5):325–340, 2014.

[140] Hassan A Yousef, Mohamed Hamdy, and Kyrillos Nashed. $\mathscr{L}_1$ adaptive fuzzy controller for a class of nonlinear systems with unknown backlash-like hysteresis. *International Journal of Systems Science*, 48(12):2522–2533, 2017.

[141] Roshni Maiti, Kaushik Das Sharma, and Gautam Sarkar. Fuzzy predictor based $\mathscr{L}_1$ adaptive controller for nonlinear systems with disturbances. In *2017 IEEE Calcutta Conference (CALCON)*, pages 253–257. IEEE, 2017.

[142] Rusong Zhu, Mingwei Xie, Zili Guo, Wen Gai, and Gengsheng Tang. Nonlinear $\mathscr{L}_1$ adaptive control with feedforward control action and its application in wind tunnel. In *2019 Chinese Control Conference (CCC)*, pages 386–391. IEEE, 2019.

[143] Tieshan Li, Dan Wang, and Naxin Chen. Adaptive fuzzy control of uncertain MIMO non-linear systems in block-triangular forms. *Nonlinear Dynamics*, 63:105–123, 2011.

[144] Ling Li and Yeguo Sun. Adaptive fuzzy control for nonlinear fractional-order uncertain systems with unknown uncertainties and external disturbance. *Entropy*, 17(8):5580–5592, 2015.

[145] Shuai Song, Ju H Park, Baoyong Zhang, and Xiaona Song. Observer-based adaptive hybrid fuzzy resilient control for fractional-order nonlinear systems with time-varying delays and actuator failures. *IEEE Transactions on fuzzy systems*, 29(3):471–485, 2019.

[146] Tahereh Binazadeh and Mohammad H Shafiei. Output tracking of uncertain fractional-order nonlinear systems via a novel fractional-order sliding mode approach. *Mechatronics*, 23(7):888–892, 2013.

[147] Shabnam Pashaei and Mohammad Ali Badamchizadeh. Control of a class of fractional-order systems with mismatched disturbances via fractional-order sliding mode controller. *Transactions of the Institute of Measurement and Control*, 42(13):2423–2439, 2020.

[148] Seongik Han. Fractional-order command filtered backstepping sliding mode control with fractional-order nonlinear disturbance observer for nonlinear systems. *Journal of the Franklin Institute*, 357(11):6760–6776, 2020.

[149] Fatemeh Doostdar and Hamed Mojallali. An ADRC-based backstepping control design for a class of fractional-order systems. *ISA transactions*, 121:140–146, 2022.

[150] Liping Chen, Jianfeng Qu, Yi Chai, Ranchao Wu, and Guoyuan Qi. Synchronization of a class of fractional-order chaotic neural networks. *Entropy*, 15(8):3265–3276, 2013.

[151] Fei Qi, Jianfeng Qu, Yi Chai, Liping Chen, and António M Lopes. Synchronization of incommensurate fractional-order chaotic systems based on linear feedback control. *Fractal and Fractional*, 6(4):221, 2022.

[152] Milad Mohadeszadeh and Hadi Delavari. Synchronization of fractional-order hyper-chaotic systems based on a new adaptive sliding mode control. *International Journal of Dynamics and Control*, 5:124–134, 2017.

[153] Jooyoung Park and Irwin W Sandberg. Universal approximation using radial-basis-function networks. *Neural computation*, 3(2):246–257, 1991.

[154] Federico Girosi and Tomaso Poggio. Networks and the best approximation property. *Biological cybernetics*, 63(3):169–176, 1990.

[155] Mohammad Pourmahmood Aghababa. A Lyapunov-based control scheme for robust stabilization of fractional chaotic systems. *Nonlinear Dynamics*, 78(3):2129–2140, 2014.

[156] Nadia Djeghali, Maamar Bettayeb, and Said Djennoune. Sliding mode active disturbance rejection control for uncertain nonlinear fractional-order systems. *European Journal of control*, 57:54–67, 2021.

[157] Salim Labiod and Thierry Marie Guerra. Direct adaptive fuzzy control for a class of MIMO nonlinear systems. *International Journal of systems science*, 38(8):665–675, 2007.

[158] Li-Xin Wang. *Adaptive fuzzy systems and control: design and stability analysis*. Prentice-Hall, Inc., 1994.

[159] Mohammad Reza Faieghi and Hadi Delavari. Chaos in fractional-order Genesio–Tesi system and its synchronization. *Communications in Nonlinear Science and Numerical Simulation*, 17(2):731–741, 2012.